July 2020

Benefits of Continuously Spaced Energies and Scanned Beams for Electron Bolus Conformal Therapy for Left-Side Post-Mastectomy Chest Wall

Stephanie Lianglei Wang
Louisiana State University and Agricultural and Mechanical College

BENEFITS OF CONTINUOUSLY SPACED ENERGIES AND SCANNED BEAMS FOR ELECTRON BOLUS CONFORMAL THERAPY FOR LEFT-SIDE POST-MASTECTOMY CHEST WALL

A Thesis

Submitted to the Graduate Faculty of the
Louisiana State University and
Agricultural and Mechanical College
in partial fulfillment of the
requirements for the degree of
Master of Science

in

The Department of Physics and Astronomy

by
Stephanie Lianglei Wang
B.S., College of William and Mary, 2017
August 2020

Acknowledgements

I thank my thesis advisor, Dr. Robert Carver, for all his support and guidance, and I acknowledge Dr. Kenneth Hogstrom for providing his expertise and mentorship throughout this project. Also, I thank my other graduate committee members Drs. James Matthews, Garrett Pitcher, and Rui Zhang for monitoring the progress of this work. I also acknowledge Dr. Kevin Erhart of .decimal, LLC for providing the research version of p.d used in this project.

I acknowledge funding support for this project from Mary Bird Perkins Cancer Center. Also, this research was supported in part by the Kenneth R. Hogstrom Superior Graduate Student Scholarship in Medical Physics from the Louisiana State University-Mary Bird Perkins Cancer Center Medical Physics Program.

I am grateful to the medical physics faculty at LSU who taught me everything I know about medical physics from attenuation to the Zeeman effect. I also express my sincerest thanks and appreciation for Susan Hammond, Paige Whittington, and Yao Zeng for helping with administrative logistics and paperwork during my time at LSU.

I also thank my student colleagues I have known during my time at LSU for their camaraderie, particularly Ana Dieguez, Troy Jacobs, Rachel Malecek, Phillip Wall, and Yibo Xie. I also owe thanks to Eddy Wang and Dmitriy Zhigunov for all their moral support.

Finally, I thank my mom, dad, and sister, Katie, for encouraging me to pursue a career in medical physics.

Table of Contents

List of Tables

List of Figures

Abstract

Purpose: This study assessed the benefits to the heart and lung of using scanned electron beams and continuous energy spacing (ΔR_{90}=0.1 cm) for left-side post-mastectomy radiotherapy (PMRT) patients previously treated with volumetric modulated arc therapy (VMAT). Such beams offer a sharper distal falloff (R_{90-10}) than do currently available scattered, discrete energy beams, which increases sparing of healthy organs distal to the target.

Methods: Seven left-side PMRT patients previously treated with VMAT at the Mary Bird Perkins Cancer Center were planned in this study. The patients were divided into two sets; Patient Sets 1 (three patients) and 2 (four patients) used one and two fields, respectively, to plan chest wall irradiation. Four and five intensity modulated bolus electron conformal therapy (IM-BECT) plans, respectively, were created per patient using combinations of scattered/scanned and discrete/continuous energy beam data. For Patient Set 2 the inferior edge of the upper field was feathered to match the penumbra of the superior edge of the lower field. Dose distributions and dose volume histograms (DVHs) were used to evaluate plan quality, to calculate physical dose metrics for the target, heart, and lung, and to calculate the biological metrics, normal tissue complication probability (NTCP), and secondary cancer complication probability (SCCP) for the heart and lung.

Results: Scanned and/or continuous energy electron beams showed patient-dependent, sometimes significant reductions in both physical and biological dose metrics for the heart and lung. For patient CW1, as compared to scattered, discrete energy beams, scanned, continuous energy beams reduced $V_{22.5Gy}$ from 10.4% to 2.3%, V_{30Gy} from 3.1% to 0.1%, D_{mean} from 8.3 Gy to 4.3 Gy, and NTCP from 0.4% to 0.1% for the heart. The comparison reduced V_{20Gy} from 17.2% to 10.7% and $SCCP_{lin}$ from 14.4% to 8.7% for the lungs. Such reductions tended to

increase as R_{90} increased. Compared to VMAT, IM-BECT plans with scanned beams on average reduced $V_{22.5Gy}$ from 9.4% to 3.4%, D_{mean} from 9.3 Gy to 4.4 Gy, and NTCP from 1.0% to 0.2% for heart and D_{mean} from 8.8 Gy to 7.1 Gy, NTCP from 2.8% to 0.2%, and $SCCP_{lin}$ from 15.1% to 10.2% for lung.

Conclusion: Scanned and/or continuous energy electron beam treatment plans showed reduced physical and biological dose metrics for heart and lung compared to scattered, discrete energy beams. These improvements were patient dependent, although patients requiring higher energy beam(s) tended to show the greatest benefits.

Chapter 1. Introduction

1.1. Background and Significance

1.1.1. Breast Cancer and Post- Mastectomy Chest Wall Irradiation

In 2019, breast cancer comprised 30% of all new cancer diagnoses in women, the highest incidence rate of all cancers in women.[1] While the overall cancer incidence rate for women has stayed relatively constant over the past few decades, breast cancer incidence rates have been on the rise. From 2006 to 2015 in the United States, breast cancer incidence increased by 0.3%-0.4% per year in non-Hispanic white and Hispanic women, by 0.7%-0.8% per year in black and American Indian/ Alaska Native women, and by 1.8% per year in Asian/ Pacific Islander women.[2] Contributing factors may be the obesity epidemic and declining parity.[3, 4]

15% of all deaths due to cancer, corresponding to 41,760 total patients, were attributed to breast cancer in the United States, which has the second highest mortality rate of all cancers in women. However, the 5-year survival rate for all stages of breast cancer is 90%, which is the third highest of all cancers.[1] This suggests that the high mortality rate is primarily due to its high incidence rate.

Surgery, radiation, or a combination of the two are common treatment options for breast cancer. A mastectomy, complete removal of the breast tissue, is often combined with radiotherapy to eradicate microscopic disease in the remaining chest wall, referred to as post-mastectomy radiotherapy (PMRT).

When planning post-mastectomy radiation treatments, the chest wall is defined by the following anatomical boundaries based on consensus definitions from RTOG breast cancer Atlas: to the caudal border of the clavicle head on the cranial side, to the skin on the anterior side, to the rib-pleural interface (including the pectoralis muscles, chest wall muscles, and ribs) on the posterior side, to the mid axillary line (excluding latissimus dorsi) on the lateral side, to the sternal-

rib junction on the medial side, to the clinical reference on the caudal side.[5] The supraclavicular region, which is treated with photon radiotherapy, has the following anatomical boundaries based on the RTOG breast cancer Atlas: the upper border is below the level of the cricoid, the medial border is at the vertebral pedicles and lateral border consists of the portion of the axilla that remained undissected, and the inferior border extends to the caudal aspect of the clavicular head.[5] See Figure 1.1 for outlines of the regions and heart.

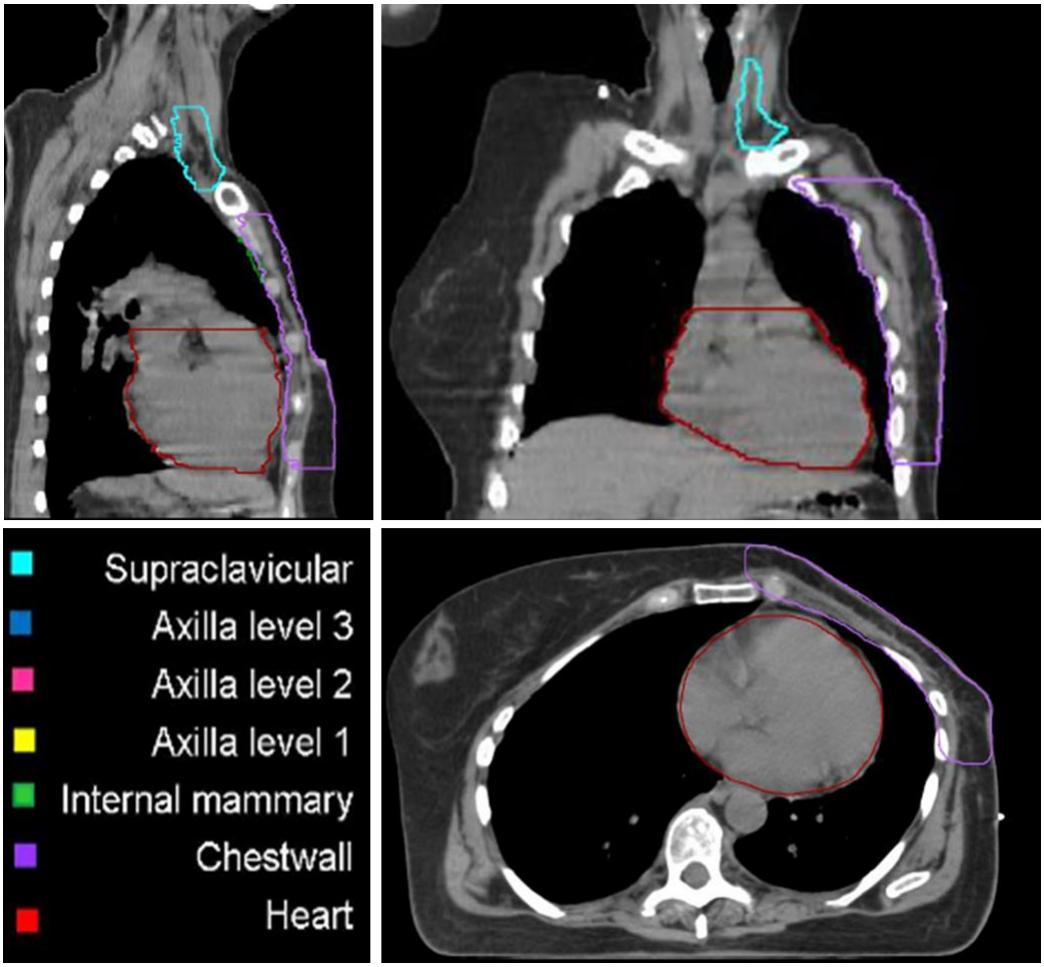

Figure 1.1. RTOG breast cancer atlas image of chest wall: sagittal (upper left), coronal (upper right), and transverse (lower right) planes. Shown are the chest wall, heart, and internal mammary glands.[6]

The standard radiation dose for post-mastectomy radiotherapy is 50 Gy to the target, delivered as 2 Gy daily fractions over 5 weeks. Monitor units are calculated to give the prescribed

dose to 95% of the target volume.[7, 8] Due to the high survival rate, the long-term side effects of post-mastectomy radiotherapy must be examined. For any post-mastectomy radiotherapy treatment, the lung is a primary organ at risk. In addition, for cases involving left-side post-mastectomy chest wall irradiation, the heart is also of concern, as the heart is distal to the left side of the chest wall. Cardiac late effects such as pericarditis, ischemic heart disease, congestive heart failure, and coronary atherosclerosis can occur if the dose delivered to the heart is too high.[9] However, if the heart receives under 30 Gy of dose, there is not an increased risk of cardiac mortality.[10] Thus, the present study evaluates the risk of developing radiotherapy side effects to the heart with $V_{30\,Gy}$, the volume of the heart receiving at least 30 Gy of dose compared to the total heart volume. Radiation pneumonitis, or acute inflammation of the lung, and pulmonary fibrosis, or scarring and stiffening of scar tissue, can both occur if too large a volume of the lung is irradiated.[11] Thus, the present study evaluates the risk of developing radiotherapy side effects to the lung with $V_{20\,Gy}$, the volume of the lungs receiving at least 20 Gy of dose compared to the total lung volume.[12, 13]

Because of the improvement in overall survivorship for invasive breast cancer patients when using PMRT, many different advanced radiotherapy techniques have been developed. These techniques include fixed-beam intensity-modulated radiotherapy,[14] non-coplanar volumetric modulated arc therapy (VMAT),[15] multiple arc VMAT,[16] mixed beam therapy (photons and electrons),[17] electron arc therapy,[18] and helical tomotherapy[19]. A previous study conducted by Xie et al.[20] evaluated many of these different treatment modalities for treating PMRT patients by the following metrics: planning target volume (PTV) coverage, dose homogeneity index (DHI), conformity index (CI), dose to organs at risk (OARs), normal tissue complication probability (NTCP) of pneumonitis, lifetime attributable risk (LAR) of second cancers, and risk of coronary

events (RCE). They found that fixed-beam IMRT delivered the lowest mean dose to contralateral breast and exhibited lowest LAR of secondary contralateral breast cancer; non-coplanar-VMAT delivered the lowest mean dose to lungs, exhibited lowest LAR of secondary lung cancer and lowest NTCP of pneumonitis; mixed beam therapy delivered the lowest mean dose to heart and exhibited lowest RCE for the heart; and tomotherapy plans provided the most optimal target coverage while delivering higher dose to OARs than other techniques.

Opp et al.[21] performed a similar study to compare the following PMRT techniques: opposed tangents with wedges, opposed tangents with field in field modulation, 8-field IMRT, and bolus electron conformal therapy (BECT). They compared the dose homogeneity and normal tissue dose parameters for these four sets of plans while maintaining a constant PTV coverage. They found that IMRT and BECT provided the lowest $V_{25\ Gy}$ doses for the heart, while field in field had the lowest average lung dose. In addition, IMRT provided the lowest $V_{20\ Gy}$ doses for the lung and BECT provided the lowest mean heart dose. This study, along with Xie et al.'s study shows that using electron radiotherapy for PMRT has OAR sparing benefits while maintaining adequate PTV coverage.

1.1.2. Electron Beam Radiation Therapy

Therapeutic electron beams are characterized by a unique depth dose profile and finite range that can be useful for irradiating planning target volumes (PTVs) within 6 cm of the patient skin surface while sparing distal organs and tissues. Superficial cancers and shallow tumor sites, such as skin, spinal cord, head and neck, and chest wall are effectively treated with electron beams.[22–24] This includes PMRT, for which there are many electron beam techniques, such as abutted beams of different energies,[19] electron arc therapy,[18] and BECT.[21, 25, 26]

Clinically available electron beams typically have energies ranging from approximately 7 MeV to 20 MeV, which have therapeutic ranges (R_{90}) of approximately 2.0 cm to 6.0 cm,

respectively. Such electron beams deliver a fairly uniform dose from the surface to R_{90}, with a sharp distal falloff (R_{90-10}), which spares underlying healthy tissue and critical organs. This rapid dose falloff beyond the target volume depth decreases the normal tissue complication probability while preserving high tumor control. This is the primary advantage of electron beam therapy over conventional photon therapy. Figure 1.2 characterizes the depth dose profile of an electron beam.

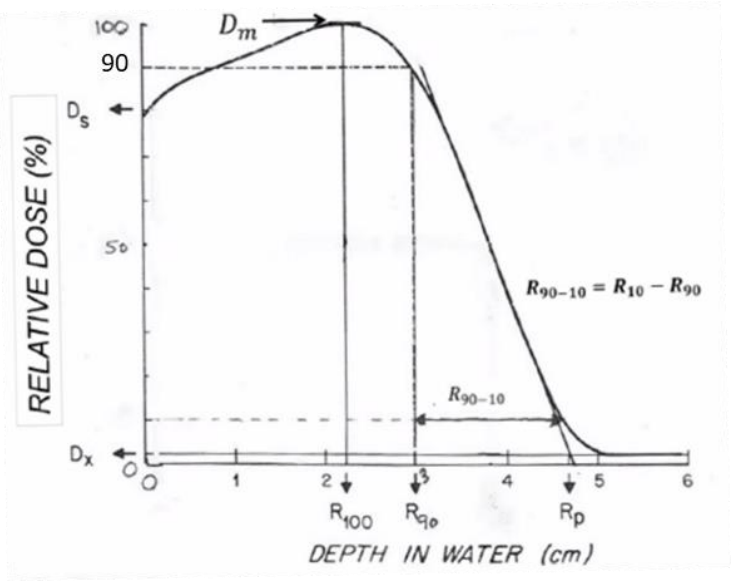

Figure 1.2. Characteristic depth dose curve of a megavoltage electron beam. The dose is normalized at R_{100}, the depth of maximum dose. The maximum dose, D_m or 100%, does not occur at the surface, but deeper in the volume, due to multiple Coulomb scattering. Typically the dose ranges from the lesser of D_s or 90% to 100% in the planning target volume (PTV). [27, 28]

Typically, electron beams are delivered in such a way that as much of the PTV is contained in the plateau (surface to R_{90} depth) with dose ranging from 100% to 90% (or D_s, if lower) without overdosing distal healthy tissue. In three dimensions, distal PTV depth varies with off-axis position, and ideally, the lowest energy that can contain the PTV within the 90% isosurface should be used. Often a higher than required energy is used in conjunction with a tissue-equivalent bolus to treat the PTV, due to the discretely spaced energies of clinically available electron beams, as illustrated in Figure 1.3 for the Elekta radiotherapy accelerator. In such a case, a tissue-equivalent bolus usually is placed superficial to the target, shifting the dose distribution towards the surface

and R_{90} toward the distal PTV surface. Note in Figure 1.3 that higher energy electron beams have a more gradual falloff (increased R_{90-10}), delivering more dose to healthy tissues distal to the PTV. This effect is amplified in lung, compared to unit density tissue, due to its lower density (approximately 0.25-0.33 times that of unit density tissue).

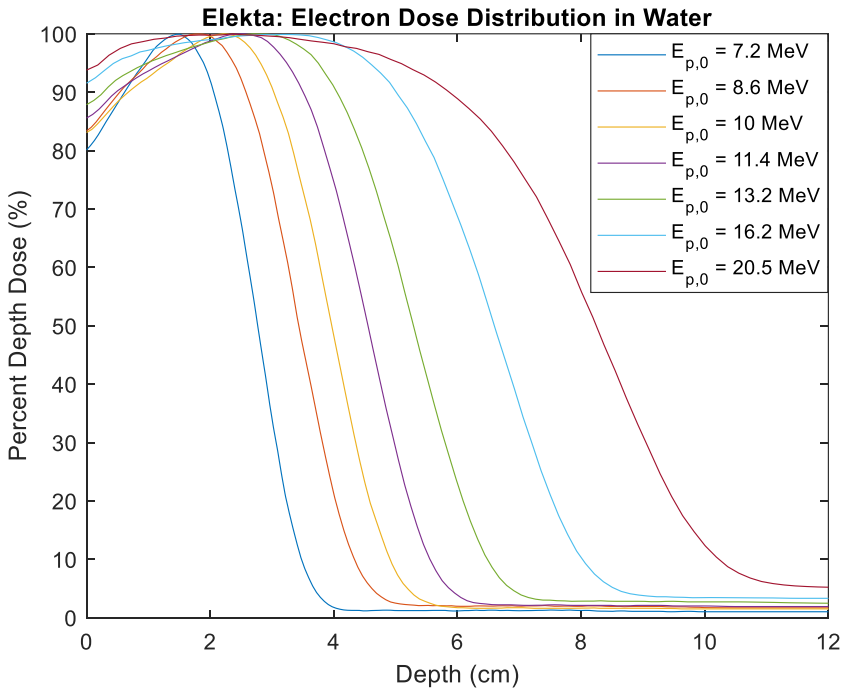

Figure 1.3 Percent depth dose curves for clinically available Elekta energies at Mary Bird Perkins Cancer Center (MBPCC). Note that higher energy beams that are more penetrative have a greater dose falloff region (R_{90-10}).

1.1.3. Scanned Electron Beams

Historically, two methods have been used for broadening and flattening therapeutic electron beams: dual scattering foil and scanned beams. Dual scattered electron beams use a thin high-Z metal foil (placed 90-100 cm upstream of isocenter) to broaden the beam and a Gaussian-shaped metal foil, typically aluminum (placed 5-20 cm downstream of primary foil) to flatten the resulting forward peaked beam.[29, 30] Scanned electron beams use two scanning dipole magnets to scan the electron beam in orthogonal directions to spread and flatten the beam. The scanning patterns can

be row by row, spiraled, or quasi random.[31] Because scanned beams do not have the thick primary scattering foil, there is less bremsstrahlung production and energy straggling in the treatment head, reducing $R_{90\text{-}10}$.

Hence, scanned beams can offer superior dose distributions compared to scattered beams, which can have clinical advantages. This is illustrated in Figure 1.4, which compares a scattered and a scanned beam, each having an R_{90} of 5.0 cm. Note the difference in the dose falloff region: the scanned beam having a lower $R_{90\text{-}10}$, reduced R_p (corresponding reduced beam energy, $E_{p,0}$), and reduced D_γ.

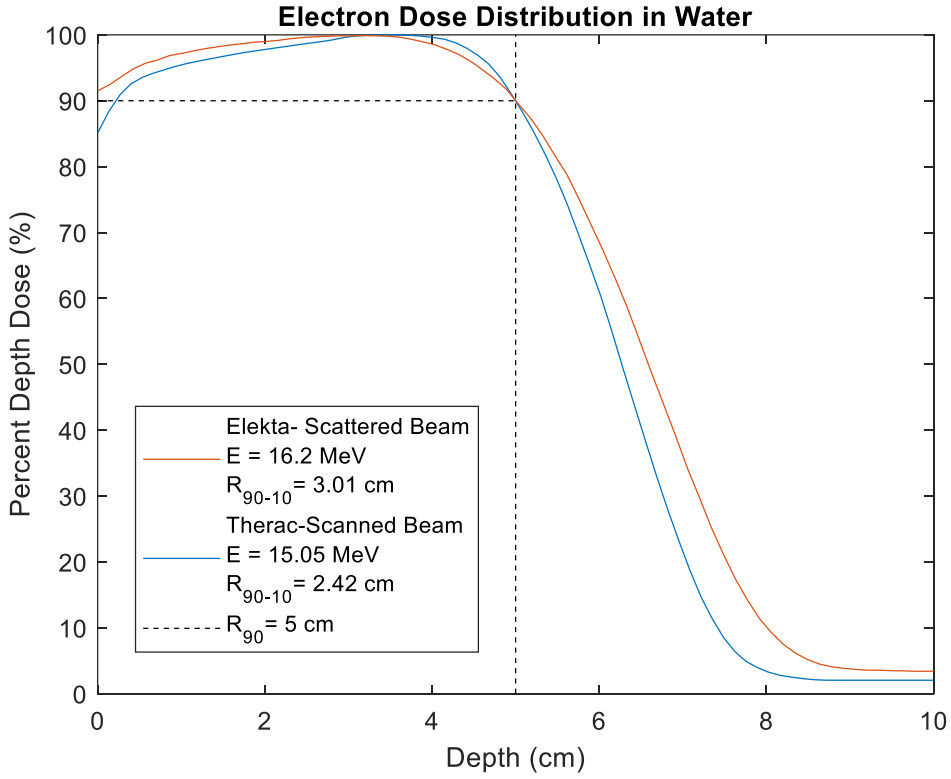

Figure 1.4. Percent depth dose curve for both a scanned (Therac 20) and scattered (Elekta) electron beam with R_{90} of 5.0 cm. The $R_{90\text{-}10}$ of the scanned beam is 2.42 cm, versus 3.01 cm for the scattered beam, which corresponds to 0.59 cm of additional normal tissue sparing.

These effects are illustrated in Figure 1.5, which compares plots of R_{90} vs $E_{p,0}$ and $R_{90\text{-}10}$ vs $E_{p,0}$ for scattered and scanned beams. The increased benefit of scanned beams can be better

appreciated by combining the data of Figure 1.5 into a plot of R_{90-10} versus R_{90} for scattered and scanned beams, shown in Figure 1.6. For example, an R_{90} of 5.0 cm requires a 16.2 MeV scattered beam versus a 15.05 MeV scanned beam (demarcated in Figure 1.5), which results in a decreased R_{90-10} (3.0 cm versus 2.4 cm), decreased R_p (7.9 cm vs 7.4 cm), and decreased D_γ. Thus, a lower energy scanned beam can be used to treat the same target as a scattered beam, while providing additional healthy tissue sparing. Unfortunately, due to specific cases of overdose due to scanning failures, scanning beam electron therapy machines were phased out in the 1990s, and currently scattered electron beams are almost exclusively used clinically.[32]

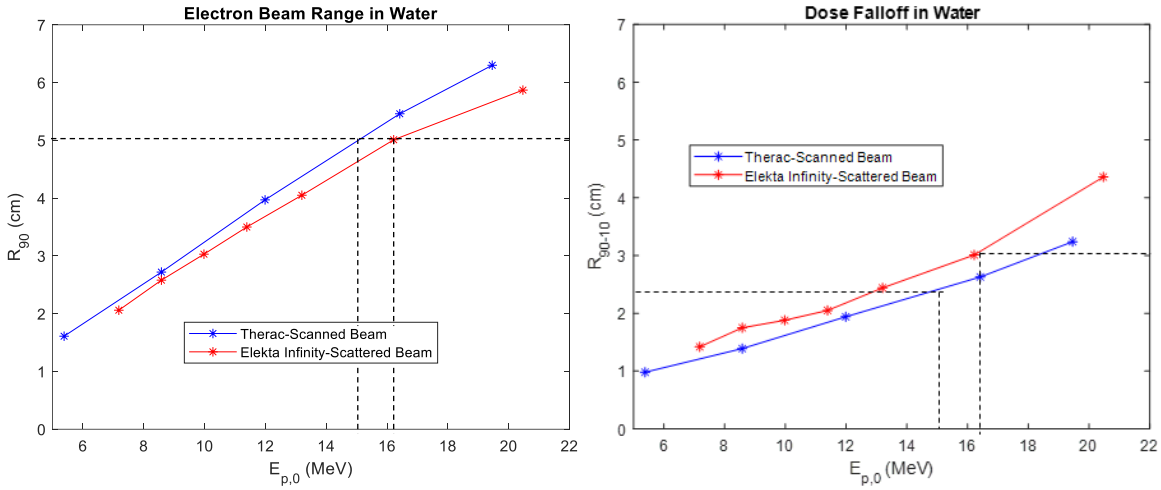

Figure 1.5. R_{90} and R_{90-10} as a function of energy for both scanned and scattered beams in water. The scanned electron beam has a greater R_{90} for each energy compared to the scattered beam and has a lower R_{90-10} for each energy compared to the scattered beam. Points demarcate discrete energies on selected Therac 20 and Elekta machines, and solid lines are guides for the eye. The dashed lines indicate $E_{p,0}$ of beams having R_{90} of 5.0 cm.

1.1.4. Continuous Beam Energy

Another impact on the distal dose falloff is the spacing between discrete electron beam energies for both scattered and scanned electron beam radiotherapy machines. This is illustrated in Figure 1.6, where electron beam energies are indicated by the points, showing that energies are spaced at approximately 0.5 to 1.0 cm R_{90} intervals in water, which corresponds to approximately

1.5 to 4.0 MeV intervals in $E_{p,0}$. The impact of this is illustrated in Figure 1.7, which compares scattered beam %DD curves of a beam with an R_{90} of 5.2 cm with one having an R_{90} value of 5.9 cm with 0.7 cm of bolus. In such a case, the $R_{90\text{-}10}$ is 3.4 cm vs. 4.3 cm, illustrating the downside of having to use a higher energy with bolus when continuous energies are not available.

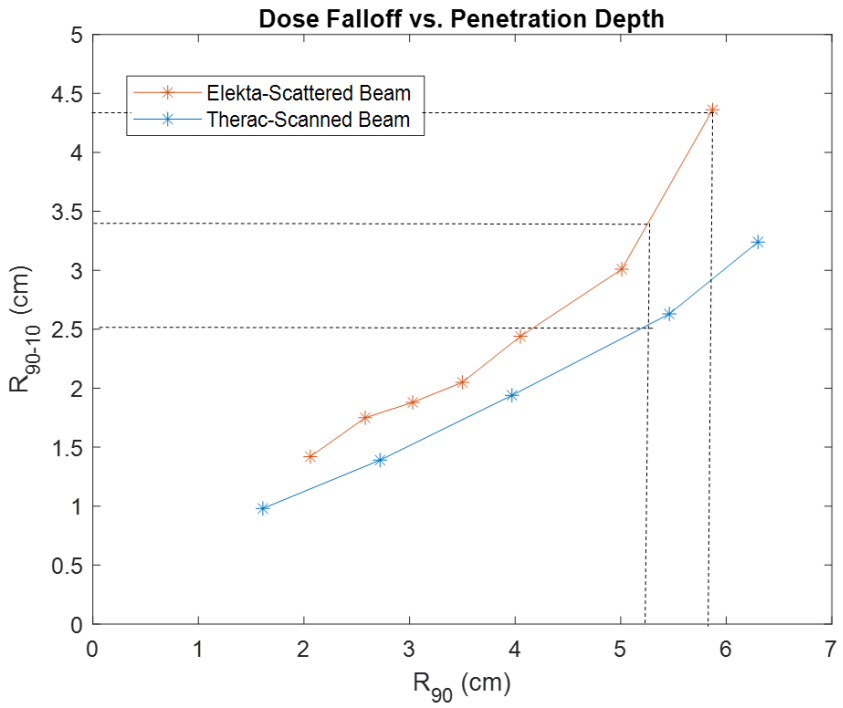

Figure 1.6. $R_{90\text{-}10}$ as a function of R_{90} for both scanned and scattered beams in water. The scanned beam has a lower $R_{90\text{-}10}$ for each R_{90} than the scattered beam, so that there is less dose falloff for treating the same depth. Points demarcate discrete energies on selected Therac 20 and Elekta machines. Solid lines are guides for the eye, and the dashed lines indicate scattered beams with R_{90}=5.9 cm + 0.7 cm bolus and R_{90}=5.2 cm and a scanned beam with R_{90}=5.2 cm.

In addition to continuous energy beams, if scanned beams were available, $R_{90\text{-}10}$ would be further reduced to 2.5 cm. Hence, compared to the scattered, discrete energy beam, the scanned continuous energy beam reduces $R_{90\text{-}10}$ by almost 2 cm (from 4.3 to 2.5 cm). This advantage is further illustrated by comparing the corresponding depth dose curves in Figure 1.7, which first simulates the water-equivalent heart lying 0.5 cm distal to the 5.2 cm deep PTV, and second it simulates the 0.25 density lung lying 1.0 cm distal to the 5.2 cm deep PTV.

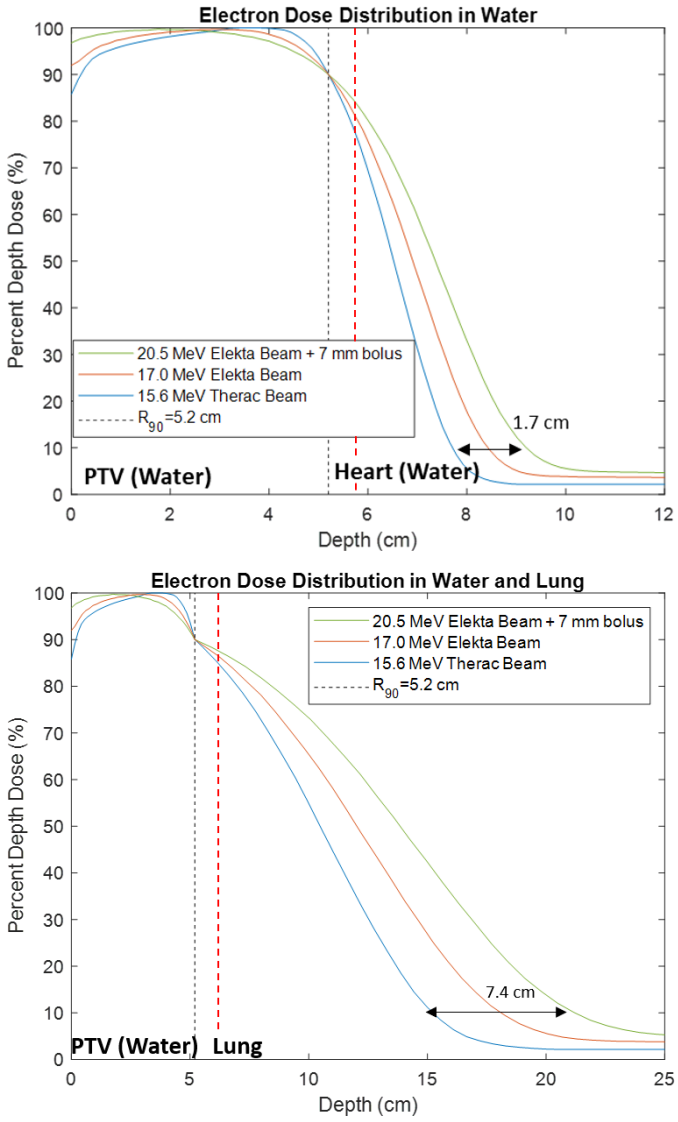

Figure 1.7. Comparison of percent depth doses curves for continuous versus discrete spacing for two scattered Elekta beams and for scanned, continuous energy Therac beam. Percent depth dose curves for the scattered electron beams have an $E_{p,0}$=17 MeV and $E_{p,0}$=20.5 MeV+0.7 cm bolus (both corresponding to R_{90}=5.2 cm). Percent depth dose curves for the scanned beam have an $E_{p,0}$=15.6 MeV (corresponding to R_{90}=5.2 cm). Shown for heart lying distal to the PTV (top) and lung lying distal to PTV (bottom). The red dashed lines indicate the starting depth for which the DVHs in Figure 1.8 are generated.

These effects of using scanned, continuous energy beams over scattered, continuous energy beams over currently available scattered, discrete energy beams are demonstrated in DVHs for a simulated patient geometry, as shown in Figure 1.8. These DVHs are generated from the percent depth dose curves shown in Figure 1.7.

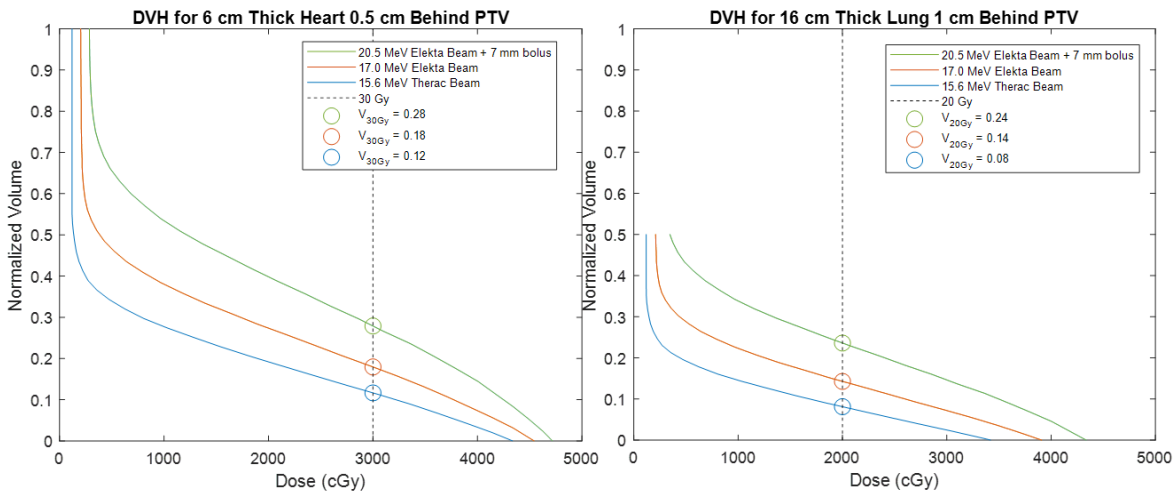

Figure 1.8. Simulated DVHs for a generic patient, shown for the heart (left) and lung (right). All three beams shown are used to treat a target that is 5.2 cm thick. Using percent depth dose curves in Figure 1.7, the heart V_{30Gy} is reduced from 28% to 18% to 12%, and the lung V_{20Gy} is reduced from 24% to 14% to 8%, when using scattered, discrete energy beams (green line)scanned, continuous energy beams (blue line) versus scanned, continuous energy beams (blue line), respectively.

While these discretely spaced electron energies can effectively treat patients, they can introduce greater dose to normal tissue than an ideal treatment. The ability to select the optimal beam energy from a set of continuously variable electron energies and/or use scanned beams versus scattered beams could provide the ability to improve patient treatments by delivering less dose to normal tissues than using currently available electron beams. To further investigate this concept, we believe it appropriate to utilize the most technically advanced method for electron planning and delivery currently available, intensity modulated bolus electron conformal therapy (IM-BECT).[33, 34]

1.1.5. Intensity Modulated-Bolus Electron Conformal Therapy (IM-BECT)

Electron conformal therapy (ECT) is the use of one or more electron beams to contain the PTV to the 90% dose surface, achieve as homogenous dose distribution as possible or a prescribed heterogeneous dose distribution to the PTV, and deliver minimal dose to underlying critical

structures and normal tissues.[35] Bolus ECT (BECT) has been shown clinically useful for posterior chest wall,[25, 36] PMRT,[21, 25, 26] head and neck,[33, 37] and extremities.[36] Currently, BECT planning and delivery technology is commercially available from .decimal LLC (Sanford, FL) and from Adaptiiv (Halifax, NS, Canada), which are based on the original work of Low et al.[38] and a later, similar work by Su et al,[36] respectively. These technologies use a bolus (tissue equivalent range compensator) that shapes the distal side of the dose distribution (e.g. 90% dose surface) to the PTV. The bolus can be milled machinable wax[39] or 3D printed polyethylene terephthalate glycol-modified (PETG) or polylactic acid (PLA).[36, 40] The bolus is patient-specific, and its distal surface conforms to the patient surface. However, bolus electron conformal therapy (BECT) can produce increased dose heterogeneity in the PTV due to the irregular proximal surface of the bolus creating lateral side scatter disequilibrium.

Kudchadker et al. showed that intensity modulation used in conjunction with BECT can significantly improve dose homogeneity in the PTV.[33] In this case, the bolus provides a high level of dose conformation to the PTV, and the intensity modulation improves dose homogeneity, reducing hot and cold spots.

Recently, a new technology for passive electron intensity modulation has been developed and studied.[34, 41–43] For intensities 50% or greater of the incident beam, modulation is achieved using tungsten island blocks of varying diameters placed on a hexagonal grid and embedded in low density, machinable foam within the patient collimating aperture. The block diameters are selected to modulate electron fluence, analogous to metal compensators used in intensity modulated x-ray therapy.[34] Intensity modulation is useful for delivering a highly conformal and homogenous (or prescribed heterogeneous) dose distribution.

A later study by Kudchadker et al. showed the improvement in dose distribution as well as the reduction of hot and cold spots when using IM-BECT over BECT for the post-mastectomy chest wall.[33] These results are shown in Figure 1.9.

1.2. Motivation for Research

Opp et al. compared bolus electron conformal therapy with conventional techniques for the treatment of left-side chest-wall post-mastectomy patients.[21] That study completed treatment plans for twenty-five patients comparing opposed tangents with wedges, opposed tangents with field-in-field modulation, 8-field IMRT, and BECT. Results showed that IMRT and BECT provided the lowest heart $V_{25\,Gy}$ doses, and BECT had the lowest mean heart dose. Field-in-field provided the lowest mean total lung dose and IMRT provided the lowest total lung $V_{20\,Gy}$. In some cases, BECT could not provide adequate coverage, and IMRT showed better dose homogeneity. When using IMRT, the contralateral breast and lung receive slightly higher doses compared to other techniques. Patient anatomy determines whether BECT is suitable, and patients with a maximal target depth of <5.7 cm could be treated with BECT. If the maximal depth of the target is >5.7 cm, IMRT provides better dose homogeneity and normal tissue sparing.[21]

Previous work has shown that using IM-BECT over the heart and opposed IMXT elsewhere for PMRT has statistically significant advantages over using conventional techniques such as VMAT in some patients.[43] Delivering IM-BECT treatments to the chest wall with scanned beams and continuously spaced energies should further reduce the dose to the heart and lung in PMRT.

In the present study, only the chest wall portion of the PTV treated in PMRT, which can be treated with IM-BECT, will be studied, i.e. the supraclavicular PTV, normally requiring x-ray radiotherapy will be ignored. The chest wall treatment will be planned using one field, or if needed, two abutted fields, the lower “heart field” and upper “lung field.” The heart field will be treated with a lower energy, and the lung field will be treated with a higher energy. The objective of this

study is to verify and quantify the benefits of using scanned electron beams and/or continuously spaced electron beam energies for chest wall PMRT.

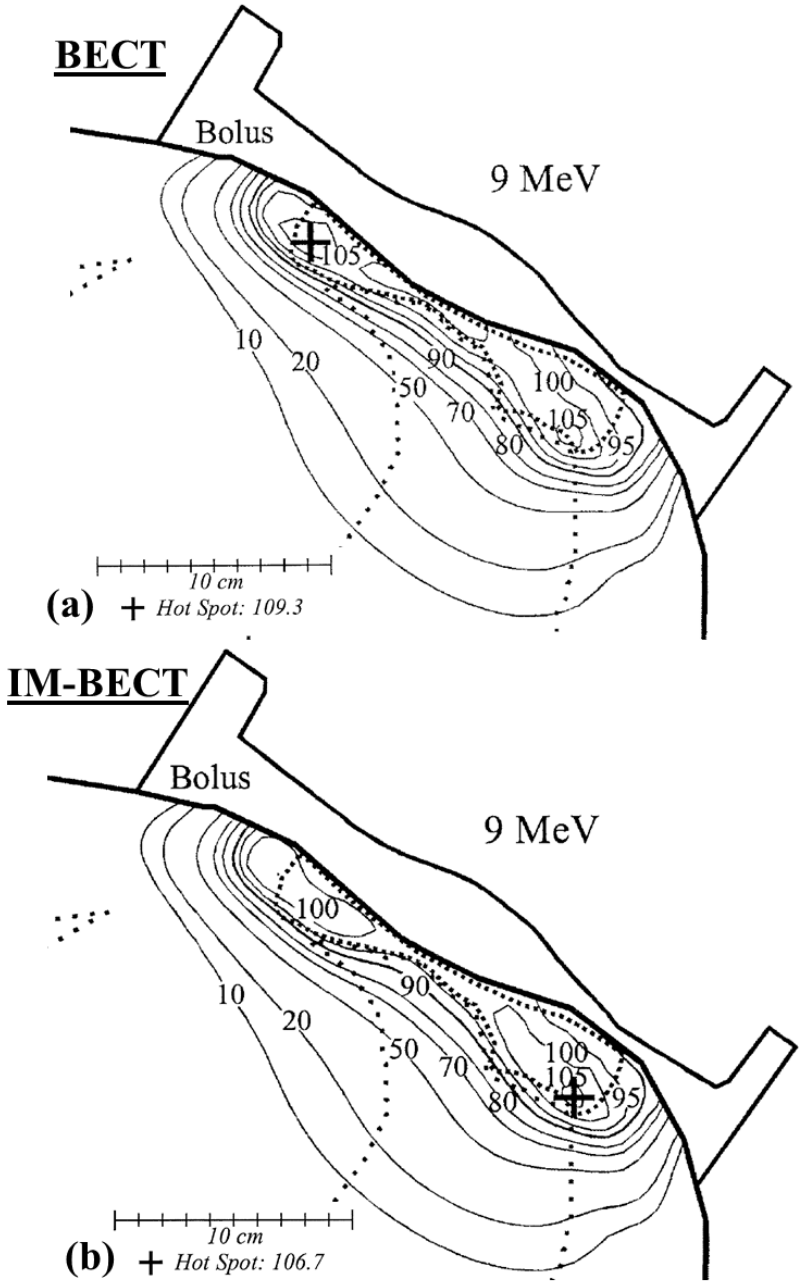

Figure 1.9. Dose distributions comparing BECT and IM-BECT for post-mastectomy chest wall.[33] The PTV is marked with the dashed line in the transverse plane shown. (a) BECT resulting in a hot spot of 109.3% and (b) IM-BECT resulting in a reduced hot spot of 106.7%.

1.3. Hypothesis and Specific Aims

1.3.1. Hypothesis

For seven post-mastectomy radiotherapy left-side chest wall patients previously treated with volumetric modulated arc therapy (VMAT), treatment plans using intensity modulated bolus electron conformal therapy (IM-BECT) with a scanned electron beam and/or the capability of continuous energy spacing can be superior (increased sparing of heart and lung and reduced chance of secondary cancer) to plans made using IM-BECT with a passively scattered electron beam and discrete Elekta energy spacing.

1.3.2. Specific Aims

Aim 1, Generate Treatment Plans Assuming Different Electron Beam Technology: Generate IM-BECT treatment plans for seven post-mastectomy radiotherapy (PMRT), left-side chest wall patients previously treated with volumetric modulated arc therapy (VMAT) using a range of applicable energies from 13 to 20 MeV. Treatment plans will be generated for combinations of scanned or passively scattered electron beams and discrete or continuous electron energy beams. Plans will be developed for the entire chest wall PTV, which had been contoured in accordance with RTOG breast cancer atlas guidelines while maintaining healthy tissue dose limits. Compute 3D dose distributions and DVHs for each plan.

Aim 2, Physical and Biological Dose Metrics for Plans: Compute physical dose metrics and resulting biological metrics for each of the plans for each of the seven patients. Physical dose metrics include (1) PTV: D_{max}(maximum dose), D_{mean} (mean dose), $D_{97\%}$ (Dose given to 97% of PTV volume) and $V_{47.5\ Gy}$ (relative volume of PTV receiving 47.5 Gy, or 95% of the prescribed dose of 50 Gy), (2) Heart: D_{min}, D_{max}, D_{mean}, $V_{22.5\ Gy}$ (relative volume of heart receiving 22.5 Gy), and $V_{30\ Gy}$ (relative volume of heart receiving 30 Gy), and (3) Lung: D_{min}, D_{max}, D_{mean}, and $V_{20\ Gy}$ (relative volume of lung receiving 20 Gy). Biological dose metrics include (1) Heart: NTCP

(normal tissue complication probability) and (2) Lung: NTCP, $SCCP_{lin}$ (secondary cancer complication probability, linear model), and $SCCP_{lin\text{-}exp}$ (secondary cancer complication probability, linear-exponential model).

Aim 3, Analyze and Compare Plans using Metrics: Analyze the seven different sets of patient plans and determine the patient indications for using continuously spaced electron energies and scanned electron beams. Determine the differences in patient geometry and beam conditions that affect the utility of scanned versus scattered beams and continuous versus discrete energy spacing (Comparisons made in this aim are presented in the discussion section).

Chapter 2. Methods and Materials

2.1. Aim 1—Generating Treatment Plans Assuming Different Electron Beam Technology

The goal of Aim 1 is to develop IM-BECT plans for seven post-mastectomy radiotherapy left-side chest wall patients previously treated with volumetric modulated arc therapy (VMAT).[17] For each plan, this involves the following steps:

1. Create initial electron plan.
    a. Beam Angle Selection
    b. PTV Segmentation
    c. Field Construction
    d. Energy Selection
2. Improve beam penumbra matching using edge feathering.
3. Design electron bolus for each field.
4. Compute dose distributions for each field.
5. Sum for the composite chest wall dose distribution.

Steps 1 and 2 were completed using Pinnacle v9.10 (Philips Radiation Oncology Systems, Fitchburg, WI) treatment planning system and MATLAB code developed for this project. Steps 3 and 4 were completed using a research version of p.d (.decimal LLC, Samford, FL). MIM (MIM Software Inc., Cleveland, OH) was used to assist in transferring files between platforms, completing step 5, and evaluating plan quality.

For all plans, the prescription was 50 Gy to the 90% isodose line (100%, or 55.6 Gy, is the given dose for each field) in 25 fractions. However, to compare plans for the same patient, dose distributions were rescaled, so all plans delivered an identical dose to 50% of the PTV, based on the dose given to 50% of the PTV for Plan 1, defined later.

2.1.1. Patient Selection

Seven left-side post-mastectomy chest wall patients were selected, each of whom fulfilled the following criteria:

1. Received prior treatment with VMAT at the Mary Bird Perkins Cancer Center
2. Part of a HIPAA compiled data set
3. Subjects of previous retrospective treatment planning study by Heins[8] (2016) and Doiron[41] (2018).

Each anonymized patient data set included previously defined contours (PTVs, normal structures, and skin surface) and CT images acquired on a 120 kVp large bore GE Lightspeed 16 CT scanner (General Electric Medical Systems). Transverse CT planes were acquired every 0.25 cm. The chest wall PTV and organs at risk, i.e. lung and heart, were previously contoured by the treating radiation oncologist. The patients and their corresponding data sets are referred to as CW1 through CW9 (CW5 and CW9 were not included in this study due to software issues in our research version of p.d), matching the designations in Heins and Doiron.[8, 41]

For planning purposes, the patient data was divided into two subsets, Patient Set 1 (CW1, CW3, CW6) and Patient Set 2 (CW2, CW4, CW7, CW8). Patient Set 1 was planned using a single field (single energy); Patient Set 2 was planned using two abutting fields (having different beam energies).

2.1.2. Field Specifications for Patient Set 1

For three patients (CW1, CW3, and CW6), further referred to as Patient Set 1, one electron field (energy) was sufficient to cover the entire PTV. In these cases, the deepest part of the PTV superficial to the heart is as deep or deeper than the portion of the PTV superior to the heart. Hence, only one PTV and one beam energy were necessary. The superior and inferior margins were set as 2 cm, and the two lateral margins are set as 1.5 cm. Only four plans, Plan 1, Plan 3, Plan 4, and

Plan 5, were created for these patients (CW1, CW3, and CW6), corresponding to the plan designations described for Patient Set 2. A schematic of the fields and PTVs for each plan is shown in Figure 2.1.

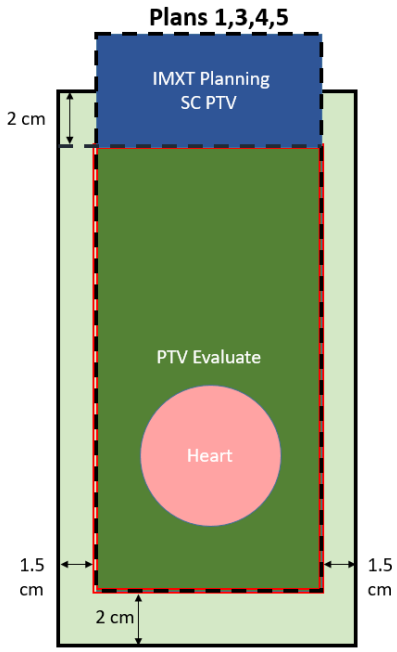

Figure 2.1. Schematic of PTVs and fields for Patient Set 1. For these patients, the superior border of the CW PTV (PTV Evaluate) is at the inferior border of the supraclavicular PTV (SC PTV).

2.1.3. Field Specifications for Patient Set 2

For four of the seven patients (CW2, CW4, CW7, and CW8), further referred to as Patient Set 2, the chest wall PTV was divided into two separate PTVs: the inferior (lower) PTV which is anterior to the heart and the inferior portion of the left lung, and the superior (upper) PTV which is anterior to lung, extending from the superior border of the inferior field to just inferior to the PTV for the supraclavicular nodes. The supraclavicular nodes were assumed to have been planned with x-rays which contribute insignificant dose to lung, hence not included in this study. The superior border of the PTV was located at the caudal aspect of the clavicular head. The lower PTV was shallower and treated with a lower energy electron beam, while the upper PTV was deeper and treated with a higher energy electron beam. This allowed dose to the heart to be minimized.

For these patients, the planned treatment used two abutted fields, each having different energies and irradiating separately the previously defined PTVs. Five plans were created for each patient; Plans 1,2, and 4 had the same PTVs (fields), illustrated in Figure 2.2, while Plans 3 and 5 had the same PTVs (fields), illustrated in Figure 2.3.

For Plans 1, 2, and 4 (Figure 2.2) the lower PTV extended from the inferior extent of the PTV to the farthest extent superior to the heart that could be treated using the lowest energy from the set of available discrete energies sufficient to treat the PTV anterior to the heart. For planning purposes, a 2 cm junction PTV was placed between the lower and upper PTVs. The upper PTV extended from the superior extent of the junction PTV to the supraclavicular PTV, which has an inferior border at the caudal aspect of the clavicular head. The lower PTV, junction PTV, and upper PTV together comprised the chest wall PTV used to evaluate plan quality, also referred to as the PTV Evaluate. The lower PTV was treated with the lower field, which had a 1.5 cm lateral expansion, a 2.0 cm inferior expansion, and a 1 cm superior expansion of the lower PTV. The upper PTV was treated with the upper field, which had a 1.5 cm lateral expansion, a 1 cm inferior expansion, and a 2.0 cm superior expansion of the upper PTV.

For Plans 3 and 5 (Figure 2.3), the lower PTV extended from the inferior extent of the PTV to the superior extent of the heart. The selected energy is the lowest from a set of available continuous energies sufficient to treat the PTV superficial to the heart. For planning purposes, a 2 cm junction was placed between the lower and upper PTVs. The upper PTV extended from the superior extent of the junction PTV (PTV Evaluate) to the supraclavicular region, which has an inferior border at the caudal aspect of the clavicular head. The lower PTV, junction, and upper PTV together comprised the PTV used to evaluate plan quality, also referred to as the Chest Wall PTV. The lower PTV was treated with the lower field, which had a 1.5 cm lateral expansion, a 2.0

cm inferior expansion, and a 1 cm superior expansion of the lower PTV. The upper PTV was treated with the upper field, which had a 1.5 cm lateral expansion, a 1 cm inferior expansion, and a 2.0 cm superior expansion of the upper PTV.

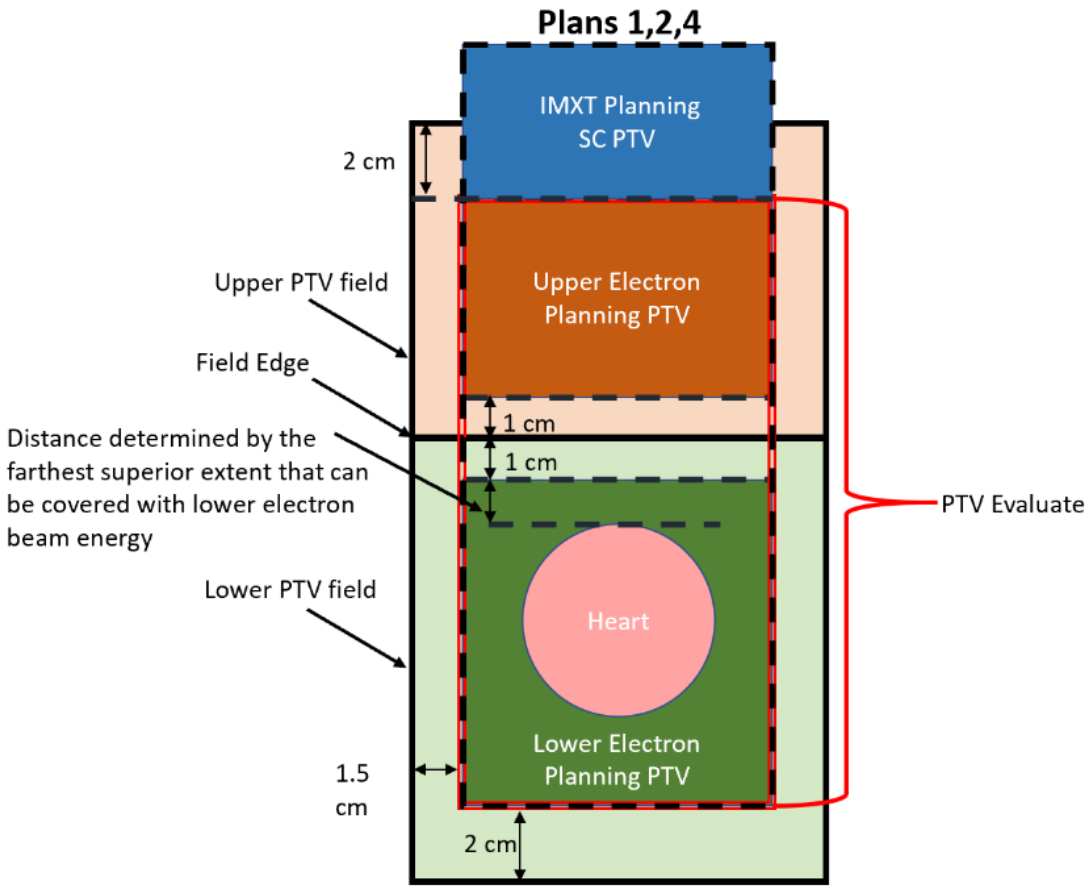

Figure 2.2. Schematic of the PTVs and fields for Plans 1,2, and 4 for each patient. For these plans the superior border of the lower PTV is at the farthest superior extent that can be covered with the lower energy beam. The chest wall PTV (PTV Evaluate) is comprised of the upper PTV (orange region outlined by dashed lines), the lower PTV (green region outlined by dashed lines), and the intervening junction PTV (outlined by dashed lines). Lower field is light green region outlined by solid black line; upper field is light orange region outlined by solid black line.

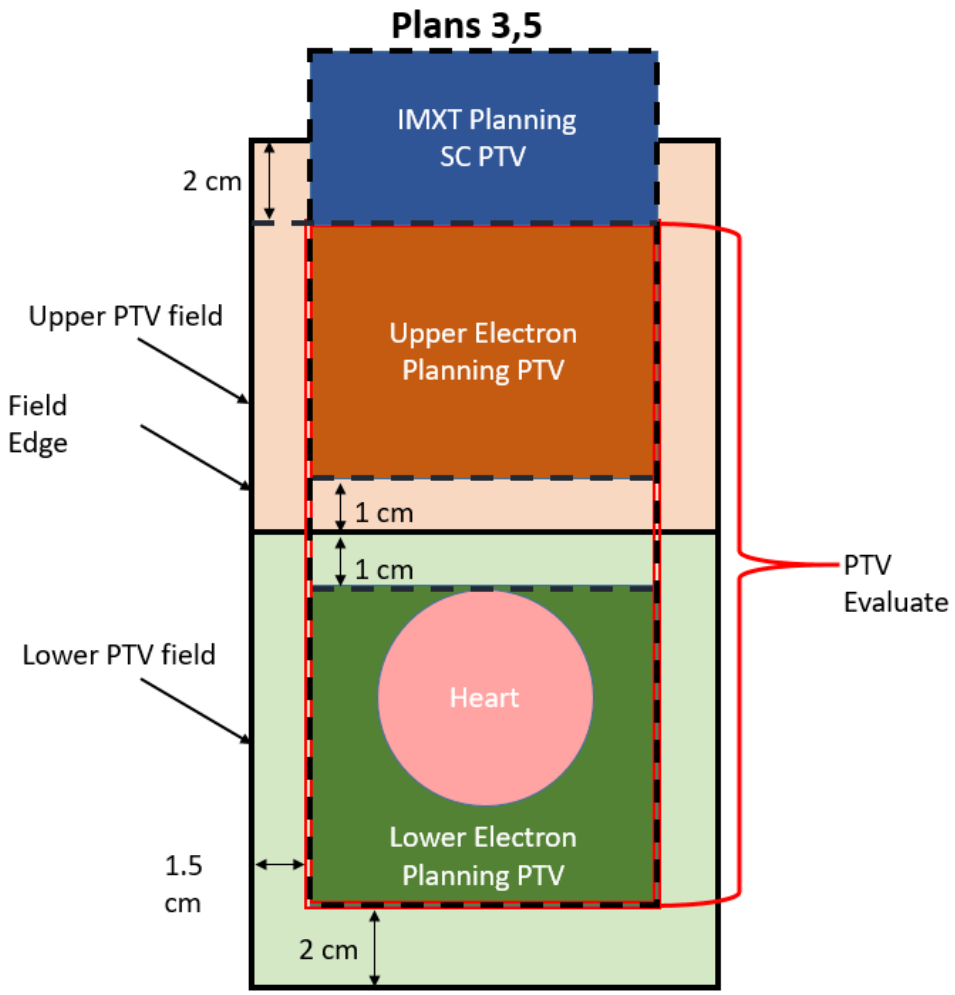

Figure 2.3. Schematic of PTVs and fields for Plans 3 and 5 for each patient in Patient Set 2. For these plans the superior border of the lower PTV is at the superior edge of the heart. Assuming availability of beams with continuous energy, Plans 3 and 5 beams are flattened using dual scattering foils and scanned beams, respectively. The chest wall PTV (PTV Evaluate) is comprised of the upper PTV (orange region outlined by dashed lines), the lower PTV (green region outlined by dashed lines), and the intervening junction PTV (outlined by dashed lines). Lower field is light green region outlined by solid black line; upper field is light orange region outlined by solid black line.

2.1.4. Electron beam arrangements for Patient Set 1

For Patient Set 1 an SSD of 105 cm was used, and the gantry angle was selected so the beam central axis was approximately perpendicular to the distal PTV surface, typical of BECT plans, which resulted in a left, anterior, oblique field. The beam parameters (i.e. gantry angles,

SSD, and field shape) were determined in Pinnacle[3] and exported to p.d for use during bolus design.

2.1.5. Electron beam arrangements for Patient Set 2

For Patient Set 2, each plan consisted of three beams, one lower energy beam that covered the lower field, and two higher energy beams covered the upper field. The two upper fields were identical except for their lower edges, which were feathered so that their composite penumbra closely matched that of the lower field, maximizing dose homogeneity in the abutment region. All three beams shared a common isocenter and a common virtual source, i.e. common beam central axis. Each beam had a source-to-surface distance (SSD) of 105 cm along the common central axis, typically used to prevent collisions between the electron applicator and electron bolus. As was the case for Patient Set 1, the gantry angle was selected so that the beam central axis was approximately perpendicular to the distal PTV surface, typical of BECT treatment plans. The beam parameters (i.e. gantry angles, SSD, and field shape) were determined in Pinnacle[3] and exported to p.d for use during bolus design.

2.1.5.1. Upper field edge feathering for dose homogeneity at abutment of high and low energy fields

Perfect penumbra matching between the upper and lower fields was impossible due to the different beam energies, as well as patient surface irregularities. To mitigate hot and cold spots, edge feathering of the upper (higher) energy beams was used. Figure 2.4 illustrates the need for edge feathering by using CW2 fields in water as an example, and Figure 2.5 illustrates how edge feathering was implemented in this study to improve dose homogeneity in the abutting region. Two identical copies of the upper field were created, then the inferior borders of the fields were shifted +/- Δ, where Δ depended on six factors: beam energy, PTV depth (z), and distance between the collimator and bolus surface (L_0) for the lower and upper fields. These factors are illustrated

in Figure 2.6. The parameters used to determine Δ for patient plans in Patient Set 2 are shown in Table 2.1.

The optimal edge feathering parameter, Δ, was determined by matching the penumbra of the lower and upper fields. This was done by minimizing the square of the residuals between the relative intensity functions for the lower field, $f(x)$, and for the upper field, $(g_{+\Delta}(x) + g_{-\Delta}(x))/2$, where f and g were found by following:

$$f(x) = \frac{1}{2}\left[\mathrm{erf}\left(\frac{\frac{w_0}{2}-x}{\sqrt{2}\sigma_x}\right) + \mathrm{erf}\left(\frac{\frac{w_0}{2}+x}{\sqrt{2}\sigma_x}\right)\right]$$

$$g_{\pm\Delta}(x) = \frac{1}{2}\left[\mathrm{erf}\left(\frac{\frac{w_0\pm\Delta}{2}-x}{\sqrt{2}\sigma_x}\right) + \mathrm{erf}\left(\frac{\frac{w_0\pm\Delta}{2}+x}{\sqrt{2}\sigma_x}\right)\right].$$

Here, x is the distance from the center of the upper field to the edge of the abutting edge. w_0 and σ_x are patient dependent, depending on the energy and geometry of each of the abutted fields, illustrated in Figure 2.6. The latter is given by

$$\sigma_x^2 = (z + L_0)^2\sigma_{\theta_x}^2 + a_2(z)$$

z is the distance from the bolus surface to a depth equal to half the chest wall PTV thickness below the skin surface at the abutment location, L_0 is the distance from the bottom edge of the electron cutout/applicator to the bolus surface, and $a_2(z)$ is the RMS spread of the lateral distribution of electron beams incident on the bolus at depth (z) equal to the distance from the bolus surface to half the chest wall PTV thickness in the patient. $a_2(z)$ was determined using the formalism of Werner et al.[44] The optimization of Δ was determined using the L2 norm in a MATLAB program developed for this study.

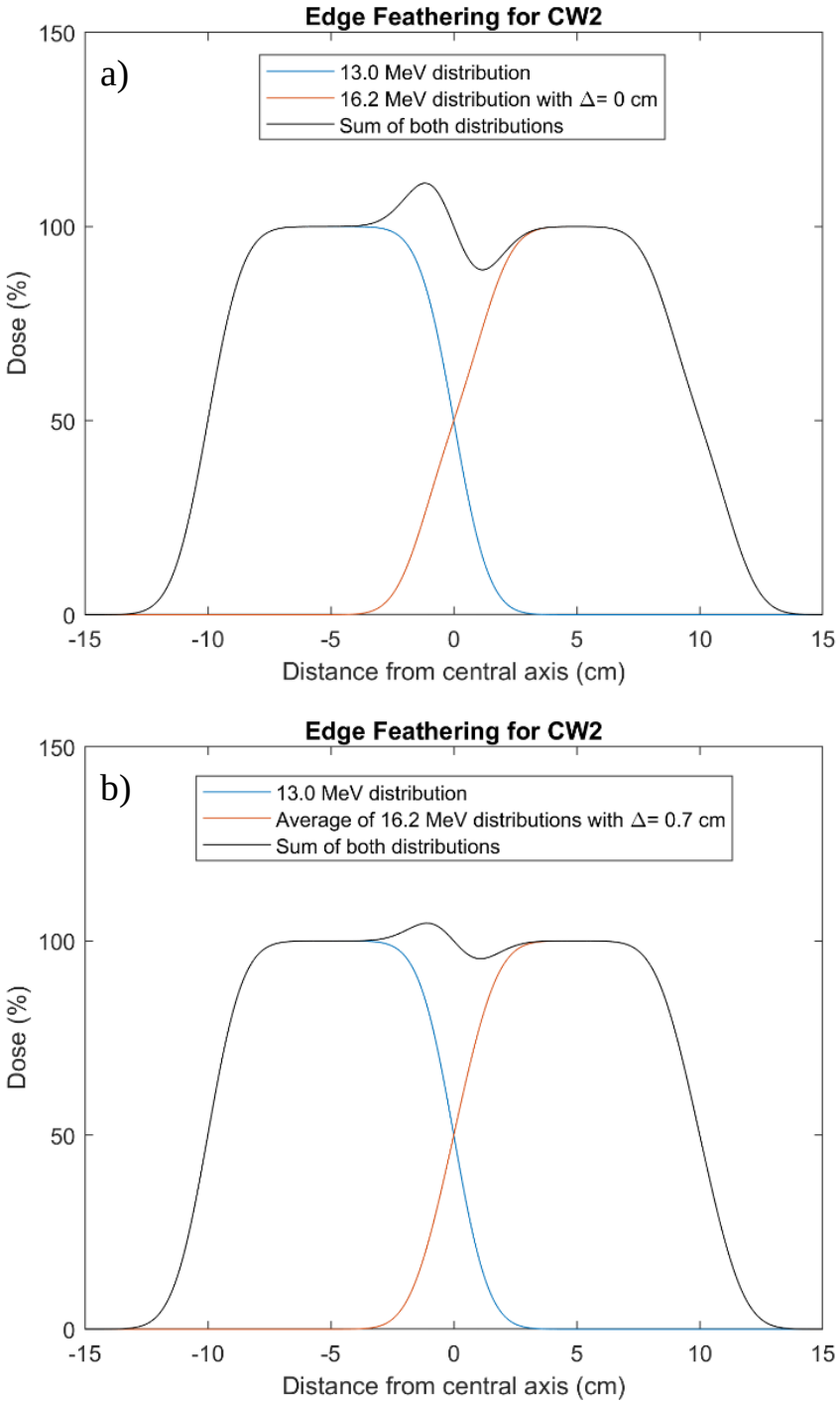

Figure 2.4. Off-axis dose distributions for two abutting fields are shown for CW2. (a) Without feathering, there is a +/- 11% dose heterogeneity. (b) When feathering the lower border of the upper field, the dose heterogeneity has been reduced to +/- 4%. See Table 2.1 for values of six parameters.

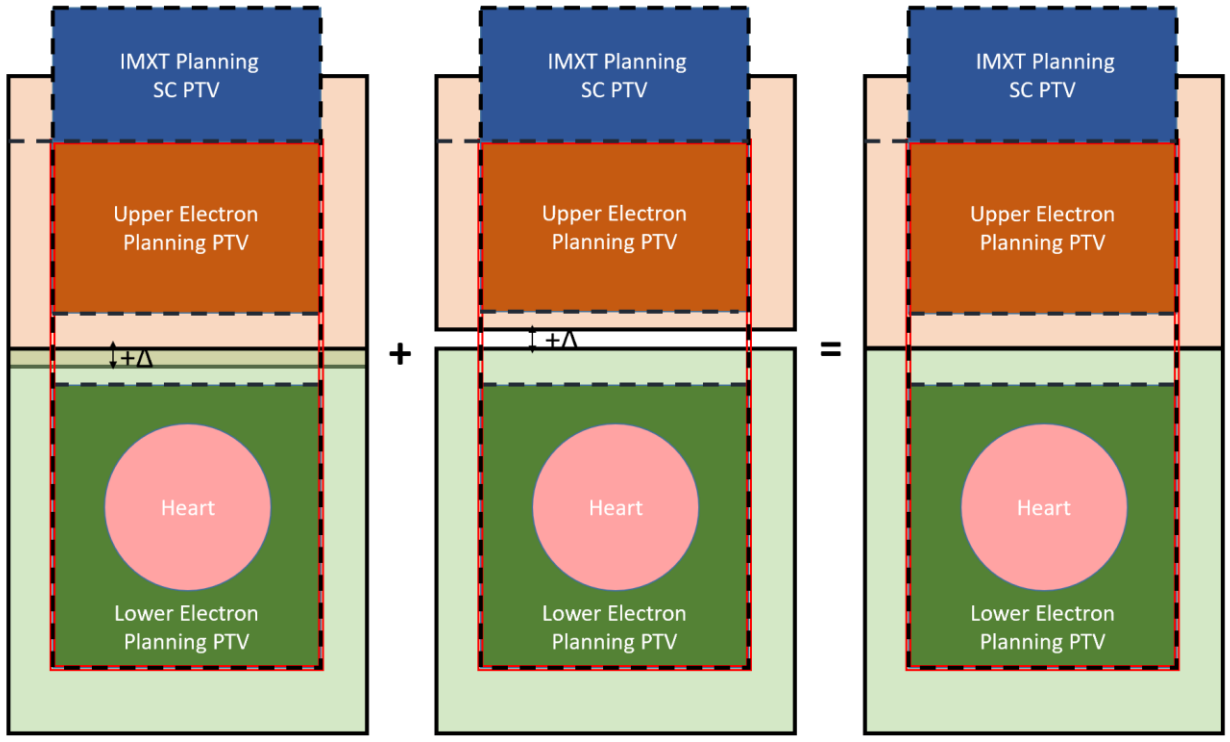

Figure 2.5. Beam's eye view illustrating feathering lower edge of the upper field (±Δ) abutted to lower field.

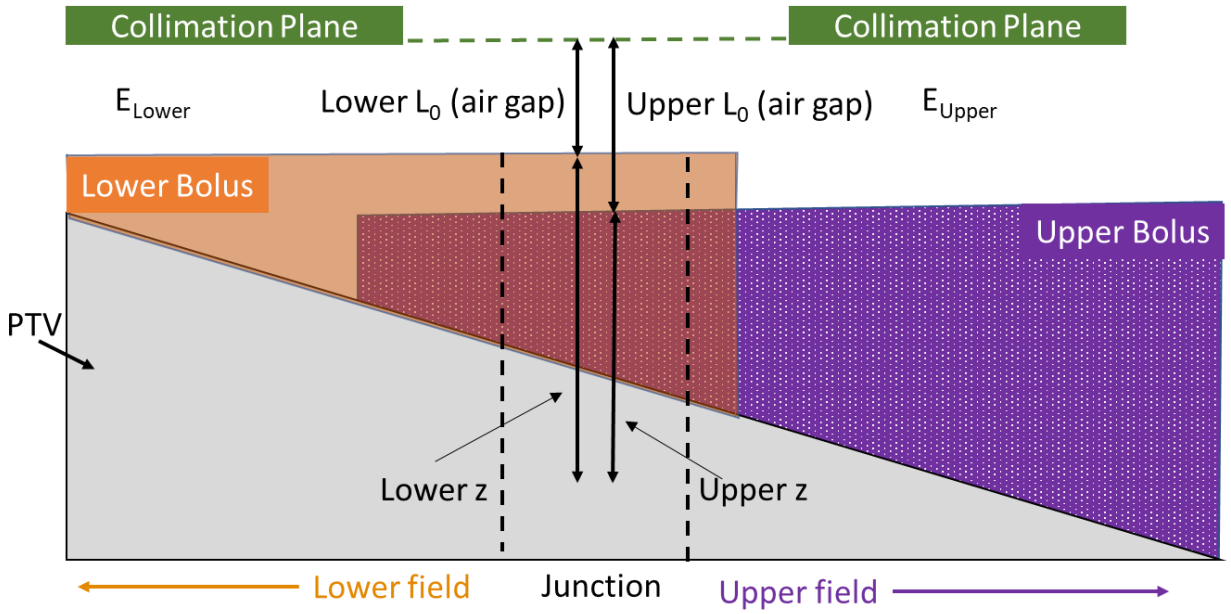

Figure 2.6. Side view illustrating six parameters that affect Δ when determining feathering of upper field penumbra to match that of lower field.

Table 2.1. Parameters used to calculate Δ for Patient Set 2. All values are shown for Plan 1, which has discrete energy spacing and uses scattered electron beams.

Patient	Lower Energy (MeV)	Lower R_{90} (cm)	Lower L_0 (cm)	Lower z (cm)	Upper Energy (MeV)	Upper R_{90} (cm)	Upper L_0 (cm)	Upper z (cm)	Δ (cm)
CW2	13.0	4.0	6.9	3.6	16.2	5.0	5.9	4.6	0.7
CW4	16.2	5.0	8.0	4.0	21.3	6.0	7.0	5.0	0.8
CW7	16.2	5.0	6.1	4.5	21.3	6.0	5.1	5.5	0.7
CW8	13.0	4.0	7.6	3.2	16.2	5.0	6.6	4.2	0.6

2.1.6. Energy Selection for Different Plans

Table 2.2 lists R_{90} and R_{90-10} values for the energies available on the Elekta Infinity (scattered beams), and Table 2.3 shows the R_{90} and R_{90-10} values for R_{90} values corresponding to the Elekta Infinity for the Therac 20 (scanned beam). These discrete energies were used to create and evaluate treatment plans with discrete energy spacing.

For each patient, either four plans (Pans 1,2,4,5) were created (Patient Set 1) or five plans (Plans1-5) were created (Patient Set 2). Described as follows, the different plans investigated the effects of scattered versus scanned beams as well as the effects of continuous energy spacing.

Table 2.2. Available electron energies on the Elekta Infinity at MBPCC, as well as corresponding R_{90} and R_{90-10} values in water. In the case where the depth of the target falls between two R_{90} values, the higher energy must be used. Continuously spaced electron energies will prevent unnecessary additional dose to distal normal tissue.

Nominal Energy (MeV)	$E_{p,0}$ (MeV)	R_{90} (cm)	R_{90-10} (cm)
7	7.0	2.0	1.4
9	8.4	2.5	1.7
10	9.9	3.0	1.9
11	11.4	3.5	2.1
13	13.0	4.0	2.4
16	16.2	5.0	3.0
20	21.3	6.0	4.4

Table 2.3. Beam parameters of Therac 20 for R_{90} values corresponding to the same R_{90} values as available electron energies on the Elekta Infinity. Also shown are the corresponding $E_{p,0}$ and R_{90-10} values. In the case where the depth of the target falls between two R_{90} values, the higher energy must be used. Continuously spaced electron energies will prevent unnecessary additional dose to distal normal tissue.

Nominal Energy (MeV)	**$E_{p,0}$ (MeV)**	**R_{90} (cm)**	**R_{90-10} (cm)**
7	6.5	2.0	1.1
9	8.9	2.5	1.4
10	9.4	3.0	1.5
11	10.8	3.5	1.8
12	12.1	4.0	2.0
15	15.1	5.0	2.4
18	18.3	6.0	3.0

Plan 1, Scattered, Discrete Energy Beams:

For Plan 1, Patient Set 1, the PTV and field were planned as shown in Figure 2.1. The minimum commercially available energy (from Table 2.2), whose 90% dose surface (R_{90}) could sufficiently cover the entire PTV, was selected.

For Plan 1, Patient Set 2, the PTVs and fields were planned as shown in Figure 2.2. The minimum commercially available Elekta scattered beam energy (see Table 2.2) for each beam, whose 90% dose surface (R_{90}) could sufficiently cover the lower or upper PTVs, was selected.

Plan 2, Scattered, Discrete and Continuous Energy Beams:

For Patient Set 1 no Plan 2 was created, as there was no upper field. For Plan 2, Patient Set 2, the PTVs and fields were created as shown in Figure 2.2. The lower field was planned using the same field as in Plan 1. Different from Plan 1, the upper field was planned with the minimum energy, assuming continuous energy beams, whose 90% dose surface (R_{90}) could sufficiently cover the upper PTV, assuming availability of continuous energy spacing. Both fields were treated with scattered electron beams.

Plan 3, Scattered, Continuous Energy Beams:

For Plan 3, Patient Set 1, the PTV and field were planned as shown in Figure 2.1. The PTV was planned using a single beam with the minimum energy whose 90% dose surface (R_{90}) could sufficiently cover the upper PTV, assuming availability of continuous energy spacing for scattered Elekta beams.

For Plan 3, Patient Set 2, the PTVs and fields were created as shown in Figure 2.3. The lower field was planned using the minimum energy whose 90% dose surface (R_{90}) could sufficiently cover the lower PTV, assuming availability of continuous energy spacing for scattered Elekta beams. The upper field was treated with the lowest energy, whose 90% dose surface (R_{90}) could sufficiently cover the upper PTV, assuming availability of continuous energy spacing for scattered Elekta beams.

Plan 4, Scanned, Discrete Energy Beams:

For Plan 4, Patient Set 1, the PTV and field were planned as shown in Figure 2.1. The PTV was planned using a single beam by selecting the minimum discrete beam energy, whose 90% dose surface (R_{90}) could sufficiently cover the entire PTV. The single scanned beam energy was selected from Therac 20 scanned electron beams energies, assumed to have the same discrete R_{90} values as commercially available Elekta beams (from Table 2.3).

For Plan 4, Patient Set 2, the PTVs and fields were created as shown in Figure 2.2. Assuming Therac 20 scanned electron beams energies, having the same discrete R_{90} values as commercially available Elekta beams (from Table 2.2), a plan was developed the same as done using scattered beams in Plan 1. That is, the minimum energy beams whose 90% dose surface (R_{90}) could sufficiently cover the lower and upper PTVs, were selected.

Plan 5, Scanned, Continuous Energy Beams:

For Plan 5, Patient Set 1, the PTV and field were planned as shown in Figure 2.1. The single field was treated with the lowest energy whose 90% dose surface (R_{90}) could sufficiently cover the PTV, assuming continuous energy spacing and scanned electron beams.

For Plan 5, Patient Set 2, the PTVs and fields were created as shown in Figure 2.3. This plan was developed using the same methods as detailed in Plan 3 with the exception that Therac 20 scanned beams with continuous beam energies rather than Elekta scattered beams with continuous energy were assumed available and used. That is, the lower field was planned with the minimum energy whose 90% dose surface (R_{90}) could sufficiently cover the lower PTV, and the upper field was treated with the minimum energy whose 90% dose surface (R_{90}) could sufficiently cover the upper PTV.

The parameters for each plan for Patient Set 1 are summarized in Table 2.4. The parameters for each plan for Patient Set 2 are summarized in Table 2.5.

Table 2.4. Summary of energy availability for each of the four plans for patients in Patient Set 1. See geometry for plans in Figure 2.1.

Plan	Energy Spacing	Beam Flattening
1	Discrete	Scattered
2	N/A	N/A
3	Continuous	Scattered
4	Discrete	Scanned
5	Continuous	Scanned

Table 2.5. Summary of energy availability for each of the five plans for each patient in Patient Set 2. See geometry for plans 1,2 and 4 in Figure 2.2.

Plan	Energy Spacing: Lower PTV	Energy Spacing: Upper PTV	Beam Flattening
1	Discrete	Discrete	Scattered
2	Discrete	Continuous	Scattered
3	Continuous	Continuous	Scattered
4	Discrete	Discrete	Scanned
5	Continuous	Continuous	Scanned

2.1.7. Design of Bolus and Intensity Modulation for IM-BECT Patient Plans

Bolus and intensity modulations for each field were designed using a research version of p.d, which included intensity modulation.[42] Each bolus was designed using a set of operators from Low et al.[38] that were clinically available and manually optimized to fulfill the design goals of circumscribing the PTV with the 90% dose surface. Intensity modulation was designed to improve dose homogeneity in the PTV. Dose calculations in p.d were performed using a 3-dimentional implementation of the pencil beam redefinition algorithm (PBRA)[45–47] with intensity modulation.[34]

Operators to create the bolus fall into three categories: bolus creation operators, bolus modification operators, and bolus extension operators. A description of these operators can be found in Appendix A. For a specific patient, the sequence of bolus operators for each field are identical for each plan. The operators used for each patient in Patient Set 1 are almost identical, with slight variation. Likewise, the operators used for each patient in Patient Set 2 are almost identical, with slight variation. The operator sequences for Patient Set 1 and Patient Set 2 are listed in Table 2.6 and Table 2.7, respectively.

Table 2.6. Summary of bolus design operator sequences for Patient Set 1. See Appendix A for explanation of operators.

Number	PTV Field
1	Create (1.5 cm)
2	Truncate
3	Smooth (1,1)
4	IM (1.1)
5	Isodose shift (90%)
6	Smooth (1,1)
7	Specified shift (-0.2 cm)
8	Isodose shift (90%)
9	Smooth (1,0.5)
10	IM (1.0)

Table 2.7. Summary of bolus design operator sequences for Patient Set 2. See Appendix A for explanation of operators.

Number	Lower Field	Upper Field (shifted +Δ)	Upper Field (shifted -Δ)
1	Create (1.5 cm)	Create (0.75 cm)	Create (0.75 mm)
2	Truncate	Truncate	Truncate
3	Smooth (1,1)	Smooth (1,1)	Smooth (1,1)
4	IM (1.1)	Isodose shift (90%)	Specified Shift (-0.8 cm)
5	Isodose shift (90%)	Smooth (1,1)	
6	Smooth (1,1)	IM (1.1)	
7	Specified shift (-0.2 cm)		
8	Isodose shift		
9	Smooth (1,0.5)		
10	IM (1.0)		

For the lower PTV of plans in Patient Set 2, a bolus is created with an inner margin of 1.5 cm (border between the outer portion of bolus created and outer edge of PTV). Then the truncation operator was used to minimize the height of the rim of the bolus outside the treatment area, as to avoid collision between the electron applicator and bolus. The creation operator creates height irregularities in the bolus surface since the distal surface of the PTV is not smooth, potentially causing hot and cold spots in the PTV. So, the next step used a smoothing operator to reduce surface irregularities on the proximal side of the bolus. Intensity modulation further reduced the hot and cold spots in the PTV. Next, an isodose shift was used to shift the 90% isodose surface towards the distal PTV surface. The isodose shift operator is a one-dimensional operator, which means it only considers the difference between the physical distal target depth and the 90% dose line along each fan line diverging from the source. However, because electrons scatter laterally, multiple applications of the isodose shift operator were needed for larger targets. Following each isodose shift operator, the smoothing operator was applied to reduce the hot and cold hots in the PTV. Following the first isodose shift –smoothing operator sequence, to better visualize PTV coverage, a specified shift of 0.2 cm was used to shift the 90% dose surface towards the distal

surface of the PTV (though this step does not influence the final bolus design). The final steps were isodose shift, smooth, and intensity modulation to improve the homogeneity of the dose distribution. This was the baseline set of operators used for all patients in Patient Set 1. However, this baseline was adjusted on a patient by patient basis to achieve more optimal bolus. For plans in Patient Set 2, the bolus design operator sequence for the lower field was identical to the sequence used for Patient Set 1.

2.1.8. Normalization and Summation of Dose

Dose was normalized in p.d for each field such that 100% corresponded to the given dose. Given dose is defined as the maximum central axis dose (D_{max}) in a water phantom at the planned SSD for the rectangular field with least area that circumscribes the treatment field. The SSD is the distance from a point 100 cm upstream of isocenter (nominal source location) to the surface of the bolus along central axis of the beam. Because central axis was in the abutment region for our beams in Patient Set 2, its SSD was not necessarily representative of that at the center of the field; therefore, this required that the dose be renormalized so that the mean value of the dose along the depth of maximum dose was 100%. This was achieved visually by achieving intermittent islands of the 100% isodose lines in the transverse plane near the field center. These normalization factors ranged from 0.97 to 1.03 for all twenty plans generated in Patient Set 2. Similar normalization was used for plans in Patient Set 1 and ranged from 0.99 to 1.01.

After finalizing the beams in p.d for each of the plans for each patient, the dose distributions for each plan were exported to MIM for summation and conversion from percent dose to dose in Gy. For Patient Set 2, the composite percent dose distribution equaled the percent dose distribution for the lower field plus the sum of 50% of the percent dose distributions ($\pm\Delta$) for the upper fields (see Figure 2.5), i.e. equal weighting given to both the $+\Delta$ and $-\Delta$ fields. Percent doses were converted to dose by prescribing 50 Gy to the 90% contour, i.e. multiplying all values by (50

Gy/90%). The summed dose distributions for both Patient Set 1 and Patient Set 2 are shown in the isodose distributions in Appendix B, where 100%=55.5 Gy. The isodose distributions were also created in MIM.

Finally, for comparing dose distributions for each plan of a single patient, each plan's composite dose distribution was scaled relative to that of Plan 1, so all had the same PTV D_{50}, that is the same dose value for 50% PTV coverage. This scaling was chosen because Plan 1 is the currently clinically available planning strategy; however, because D_{50} values of all plans were within a few percent, this scaling had little impact on the results and conclusions.

2.2. Aim 2—Physical and Biological Dose Metrics for Plans

2.2.1. Dose and Biological Metrics

The cumulative DVHs for the heart, lungs, and PTV were extracted from MIM and imported to MATLAB, where an in-house script was used to determine the following dose and biological metrics.

(1) PTV Metrics:

a. $D_{97\%}$-Dose given to 97% of PTV volume

b. D_{max}-maximum dose to PTV

c. D_{mean}-mean dose to PTV

d. $V_{47.5\ Gy}$-volume of PTV receiving 47.5 Gy (95% of 50 Gy prescription)

(2) Heart Metrics:

a. D_{min}-minimum dose to heart

b. D_{max}-maximum dose to heart

c. D_{mean}-mean dose to heart

d. $V_{22.5\ Gy}$-volume of heart receiving 22.5 Gy

e. $V_{30\ Gy}$-volume of heart receiving 30 Gy

f. NTCP-normal tissue complication probability

(3) Lung Metrics:

a. D_{min}-minimum dose to lungs

b. D_{max}-maximum dose to lungs

c. D_{mean}-mean dose to lungs

d. $V_{20\ Gy}$-volume of heart receiving 30 Gy

e. NTCP-normal tissue complication probability

f. $SCCP_{lin}$-Secondary cancer complication probability, linear model

g. $SCCP_{lin\text{-}exp}$-Secondary cancer complication probability, linear-exponential model

2.2.2. NTCP-Lungs

NTCP values for the lungs were calculated using the Lyman-Kutcher-Burman (LBK) model.[48, 49] The endpoint, which was used in the present study, was grade two radiation pneumonitis or higher, whose model follows:

$$NTCP = \frac{1}{\sqrt{2\pi}} \int_{-\infty}^{t} e^{\frac{-x^2}{2}} dx,$$

where

$$t = \frac{EUD - TD_{50}}{m * TD_{50}},$$

and

$$EUD = \left(\sum_i D_i^{\frac{1}{n}} \frac{V_i}{V_{tot}} \right)^n.$$

The definitions and values of the various parameters are found in Table 2.8.

.

Table 2.8. Parameters for computing lung NTCP (from Seppenwoolde et al., 2003[48])

Parameter	Definition/ Value
D_i	dose per fraction to the sub-volume i
V_i	volume irradiated to dose D_i
V_{tot}	total volume of lung
m	Slope of the dose-response curve, 0.37
EUD	Dose from a non-uniform dose distribution that results in the same NTCP as a non-uniform dose distribution
TD_{50}	Dose that would cause a 50% risk of complication if given uniformly, 30.8 Gy
n	0.99

2.2.3. NTCP-Heart

The NTCP for the whole heart was calculated using Kallman's relative seriality model, which takes into account both the parallel and serial arrangements of functional subunits within the heart.[50] When finding the NTCP, cardiac mortality was used as the endpoint, i.e.

$$NTCP = \{1 - \prod_i (1 - P(D_i)^s)^{V_i}\}^{\frac{1}{s}},$$

where

$$P(D_i) = 2^{-e^{e\gamma\left(1-\frac{D_i}{D_{50}}\right)}}.$$

The definitions and values of the various parameters are found in Table 2.9.

Table 2.9. Parameters for computing heart NTCP (from Gagliardi et al., 2001[10])

Parameter	Definition/ Value
D_i	dose to the sub-volume i
V_i	volume irradiated to dose D_i
s	Ratio of serial function subunits to total functional subunits, 1
TD_{50}	Dose that would cause a 50% risk of complication if given uniformly, 52.3 Gy
γ	Maximum relative slope of the dose-response curve, 1.28

2.2.4. SCCP-Lungs

In addition to NTCP, the secondary cancer complication probability (SCCP) was calculated for the lungs using two different models, the linear dose response model ($SCCP_{lin}$) and the linear-exponential dose response ($SCCP_{lin\text{-}exp}$). Here, the Schneider model[51] was used, i.e.

$$SCCP_l = \mathrm{In}_{\mathrm{org}}\, OED_{org,linear}\,,$$

where

$$\mathrm{OED}_{\mathrm{org,linear}} = \frac{1}{V_{org}} \sum_i V_i D_i\,,$$

and

$$SCCP_{lin-exp} = \mathrm{In}_{\mathrm{org}}\, OED_{org,linear-exponential}\,,$$

where

$$\mathrm{OED}_{\mathrm{org,linear-exponential}} = \frac{1}{V_{org}} \sum_i V_i D_i e^{-\alpha D_i}\,.$$

The definitions and values of the various parameters are found in Table 2.10.

Table 2.10. Parameters for computing lung SCCP (from Schneider et al., 2005[51])

Parameter	Definition/ Value
α	Organ specific cell sterilization parameter, 0.085 Gy^{-1}
D_i	dose to the sub-volume i
V_i	volume irradiated to dose D_i
V_{org}	Volume to the total organ
OED_{org}	Dose from a non-uniform dose distribution that results in the same cancer incidence as a non-uniform dose distribution
IN_{org}	Organ specific absolute cancer incidence as a percentage per gray, representing the lifetime risk for a residual lifetime expectancy of 50 years, 1.68% per Gy

Chapter 3. Results

Aim 1 and Aim 2 results are presented together for each of the seven patients studied. The first section below describes the beams comprising the treatment plans. The second section shows and compares dose distributions, dose metrics, and biological metrics for multiple plans for each patient.

3.1. Description of Treatment Plans for Different Electron Beam Technologies

Aim 1 results show the resulting treatment beams and dose distribution for each of the four or five treatment plans developed for each of the seven patients. Treatment planning results are described below, partitioned into the two patent data sets. Plans for Patient Set 1 (CW1, CW3, CW6) required only a single electron field. Plans for Patient Set 2 (CW2, CW4, CW7, CW8) required two electron fields (upper and lower).

3.1.1. Treatment Planning Beam Parameters (Patient Set 2)

Patient plans were developed in accordance with the methods described above. For Patient Set 1 (CW1, CW3, CW6), the beam parameters for Plans 1-4 are listed in Table 3.1.

Table 3.1. Summary of beam parameters for each patient and plan in Patient Set 1.

Patient	Plan	Beam Type	Energy Spacing	Energy (MeV)	R_{90} (cm)	Gantry Angle (°)
CW1	1	Scattered	Discrete	21.3	6.0	130
	3	Scattered	Continuous	19.5	5.7	
	4	Scanned	Discrete	18.4	6.0	
	5	Scanned	Continuous	17.3	5.7	
CW3	1	Scattered	Discrete	13.0	4.0	40
	3	Scattered	Continuous	12.4	3.8	
	4	Scanned	Discrete	12.2	4.0	
	5	Scanned	Continuous	11.6	3.8	
CW6	1	Scattered	Discrete	16.2	5.0	45
	3	Scattered	Continuous	15.6	4.8	
	4	Scanned	Discrete	15.1	5.0	
	5	Scanned	Continuous	14.5	4.8	

For patients in Patient Set 2 (CW2, CW4, CW7, and CW8) the PTVs were partitioned as illustrated in Figure 2.2 for Plans 1, 2, and 4, and in Figure 2.3 for Plans 3 and 5. The resulting beam energies ($E_{p,0}$), therapeutic ranges (R_{90}), and beam angles of all five plans for each of the four patients are listed for the lower and upper fields in Table 3.2.

Table 3.2. Summary of beam parameters for each patient and plan in Patient Set 2.

Patient	Plan	Beam Type	Energy Spacing	Lower Field E (MeV)	Lower Field R_{90} (cm)	Upper Field E (MeV)	Upper Field R_{90} (cm)	Gantry Angle (°)	Δ (cm)
CW2	1	Scattered	Discrete	13.0	4.0	16.2	5.0	38	0.7
	2	Scattered	Discrete	13.0	4.0	15.9	4.9		
	3	Scattered	Continuous	13.0	4.0	15.9	4.9		
	4	Scanned	Discrete	12.2	4.0	15.1	5.0		
	5	Scanned	Continuous	12.2	4.0	14.8	4.9		
CW4	1	Scattered	Discrete	16.2	5.0	21.3	6.0	150	0.8
	2	Scattered	Discrete	16.2	5.0	21.3	6.0		
	3	Scattered	Continuous	16.2	5.0	21.3	6.0		
	4	Scanned	Discrete	15.1	5.0	18.4	6.0		
	5	Scanned	Continuous	15.1	5.0	18.4	6.0		
CW7	1	Scattered	Discrete	16.2	5.0	21.3	6.0	50	0.7
	2	Scattered	Discrete	16.2	5.0	21.3	6.0		
	3	Scattered	Continuous	16.2	5.0	21.3	6.0		
	4	Scanned	Discrete	15.1	5.0	18.4	6.0		
	5	Scanned	Continuous	15.1	5.0	18.4	6.0		
CW8	1	Scattered	Discrete	13.0	4.0	16.2	5.0	40	0.6
	2	Scattered	Discrete	13.0	4.0	15.6	4.8		
	3	Scattered	Continuous	11.1	3.4	15.6	4.8		
	4	Scanned	Discrete	12.2	4.0	14.5	4.8		
	5	Scanned	Continuous	10.5	3.4	14.5	4.8		

Also, for all five plans, the abutment region was managed by feathering the upper beam, as illustrated in Figure 2.6. A profile of the abutting scheme for CW2 is illustrated in Figure 2.4 and the resulting profiles for all four patients are plotted in Figure 3.1. They show the dose heterogeneity being reduced to less than ±6% in the abutment region of the PTV.

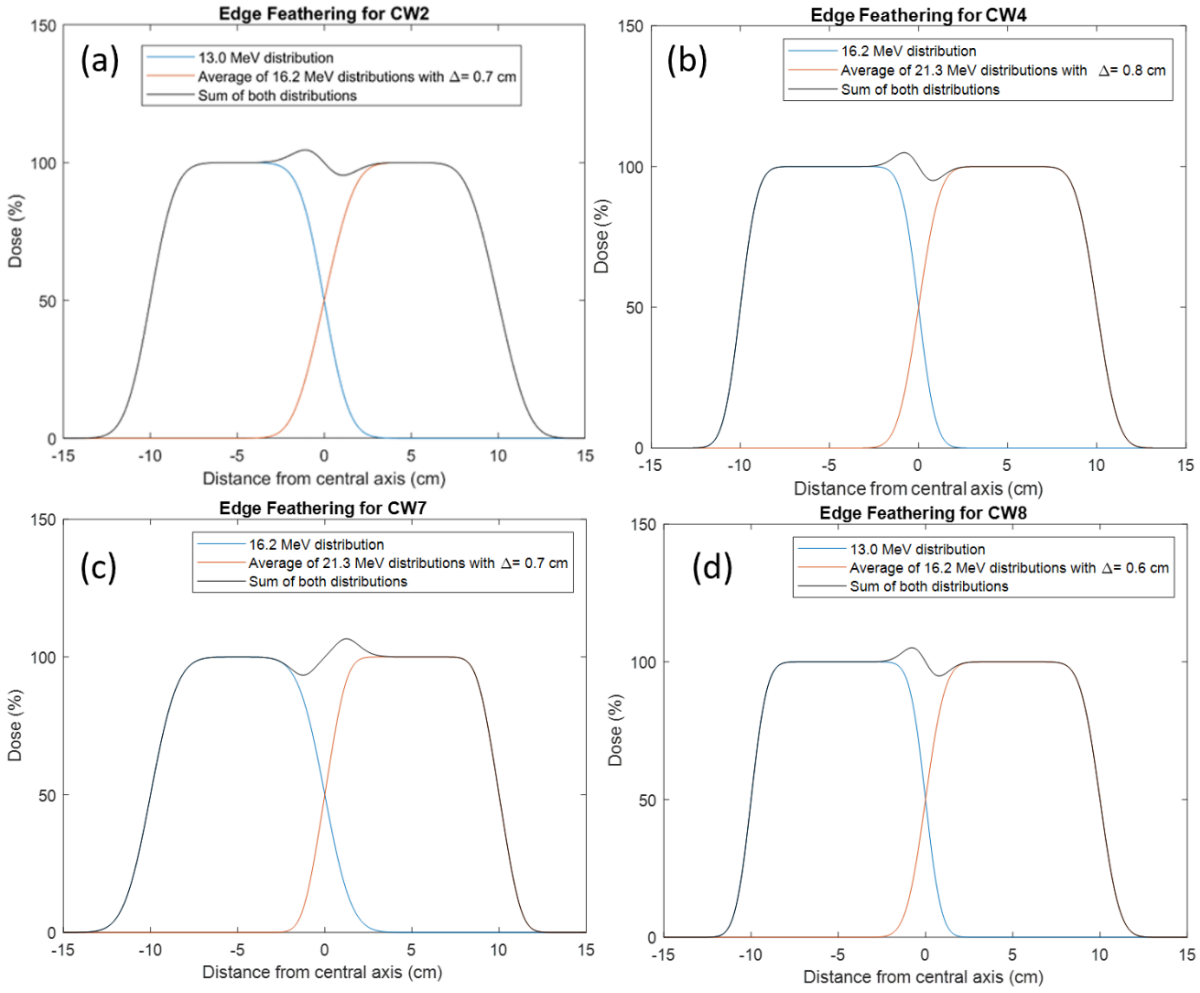

Figure 3.1. Feathering results for all four patients in Patient Set 2. (a) For CW2, Δ=0.7 cm which results in dose heterogeneities of +/-4%. (b) For CW4, Δ=0.8 cm which results in dose heterogeneities of +/-5% (c) For CW7, Δ=0.7 cm which results in dose heterogeneities of +/-6% (d) For CW8, Δ=0.6 cm which results in dose heterogeneities of +/-4%.

For each plan three transverse and one sagittal-coronal oblique planar dose distributions are plotted over the CT images. Also, for each patient, DVHs for the PTV, heart, and lungs are plotted for each plan. Using the DVHs, dose and biologic metrics are calculated and compared in a single table. Dose metrics include: (1) PTV: $D_{97\%}$ (Dose given to 97% of PTV volume), D_{max} (maximum dose), D_{mean} (mean dose), and $V_{47.5\ Gy}$ (relative volume of PTV receiving 47.5 Gy, or 95% of the prescribed dose), (2) Heart: D_{min}, D_{max}, D_{mean}, $V_{22.5\ Gy}$ (relative volume of heart receiving 22.5 Gy), and $V_{30\ Gy}$ (relative volume of heart receiving 30 Gy), and (3) Lung: D_{min},

D_{max}, D_{mean}, and $V_{20\,Gy}$ (relative volume of lung receiving 20 Gy). Biological dose metrics include: (1) Heart: NTCP (normal tissue complication probability) and (2) Lung: NTCP, $SCCP_{lin}$ (secondary cancer complication probability, linear model), $SCCP_{lin\text{-}exp}$ (secondary cancer complication probability, linear-exponential model).

3.2. Dose Distributions, DVHs, Dose Metrics, and Biological Metrics for All Plans for Each Patient

Results are presented for three patients in Patient Set 1 (CW1, CW3, and CW6) and four patients in Patient Set 2 (CW2, CW4, CW7, and CW8). Results for Patient Set 1, for which there are four plans (Plan 1, Plan 3, Plan 4, and Plan 5 as detailed earlier), are shown first because they required only a single electron beam and are easier to compare and interpret. Results for Patient Set 2, for which there are five plans (Plan 1, Plan 2, Plan 3, Plan 4, and Plan 5 as detailed earlier), are shown second, as they required upper and lower fields, the upper having edge feathering, hence three electron beams. As such, these plans are more complex to compare and interpret.

The trends indicated by the metrics above can be visualized by comparing the isodose plots for the four plans being compared. The PTV coverage is appreciated by viewing the PTV and the 80% and 90% isodose lines. The heart dose is appreciated by comparing isodose lines in the dose falloff region, particularly the 40% isodose line that equals approximately 22.5 Gy, with the anterior heart in the sagittal-coronal oblique and two inferior planes demarcated on the former. Lung dose is appreciated by comparing isodose lines in the dose falloff region, particularly the 40% isodose line that is just greater than 20 Gy, within the lung (superior to heart) in the sagittal-coronal oblique and the superior plane demarcated on the former. For the remaining comparisons, the sagittal-coronal oblique plane and the transverse plane through mid-heart will be shown in the text, and isodose plots for their respective transverse planes through the region superior to the heart and through the inferior heart are plotted in Appendix B.

3.2.1. Result for Patient Set 1

Treatment planning results for patients in Patient Set 1 (CW1, CW3, and CW6) are shown using isodose plots for three transverse planes and one sagittal-coronal oblique plane for Plans 1, 3, 4, and 5. Inspection of these plots shows utilization of continuous rather than discrete energy beams usually resulted in lower beam energies. Because lower energy beams have a sharper dose falloff, this usually resulted in less normal tissue dose and lower complication probabilities. Also, utilization of scanned versus scattered electron beams, which results in sharper dose falloff, resulted in less normal tissue dose and lower complication probabilities. The combination of the two effects is greater than either alone and is illustrated by comparing Plan 1 (scattered, discrete energy beams) and Plan 5 (scanned beam, continuous energy beams), which represent the worst and best plans, respectively.

3.2.1.1. Results for Patient CW1

Treatment planning results for CW1 (Patient Set 1) include isodose plots for three transverse planes and one sagittal-coronal oblique plane for Plans 1, 3, 4, and 5. All such results are shown in Appendix B, and one sagittal-coronal oblique plane and one transverse plane for each plan are shown in Figure 3.2 to Figure 3.5. DVHs for PTV, heart, and lungs for each of the four plans were computed and plotted for comparison in Figure 3.6. Dose and biologic metrics computed from the DVHs are compared in Table 3.3. These results likely have some dependence on the location of the distal PTV surface, and for CW1 the distance between the distal edge of the PTV and the distal side of the chest wall (Δt) was 1.3 cm on central axis.

PTV Coverage: Dose plots (Figure 3.2 to Figure 3.5) show that the 90% isodose lines closely cover the distal PTV surface, or in some locations the 80% isodose surface due to the jagged nature of the PTV. Most evident at the lateral edges of the PTV, coverage could be improved by increasing the lateral margin between the PTV and field edge or by a more realistic

PTV (smoother edges). The PTV DVHs are similar for all plans; $V_{47.5\ Gy}$ values of the scanned beams are slightly less than those of the scattered beams. Maximum doses are less than 57 Gy (<103%).

Effect of Scanned vs. Scattered Beams: Comparing Plan 1 (scattered, discrete energy 21.3 MeV beam) and Plan 4 (scanned, discrete energy 18.4 MeV beam) showed that the scanned electron beam reduced (1) mean dose to the heart by 2.7 Gy (8.3 to 5.6 Gy) and (2) V_{20} Gy to the lung by 3.7% (17.2 to 13.5%). This resulted in reduced (1) $NTCP_{heart}$ by 0.2% (0.4 to 0.1%), (2) $NTCP_{lungs}$ by 0.01% (0. 02 to 0.01%), and (3) $SCCP_{lin}$ by 3.5% (14.4 to 10.8%).

Comparing Plan 3 (scattered, continuous energy 19.5 MeV beam) and Plan 5 (scanned, continuous energy 17.3 MeV beam) showed that the scanned electron beam reduced (1) mean dose to the heart by 2.0 Gy (6.4 to 4.3 Gy) and (2) V_{20Gy} to the lung by 3.4% (14.1 to 10.7%). This resulted in reduced (1) $NTCP_{heart}$ by 0.1% (0.2 to 0.1%), (2) $NTCP_{lungs}$ by 0.0% (0. 01 to 0.01%), and (3) $SCCP_{lin}$ by 3.1% (11.7 to 8.7%).

Effect of Continuous vs. Discrete Beam Energies: The same data above can be used to evaluate the benefit of continuous versus discrete energy beams. Comparing Plan 1 (scattered, discrete energy 21.3 MeV beam) with Plan 3 (scattered, continuous energy 19.5 MeV beam) showed that continuous energy beams reduced (1) mean dose to the heart by 1.9 Gy (8.3 to 6.4 Gy) and (2) V_{20Gy} to the lung by 3.2% (17.2 to 14.1%). This resulted in reduced (1) $NTCP_{heart}$ by 0.2% (0.4 to 0.2%), (2) $NTCP_{lungs}$ by 0.01% (0. 02 to 0.01%), and (3) $SCCP_{lin}$ by 2.6% (14.4% to 11.7%).

Comparing Plan 4 (scanned, discrete energy 18.4 MeV beam) with Plan 5 (scanned, continuous energy 17.3 MeV beam) showed that continuous energy beams reduced (1) mean dose to the heart by 1.3 Gy (5.6 to 4.3 Gy) and (2) V_{20Gy} to the lung by 2.8% (13.5 to 10.7%). This

resulted in reduced (1) $NTCP_{heart}$ by 0.09% (0.14 to 0.05%), (2) $NTCP_{lungs}$ by 0.00% (0. 01 to 0.01%), and (3) $SCCP_{lin}$ by 2.1% (10.8% to 8.7%).

Effect of Scanned, Continuous Energy Beams vs. Scattered, Discrete Energy Beams: The greatest plan improvement was comparing Plan 1 (scattered, discrete energy 21.3 MeV beam), current technology, with Plan 5 (scanned, continuous energy 17.3 MeV beam), possible future technology, which reduced (1) mean dose to the heart by 3.9 Gy (8.3 to 4.3 Gy) and (2) V_{20Gy} to the lung by 6.5% (17.2 to 10.7%). This resulted in reduced (1) $NTCP_{heart}$ by 0.3% (0.4 to 0.05%), (2) $NTCP_{lungs}$ by 0.01% (0.02 to 0.01%), and (3) $SCCP_{lin}$ by 5.7% (14.4% to 8.7%).

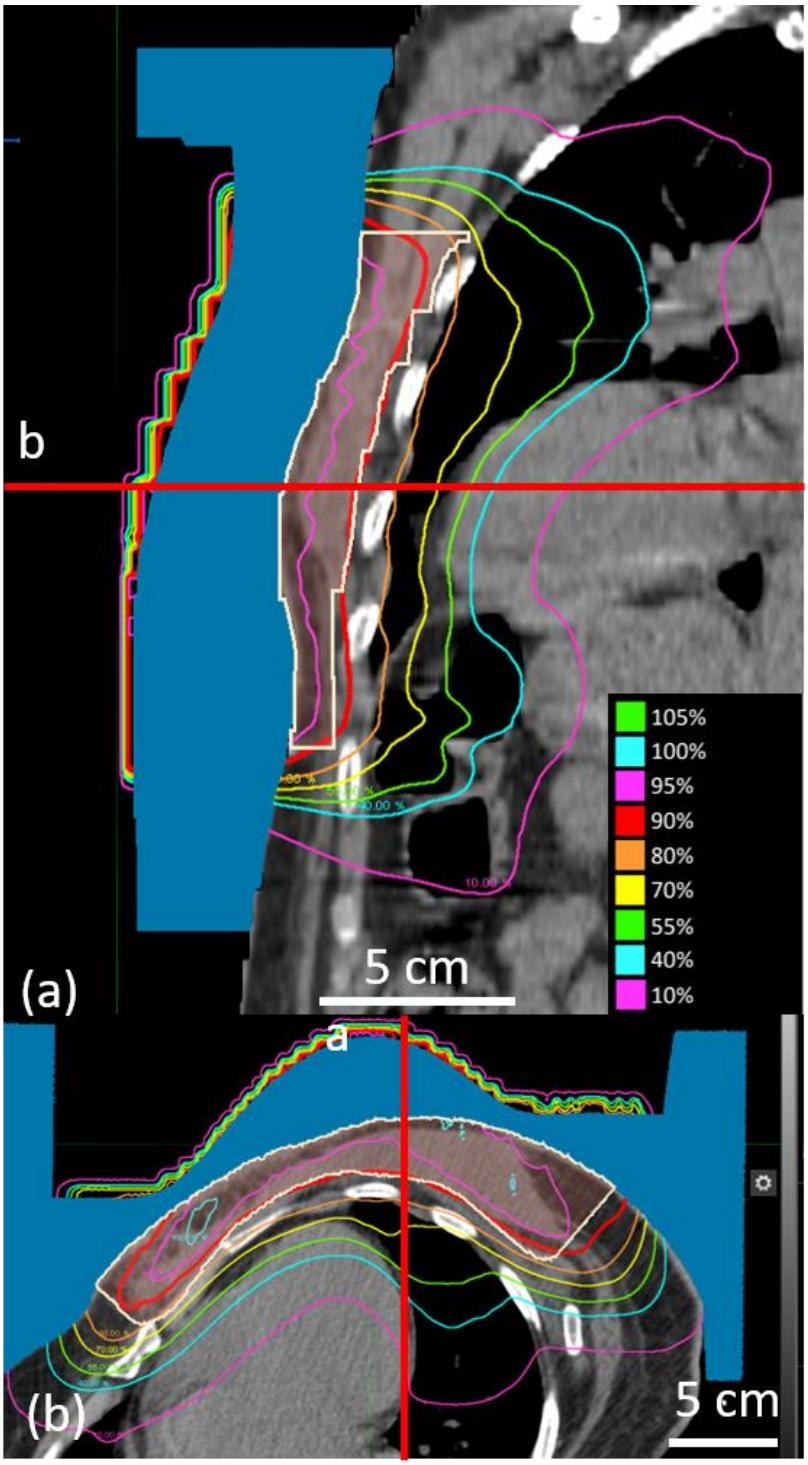

Figure 3.2. Sagittal and axial images of CW1, Plan 1. CW1 (Patient Set 1) was planned using scattered electron beams and discrete energy spacing. (a) Dose plan in the sagittal-coronal, oblique plane demarcated by the red line in figure (b)'s transverse plane; (b) Dose plan in transverse plane passing through central heart region, demarcated by red line in figure (a)'s oblique plane. Bolus is shaded blue, and PTV is outlined in white. Key shows dose values.

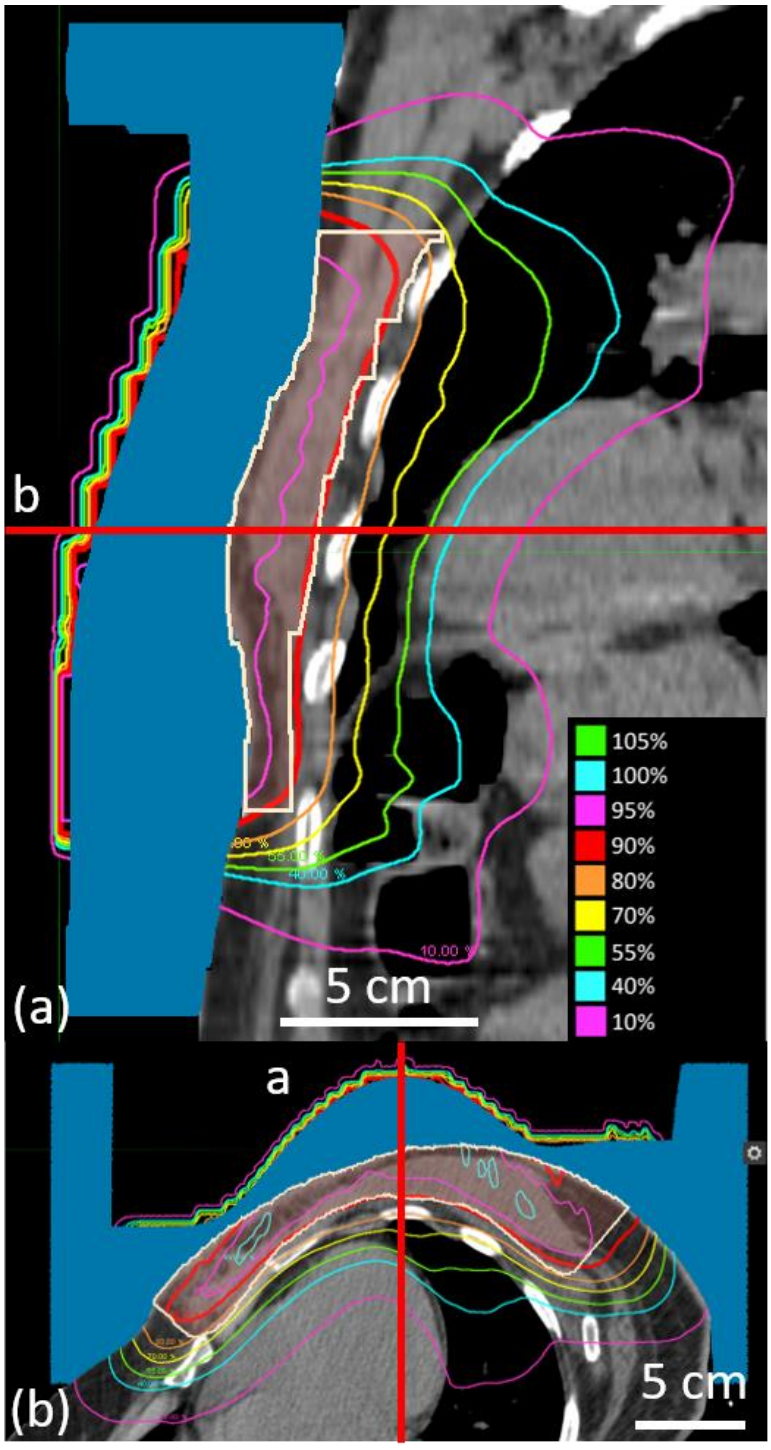

Figure 3.3. Sagittal and axial images of CW1, Plan 3. CW1 (Patient Set 1) was planned using scattered electron beams and continuous energy spacing. (a) Dose plan in the sagittal-coronal, oblique plane demarcated by the red line in figure (b)'s transverse plane; (b) Dose plan in transverse plane passing through central heart region, demarcated by red line in figure (a)'s oblique plane. Bolus is shaded blue, and PTV is outlined in white. Key shows dose values.

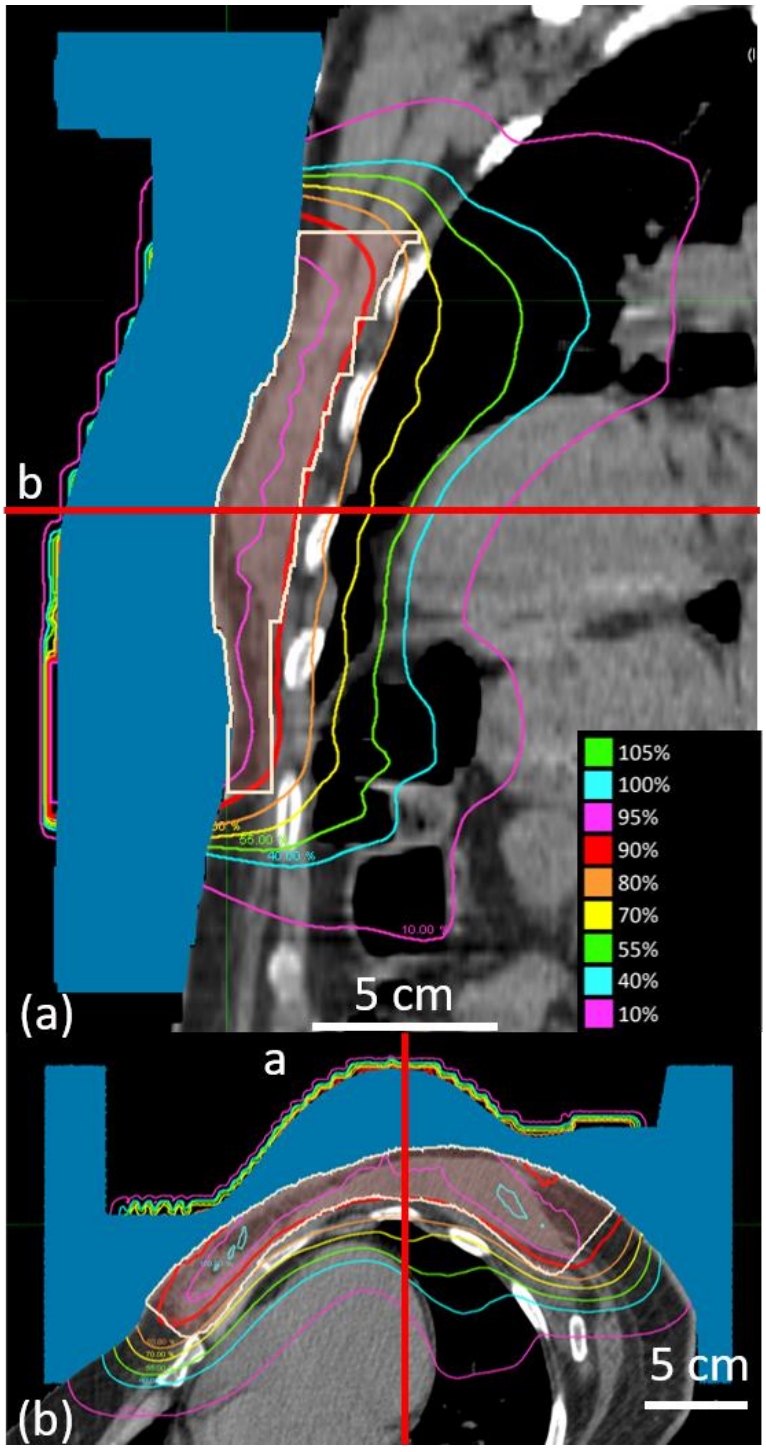

Figure 3.4. Sagittal and axial images of CW1, Plan 4. CW1 (Patient Set 1) was planned using scanned electron beams and discrete energy spacing. (a) Dose plan in the sagittal-coronal, oblique plane demarcated by the red line in figure (b)'s transverse plane; (b) Dose plan in transverse plane passing through central heart region, demarcated by red line in figure (a)'s oblique plane. Bolus is shaded blue, and PTV is outlined in white. Key shows dose values.

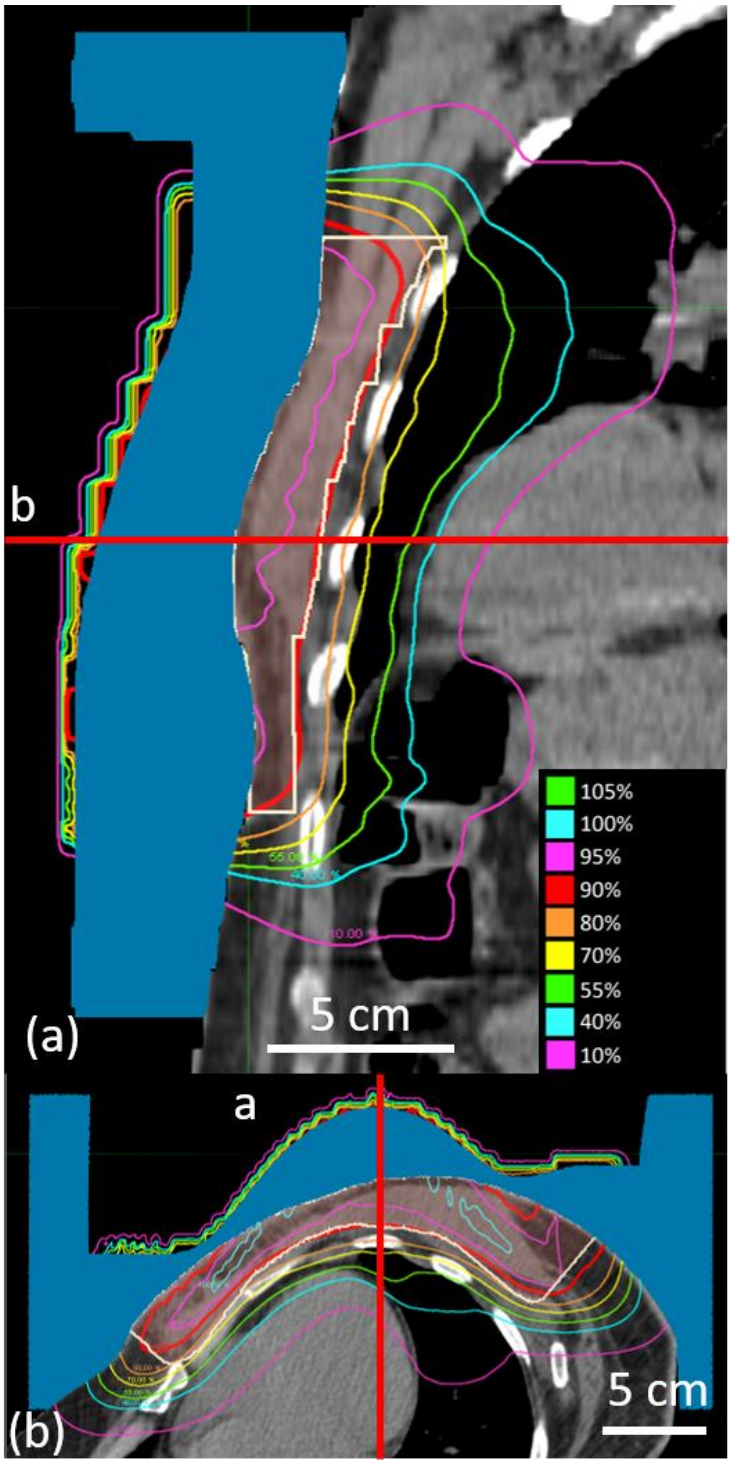

Figure 3.5. Sagittal and axial images of CW1, Plan 5. CW1 (Patient Set 1) was planned using scanned electron beams and continuous energy spacing. (a) Dose plan in the sagittal-coronal, oblique plane demarcated by the red line in figure (b)'s transverse plane; (b) Dose plan in transverse plane passing through central heart region, demarcated by red line in figure (a)'s oblique plane. Bolus is shaded blue, and PTV is outlined in white. Key shows dose values.

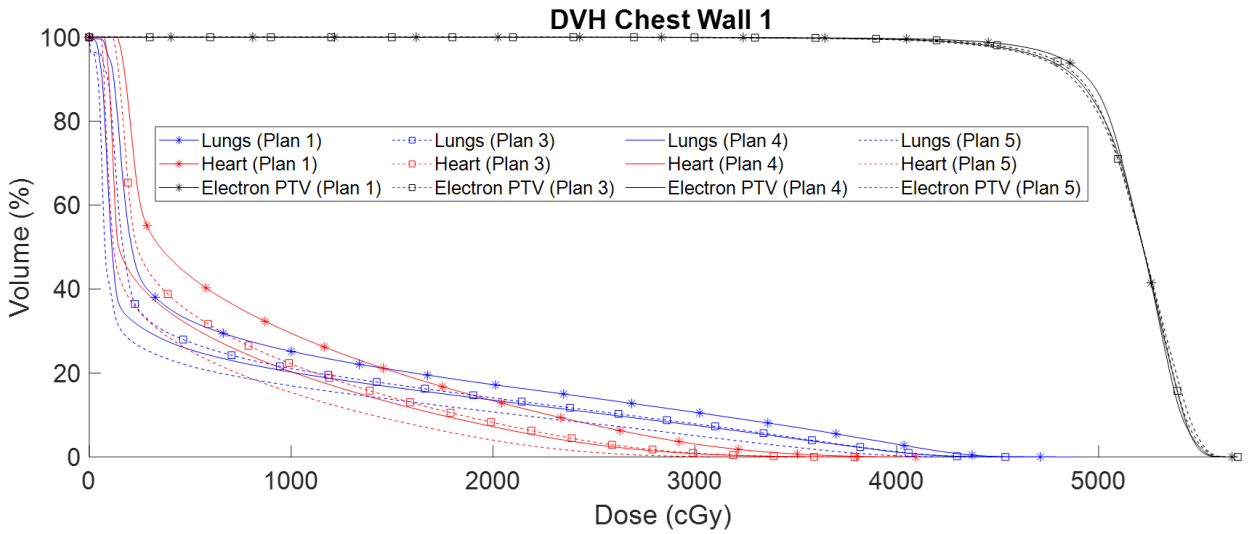

Figure 3.6. Comparison of cumulative DVH plots for CW1 (Patient Set 1) Plans. DVH plots for PTV, heart, and lung are compared for Plans 1, 3, 4, and 5, as indicated in key.

Table 3.3. Comparison of metrics for CW1 (Patient Set 1) Plans. Dose metrics are shown for PTV, heart, and lungs. NTCP and SCCP values are shown for heart and lungs.

		Plan 1	Plan 3	Plan 4	Plan 5
PTV	$D_{97\%}$ (Gy)	46.9	46.4	46.2	45.9
	$V_{47.5\ Gy}$ (%)	96.2	95.3	94.6	94.1
	Max dose (Gy)	56.6	56.9	56.7	56.7
	Mean dose (Gy)	51.9	51.8	51.7	51.7
	Std Dev (Gy)	2.2	2.5	2.6	2.8
Heart	$V_{22.5\ Gy}$ (%)	10.4	5.7	4.9	2.3
	$V_{30\ Gy}$ (%)	3.1	0.9	0.8	0.1
	Min dose (Gy)	1.3	1.1	0.7	0.5
	Max dose (Gy)	40.9	37.9	38.2	34.1
	Mean dose (Gy)	8.3	6.4	5.6	4.3
	Std Dev (Gy)	8.3	7.2	7.2	6.0
	NTCP (%)	0.4	0.2	0.1	0.1
Lungs	$V_{20\ Gy}$ (%)	17.2	14.1	13.5	10.7
	Min dose (Gy)	0.0	0.0	0.0	0.0
	Max dose (Gy)	47.1	45.4	49.0	43.8
	Mean dose (Gy)	8.6	7.0	6.5	5.2
	Std Dev (Gy)	11.9	10.7	10.7	9.4
	NTCP (%)	0.02	0.01	0.01	0.01
	$SCCP_{lin}$ (%)	14.4	11.7	10.8	8.7
	$SCCP_{lin\text{-}exp}$ (%)	3.4	3.0	2.6	2.2

3.2.1.2. Results for Patient CW3

Treatment planning results for CW3 (Patient Set 1) include isodose plots for three transverse planes and one sagittal-coronal oblique plane for Plans 1, 3, 4, and 5. All such results are shown in Appendix B, and one sagittal-coronal oblique plane and one transverse plane for each plan are shown in Figure 3.7 to Figure 3.10. DVHs for PTV, heart, and lungs for each of the four plans were computed and plotted for comparison in Figure 3.11. Dose and biologic metrics computed from the DVHs are compared in Table 3.4. These results likely have some dependence on the location of the distal PTV surface, and for CW3 the distance between the distal edge of the PTV and the distal side of the chest wall (Δt) was 1.1 cm on central axis.

PTV Coverage: Dose plots (Figure 3.7 to Figure 3.10) show that the 90% isodose lines closely cover the distal PTV surface, or in some locations the 80% isodose surface due to the jagged nature of the PTV. Most evident at the lateral edges of the PTV, coverage could be improved by increasing the lateral margin between the PTV and field edge or by a more realistic PTV (smoother edges). The PTV DVHs are similar for all plans; $V_{47.5\ Gy}$ values of the scanned beams are slightly less than those of the scattered beams. Maximum doses are less than 59 Gy (<106%).

Effect of Scanned vs. Scattered Beams: Comparing Plan 1 (scattered, discrete energy 13.0 MeV beam) and Plan 4 (scanned, discrete energy 12.2 MeV beam) showed that the scanned electron beam reduced (1) mean dose to the heart by 0.2 Gy (4.3 to 4.1 Gy) and (2) V_{20} Gy to the lung by 1.7% (15.8 to 14.1%). This resulted in reduced (1) $NTCP_{heart}$ by 0.05% (0.1 to 0.05%), (2) $NTCP_{lungs}$ by 0.00% (0.01 to 0.01%), and (3) $SCCP_{lin}$ by 1.3% (11.8 to 10.5%).

Comparing Plan 3 (scattered, continuous energy 12.4 MeV beam) and Plan 5 (scanned, continuous energy 11.6 MeV beam) showed that the scanned electron beam reduced (1) mean dose to the heart by 0.0 Gy (3.7 to 3.7 Gy) and (2) V_{20Gy} to the lung by 2.0% (14.5 to 12.5%). This

resulted in reduced (1) $NTCP_{heart}$ by 0.03% (0.06 to 0.03%), (2) $NTCP_{lungs}$ by 0.0% (0.1 to 0.1%), and (3) $SCCP_{lin}$ by 1.3% (10.7 to 9.4%).

Effect of Continuous vs. Discrete Beam Energies: The same data above can be used to evaluate the benefit of continuous versus discrete energy beams. Comparing Plan 1 (scattered, discrete energy 13.0 MeV beam) with Plan 3 (scattered, continuous energy 12.4 MeV beam) showed that continuous energy beams reduced (1) mean dose to the heart by 0.6 Gy (4.3 to 3.7 Gy) and (2) V_{20Gy} to the lung by 1.4% (15.8 to 14.5%). This resulted in reduced (1) $NTCP_{heart}$ by 0.04% (0.1 to 0.06%), (2) $NTCP_{lungs}$ by 0.00% (0.01 to 0.01%), and (3) $SCCP_{lin}$ by 1.1% (11.8% to 10.7%).

Comparing Plan 4 (scanned, discrete energy 12.2 MeV beam) with Plan 5 (scanned, continuous energy 11.6 MeV beam) showed that continuous energy beams reduced (1) mean dose to the heart by 0.4 Gy (4.1 to 3.7 Gy) and (2) V_{20Gy} to the lung by 1.6% (14.1 to 12.5%). This resulted in reduced (1) $NTCP_{heart}$ by 0.02% (0.05 to 0.03%), (2) $NTCP_{lungs}$ by 0.0% (0.1 to 0.1%), and (3) $SCCP_{lin}$ by 1.1% (10.5% to 9.4%).

Effect of Scanned, Continuous Energy Beams vs. Scattered, Discrete Energy Beams: The greatest plan improvement was comparing Plan 1 (scattered, discrete energy 13.0 MeV beam), current technology, with Plan 5 (scanned, continuous energy 11.6 MeV beam), possible future technology. This reduced (1) mean dose to the heart by 0.6 Gy (4.3 to 3.7 Gy) and (2) V_{20Gy} to the lung by 3.3% (15.8 to 12.5%). This resulted in reduced (1) $NTCP_{heart}$ by 0.07% (0.1 to 0.03%), (2) $NTCP_{lungs}$ by 0.00% (0.01 to 0.01%), and (3) $SCCP_{lin}$ by 2.4% (11.8% to 9.4%).

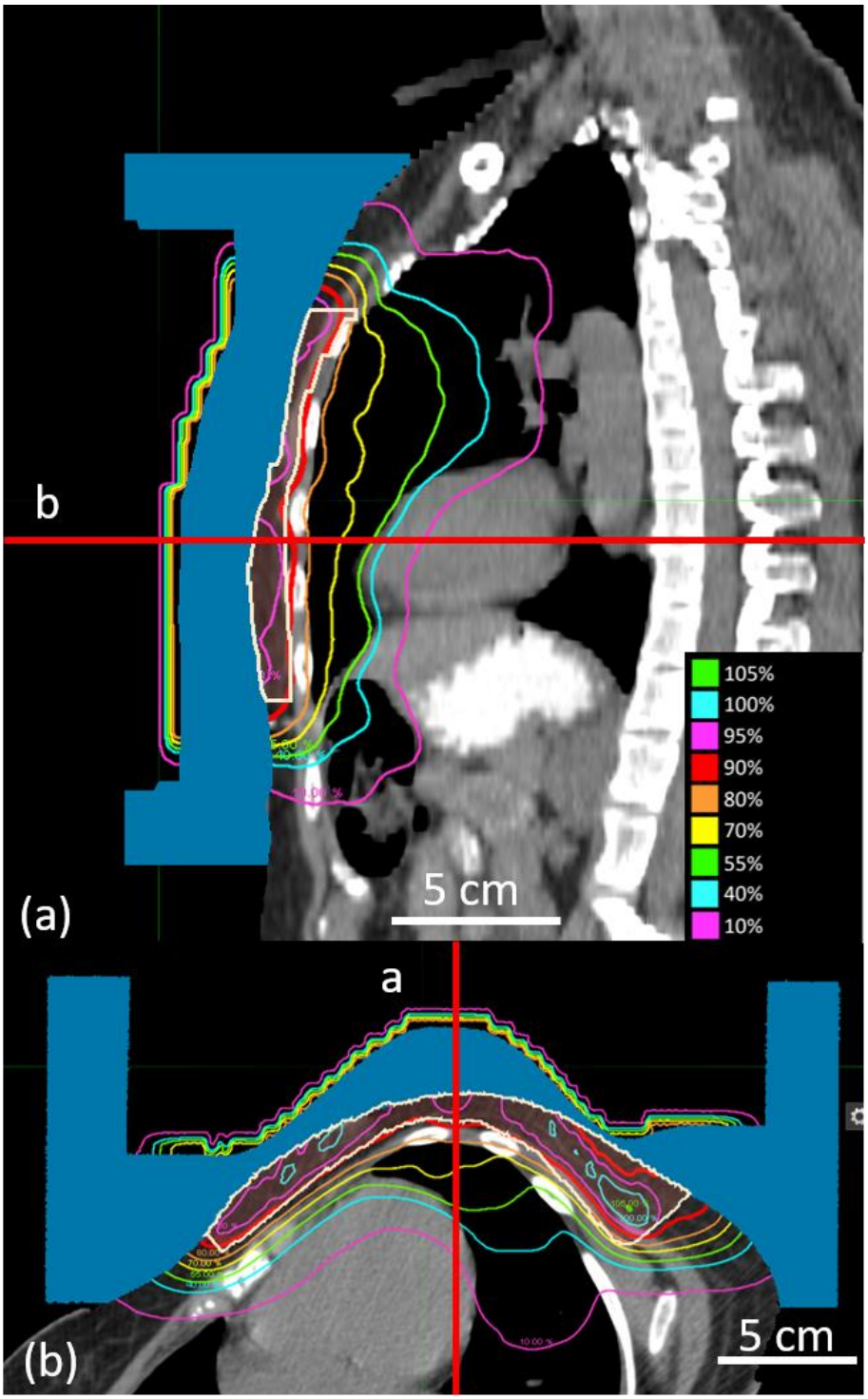

Figure 3.7. Sagittal and axial images of CW3, Plan 1. CW3 (Patient Set 1) was planned using scattered electron beams and discrete energy spacing. (a) Dose plan in the sagittal-coronal, oblique plane demarcated by the red line in figure (b)'s transverse plane; (b) Dose plan in transverse plane passing through central heart region, demarcated by red line in figure (a)'s oblique plane. Bolus is shaded blue, and PTV is outlined in white. Key shows dose values.

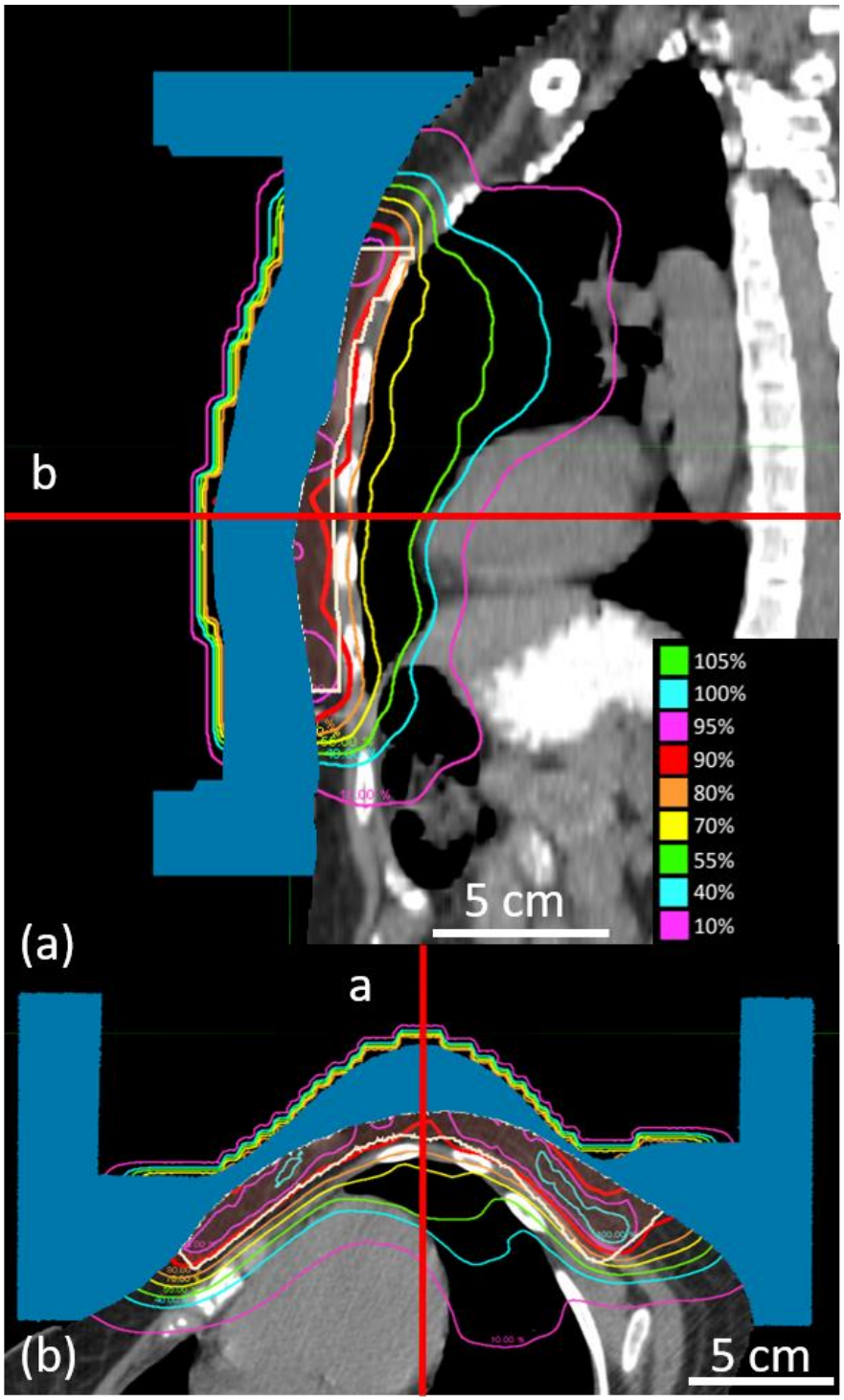

Figure 3.8. Sagittal and axial images of CW3, Plan 3. CW3 (Patient Set 1) was planned using scattered electron beams and continuous energy spacing. (a) Dose plan in the sagittal-coronal, oblique plane demarcated by the red line in figure (b)'s transverse plane; (b) Dose plan in transverse plane passing through central heart region, demarcated by red line in figure (a)'s oblique plane. Bolus is shaded blue, and PTV is outlined in white. Key shows dose values.

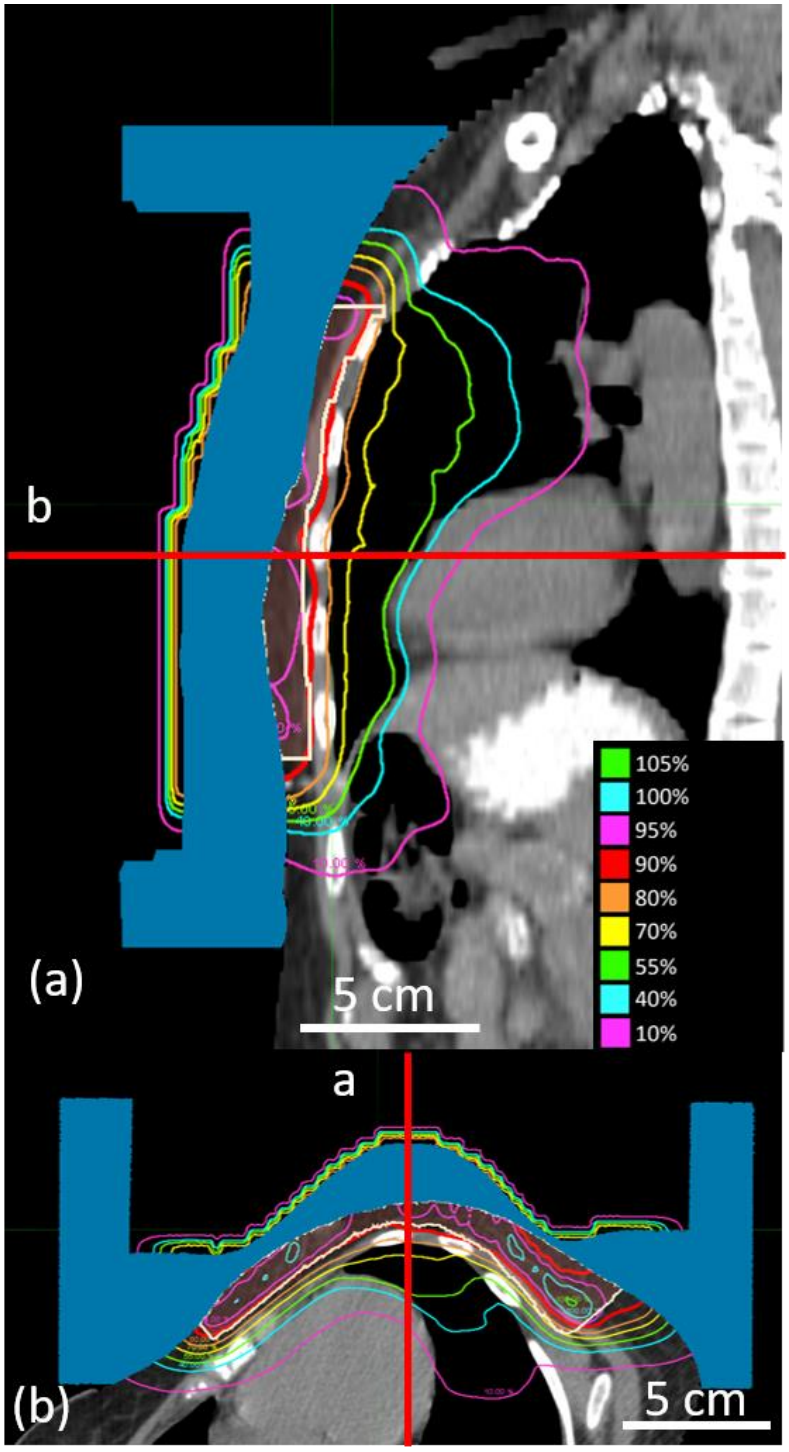

Figure 3.9. Sagittal and axial images of CW3, Plan 4. CW3 (Patient Set 1) was planned using scanned electron beams and discrete energy spacing. (a) Dose plan in the sagittal-coronal, oblique plane demarcated by the red line in figure (b)'s transverse plane; (b) Dose plan in transverse plane passing through central heart region, demarcated by red line in figure (a)'s oblique plane. Bolus is shaded blue, and PTV is outlined in white. Key shows dose values.

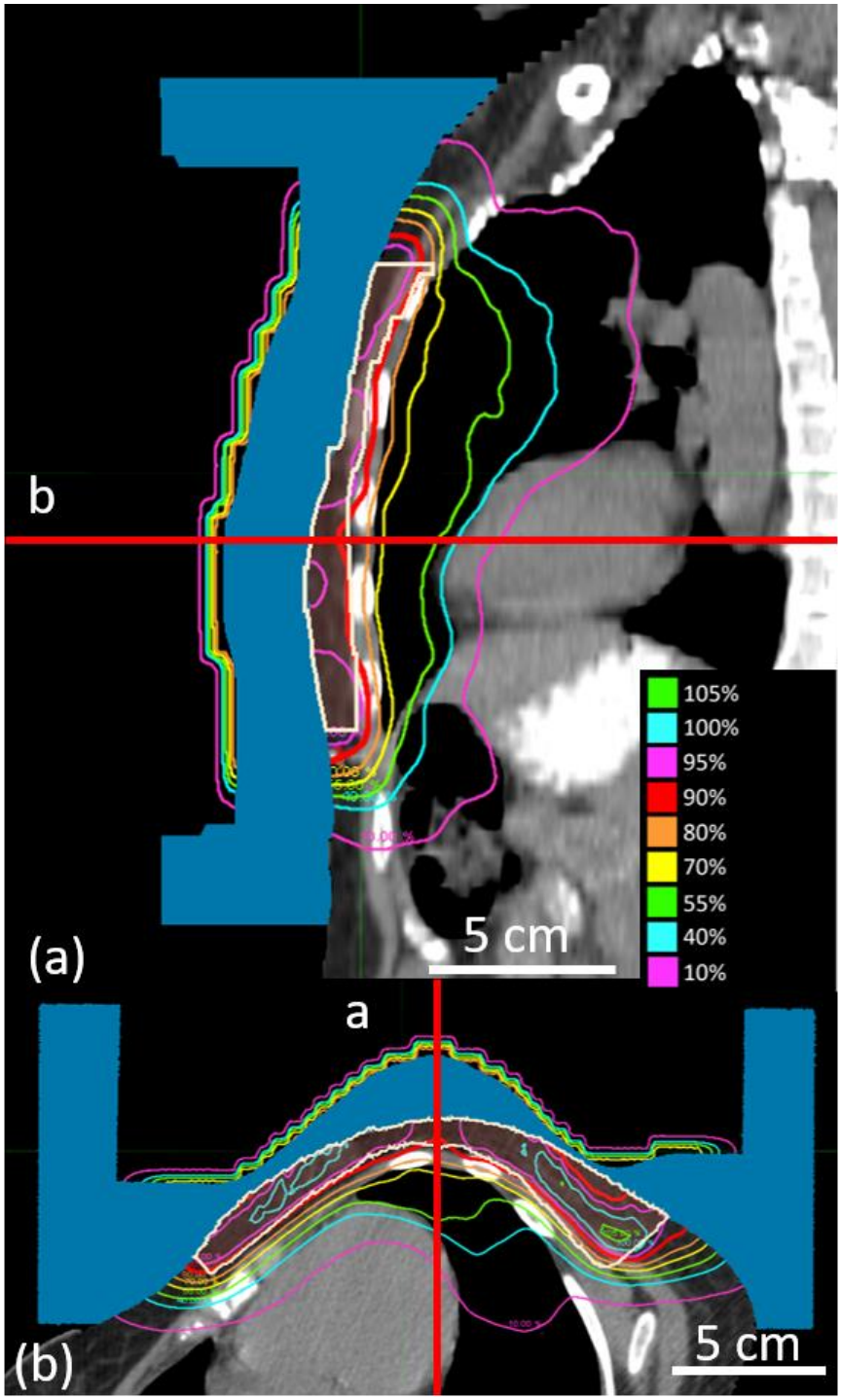

Figure 3.10. Sagittal and axial images of CW3, Plan 5. CW3 (Patient Set 1) was planned using scanned electron beams and continuous energy spacing. (a) Dose plan in the sagittal-coronal, oblique plane demarcated by the red line in figure (b)'s transverse plane; (b) Dose plan in transverse plane passing through central heart region, demarcated by red line in figure (a)'s oblique plane. Bolus is shaded blue, and PTV is outlined in white. Key shows dose values.

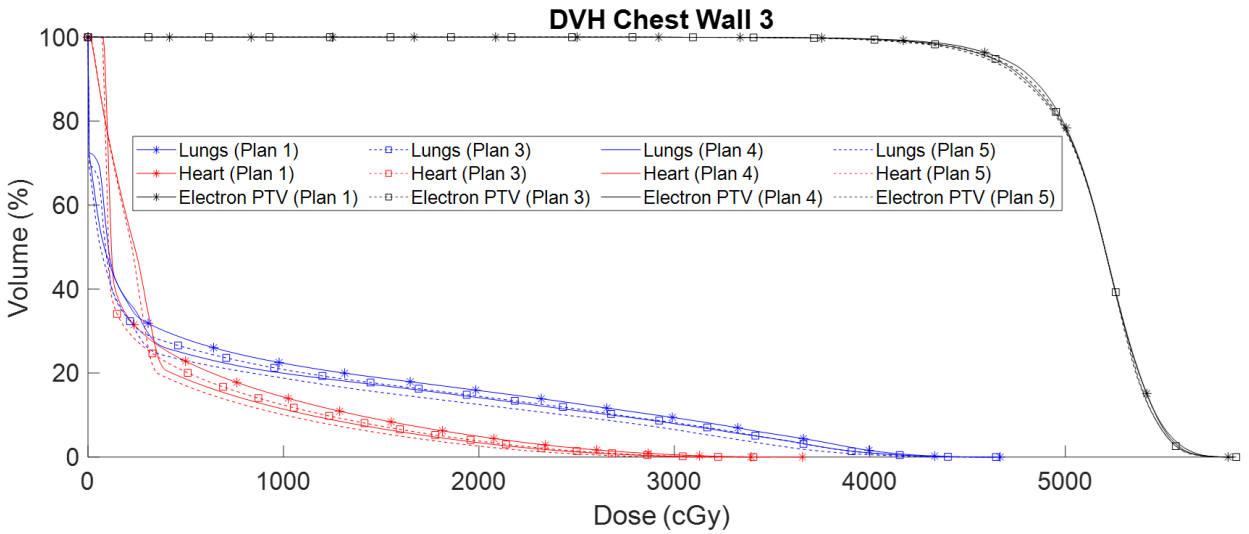

Figure 3.11. Comparison of cumulative DVH plots for CW3 (Patient Set 1) Plans. DVH plots for PTV, heart, and lung are compared for Plans 1, 3, 4, and 5, as indicated in key.

Table 3.4. Comparison of metrics for CW3 (Patient Set 1) Plans. Dose metrics are shown for PTV, heart, and lungs. NTCP and SCCP values are shown for heart and lungs.

		Plan 1	Plan 3	Plan 4	Plan 5
PTV	$D_{97\%}$ (Gy)	45.4	44.9	44.8	44.4
	$V_{47.5\ Gy}$ (%)	93.2	92.2	91.7	91.0
	Max dose (Gy)	58.3	58.8	58.6	58.6
	Mean dose (Gy)	51.6	51.6	51.6	51.5
	Std Dev (Gy)	2.7	2.8	2.9	3.0
Heart	$V_{22.5\ Gy}$ (%)	3.4	2.5	2.2	1.5
	$V_{30\ Gy}$ (%)	0.5	0.2	0.2	0.0
	Min dose (Gy)	0.7	0.7	0.0	0.1
	Max dose (Gy)	36.6	34.1	35.0	32.7
	Mean dose (Gy)	4.3	3.7	4.1	3.7
	Std Dev (Gy)	6.3	5.8	5.4	4.9
	NTCP (%)	0.1	0.1	0.1	0.03
Lungs	$V_{20\ Gy}$ (%)	15.8	14.5	14.1	12.5
	Min dose (Gy)	0.0	0.0	0.0	0.0
	Max dose (Gy)	46.7	46.5	46.4	46.3
	Mean dose (Gy)	7.0	6.4	6.2	5.6
	Std Dev (Gy)	11.6	11.1	11.0	10.3
	NTCP (%)	0.0	0.0	0.0	0.0
	$SCCP_{lin}$ (%)	11.8	10.7	10.5	9.4
	$SCCP_{lin\text{-}exp}$ (%)	2.3	2.1	2.1	2.0

3.2.1.3. Results for Patient CW6

Treatment planning results for CW6 (Patient Set 1) include isodose plots for three transverse planes and one sagittal-coronal oblique plane for Plans 1, 3, 4, and 5. All such results are shown in Appendix B, and one sagittal-coronal oblique plane and one transverse plane for each plan are shown in Figure 3.12 to Figure 3.15. DVHs for PTV, heart, and lungs for each of the four plans were computed and plotted for comparison in Figure 3.16. Dose and biologic metrics computed from the DVHs are compared in Table 3.5. These results likely have some dependence on the location of the distal PTV surface, and for CW6 the distance between the distal edge of the PTV and the distal side of the chest wall (Δt) was 0.4 cm on central axis.

PTV Coverage: Dose plots (Figure 3.12 to Figure 3.15) show that the 90% isodose lines closely cover the distal PTV surface, or in some locations, the 80% isodose line due to the large variation of thickness of the PTV in the lateral direction. Most evident at the lateral edges of the PTV, coverage could be improved by increasing the lateral margin between the PTV and field edge or by a more realistic PTV (smoother edges). The PTV DVHs are similar for all plans; $V_{47.5Gy}$ values of the scanned beams are slightly less than those of the scattered beams. Maximum doses are less than 59 Gy (<106%).

Effect of Scanned vs. Scattered Beams: Comparing Plan 1 (scattered, discrete energy 16.2 MeV beam) and Plan 4 (scanned, discrete energy 15.1 MeV beam) showed that the scanned electron beam reduced (1) mean dose to the heart by 1.9 Gy (8.3 to 6.4 Gy) and (2) V_{20} Gy to the lung by 2.0% (19.8 to 17.8%). This resulted in reduced (1) $NTCP_{heart}$ by 0.2% (0.7 to 0.5%), (2) $NTCP_{lungs}$ by 0.01% (0.03 to 0.02%), and (3) $SCCP_{lin}$ by 2.2% (15.9 to 13.7%).

Comparing Plan 3 (scattered, continuous energy 15.6 MeV beam) and Plan 5 (scanned, continuous energy 14.5 MeV beam) showed that the scanned electron beam reduced (1) mean dose to the heart by 2.0 Gy (7.8 to 5.8 Gy) and (2) V_{20Gy} to the lung by 2.4% (19.1 to 16.8%). This

resulted in reduced (1) $NTCP_{heart}$ by 0.2% (0.6 to 0.4%), (2) $NTCP_{lungs}$ by 0.00% (0.02 to 0.02%), and (3) $SCCP_{lin}$ by 2.5% (15.3 to 12.8%).

Effect of Continuous vs. Discrete Beam Energies: The same data above can be used to evaluate the benefit of continuous versus discrete energy beams. Comparing Plan 1 (scattered, discrete energy 16.2 MeV beam) with Plan 3 (scattered, continuous energy 15.6 MeV beam) showed that continuous energy beams reduced (1) mean dose to the heart by 0.5 Gy (8.3 to 7.8 Gy) and (2) V_{20Gy} to the lung by 0.7% (19.8 to 19.1%). This resulted in reduced (1) $NTCP_{heart}$ by 0.1% (0.7 to 0.6%), (2) $NTCP_{lungs}$ by 0.01% (0.03 to 0.02%), and (3) $SCCP_{lin}$ by 0.6% (15.9% to 15.3%).

Comparing Plan 4 (scanned, discrete energy 15.1 MeV beam) with Plan 5 (scanned, continuous energy 14.5 MeV beam) showed that continuous energy beams reduced (1) mean dose to the heart by 0.7 Gy (6.4 to 5.8 Gy) and (2) V_{20Gy} to the lung by 1.0% (17.8 to 16.8%). This resulted in reduced (1) $NTCP_{heart}$ by 0.09% (0.5 to 0.4%), (2) $NTCP_{lungs}$ by 0.00% (0.02 to 0.02%), and (3) $SCCP_{lin}$ by 0.9% (13.7 to 12.8%).

Effect of Scanned, Continuous Energy Beams vs. Scattered, Discrete Energy Beams: The greatest plan improvement was comparing Plan 1 (scattered, discrete energy 16.2 MeV beam), current technology, with Plan 5 (scanned, continuous energy 14.5 MeV beam), possible future technology. This reduced (1) mean dose to the heart by 2.5 Gy (8.3 to 5.8 Gy) and (2) V_{20Gy} to the lung by 3.0% (19.8 to 16.8%). This resulted in reduced (1) $NTCP_{heart}$ by 0.3% (0.7 to 0.4%), (2) $NTCP_{lungs}$ by 0.01% (0.03 to 0.02%), and (3) $SCCP_{lin}$ by 3.1% (15.9% to 12.8%).

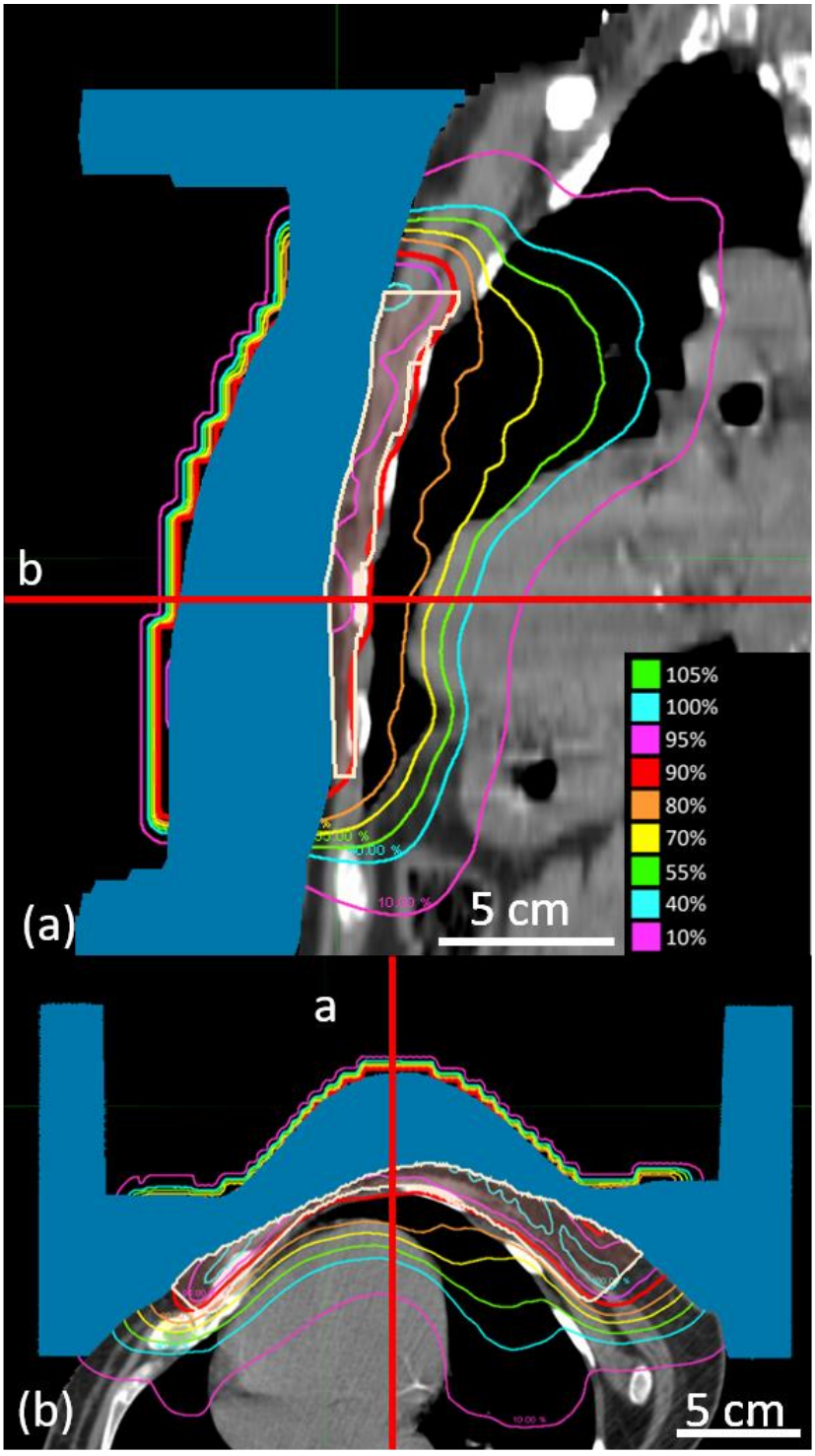

Figure 3.12. Sagittal and axial images of CW6, Plan 1. CW6 (Patient Set 1) was planned using scattered electron beams and discrete energy spacing. (a) Dose plan in the sagittal-coronal, oblique plane demarcated by the red line in figure (b)'s transverse plane; (b) Dose plan in transverse plane passing through central heart region, demarcated by red line in figure (a)'s oblique plane. Bolus is shaded blue, and PTV is outlined in white. Key shows dose values.

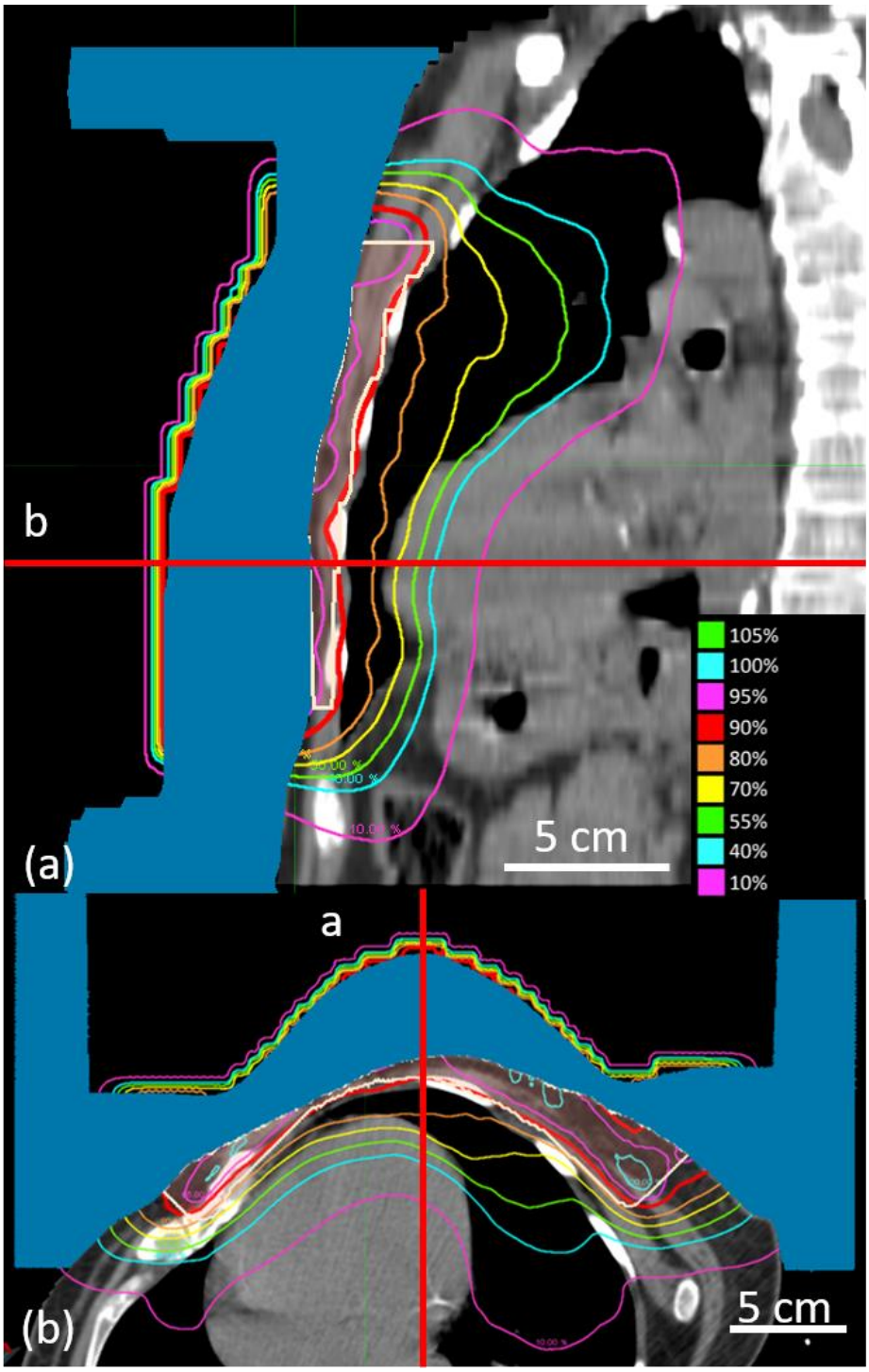

Figure 3.13. Sagittal and axial images of CW6, Plan 3. CW6 (Patient Set 1) was planned using scattered electron beams and continuous energy spacing. (a) Dose plan in the sagittal-coronal, oblique plane demarcated by the red line in figure (b)'s transverse plane; (b) Dose plan in transverse plane passing through central heart region, demarcated by red line in figure (a)'s oblique plane. Bolus is shaded blue, and PTV is outlined in white. Key shows dose values.

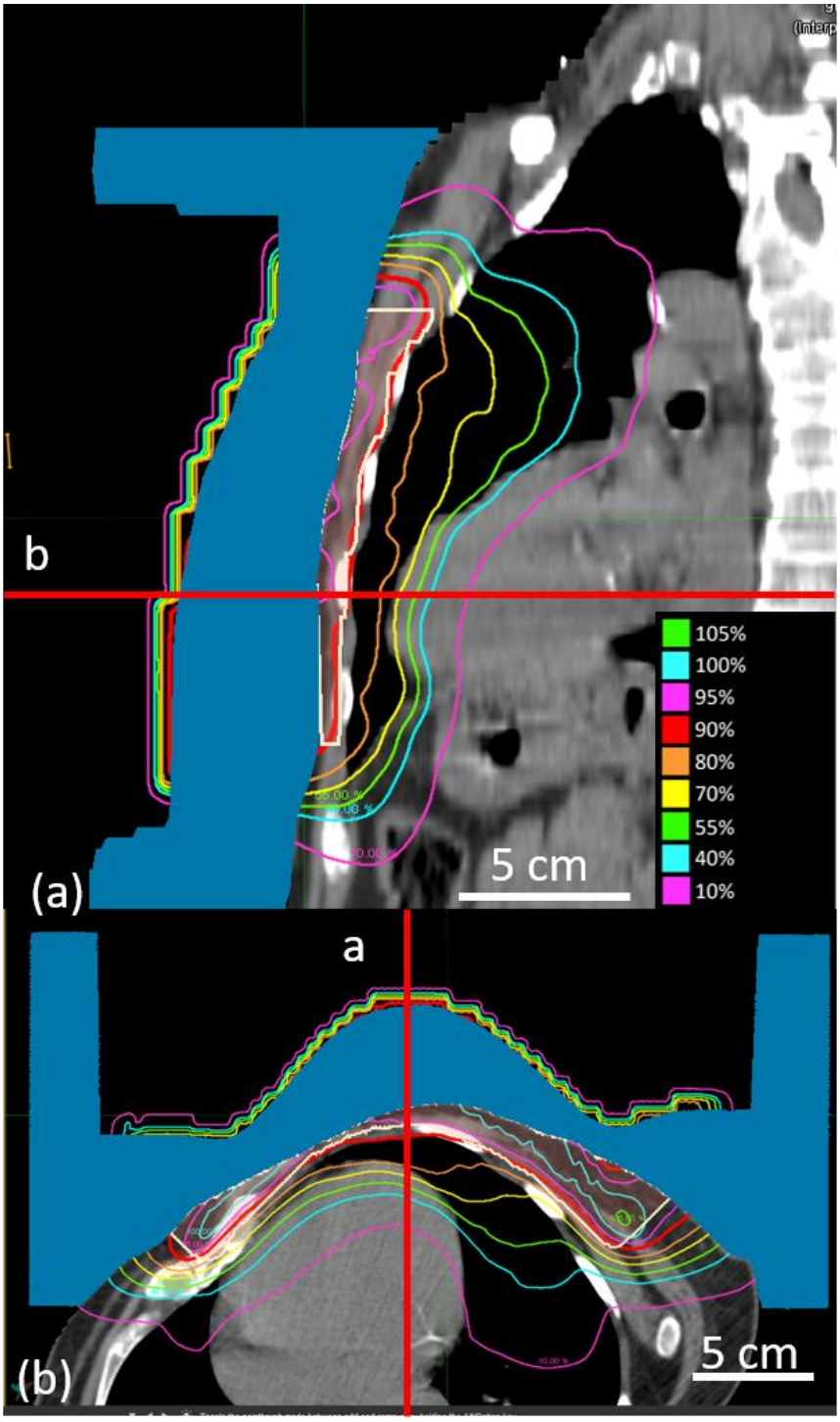

Figure 3.14. Sagittal and axial images of CW6, Plan 4. CW6 (Patient Set 1) was planned using scanned electron beams and discrete energy spacing. (a) Dose plan in the sagittal-coronal, oblique plane demarcated by the red line in figure (b)'s transverse plane; (b) Dose plan in transverse plane passing through central heart region, demarcated by red line in figure (a)'s oblique plane. Bolus is shaded blue, and PTV is outlined in white. Key shows dose values.

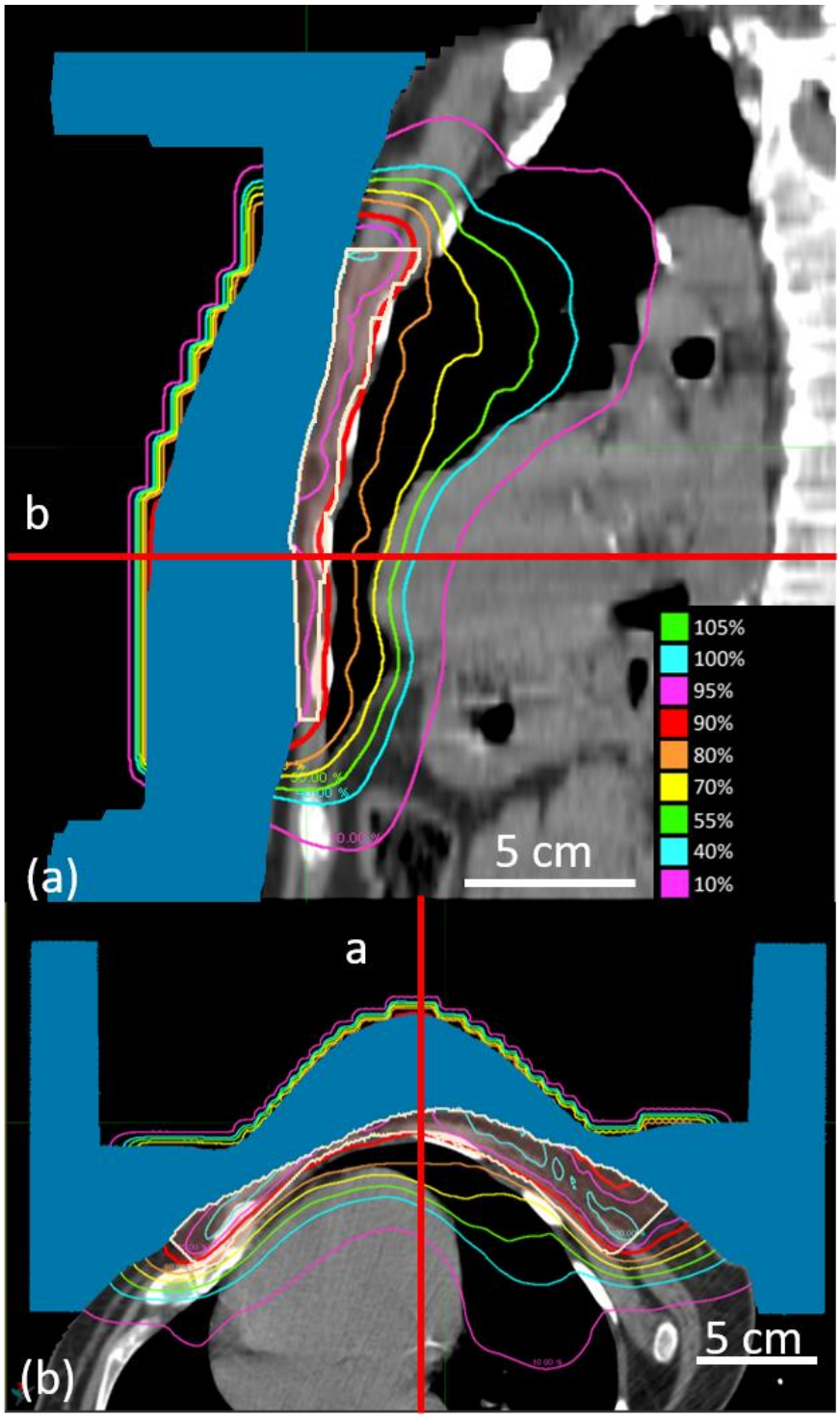

Figure 3.15. Sagittal and axial images of CW6, Plan 5. CW6 (Patient Set 1) was planned using scanned electron beams and continuous energy spacing. (a) Dose plan in the sagittal-coronal, oblique plane demarcated by the red line in figure (b)'s transverse plane; (b) Dose plan in transverse plane passing through central heart region, demarcated by red line in figure (a)'s oblique plane. Bolus is shaded blue, and PTV is outlined in white. Key shows dose values.

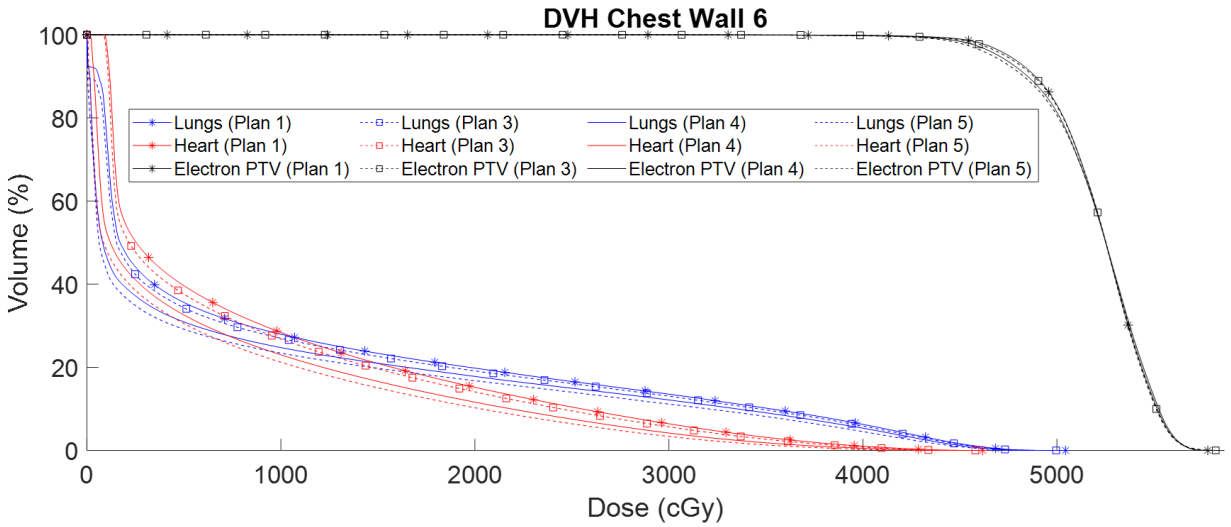

Figure 3.16. Comparison of cumulative DVH plots for CW6 (Patient Set 1) Plans. DVH plots for PTV, heart, and lung are compared for Plans 1, 3, 4, and 5, as indicated in key.

Table 3.5. Comparison of metrics for CW6 (Patient Set 1) Plans. Dose metrics are shown for PTV, heart, and lungs. NTCP and SCCP values are shown for heart and lungs.

		Plan 1	Plan 3	Plan 4	Plan 5
PTV	$D_{97\%}$ (Gy)	46.7	46.4	46.2	45.8
	$V_{47.5\ Gy}$ (%)	95.0	94.5	93.5	92.7
	Max dose (Gy)	57.8	58.2	57.9	58.6
	Mean dose (Gy)	52.2	52.2	52.1	52.0
	Std Dev (Gy)	2.6	2.6	2.8	2.8
Heart	$V_{22.5\ Gy}$ (%)	12.7	11.7	9.5	8.2
	$V_{30\ Gy}$ (%)	6.4	5.7	4.2	3.4
	Min dose (Gy)	0.9	0.8	0.2	0.0
	Max dose (Gy)	46.2	45.8	45.6	44.3
	Mean dose (Gy)	8.3	7.8	6.4	5.8
	Std Dev (Gy)	10.3	10.0	9.4	9.0
	NTCP (%)	0.7	0.6	0.5	0.4
Lungs	$V_{20\ Gy}$ (%)	19.8	19.1	17.8	16.8
	Min dose (Gy)	0.0	0.0	0.0	0.0
	Max dose (Gy)	50.4	50.0	49.9	49.3
	Mean dose (Gy)	9.5	9.1	8.2	7.6
	Std Dev (Gy)	13.5	13.4	13.2	12.8
	NTCP (%)	0.03	0.02	0.02	0.02
	$SCCP_{lin}$ (%)	15.9	15.3	13.7	12.8
	$SCCP_{lin\text{-}exp}$ (%)	3.0	2.8	2.3	12.8

3.2.2. Results for Patient Set 2

Plan comparisons for Patient Set 2 (CW2, CW4, CW7, and CW8) were more complex that those of Patient Set 1 because this study had no criteria for optimizing the location of the abutting edge of the lower field (greatest impact on heart dose) and upper fields (greatest impact on lung dose). For the scattered beams, Plan 1 placed the abutting edge as far superior as allowed for the minimum energy that could be used for the lower field. This likely represents the best plan that could be created when using scattered, discrete energy beams, which is the only plan deliverable with currently available radiotherapy accelerator technology. Plan 2 uses the same lower field as Plan 1, but assumes scattered, continuous energy beams for the upper field. Plan 3, which assumes scattered, continuous energy beams for both the lower and upper fields, places the edge at the superior aspect of the heart. The optimal location of the abutting edge is somewhere between that of Plans 2 and 3; however, no effort was made to determine that location in the current study. For such optimization, the tradeoff between heart dose and lung dose must be specified.

Plans 4 and 5 used scanned, discrete energy beams and scanned, continuous energy beams, respectively with the same field placements as Plans 1 and 3, respectively. Therefore, the impact of scanned beams was evaluated comparing Plans 1 with Plan 4 for discrete beam energies and Plan 3 with Plan 5 for continuous beam energies.

The impact of continuous energy beams was evaluated comparing Plan 1 with Plan 2 or Plan 3 (used scattered beams), whichever best, and Plan 4 with Plan 5 (used scanned beams). The latter comparison is not optimal, as abutting edges of Plan 4 and Plan 5 were different, and a Plan 6 with the same edge location as Plan 4 might have been useful.

As results will show, placing the abutting edge at the superior aspect of the heart (Plans 3 and 5) resulted in higher lung doses, due to the upper field being larger than the other beam arrangement, and higher heart doses, apparently due to the wider penumbra of the upper, higher

energy field. The effect of this will be seen in the patient results to follow. Therefore, it is not meaningful to compare any two plans to demonstrate the benefit of using scanned, continuous energy beams overs scattered, discrete energy beams as was done for Patient Set 1.

3.2.2.1. Results for Patient CW2

Treatment planning results for CW2 (Patient Set 2) include isodose plots for three transverse planes and one sagittal-coronal oblique plane for Plans 1 to 5. All such results are shown in Appendix B, and one sagittal-coronal oblique plane and one transverse plane for each plan are shown in Figure 3.17 to Figure 3.21. DVHs for PTV, heart, and lungs for each of the five dose plans were computed and plotted for comparison in Figure 3.22. Dose and biologic metrics computed from these DVHs are compared in Table 3.6. These results likely have some dependence on the location of the distal PTV surface, and the CW2 distance between the distal edge of the PTV and the distal side of the chest wall (Δt) was 1.2 cm on central axis.

PTV Coverage: Dose plots (Figure 3.17 to Figure 3.21) show that the 90% isodose lines closely cover the distal PTV surface, or in some locations the 80% isodose surface due to the jagged nature of the PTV. Most evident at the lateral edges of the PTV, coverage could be improved by increasing the lateral margin between the PTV and field edge or by a more realistic PTV (smoother edges). The PTV DVHs are similar for all plans; however, $V_{47.5\ Gy}$ values of Plans 3 and 5, which have the field arrangement used for the continuous energy beam (see Figure 2.3) are slightly greater than those of Plans 1, 2, and 4, which use a different field arrangement (see Figure 2.2). Although maximum doses are as large as approximately 65 Gy (117%), no significant volume receives more than 61 Gy (110%).

Effect of Scanned vs. Scattered Beams: Comparing Plan 1 (scattered, discrete energy beams, upper 16.2 MeV and lower 13.0 MeV) and Plan 4 (scanned, discrete energy beams, upper 15.1 MeV and lower 12.2 MeV) showed that the scanned electron beam reduced (1) mean dose to

the heart by 0.7 Gy (4.6 to 3.9 Gy) and (2) V_{20} Gy to the lungs by 2.5% (13.0 to 10.5%). This resulted in reduced (1) $NTCP_{heart}$ by 0.5% (0.9 to 0.40%), (2) $NTCP_{lungs}$ by 0.3% (1.4 to 1.0%), and (3) $SCCP_{lin}$ by 2.2% (11.0 to 8.9%).

Comparing Plan 3 (scattered, continuous energy beams, upper 15.9 MeV and lower 13.0 MeV) and Plan 5 (scanned, continuous energy beams, upper 14.8 MeV and lower 12.2 MeV) showed that the scanned electron beam reduced (1) mean dose to the heart by 2.6 Gy (8.1 to 5.5 Gy) and (2) V_{20Gy} to the lungs by 3.6% (22.2 to 18.6%). This resulted in reduced (1) $NTCP_{heart}$ by 0.2% (0.3 to 0.1%), (2) $NTCP_{lungs}$ by 1.2% (3.5 to 2.3%), and (3) $SCCP_{lin}$ by 3.5% (18.4 to 14.9%).

Effect of Continuous vs. Discrete Beam Energies: The same data above can be used to evaluate the benefit of continuous versus discrete energy beams. Comparing Plan 2 (scattered, continuous energy beams, upper 15.9 MeV and discrete energy lower 13.0 MeV beam) with Plan 3 (scattered, continuous energy beams, upper 15.9 MeV and lower 13.0 MeV) showed Plan 2 to have lower heart and lung dose because of the beam arrangements. Therefore, Plan 2, compared to Plan 1 (scattered, discrete energy beams, upper 16.2 MeV and lower 13.0 MeV), shows (1) similar mean dose to the heart (4.6 Gy) and (2) $V_{20\ Gy}$ to the lungs reduced slightly by 0.2% (13.0 to 12.8%). This resulted in (1) equal $NTCP_{heart}$ of 0.9%, (2) $NTCP_{lungs}$ reduced slightly by 0.03% (1.4 to 1.4%), and (3) $SCCP_{lin}$ reduced slightly by 0.2% (11.0% to 10.8%).

Comparing Plan 4 (scanned, discrete energy beams, upper 15.1 MeV and lower 12.2 MeV) with Plan 5 (scanned, continuous energy beams, upper 14.8 MeV and lower 12.2 MeV) showed no advantage to continuous energy. Rather, it showed the advantage of the field arrangement for Plan 4, as Plan 5 increased (1) mean dose to the heart by 1.6 Gy (3.9 to 5.5 Gy) and (2) $V_{20\ Gy}$ to the lung by 8.2% (10.5 to 18.6%). In addition, this resulted in increased (1) $NTCP_{heart}$ by 0.3% (0.40 to 0.1%), (2) $NTCP_{lungs}$ by 1.3% (1.0 to 2.3%), and (3) $SCCP_{lin}$ by 6.0% (8.9% to 14.9%).

Summary: Results showed that scanned electron beams modestly reduced heart and lung dose and their biologic effect. NTCP changes were not likely significant because of their already low value for scattered beams, which was attributed to CW2 PTV requiring only 12.5±0.5 MeV (over heart) and 15.5±0.7 MeV (over lung) beams. Continuous energy beams showed insignificant improvement over discrete energy beams, because the discrete energies available were already near optimal. More significant was the location of the edge of abutting beams, indicating the need for optimizing its location in future studies.

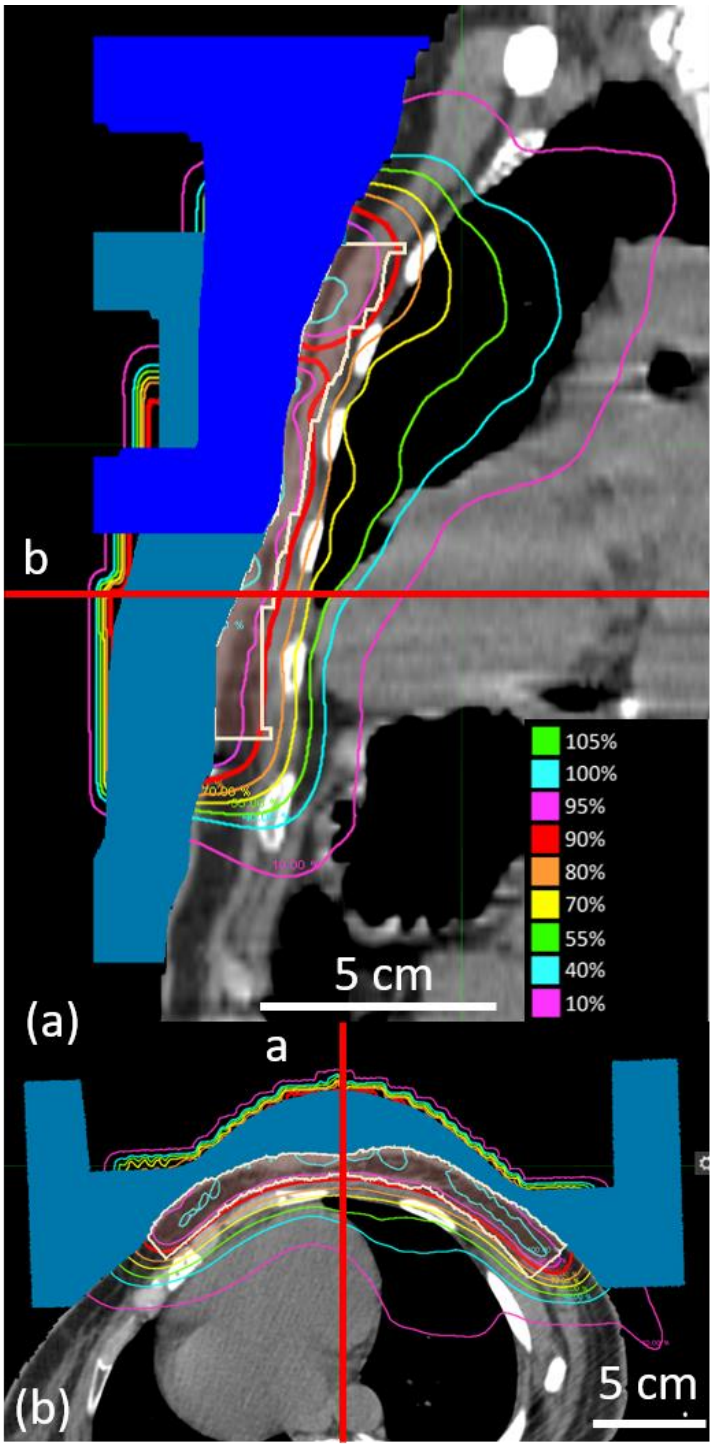

Figure 3.17. Sagittal and axial images of CW2, Plan 1. CW2 (Patient Set 2) was planned using scattered electron beams and discrete energy spacing. (a) Dose plan in the sagittal-coronal, oblique plane demarcated by the red line in figure (b)'s transverse plane; (b) Dose plan in transverse plane passing through central heart region, demarcated by red line in figure (a)'s oblique plane. Upper bolus is shaded dark blue, lower bolus is shaded light blue, and PTV is outlined in white. Key shows dose values.

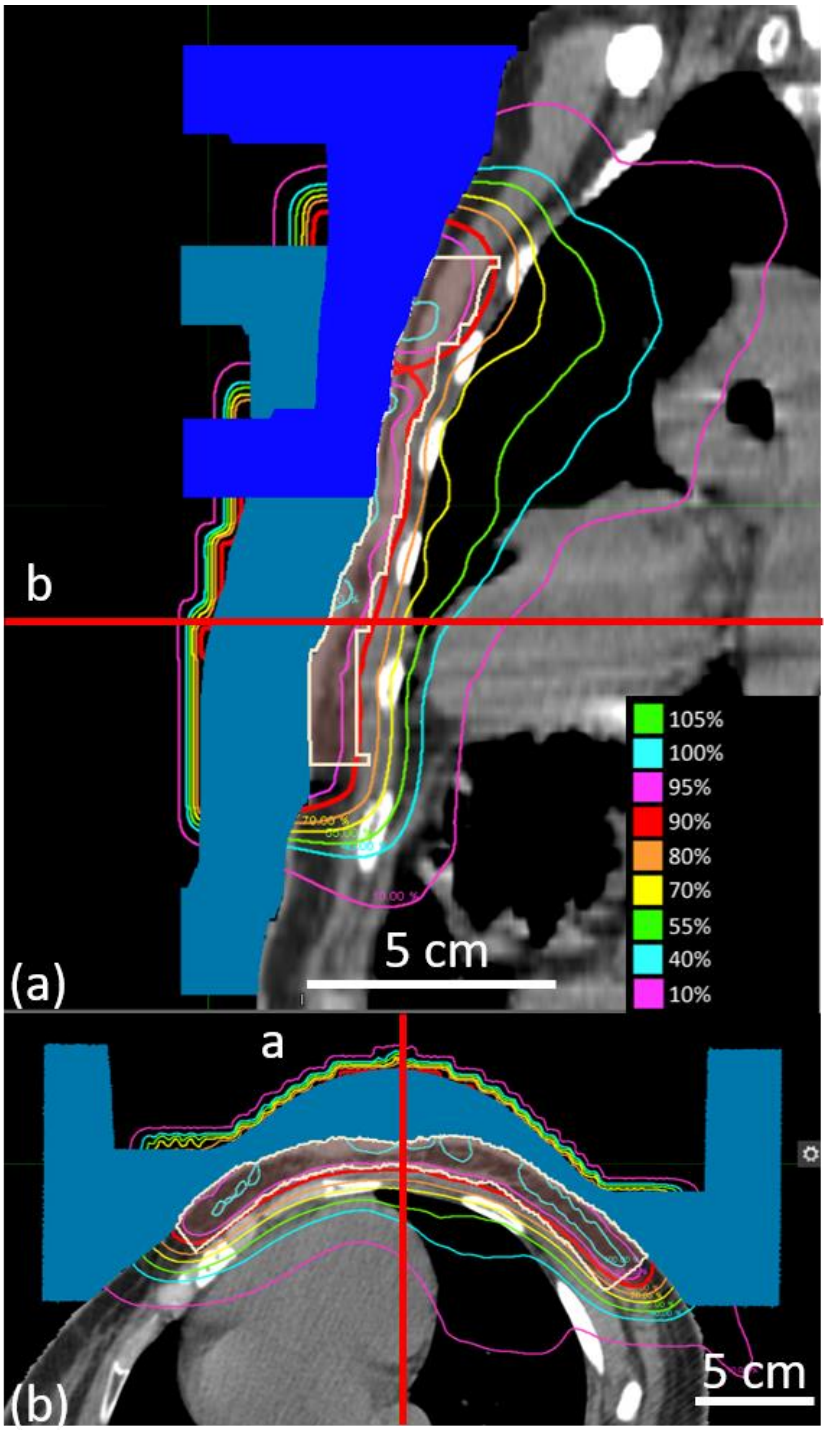

Figure 3.18. Sagittal and axial images of CW2, Plan 2. CW2 (Patient Set 2) was planned using scattered electron beams, discrete energy spacing (lower field), and continuous energy spacing (upper field). (a) Dose plan in the sagittal-coronal, oblique plane demarcated by the red line in figure (b)'s transverse plane; (b) Dose plan in transverse plane passing through central heart region, demarcated by red line in figure (a)'s oblique plane. Upper bolus is shaded dark blue, lower bolus is shaded light blue, and PTV is outlined in white. Key shows dose values.

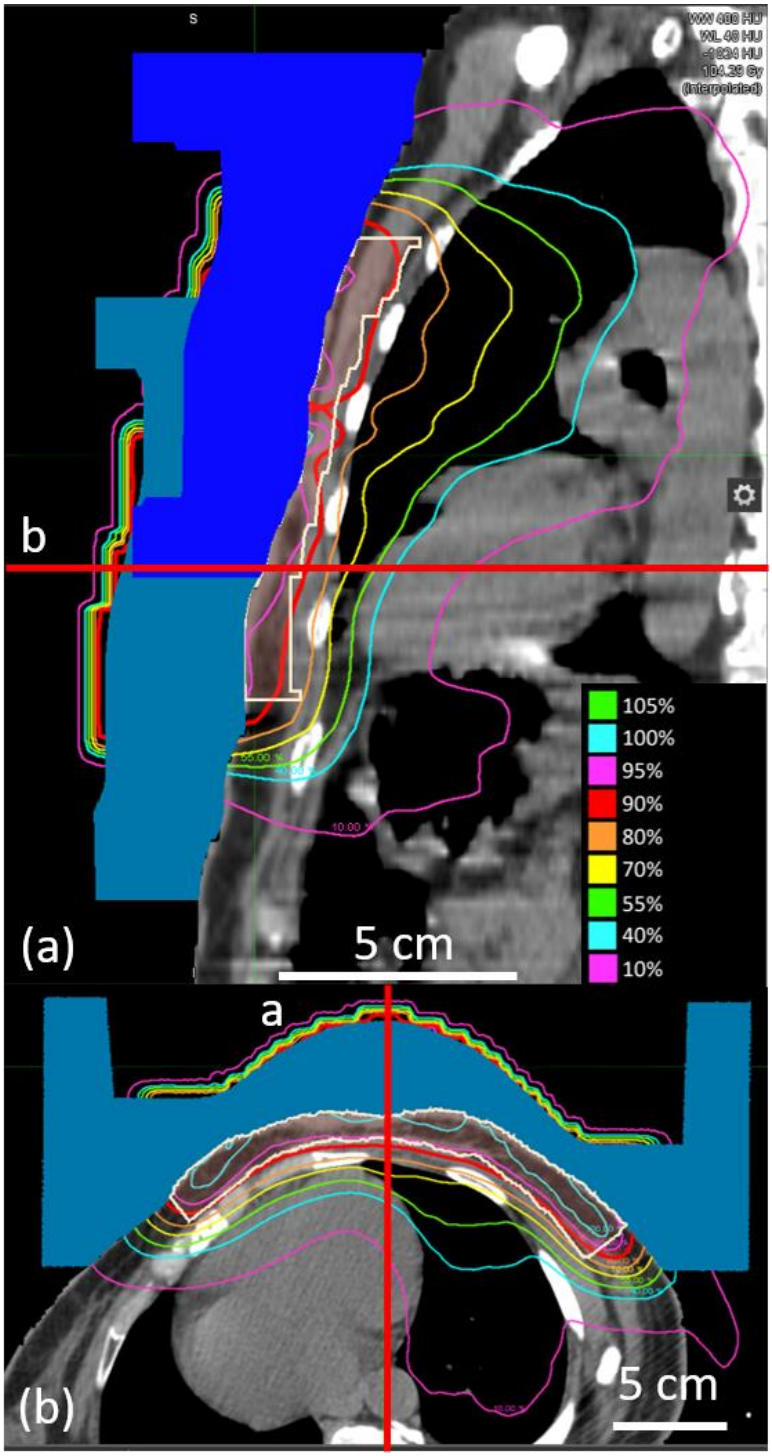

Figure 3.19. Sagittal and axial images of CW2, Plan 3. CW2 (Patient Set 2) was planned using scattered electron beams and continuous energy spacing. (a) Dose plan in the sagittal-coronal, oblique plane demarcated by the red line in figure (b)'s transverse plane; (b) Dose plan in transverse plane passing through central heart region, demarcated by red line in figure (a)'s oblique plane. Upper bolus is shaded dark blue, lower bolus is shaded light blue, and PTV is outlined in white. Key shows dose values.

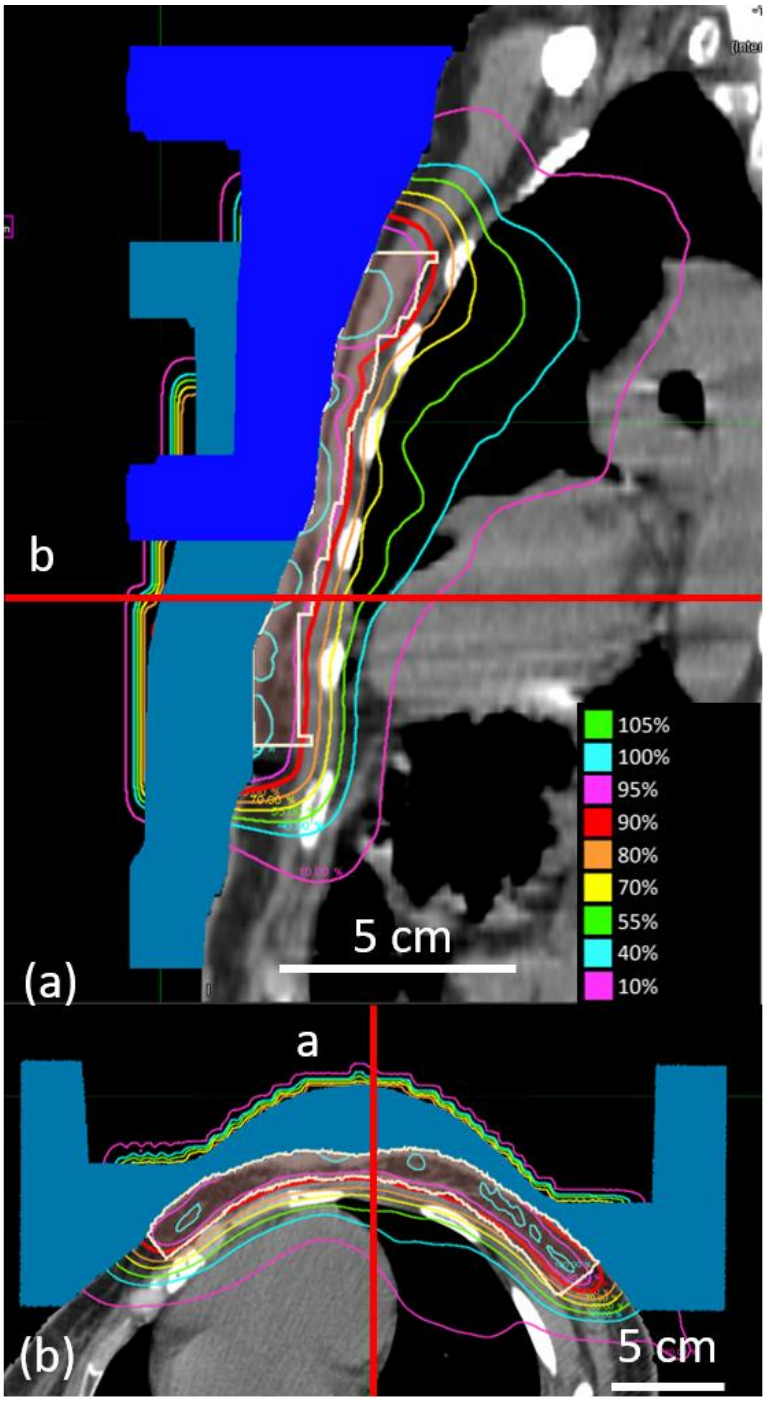

Figure 3.20. Sagittal and axial images of CW2, Plan 4. CW2 (Patient Set 2) was planned using scanned electron beams and discrete energy spacing. (a) Dose plan in the sagittal-coronal, oblique plane demarcated by the red line in figure (b)'s transverse plane; (b) Dose plan in transverse plane passing through central heart region, demarcated by red line in figure (a)'s oblique plane. Upper bolus is shaded dark blue, lower bolus is shaded light blue, and PTV is outlined in white. Key shows dose values.

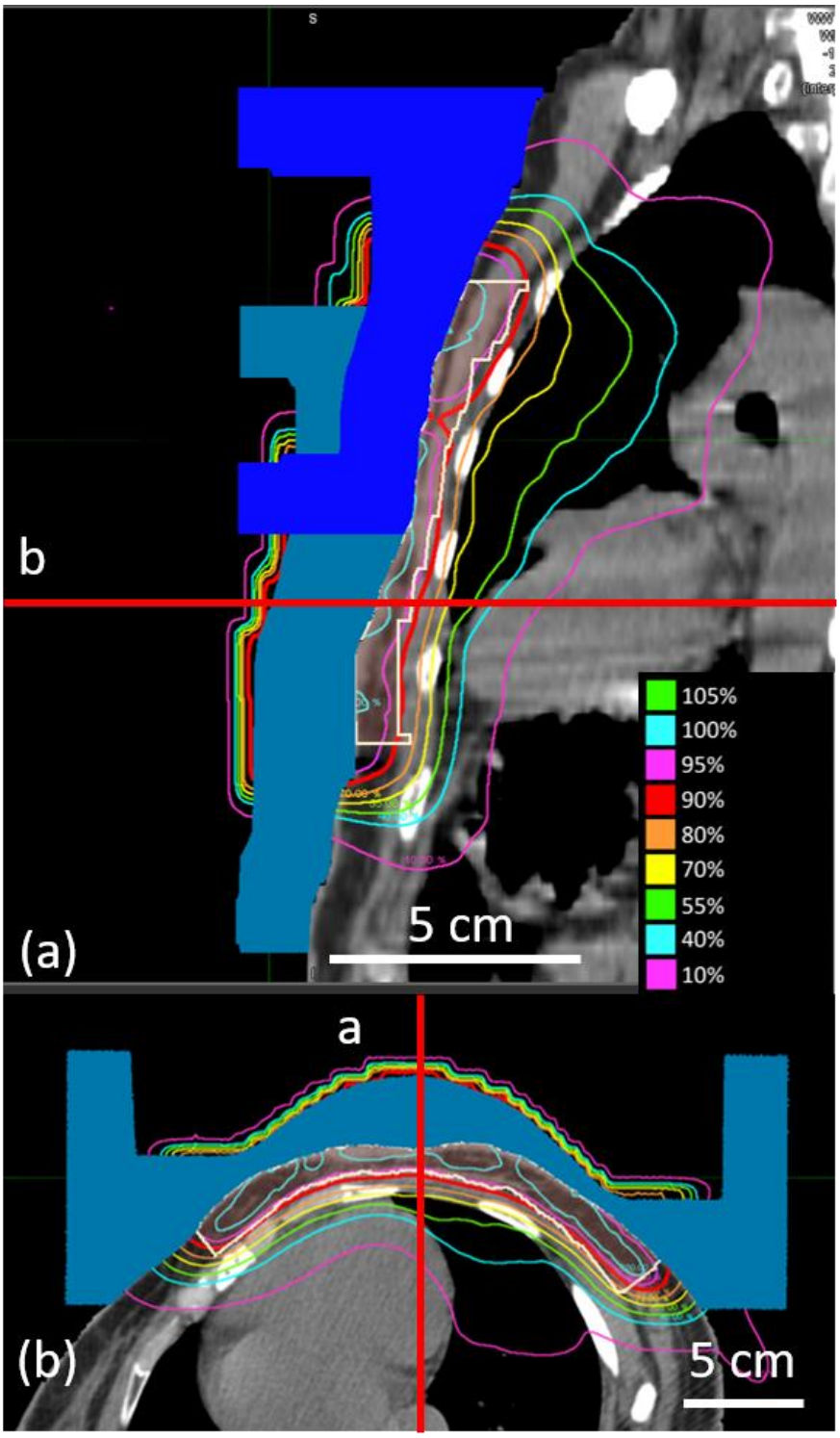

Figure 3.21. Sagittal and axial images of CW2, Plan 5. CW2 (Patient Set 2) was planned using scanned electron beams and continuous energy spacing. (a) Dose plan in the sagittal-coronal, oblique plane demarcated by the red line in figure (b)'s transverse plane; (b) Dose plan in transverse plane passing through central heart region, demarcated by red line in figure (a)'s oblique plane. Bolus is shaded blue, and PTV is outlined in white. Key shows dose values.

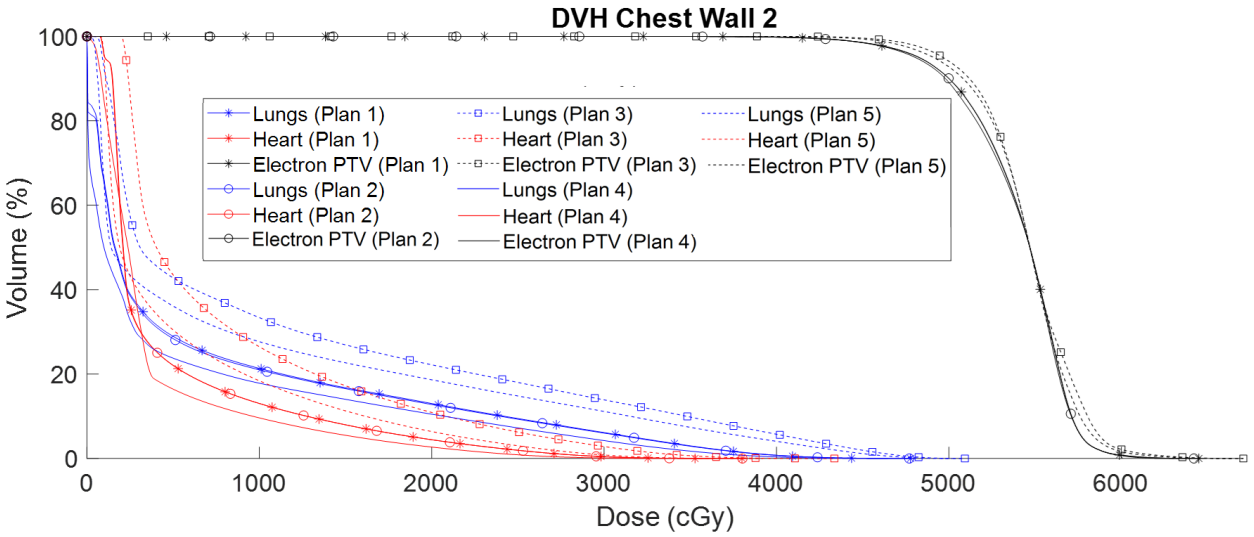

Figure 3.22. Comparison of cumulative DVH plots for CW2 (Patient Set 2) Plans. DVH plots for PTV, heart, and lung are compared for Plans 1, 2, 3, 4, and 5, as indicated in key.

Table 3.6. Comparison of metrics for CW2 (Patient Set 2) Plans. Dose metrics are shown for PTV, heart, and lungs. NTCP and SCCP values are shown for heart and lungs.

		Plan 1	Plan 2	Plan 3	Plan 4	Plan 5
PTV	$D_{97\%}$ (Gy)	46.9	46.9	48.2	46.3	47.4
	$V_{47.5\ Gy}$ (%)	96.3	96.3	98.4	96.0	97.6
	Max dose (Gy)	64.5	64.2	67.1	63.0	66.4
	Mean dose (Gy)	54.0	54.0	54.6	54.0	54.4
	Std Dev (Gy)	3.1	3.1	2.9	3.1	2.9
Heart	$V_{22.5\ Gy}$ (%)	3.1	3.1	8.4	1.7	4.6
	$V_{30\ Gy}$ (%)	0.4	0.4	2.8	0.1	0.8
	Min dose (Gy)	0.7	0.7	2.0	0.1	0.7
	Max dose (Gy)	38.0	38.0	43.4	36.1	39.2
	Mean dose (Gy)	4.6	4.6	8.1	3.9	5.5
	Std Dev (Gy)	5.8	5.8	8.0	4.9	6.9
	NTCP (%)	0.9	0.9	0.3	0.4	0.1
Lungs	$V_{20\ Gy}$ (%)	13.0	12.8	22.2	10.5	18.6
	Min dose (Gy)	0.0	0.0	0.0	0.0	0.0
	Max dose (Gy)	47.8	47.7	50.9	46.5	50.2
	Mean dose (Gy)	6.6	6.5	10.9	5.3	8.8
	Std Dev (Gy)	10.1	10.1	13.3	9.2	12.6
	NTCP (%)	1.4	1.4	3.5	1.0	2.3
	$SCCP_{lin}$ (%)	11.0	10.8	18.4	8.9	14.9
	$SCCP_{lin\text{-}exp}$ (%)	2.9	2.8	3.8	2.3	3.0

3.2.2.2. Results for Patient CW4

Treatment planning results for CW4 (Patient Set 2) include isodose plots for three transverse planes and one sagittal-coronal oblique plane for Plans 1 to 5. However, Plans 1 and 2 are identical as the optimal, continuous energy for the upper field was the same as the discrete energy used in Plan 1. All such results are shown in Appendix B, and one sagittal-coronal oblique plane and one transverse plane for each plan are shown Figure 3.23 to Figure 3.26. DVHs for PTV, heart, and lungs for each of the five dose plans were computed and plotted for comparison in Figure 3.27. Dose and biologic metrics computed from these DVHs are compared in Table 3.7. These results likely have some dependence on the location of the distal PTV surface, and the CW4 distance between the distal edge of the PTV and the distal side of the chest wall (Δt) was 1.9 cm on central axis.

PTV Coverage: Dose plots (Figure 3.23 to Figure 3.26) show that the 90% isodose lines closely cover the distal PTV surface, or in some locations the 80% isodose surface due to the jagged nature of the PTV. Most evident at the lateral edges of the PTV, coverage could be improved by increasing the lateral margin between the PTV and field edge or by a more realistic PTV (smoother edges). The PTV DVHs are similar for all plans; however, $V_{47.5\ Gy}$ values of Plans 1 and 2 (≈95%), which use scattered beams are greater than those for Plans 3 and 5 (≈91%). This is possibly due to the different dose distributions given by the scanned and scattered beams, as well as the different field arrangements. Although maximum doses are as large as approximately 66 Gy (119%), no significant volume receives more than 59 Gy (105%).

Effect of Scanned vs. Scattered Beams: Comparing Plan 1 (scattered, discrete energy beams, upper 21.3 MeV and lower 16.2 MeV) and Plan 4 (scanned, discrete energy beams, upper 18.4 MeV and lower 15.1 MeV) showed that the scanned electron beam reduced (1) mean dose to the heart by 1.4 Gy (3.8 to 2.4 Gy) and (2) V_{20} Gy to the lungs by 2.5% (11.8 to 9.2%). This

resulted in insignificant reduction to (1) $NTCP_{heart}$ by 0.01% (0.01 to 0.00%) and (2) $NTCP_{lungs}$ by 0.00% (0.01 to 0.01%), because of their already low values, and reduction to (3) $SCCP_{lin}$ by 2.8% (10.9 to 8.1%).

Comparing Plan 3 (scattered, continuous energy beams, upper 21.3 MeV and lower 16.2 MeV) and Plan 5 (scanned, continuous energy beams, upper 18.4 MeV and lower 15.1 MeV) showed that the scanned electron beam reduced (1) mean dose to the heart by 1.2 Gy (3.6 to 2.4 Gy) and (2) V_{20Gy} to the lung by 1.6% (11.7 to 10.1%). This resulted in insignificant reduction to (1) $NTCP_{heart}$ by 0.01% (0.01 to 0.00%) and (2) $NTCP_{lungs}$ by 0.00% (0.01 to 0.01%), because of their already low values, and reduction to (3) $SCCP_{lin}$ by 1.9% (10.7 to 8.8%).

Effect of Continuous vs. Discrete Beam Energies: For Plan 2, the optimal continuous energy for the upper beam was identical to the discrete energy used in Plan 1. Thus, Plan 1 and Plan 2 are identical. The optimal continuous energy for all beams in Plans 2, 3, and 5 were the same as the discrete energies for the beams in Plans 1 and 4. Thus, no conclusions can be drawn about the effect of using continuous vs. discrete energy spacing for this patient, CW4.

Impact of Location of Edges of Abutting Beams: Comparing Plan 2 (scattered, continuous energy beams, upper 21.3 MeV and discrete energy lower 16.2 MeV beam) with Plan 3 (scattered, continuous energy beams, upper 21.3 MeV and lower 16.2 MeV) showed Plan 2 to have essentially identical heart and lung dose due to the boundaries given to the upper and lower PTVs, but slightly lower $SCCP_{lin}$. Therefore, Plan 3, compared to Plan 1 (scattered, discrete energy beams, upper 21.3 MeV and lower 16.2 MeV), shows small reduced (1) mean dose to the heart by 0.2 Gy (3.8 to 3.6 Gy) and (2) $V_{20\,Gy}$ to the lung reduced slightly by 0.08% (11.8 to 11.7%). This resulted in (1) equal $NTCP_{heart}$ of 0.01%, (2) equal $NTCP_{lungs}$ 0.01%, and (3) $SCCP_{lin}$ reduced slightly by 0.2% (10.9%

to 10.7%). These differences are due to the location of the edge of abutting beams, as the energies used for each comparison are identical.

Comparing Plan 4 (scanned, discrete energy beams, upper 18.4 MeV and lower 15.1 MeV) with Plan 5 (scanned, continuous energy beams, upper 18.4 MeV and lower 15.1 MeV) showed no advantage to continuous energy; none would be expected since the selected discrete energies were the same as continuous ones. Rather, it showed the advantage of the field arrangement (abutment location) for Plan 4, as Plan 5 (1) had equal mean dose to the heart (2.4 Gy), but (2) increased $V_{20\ Gy}$ to the lung by 0.9% (9.2 to 10.1%). This resulted in (1) identical $NTCP_{heart}$ of 0.00%, (2) identical $NTCP_{lungs}$ of 0.01%, and (3) increased $SCCP_{lin}$ by 0.7% (8.1% to 8.8%).

Summary: Results showed that scanned electron beams slightly reduced heart and lung dose and their biologic effect. NTCP changes were not likely significant because of their already low value for scattered beams, which was attributed to the larger separation (1.9 cm) between the PTV and distal chest wall. Improvement of continuous energy beams over discrete energy beams was unable to be evaluated for CW4. Also, the location of the edge of abutting beams had little effect, due to the already low normal tissue doses and biologic effects. This is likely due to the larger separation between the distal PTV surface and the distal chest wall on central axis.

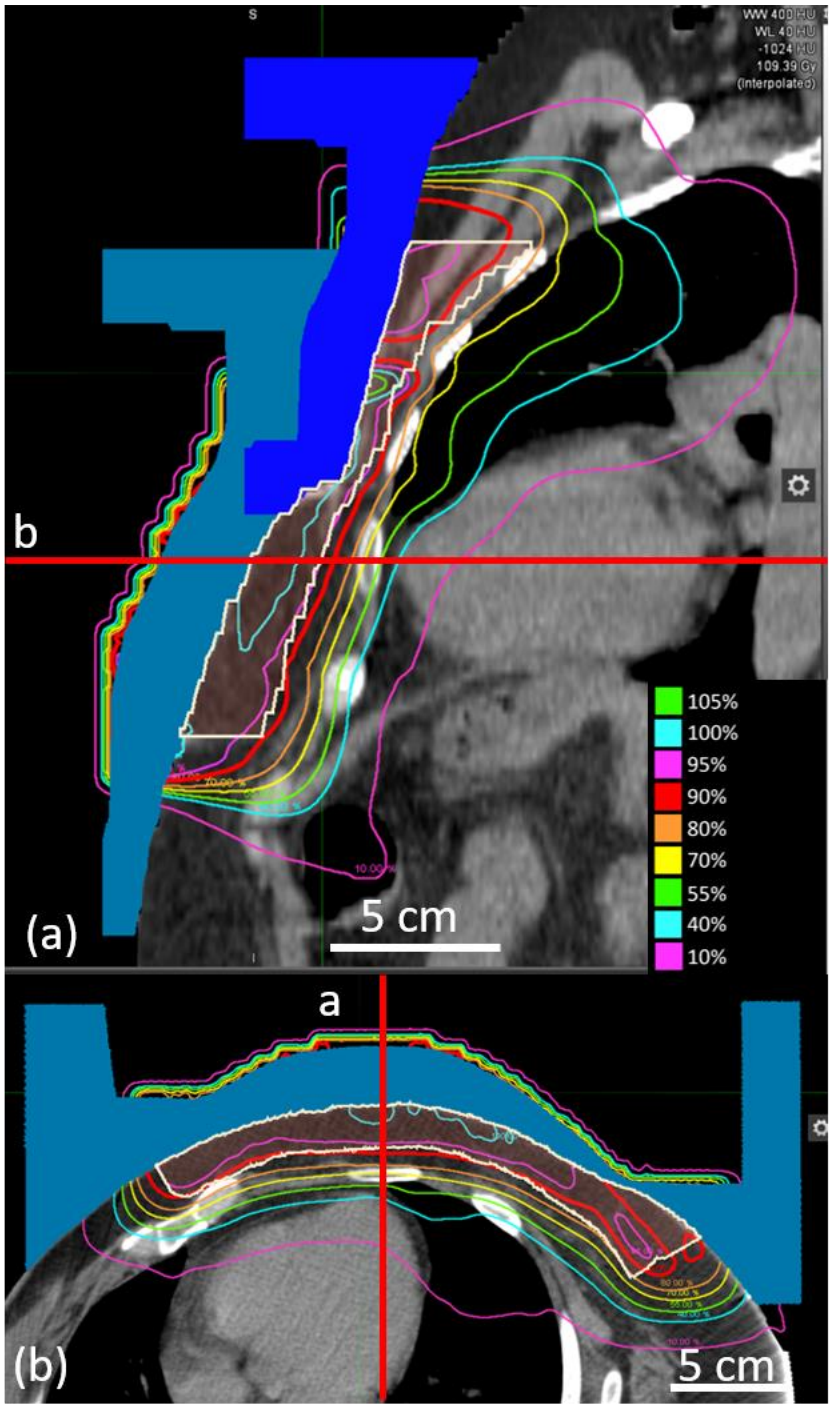

Figure 3.23. Sagittal and axial images of CW4, identical Plans 1 and 2. CW4 (Patient Set 2) was planned using scattered electron beams and discrete energy spacing for Plan 1 and scattered beams with discrete energy spacing (lower field) and continuous energy spacing (upper field) for Plan 2. (a) Dose plan in the sagittal-coronal, oblique plane demarcated by the red line in figure (b)'s transverse plane; (b) Dose plan in transverse plane passing through central heart region, demarcated by red line in figure (a)'s oblique plane. Upper bolus is shaded dark blue, lower bolus is shaded light blue, and PTV is outlined in white. Key shows dose values.

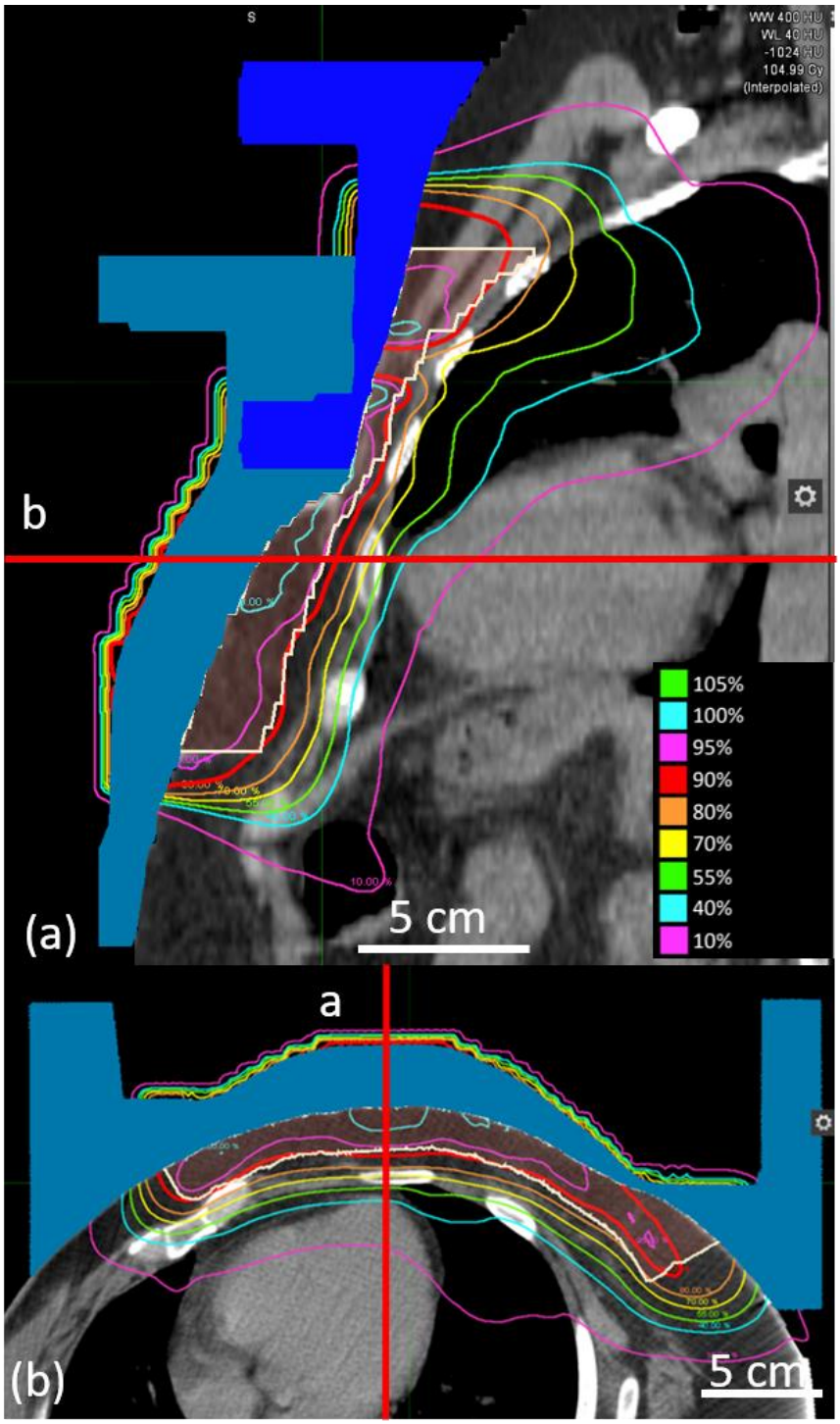

Figure 3.24. Sagittal and axial images of CW4, Plan 3. CW4 (Patient Set 2) was planned using scattered electron beams and continuous energy spacing. (a) Dose plan in the sagittal-coronal, oblique plane demarcated by the red line in figure (b)'s transverse plane; (b) Dose plan in transverse plane passing through central heart region, demarcated by red line in figure (a)'s oblique plane. Upper bolus is shaded dark blue, lower bolus is shaded light blue, and PTV is outlined in white. Key shows dose values.

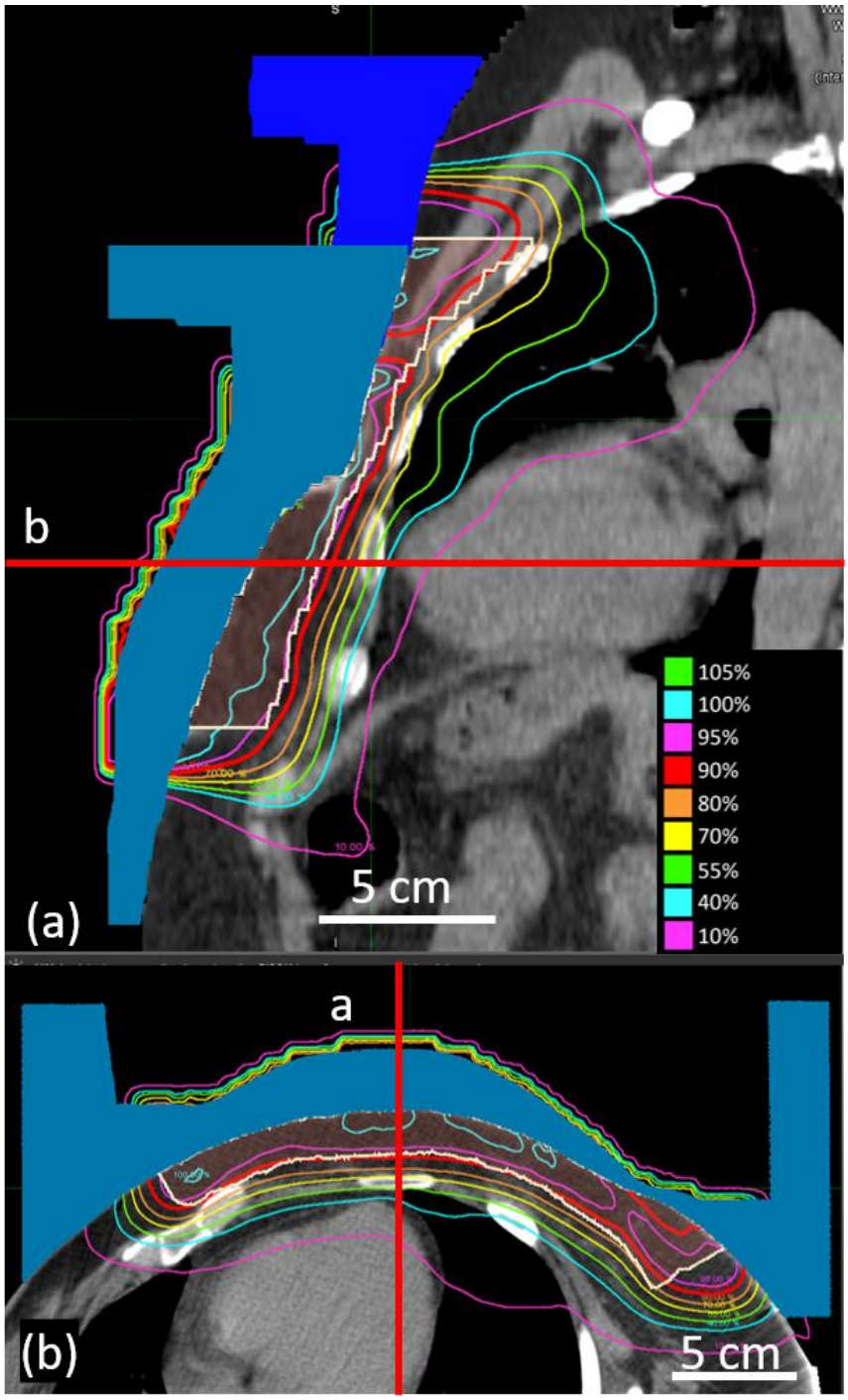

Figure 3.25. Sagittal and axial images of CW4, Plan 4. CW4 (Patient Set 2) was planned using scanned electron beams and discrete energy spacing. (a) Dose plan in the sagittal-coronal, oblique plane demarcated by the red line in figure (b)'s transverse plane; (b) Dose plan in transverse plane passing through central heart region, demarcated by red line in figure (a)'s oblique plane. Upper bolus is shaded dark blue, lower bolus is shaded light blue, and PTV is outlined in white. Key shows dose values.

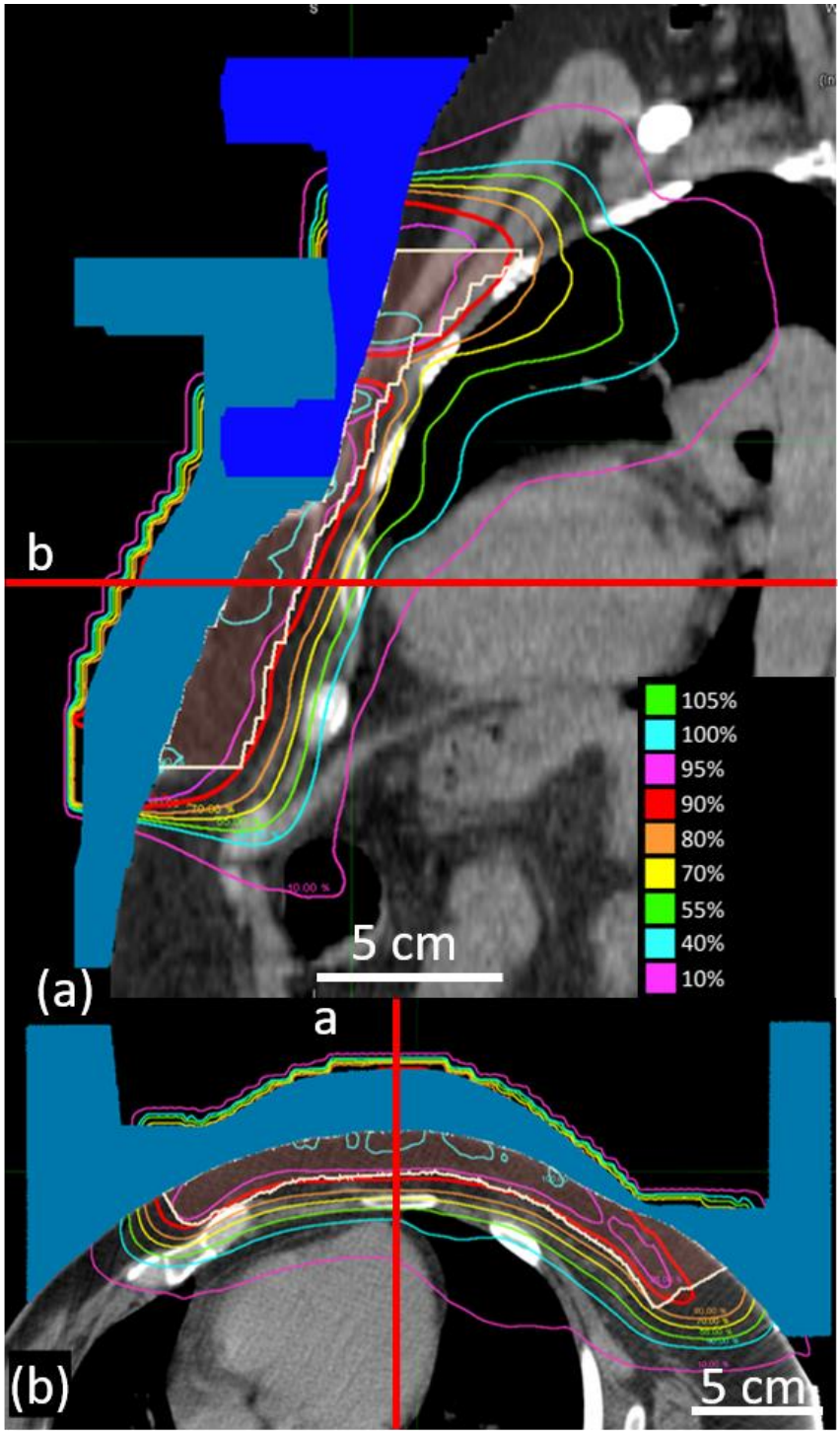

Figure 3.26. Sagittal and axial images of CW4, Plan 5. CW4 (Patient Set 2) was planned using scanned electron beams and continuous energy spacing. (a) Dose plan in the sagittal-coronal, oblique plane demarcated by the red line in figure (b)'s transverse plane; (b) Dose plan in transverse plane passing through central heart region, demarcated by red line in figure (a)'s oblique plane. Upper bolus is shaded dark blue, lower bolus is shaded light blue, and PTV is outlined in white. Key shows dose values.

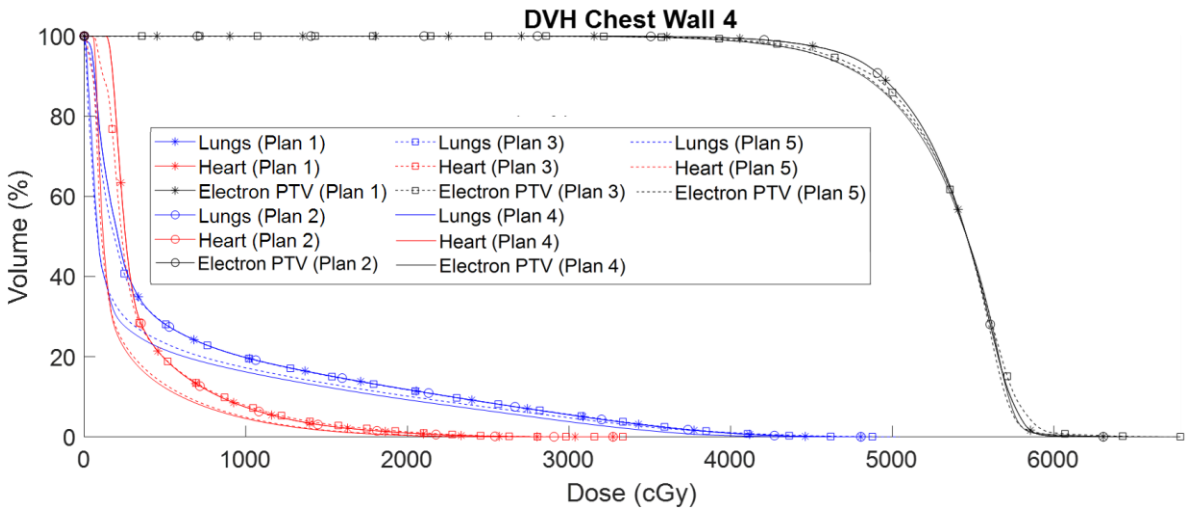

Figure 3.27. Comparison of cumulative DVH plots for CW4 (Patient Set 2) Plans. DVH plots for PTV, heart, and lung are compared for Plans 1, 2, 3, 4, and 5, as indicated in key. Note that Plans 1 and 2 are identical for CW4.

Table 3.7. Comparison of metrics for CW4 (Patient Set 2) Plans. Dose metrics are shown for PTV, heart, and lungs. NTCP and SCCP values are shown for heart and lungs. Note that Plans 1 and 2 are identical for CW4.

		Plan 1	Plan 2	Plan 3	Plan 4	Plan 5
PTV	$D_{97\%}$ (Gy)	45.7	45.7	44.3	43.2	43.5
	$V_{47.5\ Gy}$ (%)	94.75	94.75	91.63	91.87	91.02
	Max dose (Gy)	63.06	63.06	66.55	65.98	64.79
	Mean dose (Gy)	53.83	53.83	53.50	53.48	53.48
	Std Dev (Gy)	0.24	0.24	0.34	0.04	0.4
Heart	$V_{22.5\ Gy}$ (%)	0.4	0.4	0.6	0.1	0.1
	$V_{30\ Gy}$ (%)	0.0	0.0	0.0	0.1	0.2
	Min dose (Gy)	1.2	1.2	0.6	0.5	0.1
	Max dose (Gy)	32.7	32.7	33.3	27.9	28.6
	Mean dose (Gy)	3.8	3.8	3.6	2.4	2.4
	Std Dev (Gy)	3.6	3.6	3.9	3.2	3.3
	NTCP (%)	0.01	0.01	0.01	0.0	0.0
Lungs	$V_{20\ Gy}$ (%)	11.8	11.8	11.7	9.2	10.1
	Min dose (Gy)	0.0	0.0	0.0	0.0	0.0
	Max dose (Gy)	48.1	48.1	48.8	46.1	50.4
	Mean dose (Gy)	6.5	6.5	6.4	4.8	5.2
	Std Dev (Gy)	9.6	9.6	9.8	8.7	9.5
	NTCP (%)	0.01	0.01	0.01	0.01	0.01
	$SCCP_{lin}$ (%)	10.9	10.9	10.7	8.1	8.8
	$SCCP_{lin\text{-}exp}$ (%)	3.2	3.2	3.1	2.3	2.3

3.2.2.3. Results for Patient CW7

Treatment planning results for CW7 (Patient Set 2) include isodose plots for three transverse planes and one sagittal-coronal oblique plane for Plans 1 to 5. However, Plans 1 and 2 are identical as the optimal, continuous energy for the upper field was the same as the discrete energy used in Plan 1. All such results are shown in Appendix B, and one sagittal-coronal oblique plane and one transverse plane for each plan are shown in Figure 3.28 to Figure 3.31. DVHs for PTV, heart, and lungs for each of the five dose plans were computed and plotted for comparison in Figure 3.32. Dose and biologic metrics computed from these DVHs are compared in Table 3.8. These results likely have some dependence on the location of the distal PTV surface, and the CW7 distance between the distal edge of the PTV and the distal side of the chest wall (Δt) was 0.9 cm on central axis.

PTV Coverage: Dose plots (Figure 3.28 to Figure 3.31) show that the 90% isodose lines closely cover the distal PTV surface, or in some locations the 80% isodose surface due to the jagged nature of the PTV. Most evident at the lateral edges of the PTV, coverage could be improved by increasing the lateral margin between the PTV and field edge or by a more realistic PTV (smoother edges). The PTV DVHs are similar for all plans; $V_{47.5\ Gy}$ values of Plans 3 and 5, which have the field arrangement used for the continuous energy beams (see Figure 2.3) are slightly greater than those of Plans 1, 2, and 4, which use a different field arrangement (see Figure 2.2). Although maximum doses are as large as approximately 69 Gy (124%), no significant volume receives more than 62 Gy (112%).

Effect of Scanned vs. Scattered Beams: Comparing Plan 1 (scattered, discrete energy beams, upper 21.3 MeV and lower 16.2 MeV) and Plan 4 (scanned, discrete energy beams, upper 18.4 MeV and lower 15.1 MeV) showed that the scanned electron beam reduced (1) mean dose to

the heart by 2.6 Gy (9.6 to 7.0 Gy) and (2) $V_{20\ Gy}$ to the lungs by 4.1% (20.6 to 16.5%). This resulted in reduced (1) $NTCP_{heart}$ by 0.2% (0.5 to 0.3%), (2) $NTCP_{lungs}$ by 0.02% (0.04 to 0.02%), and (3) $SCCP_{lin}$ by 4.6% (18.2 to 13.7%).

Comparing Plan 3 (scattered, continuous energy beams, upper 21.3 MeV and lower 16.2 MeV) and Plan 5 (scanned, continuous energy beams, upper 18.4 MeV and lower 15.1 MeV) showed that the scanned electron beam reduced (1) mean dose to the heart by 2.2 Gy (9.7 to 7.5 Gy) and (2) $V_{20\ Gy}$ to the lungs by 1.2% (17.7 to 16.5%). This resulted in reduced (1) $NTCP_{heart}$ by 0.2% (0.6 to 0.4%), (2) $NTCP_{lungs}$ by 0.01% (0.03 to 0.02), and (3) $SCCP_{lin}$ by 1.8% (15.9 to 14.1%).

Effect of Continuous vs. Discrete Beam Energies: For Plan 2, the optimal continuous energy for the upper beam was identical to the discrete energy used in Plan 1. Thus, Plan 1 and Plan 2 are identical. The optimal continuous energy for all beams in Plans 2,3, and 5 were the same as the discrete energies for the beams in Plans 1 and 4. Thus, no conclusions can be drawn about the effect of using continuous vs. discrete energy spacing for this patient, CW7.

Impact of Location of Edges of Abutting Beams: Comparing Plan 2 (scattered, continuous energy beams, upper 21.3 MeV and discrete energy lower 16.2 MeV beam) with Plan 3 (scattered, continuous energy beams, upper 21.3 MeV and lower 16.2 MeV) showed (1) mean dose to the heart by 0.0 Gy (9.7 to 9.7 Gy) and (2) $V_{20\ Gy}$ to the lungs by 2.9% (20.6 to 17.7%). This resulted in a marginally increased (1) $NTCP_{heart}$ by 0.06% (0.5 to 0.6%) and decreased (2) $NTCP_{lungs}$ by 0.01% (0.04 to 0.03%), and (3) $SCCP_{lin}$ by 2.3% (18.2 to 15.9%). These differences are due to the location of the edge of abutting beams, as the energies used for each comparison are identical.

Comparing Plan 4 (scanned, discrete energy beams, upper 18.4 MeV and lower 15.1 MeV) with Plan 5 (scanned, continuous energy beams, upper 14.5 MeV and lower 10.5 MeV) showed

no advantage to continuous energy. Rather, it showed the advantage of the field arrangement for Plan 4, as Plan 5 increased (1) mean dose to the heart by 0.5 Gy (7.0 to 7.5 Gy) why the $V_{20\ Gy}$ to the lung remained constant at 16.5%. This resulted in increased (1) $NTCP_{heart}$ of 0.06% (0.3 to 0.4%), identical $NTCP_{lungs}$ values of 0.02%, and increased $SCCP_{lin}$ by 0.4% (13.7% to 14.1%).

Effect of Scanned, Continuous Beam Energies vs. Scattered, Discrete Beam Energies: This comparison was overshadowed by the abutting border of Plan 5 being 0.25 cm inferior to that of Plan 1. Plan 4 metrics were better than those of Plan 5, negating this comparison.

Summary: Results showed that scanned electron beams modestly reduced heart and lung dose and their biologic effects. Continuous energy beams showed insignificant improvement over discrete energy beams, because the discrete energies available were already optimal. More significant was the location of the edge of abutting beams, indicating the need for optimizing its location in future studies.

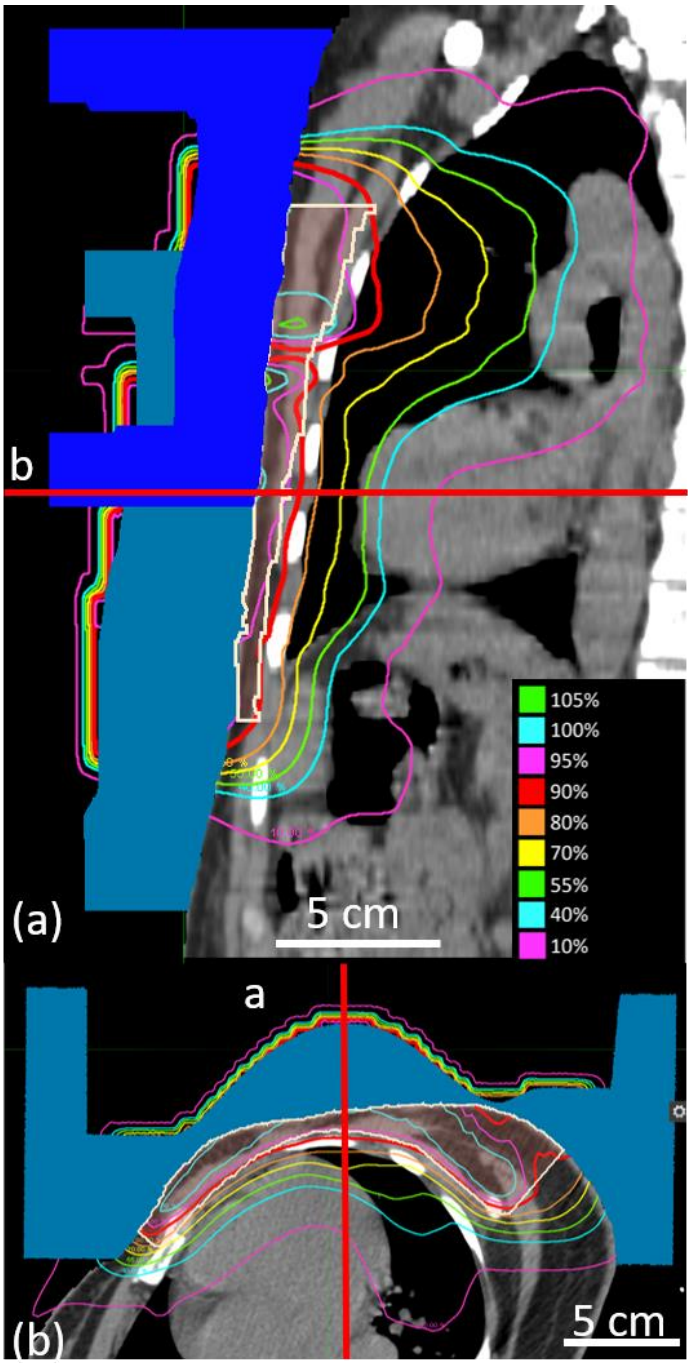

Figure 3.28. Sagittal and axial images of CW7, Plans 1 and 2. CW7 (Patient Set 2) was planned using scattered electron beams and discrete energy spacing for Plan 1 and scattered beams with discrete energy spacing (lower field) and continuous energy spacing (upper field). Because the discrete energy is the optimal energy for the upper field, Plans 1 and 2 are identical (a) Dose plan in the sagittal-coronal, oblique plane demarcated by the red line in figure (b)'s transverse plane; (b) Dose plan in transverse plane passing through central heart region, demarcated by red line in figure (a)'s oblique plane. Upper bolus is shaded dark blue, lower bolus is shaded light blue, and PTV is outlined in white. Key shows dose values.

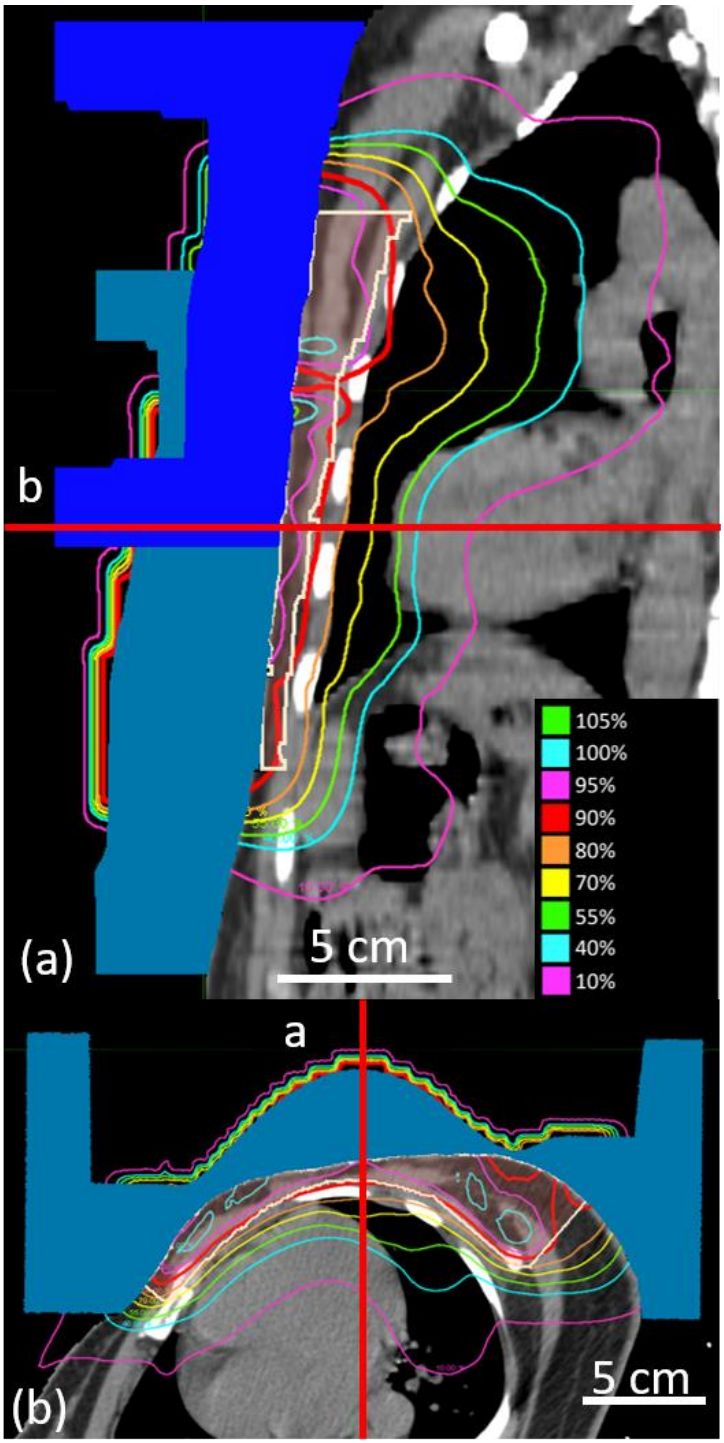

Figure 3.29. Sagittal and axial images of CW7, Plan 3. CW7 (Patient Set 2) was planned using scattered electron beams and continuous energy spacing. (a) Dose plan in the sagittal-coronal, oblique plane demarcated by the red line in figure (b)'s transverse plane; (b) Dose plan in transverse plane passing through central heart region, demarcated by red line in figure (a)'s oblique plane. Upper bolus is shaded dark blue, lower bolus is shaded light blue, and PTV is outlined in white. Key shows dose values.

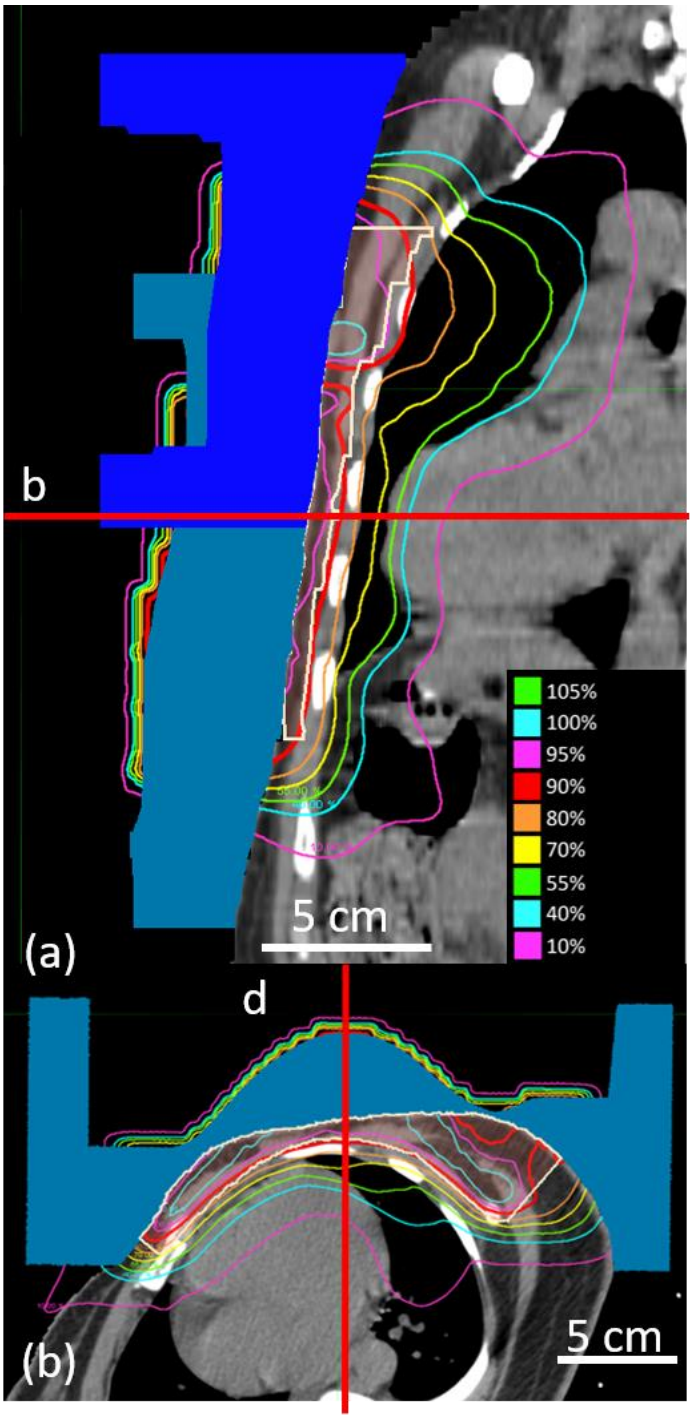

Figure 3.30. Sagittal and axial images of CW7, Plan 4. CW7 (Patient Set 2) was planned using scanned electron beams and discrete energy spacing. (a) Dose plan in the sagittal-coronal, oblique plane demarcated by the red line in figure (b)'s transverse plane; (b) Dose plan in transverse plane passing through central heart region, demarcated by red line in figure (a)'s oblique plane. Upper bolus is shaded dark blue, lower bolus is shaded light blue, and PTV is outlined in white. Key shows dose values.

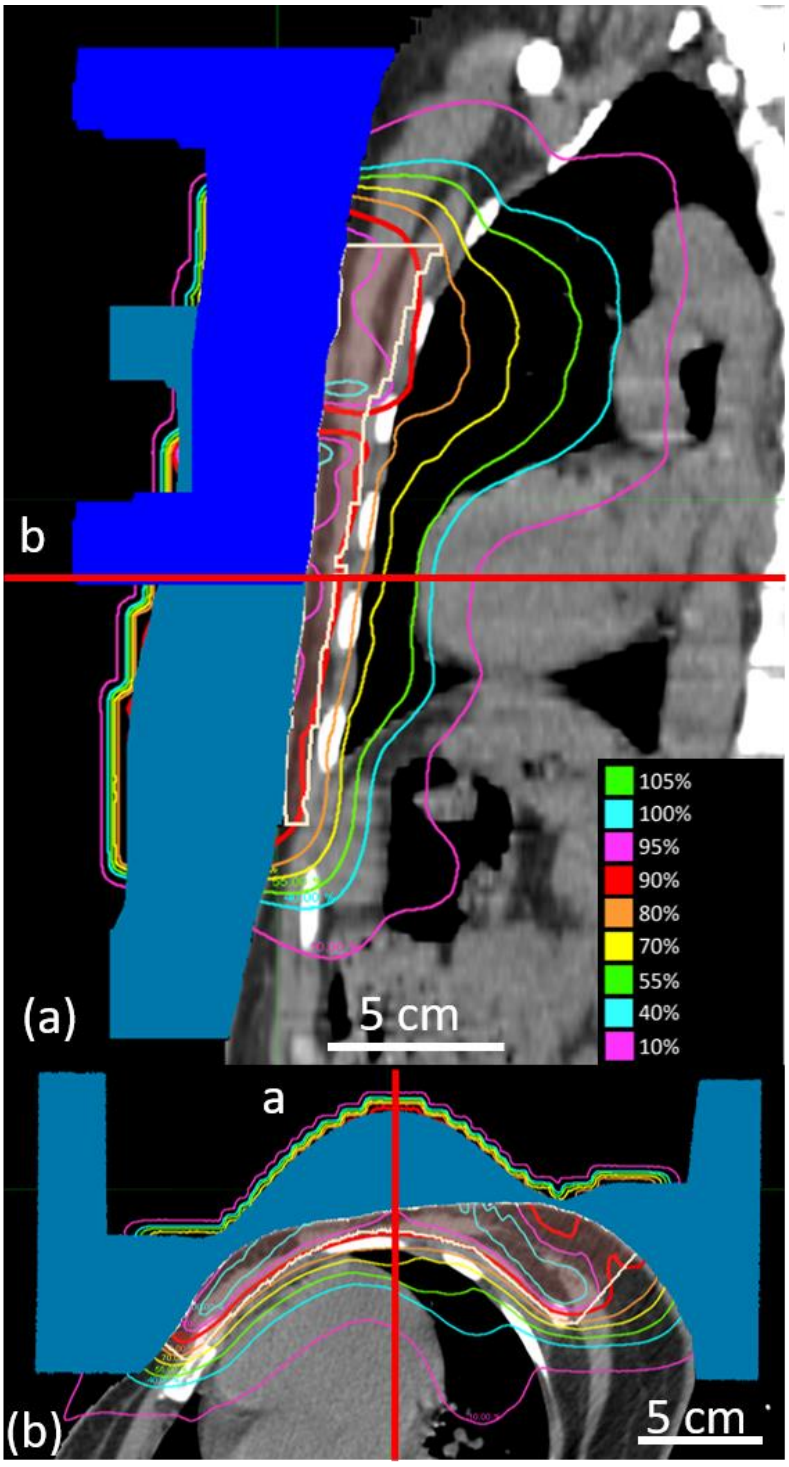

Figure 3.31. Sagittal and axial images of CW7, Plan 5. CW7 (Patient Set 2) was planned using scanned electron beams and continuous energy spacing. (a) Dose plan in the sagittal-coronal, oblique plane demarcated by the red line in figure (b)'s transverse plane; (b) Dose plan in transverse plane passing through central heart region, demarcated by red line in figure (a)'s oblique plane. Bolus is shaded blue, and PTV is outlined in white. Key shows dose values.

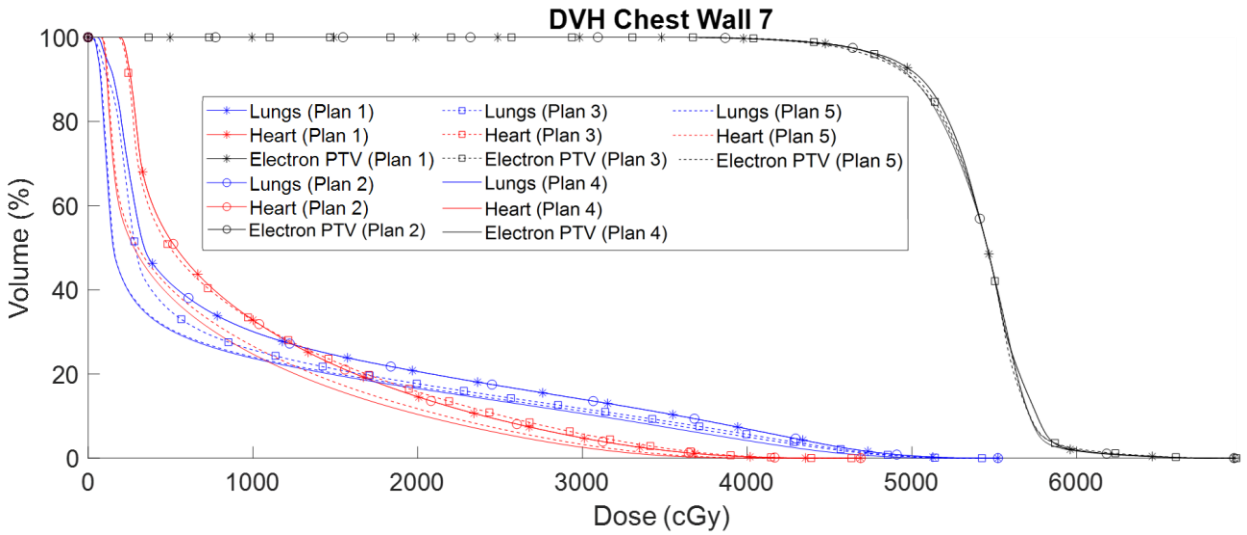

Figure 3.32. Comparison of cumulative DVH plots for CW7 (Patient Set 2) Plans. DVH plots for PTV, heart, and lung are compared for Plans 1, 2, 3, 4, and 5, as indicated in key

Table 3.8. Comparison of metrics for CW7 (Patient Set 2) Plans. Dose metrics are shown for PTV, heart, and lungs. NTCP and SCCP values are shown for heart and lungs.

		Plan 1	Plan 2	Plan 3	Plan 4	Plan 5
PTV	$D_{97\%}$ (Gy)	46.9	46.9	46.4	46.0	45.6
	$V_{47.5\ Gy}$ (%)	96.4	96.4	96.3	96.2	95.6
	Max dose (Gy)	69.6	69.6	68.4	68.4	68.3
	Mean dose (Gy)	54.2	54.2	54.1	54.0	54.0
	Std Dev (Gy)	3.2	3.2	3.2	3.2	3.3
Heart	$V_{22.5\ Gy}$ (%)	11.6	11.6	12.8	8.0	9.2
	$V_{30\ Gy}$ (%)	4.8	4.8	5.7	2.6	3.3
	Min dose (Gy)	1.9	1.9	1.8	0.7	0.8
	Max dose (Gy)	46.9	46.9	46.3	44.3	44.3
	Mean dose (Gy)	9.6	9.6	9.7	7.0	7.5
	Std Dev (Gy)	9.0	9.0	9.4	8.3	8.7
	NTCP (%)	0.5	0.5	0.6	0.3	0.4
Lungs	$V_{20\ Gy}$ (%)	20.6	20.6	17.7	16.5	16.5
	Min dose (Gy)	0.9	0.9	0.4	0.2	0.2
	Max dose (Gy)	99.4	99.4	97.7	95.7	97.5
	Mean dose (Gy)	19.5	19.5	17.0	14.6	15.1
	Std Dev (Gy)	24.3	24.3	23.1	22.3	23.1
	NTCP (%)	0.04	0.04	0.03	0.02	0.02
	$SCCP_{lin}$ (%)	18.2	18.2	15.9	13.7	14.1
	$SCCP_{lin\text{-}exp}$ (%)	4.0	4.0	3.7	3.0	3.0

3.2.2.4. Results for Patient CW8

Treatment planning results for CW8 (Patient Set 2) include isodose plots for three transverse planes and one sagittal-coronal oblique plane for Plans 1 to 5. All such results are shown in Appendix B, and one sagittal-coronal oblique plane and one transverse plane for each plan are shown in Figure 3.33 to Figure 3.37. DVHs for PTV, heart, and lungs for each of the five dose plans were computed and plotted for comparison in Figure 3.38. Dose and biologic metrics computed from these DVHs are compared in Table 3.9. These results likely have some dependence on the location of the distal PTV surface, and the CW8 distance between the distal edge of the PTV and the distal side of the chest wall (Δt) was 0.6 cm on central axis.

PTV Coverage: Dose plots (Figure 3.33 to Figure 3.37) show that the 90% isodose lines closely cover the distal PTV surface, or in some locations the 80% isodose surface due to the jagged nature of the PTV. Most evident at the lateral edges of the PTV, coverage could be improved by increasing the lateral margin between the PTV and field edge or by a more realistic PTV (smoother edges). The PTV DVHs are similar for all plans; $V_{47.5\ Gy}$ values of Plans 3 and 5, which have the field arrangement used for the continuous energy beams (see Figure 2.3) are slightly greater than those of Plans 1, 2, and 4, which use a different field arrangement (see Figure 2.2). Although maximum doses are as large as approximately 60 Gy (108%), no significant volume receives more than 58 Gy (105%).

Effect of Scanned vs. Scattered Beams: Comparing Plan 1 (scattered, discrete energy beams, upper 16.2 MeV and lower 13.0 MeV) and Plan 4 (scanned, discrete energy beams, upper 14.5 MeV and lower 12.2 MeV) showed that the scanned electron beam reduced (1) mean dose to the heart by 0.6 Gy (4.3 to 3.7 Gy) and (2) V_{20} Gy to the lungs by 2.9% (17.7 to 14.8%). This resulted in reduced (1) $NTCP_{heart}$ by 0.06% (0.1 to 0.06%), (2) $NTCP_{lungs}$ by 0.01% (0.02 to 0.01%), and (3) $SCCP_{lin}$ by 2.3% (13.1 to 10.8%).

Comparing Plan 3 (scattered, continuous energy beams, upper 15.6 MeV and lower 11.1 MeV) and Plan 5 (scanned, continuous energy beams, upper 14.5 MeV and lower 10.5 MeV) showed that the scanned electron beam reduced (1) mean dose to the heart by 0.9 Gy (3.9 to 3.0 Gy) and (2) $V_{20\,Gy}$ to the lungs by 3.2% (16.4 to 13.1%). This resulted in reduced (1) $NTCP_{heart}$ by 0.06% (0.1 to 0.06%), (2) $NTCP_{lungs}$ by 0.01% (0.02 to 0.01%), and (3) $SCCP_{lin}$ by 2.5% (12.2 to 9.7%).

Effect of Continuous vs. Discrete Beam Energies: The same data above can be used to evaluate the benefit of continuous versus discrete energy beams. Comparing Plan 2 (scattered, continuous energy beams, upper 15.6 MeV and discrete energy lower 13.0 MeV beam) with Plan 1 (scattered, discrete energy beams, upper 16.2 MeV and lower 13.0 MeV), there is insignificant differences in PTV and heart metrics, as the only difference in plans was a 0.6 MeV lower energy in the upper field. There were small changes in the lung metrics as Plan 2 showed reduced $V_{20\,Gy}$ to the lungs by 0.3% (17.7 to 17.4%) and (2) $SCCP_{lin}$ by 0.3% (13.1 to 12.9%).

Comparing Plan 2 (scattered, continuous energy beams, upper 15.6 MeV and discrete energy lower 13.0 MeV beam) with Plan 3 (scattered, continuous energy beams, upper 15.6 MeV and lower 13.0 MeV), differing only by the inferior border of the upper field being 0.75 cm inferior, showed reduced (1) mean dose to the heart by 0.3 Gy (4.2 to 3.9 Gy) and (2) V_{20Gy} to the lungs by 1.0% (17.4 to 16.4%). This resulted in reduced (1) $NTCP_{heart}$ by 0.00% (0.1 to 0.1%), (2) $NTCP_{lungs}$ by 0.00% (0.02 to 0.02%), and (3) $SCCP_{lin}$ by 0.7% (12.9 to 12.2%).

Comparing Plan 4 (scanned, discrete energy beams, upper 14.5 MeV and lower 12.2 MeV) with Plan 5 (scanned, continuous energy beams, upper 14.5 MeV and lower 10.5 MeV) showed decreased (1) mean dose to the heart by 0.6 Gy (3.7 to 3.0 Gy) and (2) V_{20Gy} to the lung by 1.6%

(14.8 to 13.1%). This resulted in identical $NTCP_{heart}$ values of 0.06% and $NTCP_{lungs}$ vales of 0.01%, and decreased $SCCP_{lin}$ by 1.2% (10.8% to 9.7%).

Effect of Scanned, Continuous Beam Energies vs. Scattered, Discrete Beam Energies: Even though the abutting border of the upper and lower fields differed, there was still benefit. Comparing Plan 5 (scanned, continuous energy beams, upper 14.5 MeV and lower 10.5 MeV) with Plan 1 (scattered, discrete energy beams, upper 16.2 MeV and lower 13.0 MeV) showed that scanned, continuous energy beams reduced (1) mean dose to the heart by 1.3 Gy (4.3 to 3.0 Gy) and (2) V_{20Gy} to the lung by 4.6% (17.7 to 13.1%). This resulted in reduced (1) $NTCP_{heart}$ by 0.0% (0.1 to 0.1%), (2) $NTCP_{lungs}$ by 0.0% (0.0 to 0.0%), and (3) $SCCP_{lin}$ by 3.4% (13.1% to 9.7%).

Summary: Results showed that scanned electron beams modestly reduced heart and lung dose and their biologic effect. NTCP changes were not likely significant because of their already low value for scattered beams. Continuous energy beams showed insignificant improvement over discrete energy beams, because the discrete energies available were already near optimal. More significant was the location of the edge of abutting beams, indicating the need for optimizing its location in future studies.

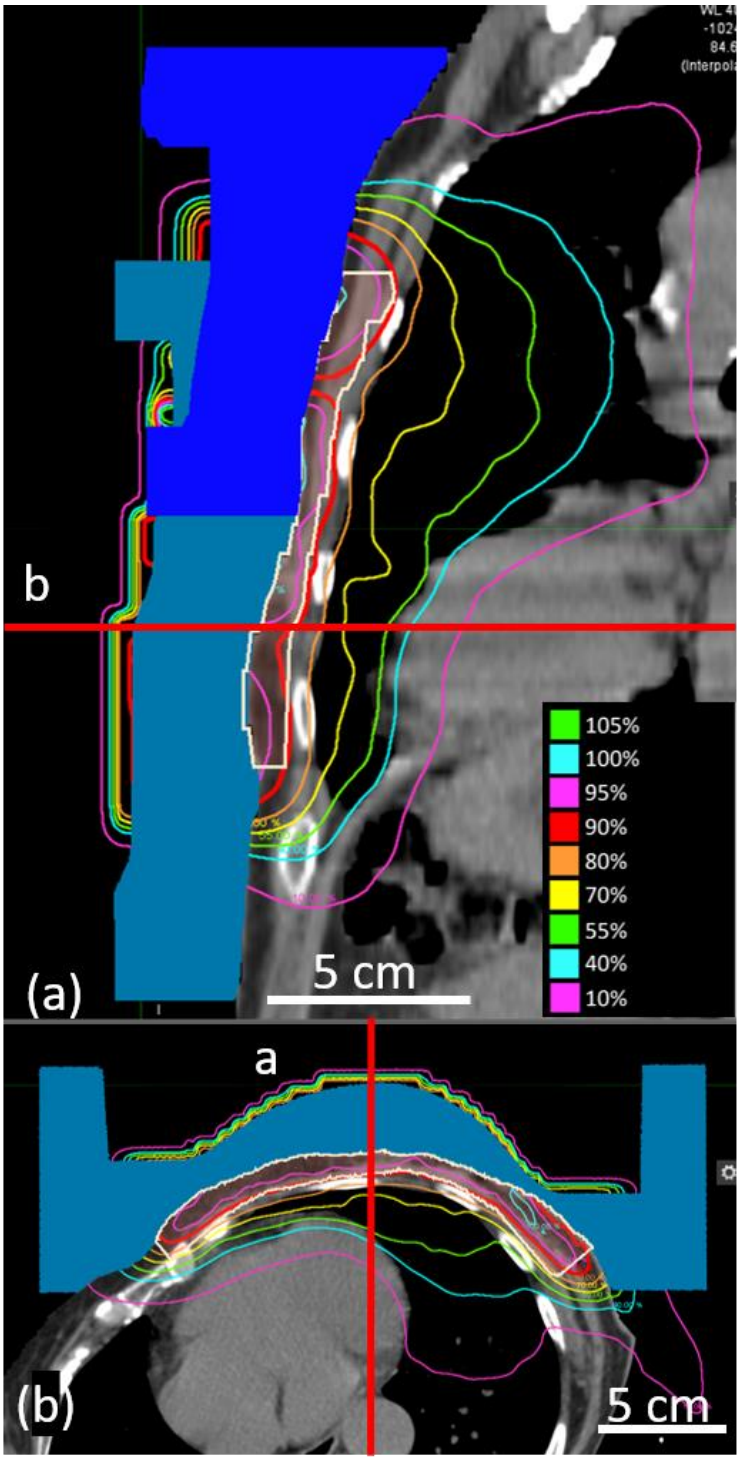

Figure 3.33. Sagittal and axial images of CW8, Plan 1. CW8 (Patient Set 2) was planned using scattered electron beams and discrete energy spacing. (a) Dose plan in the sagittal-coronal, oblique plane demarcated by the red line in figure (b)'s transverse plane; (b) Dose plan in transverse plane passing through central heart region, demarcated by red line in figure (a)'s oblique plane. Upper bolus is shaded dark blue, lower bolus is shaded light blue, and PTV is outlined in white. Key shows dose values.

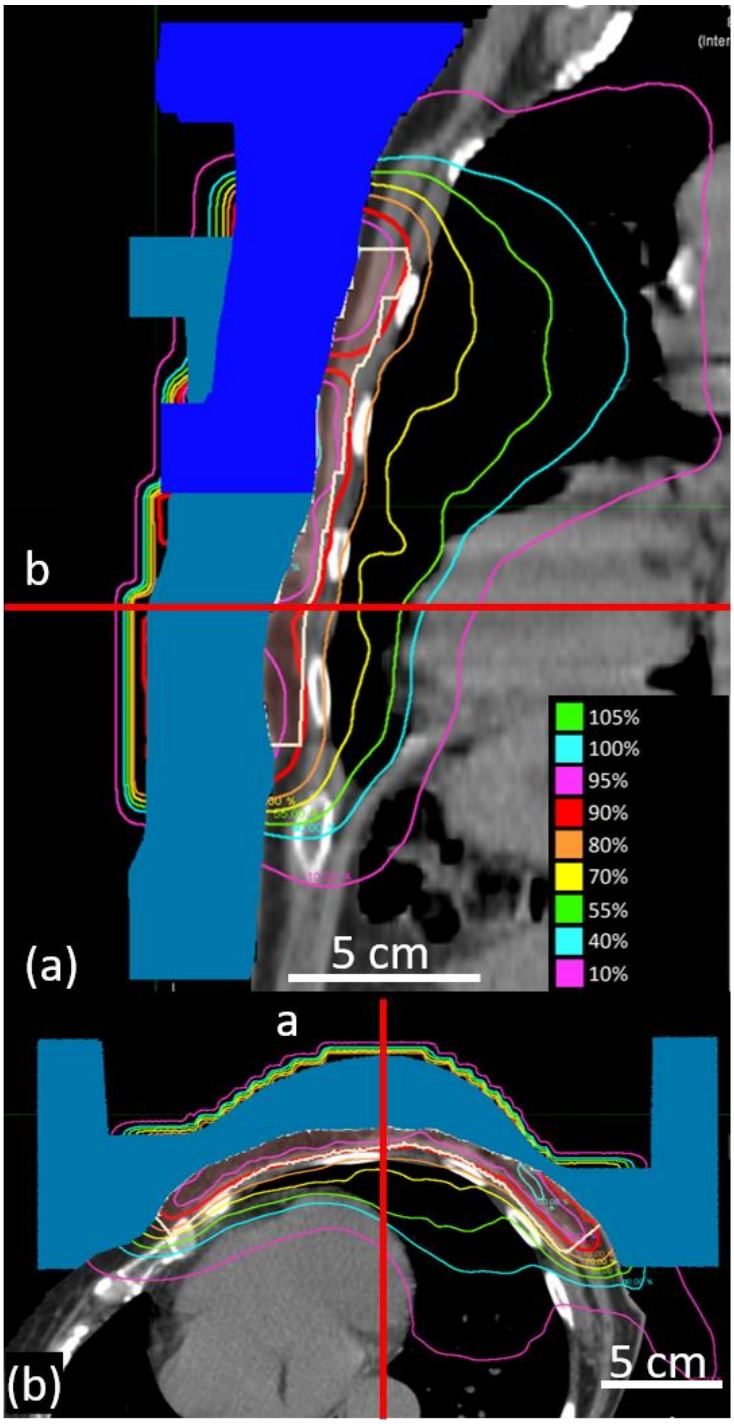

Figure 3.34. Sagittal and axial images of CW8, Plan 2. CW8 (Patient Set 2) was planned using scattered electron beams, discrete energy spacing (lower field), and continuous energy spacing (upper field). (a) Dose plan in the sagittal-coronal, oblique plane demarcated by the red line in figure (b)'s transverse plane; (b) Dose plan in transverse plane passing through central heart region, demarcated by red line in figure (a)'s oblique plane. Upper bolus is shaded dark blue, lower bolus is shaded light blue, and PTV is outlined in white. Key shows dose values.

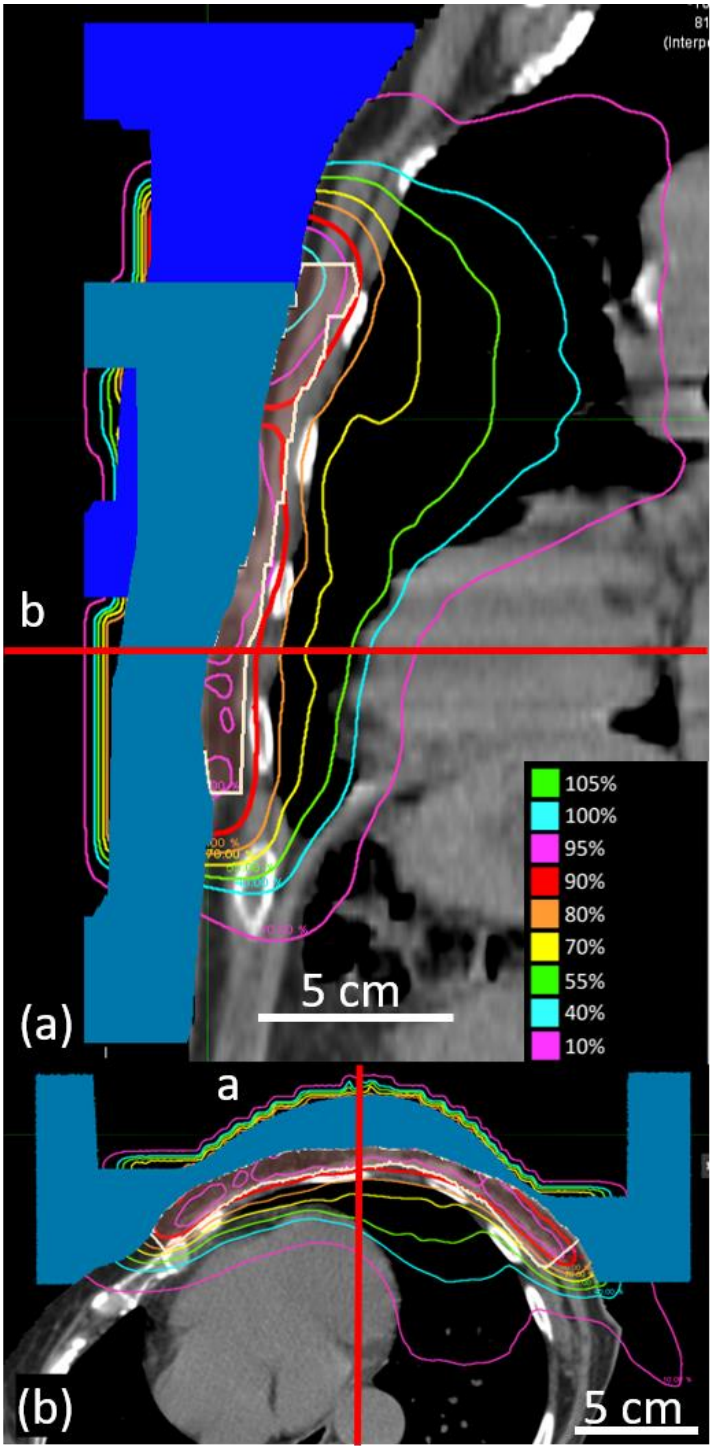

Figure 3.35. Sagittal and axial images of CW8, Plan 3. CW8 (Patient Set 2) was planned using scattered electron beams and continuous energy spacing. (a) Dose plan in the sagittal-coronal, oblique plane demarcated by the red line in figure (b)'s transverse plane; (b) Dose plan in transverse plane passing through central heart region, demarcated by red line in figure (a)'s oblique plane. Upper bolus is shaded dark blue, lower bolus is shaded light blue, and PTV is outlined in white. Key shows dose values.

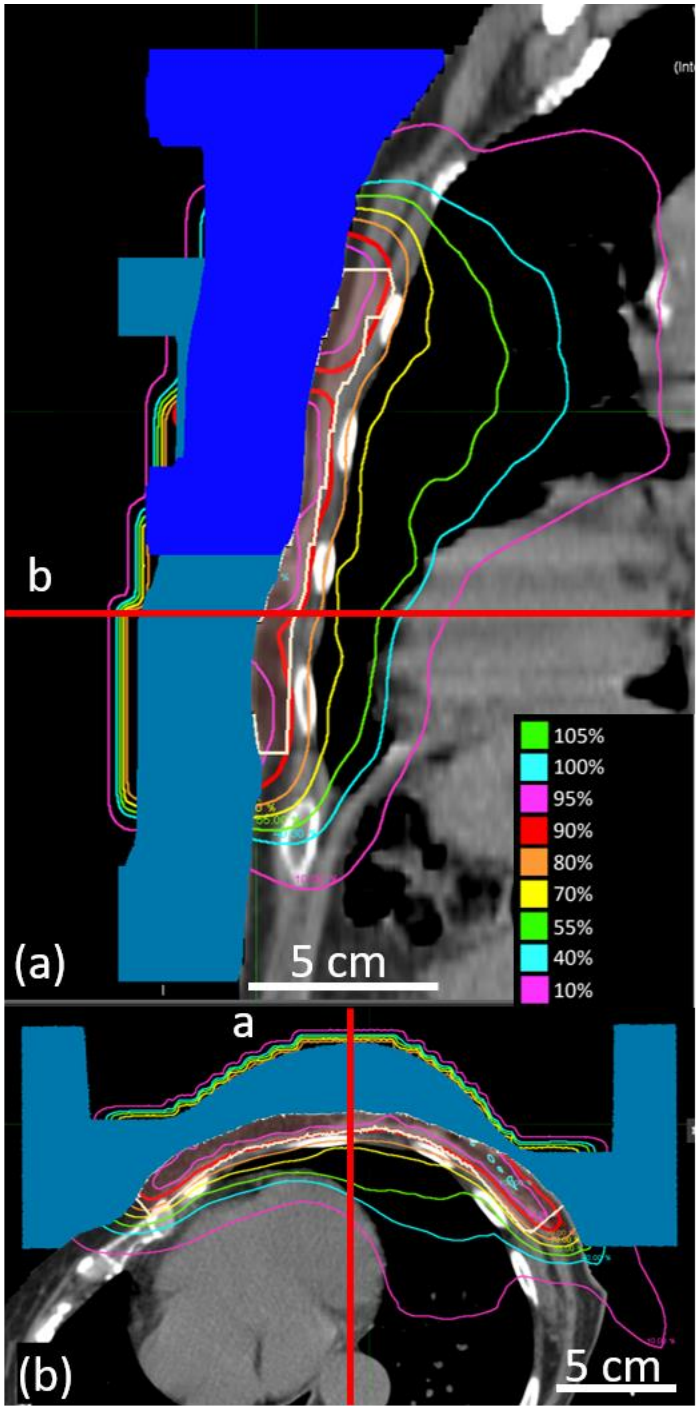

Figure 3.36. Sagittal and axial images of CW8, Plan 4. CW8 (Patient Set 2) was planned using scanned electron beams and discrete energy spacing. (a) Dose plan in the sagittal-coronal, oblique plane demarcated by the red line in figure (b)'s transverse plane; (b) Dose plan in transverse plane passing through central heart region, demarcated by red line in figure (a)'s oblique plane. Upper bolus is shaded dark blue, lower bolus is shaded light blue, and PTV is outlined in white. Key shows dose values.

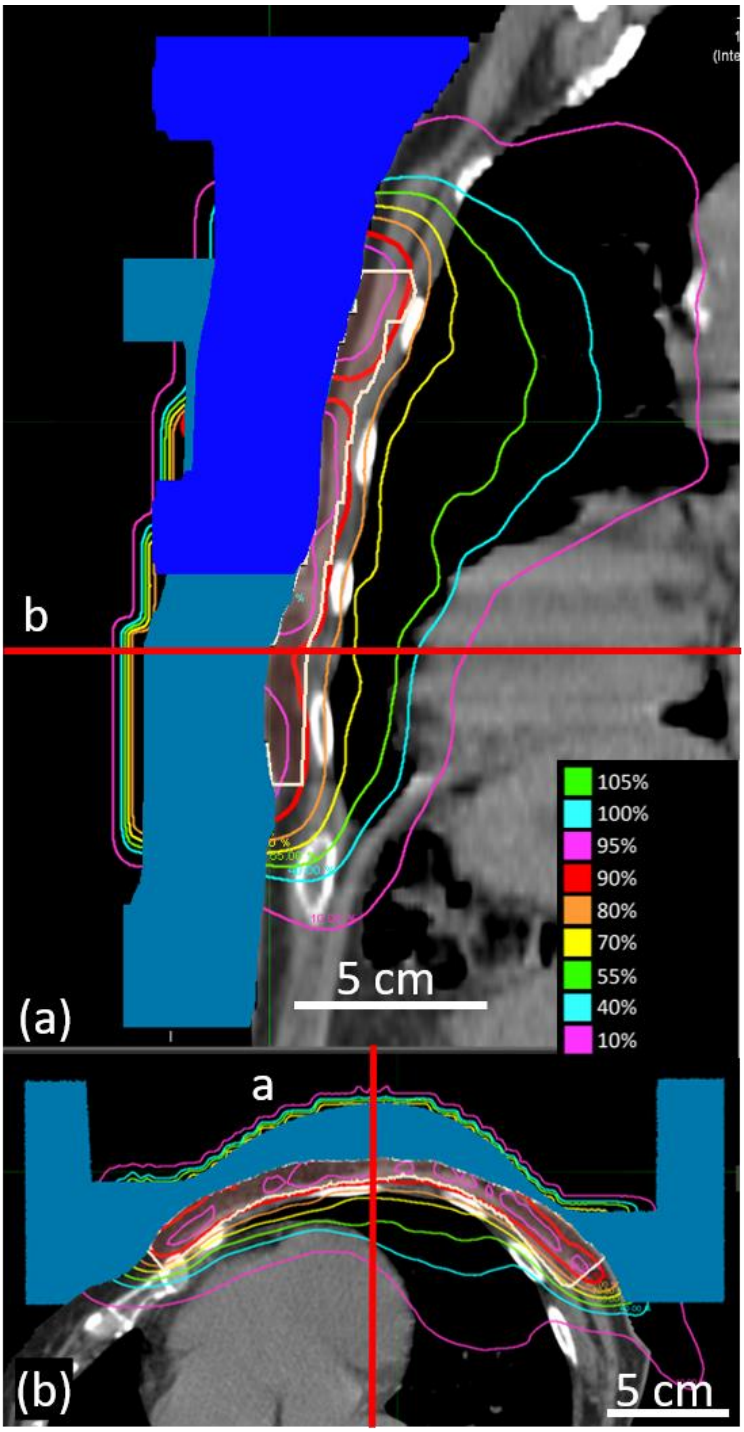

Figure 3.37. Sagittal and axial images of CW8, Plan 5. CW8 (Patient Set 2) was planned using scanned electron beams and continuous energy spacing. (a) Dose plan in the sagittal-coronal, oblique plane demarcated by the red line in figure (b)'s transverse plane; (b) Dose plan in transverse plane passing through central heart region, demarcated by red line in figure (a)'s oblique plane. Upper bolus is shaded dark blue, lower bolus is shaded light blue, and PTV is outlined in white. Key shows dose values.

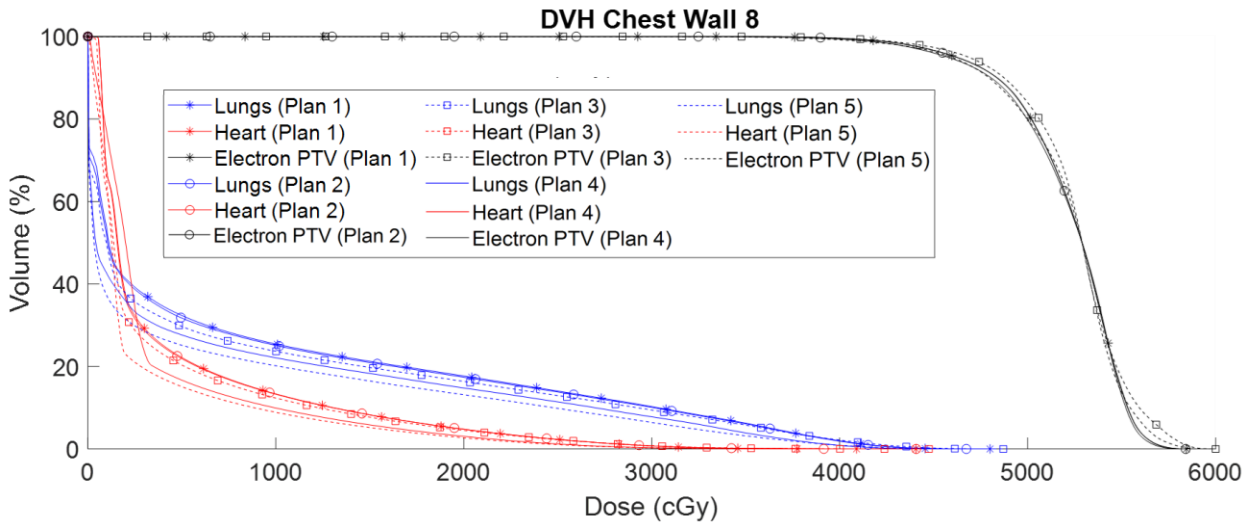

Figure 3.38. Comparison of cumulative DVH plots for CW8 (Patient Set 2) Plans. DVH plots for PTV, heart, and lung are compared for Plans 1, 2, 3, 4, and 5, as indicated in key

Table 3.9. Comparison of metrics for CW8 (Patient Set 2) Plans. Dose metrics are shown for PTV, heart, and lungs. NTCP and SCCP values are shown for heart and lungs.

		Plan 1	Plan 2	Plan 3	Plan 4	Plan 5
PTV	$D_{97\%}$ (Gy)	44.7	44.7	43.9	43.9	42.9
	$V_{47.5\ Gy}$ (%)	92.5	92.5	93.7	91.6	91.5
	Max dose (Gy)	58.4	58.4	60.0	58.4	59.1
	Mean dose (Gy)	52.2	52.2	52.5	52.1	52.2
	Std Dev (Gy)	3.1	3.0	3.1	3.2	3.3
Heart	$V_{22.5\ Gy}$ (%)	3.4	3.4	3.3	2.0	1.8
	$V_{30\ Gy}$ (%)	0.7	0.7	0.8	0.3	0.3
	Min dose (Gy)	0.5	0.5	0.0	0.0	0.0
	Max dose (Gy)	44.1	44.1	44.7	43.0	43.4
	Mean dose (Gy)	4.3	4.2	3.9	3.7	3.0
	Std Dev (Gy)	6.3	6.3	6.2	5.2	5.1
	NTCP (%)	0.1	0.1	0.1	0.1	0.1
Lungs	$V_{20\ Gy}$ (%)	17.7	17.4	16.4	14.8	13.1
	Min dose (Gy)	0.0	0.0	0.0	0.0	0.0
	Max dose (Gy)	48.0	46.7	48.7	45.7	48.0
	Mean dose (Gy)	7.8	7.7	7.2	6.5	5.8
	Std Dev (Gy)	12.1	12.0	11.9	11.1	10.5
	NTCP (%)	0.0	0.0	0.0	0.0	0.0
	$SCCP_{Lin}$ (%)	13.1	12.9	12.2	10.8	9.7
	$SCCP_{Lin\text{-}Exp}$ (%)	2.5	2.4	2.3	2.1	1.9

Chapter 4. Discussion of Results

The purpose of this study was to determine the potential impact of availability of discrete versus continuous beam energies and of beams flattened using scanned beam technology versus dual scattering foils on the treatment of post-mastectomy breast cancer patients. The quality of post-mastectomy radiotherapy treatment plans was evaluated by examining PTV coverage (chest wall, excluding supraclavicular field), heart dose, and lung dose for left sided postmastectomy patients. Both dose and biologic metrics were calculated for comparison of multiple plans for each patient. In addition to the treatment modality dependences, the results of this study also showed some dependence on beam energy, i.e. R_{90}, (related to maximum thickness of PTV), distance of tissue between distal PTV surface and distal chest wall surface (onset of lungs or heart), and number of electron fields used to treat PTV (one versus two, the upper field of the latter having a feathered edge). Below the impact of electron beam technology as well as patient and beam parameters on dose and biologic metrics are discussed.

4.1. Impact on Heart Dose

For all IM-BECT treatment plans, dose to the heart was low due to using electron beams with conformal bolus, as previously reported.[21] For the seven patients studied, the maximum values for $V_{22.5Gy}$. V_{30Gy}, and D_{mean} were 12.7%, 6.4%, and 9.6 Gy for Plan 1, which is the only plan currently deliverable using clinically available technology (scattered, discrete energy beams). These plans produced a maximum value for NTCP of 0.9%.

Effects of using scattered versus scanned beams were best assessed by comparing Plan 1 with Plan 4 and Plan 3 with Plan 5 for Patient Set 1, because they required only a single beam; however, comparisons for Patient Set 2 were also meaningful, even though Plan 5 did not have the optimal location of the abutment edge for the lower and upper fields. Plots of $\Delta V_{22.5Gy}$. ΔV_{30Gy},

and ΔD_{mean} (scattered beam value less scanned beam value) versus R_{90} showed the general trend that these metrics increased as R_{90} increased (see Figure 4.1). As expected, scanned beams showed the greatest effect (benefit) at the higher energies ($R_p \geq 5$ cm). For the seven patients studied, maximum $V_{22.5Gy}$. V_{30Gy}, and D_{mean} values for Plan 4, which could be deliverable by scanned, discrete energy beams, were reduced to 9.5%, 4.2%, and 7.0 Gy.

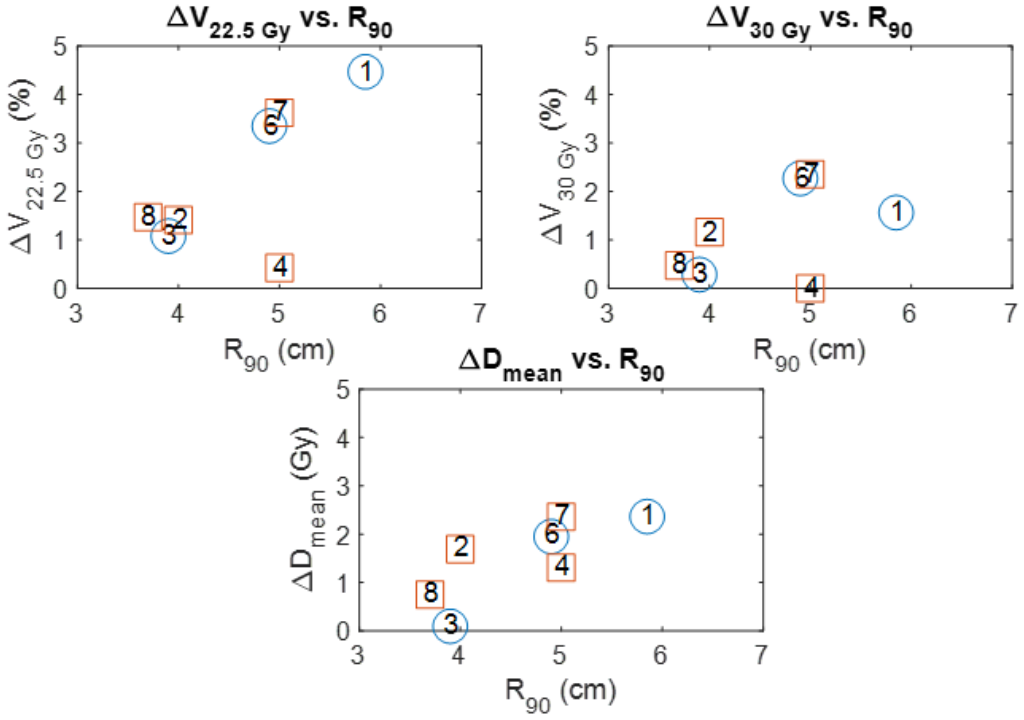

Figure 4.1. Reduction in heart dose metrics (scattered beam value less scanned beam value) versus the average R_{90} of discrete and continuous energy beams overlying heart. The values shown are the average of the differences in dose metrics between Plan 1 and Plan 4 and between Plan 3 and Plan 5 (scattered beam value less scanned beam value). These plots illustrate the effect different R_{90} values have on heart metrics. The general trend is that between scattered and scanned beams, as the R_{90} increases, so do $\Delta V_{22.5Gy}$. ΔV_{30Gy}, and ΔD_{mean}. The CW patient number is indicated inside the circles for Patient Set 1 (1,3,6) and squares for Patient Set 2 (2,4,7,8).

Effects of using continuous versus discrete energy beams were best assessed by comparing Plan 1 with Plan 3 and Plan 4 with Plan 5 for Patient Set 1. Comparisons for Patient Set 2 were not particularly informative because the location of the edge of abutting the upper and lower fields

was not optimized. Plots of $\Delta V_{22.5Gy}$. ΔV_{30Gy}, and ΔD_{mean} (discrete energy beam value less continuous energy beam value) versus R_{90} suggested the general trend that these metrics increased as R_{90} increased (see Figure 4.2). Although only data for three patients, all showed improvement with that for the highest energy beam (R_{90} = 6 cm) being the greatest; for Patient 1 $V_{22.5Gy}$, V_{30Gy}, and D_{mean} values were reduced by 5.6 %, 2.2%, and 1.9 Gy, respectively. Appreciate that this effect could be negligible if the discrete energy selected were the optimal energy; however, in some cases both effects (large R_{90} and suboptimal energy) can be considerable.

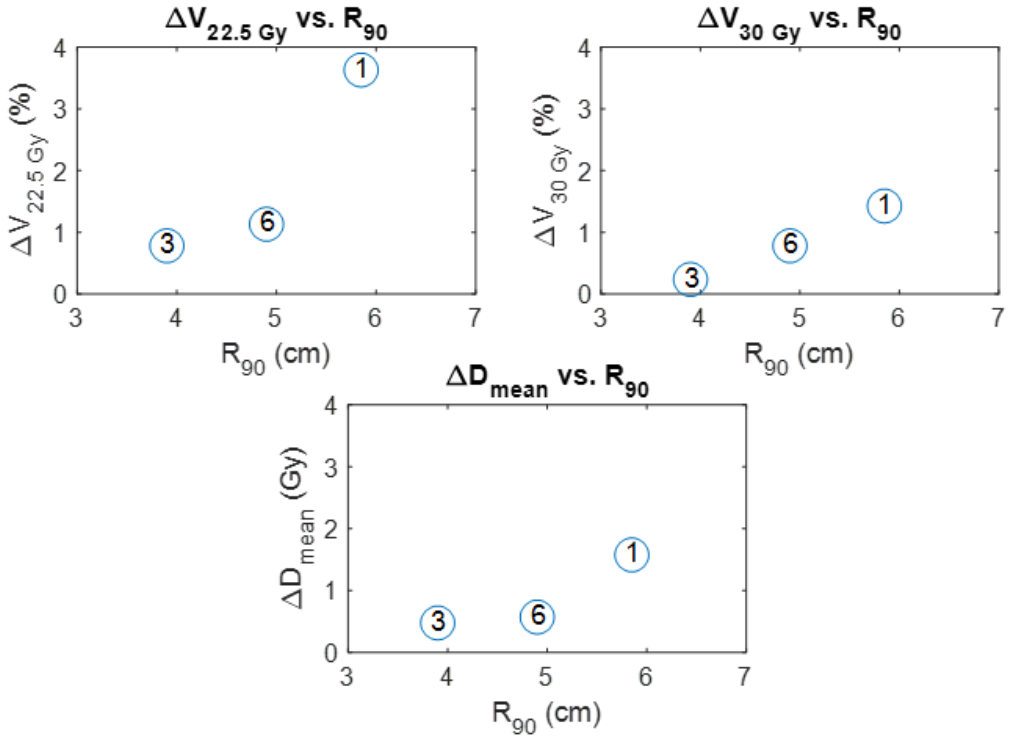

Figure 4.2. Reduction in heart dose metrics (discrete energy beam value less continuous energy beam value) versus the average R_{90} of discrete and continuous energy beams overlying heart. The values shown are the average of the differences in dose metrics between Plan 1 and Plan 3 and between Plan 4 and Plan 5 (discrete beam value less continuous beam value) for patients in Patient Set 1. These plots illustrate the effect different R_{90} values have on heart metrics. The general trend is that between discrete and continuous beams as the R_{90} increases, so do $\Delta V_{22.5Gy}$. ΔV_{30Gy}, and ΔD_{mean}. The CW patient number (1,3,6) is indicated inside the circles.

Combining these effects, scanned, continuous energy beams can provide treatment plans significantly superior to scattered, discrete energy beams. This is best illustrated by CW1, whose

metrics for Plan 1 versus Plan 5 were reduced, $V_{22.5Gy}$ from 10.4% to 2.2%, V_{30Gy} from 3.1% to 0.1%, D_{mean} from 8.3 Gy to 4.3 Gy, and NTCP from 0.4% to 0.1%.

Dose to the heart also depended on (1) the thickness of tissue (Δt) between the distal edge of the PTV and the heart and (2) the energy (hence R_{90}) required for PTV coverage. The former is illustrated by comparing $V_{22.5Gy}$. V_{30Gy}, and D_{mean} versus Δt for Plan 1 (scattered, discrete energy beams) for each of the seven patients planned in this study (see Figure 4.3), which showed the trend that the smaller the value of Δt, the greater the heart dose. The latter is confirmed by comparing $V_{22.5Gy}$. V_{30Gy}, and D_{mean} versus R_{90} for Plan 1 (scattered, discrete energy beams) for each of the seven patients planned in this study (see Figure 4.4), which showed the trend that the greater the energy (hence R_{90}), the greater the heart dose. Therefore, patient plans with the smaller Δt and the greater R_{90} are those that possibly could benefit most from availability of scanned and/or continuous energy beams.

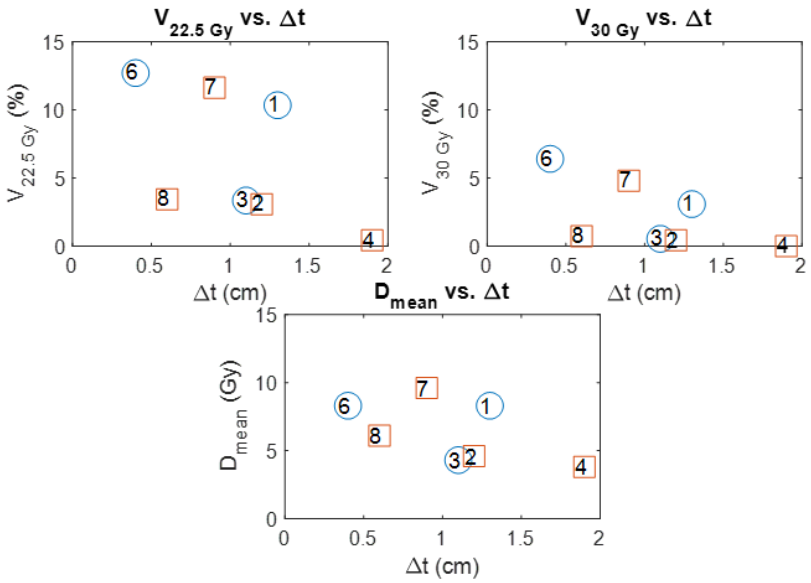

Figure 4.3. Effect of Δt on heart metrics. These plots illustrate the effect of Δt values on heart metrics for Plan 1. The general trend is that as Δt increases, $V_{22.5Gy}$. V_{30Gy}, and D_{mean} decrease. The CW patient number is indicated inside the circles for Patient Set 1 (1,3,6) and squares for Patient Set 2 (2,4,7,8).

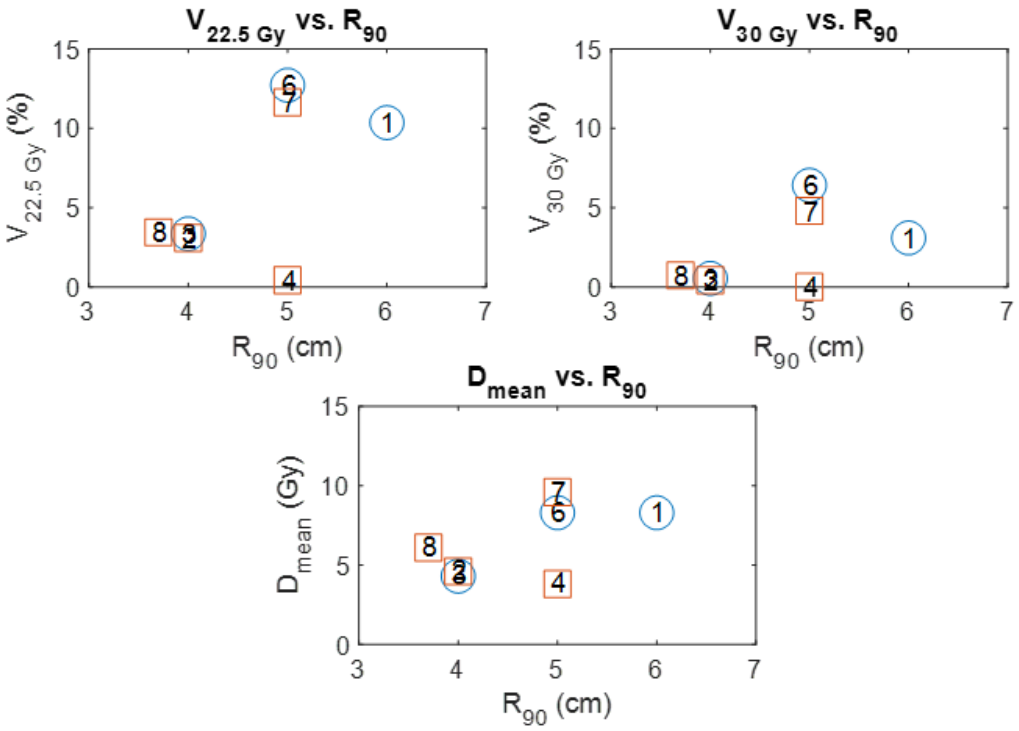

Figure 4.4. Effect of R_{90} on heart metrics. These plots illustrate the effect of R_{90} values on heart metrics for Plan 1. The general trend is that as R_{90} increases, so do $V_{22.5Gy}$. V_{30Gy}, and D_{mean}. The patient number is indicated inside the circles for Patient Set 1 (1,3,6) and squares for Patient Set 2 (2,4,7,8).

4.2. Impact on Lung Dose

For all IM-BECT treatment plans, dose to the lung was low due to using electron beams with conformal bolus, as previously reported.[21] For the seven patients studied, V_{20Gy} values ranged from 11.8% to 20.6% for Plan 1, the only plan deliverable using current scattered, discrete energy beams. These doses are acceptably low, with NTCP values ranging from 0.01% to 1.4%. However, $SCCP_{lin}$ values, which ranged from 10.9% to 18.6%, might be of greater clinical significance.

Effects of using scattered versus scanned beams were best assessed by comparing Plan 1 with Plan 4 and Plan 3 with Plan 5 for Patient Set 1, because they required only a single beam; however, comparisons for Patient Set 2 were also meaningful, even though Plan 5 did not have the ideal location of the abutment edge for the lower and upper fields. Plots of ΔV_{20Gy} and $\Delta SCCP_{lin}$

(scattered beam value less scanned beam value) versus R_{90} showed the general trend that these differences increased as R_{90} increased (see Figure 4.5). In other words, as expected, scanned beams showed greater benefit at the higher energies ($R_p \geq 5$ cm). For the seven patients studied, V_{20Gy} values were reduced to range from 9.2% to 17.8% and $SCCP_{lin}$ values were reduced to range from 8.1% to 13.7% for Plan 4, which could be deliverable by scanned, discrete energy beams.

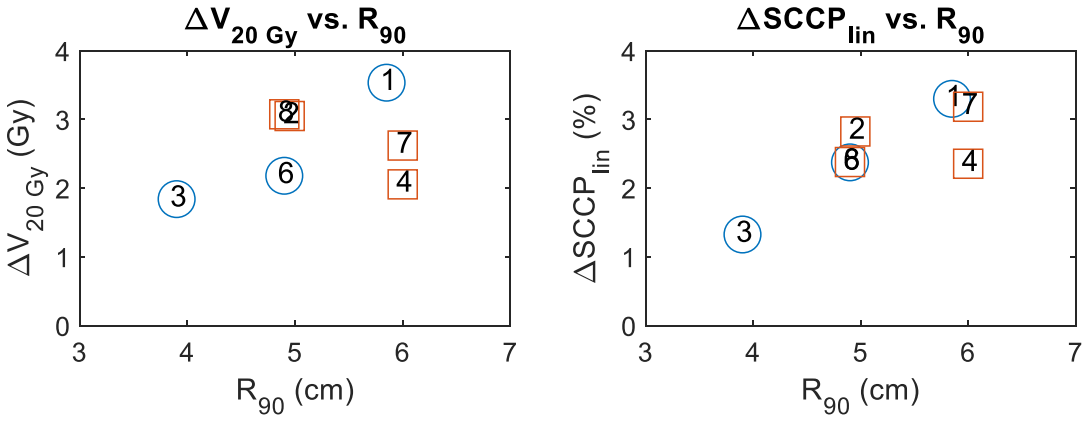

Figure 4.5. Reduction in lung dose metrics (scattered beam value less scanned beam value) versus the average R_{90} of discrete and continuous energy beams overlying lung. The values shown are the average of the differences in dose metrics between Plan 1 and Plan 4 and between Plan 3 and Plan 5 (scattered beam value less scanned beam value). These plots illustrate the effect different R_{90} values have on lung metrics. The general trend is that between scattered and scanned beams, as R_{90} increases, so do ΔV_{20Gy} and $\Delta SCCP_{lin}$. The CW patient number is indicated inside the circles for Patient Set 1 (1,3,6) and squares for Patient Set 2 (2,4,7,8).

Effects of using continuous versus discrete energy beams were best assessed by comparing Plan 1 with Plan 3 and Plan 4 with Plan 5 for Patient Set 1. Comparisons for Patient Set 2 were not particularly informative because the location of the edge of abutting the upper and lower fields abutment was not optimized. Plots of ΔV_{20Gy} and $\Delta SCCP_{lin}$ (discrete energy beam value less continuous energy beam value) versus R_{90} suggested the general trend that these differences increased as R_{90} increased (see Figure 4.6). Although only data for three patients, all showed improvement with that for the highest energy beam (R_{90} = 6 cm) being the greatest, for Patient 1, reducing V_{20Gy} and $SCCP_{lin}$ by as much as 3.1 % and 2.6%, respectively. Appreciate that this effect

could be negligible if the discrete energy selected is the optimal energy; however, in some cases both effects (large R_{90} and suboptimal energy) can be considerable.

Combining these effects, scanned, continuous energy beams can provide treatment plans significantly superior to scattered, discrete energy beams. This is best illustrated by CW1, whose metrics for Plan 1 versus Plan 5 were reduced significantly, V_{20Gy} from 17.2% to 10.7% and $SCCP_{lin}$ from 14.4% to 8.7%.

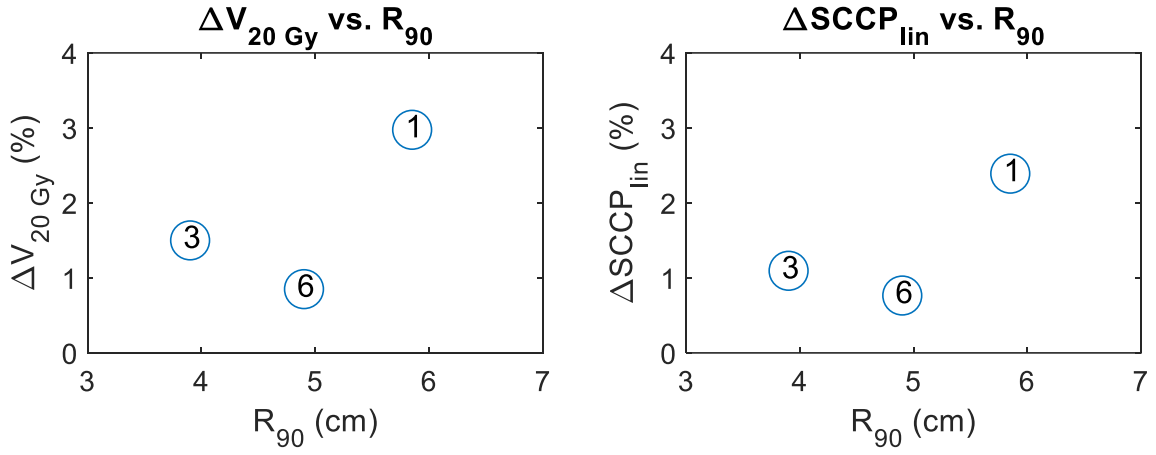

Figure 4.6. Reduction in lung dose metrics (discrete energy beam value less continuous energy beam value) versus the average R_{90} of discrete and continuous energy beams overlying lung. The values shown are the average of the differences in dose metrics between Plan 1 and Plan 3 and between Plan 4 and Plan 5 (discrete beam value less continuous beam value) for patients in Patient Set 1. These plots illustrate the effect different R_{90} values have on lung metrics. The general trend is that between discrete and continuous beams as the R_{90} increases, so do ΔV_{30Gy} and $\Delta SCCP_{lin}$. The CW patient number (1,3,6) is indicated inside the circles.

4.3. Location of Abutting Edge

Although the chest wall field can be treated with a single energy field using IM-BECT, it is often beneficial to treat a superior (upper) field using a higher electron energy and the inferior (lower) field using a lower electron energy, so as to reduce heart dose, as discussed above. This raises the questions of (1) where to put the abutting edge and (2) how to match the penumbras. The latter, described in this work, was achieved by using a common virtual source and feathering

the sharper, higher energy beam penumbra to closely match that of the broader, lower energy beam penumbra.

Regarding the former, placing the edge too superior can result in having to increase the energy of the inferior field to the detriment of increasing heart dose. Placing the edge too inferior can result in greater dose than necessary to parts of the lung, as well as additional heart dose from the bulging of the high energy penumbra of the upper field into the heart. Such was the case in the present study by placing the edge 1 cm superior to the superior extent of the heart. This is illustrated by comparing the heart doses for Plan 2 and Plan 3 in Patient Set 2. For (CW2, CW4, CW7, and CW8), the $V_{22.5Gy}$ heart dose mostly increased from (3.1, 0.4, 11.6, and 3.4 Gy) to (8.4, 0.6, 12.8, and 3.3 Gy), and the D_{mean} heart dose changed from (4.6, 3.8, 9.7, and 4.2 Gy) to (8.1, 3.6, 9.7, and 3.9 Gy); however, the NTCP decreased or remained the same from (0.9, 0.01, 0.5, and 0.1%) to (0.3, 0.01, 0.6, and 0.1%). The increased $V_{22.5Gy}$ was indicative of the encroachment of the higher energy dose, and the reduced NTCP was likely due to the differences in PTV volumes being treated.

4.4. Comparison of IM-BECT with VMAT Plans

The best IM-BECT plans can be compared with VMAT plans used to treat these patients at MBPCC, which have been previously reported.[20] For Patient Set 1, Plan 5 (scanned, continuous energy beams) gives the best results and will be used for comparison. For Patient Set 2, Plan 4 (scanned, discrete energy beams) will be used, as the optimal location of the edge of the abutting electron fields was not used in Plan 5. Plan comparisons for Patient Set 1 should be reasonable, as there was no supraclavicular field. However, comparison of plans in Patient Set 2 is somewhat presumptuous, as the current study did not include planning x-ray beams (possibly IMXT) for the supraclavicular field. However, assuming that supraclavicular fields contribute insignificantly to heart and lung dose, comparison of those metrics should be reasonable.

Selected metrics for the heart and lung are compared in Table 4.1 and Table 4.2, respectively. The results for Patient Sets 1 and 2 are similar; therefore, it is reasonable to report and discuss the results together, which are also computed (averages and standard deviations). Almost all data show that the standard deviations of VMAT plan metrics are small relative to those of the IM-BECT plans. This is possibly due to electron beam plans depending more on beam energy and Δt. Regardless, the increased spread means that some IM-BECT plans will be better or worse than the average, which means the degree of benefit of IM-BECT requires a plan comparison for the specific patient.

Table 4.1. Comparison of heart dose and biologic metrics for IM-BECT and VMAT Plans from Doiron (2018).[41] Plan 4 utilizes scanned, discrete energy beams for IM-BECT, and Plan 5 utilizes scanned, continuous energy beams for IM-BECT.

	Modality-Plan	$V_{22.5Gy}$ (%)	D_{mean} (Gy)	NTCP (%)
Patient Set 1				
CW1	VMAT	9.7	9.0	0.7
	IM-BECT Plan 5	2.3	4.3	0.05
CW3	VMAT	5.5	7.0	0.3
	IM-BECT Plan 5	1.5	3.7	0.03
CW6	VMAT	11.5	10.9	1.6
	IM-BECT Plan 5	8.2	5.8	0.40
Mean (Std Dev)	VMAT	**8.9 (3.1)**	**9.0 (2.0)**	**0.87 (0.54)**
	IM-BECT Plan 5	**4.0 (3.7)**	**4.6 (1.1)**	**0.16 (0.21)**
Patient Set 2				
CW2	VMAT	11.0	10.2	1.0
	IM-BECT Plan 4	1.7	3.9	0.40
CW4	VMAT	9.2	9.2	0.3
	IM-BECT Plan 4	0.1	2.4	0.00
CW7	VMAT	8.7	9.4	0.5
	IM-BECT Plan 4	8.0	7.0	0.31
CW8	VMAT	10.1	9.3	0.6
	IM-BECT Plan 4	2.0	3.7	0.06
Mean (Std Dev)	VMAT	**9.8 (1.0)**	**9.5 (0.5)**	**0.6 (0.3)**
	IM-BECT Plan 4	**3.0 (3.5)**	**4.3 (2.0)**	**0.2 (0.2)**
Patient Sets 1 & 2				
Mean (Std Dev)	VMAT	**9.4 (2.0)**	**9.3 (1.2)**	**1.0 (0.7)**
	IM-BECT Plan 4/5	**3.4 (3.3)**	**4.4 (1.5)**	**0.2 (0.2)**

For the heart, on average, $V_{22.5Gy}$ dose is reduced from 9.8% for VMAT to 3.0% for IM-BECT and D_{mean} is reduced from 9.3 Gy to 4.4 Gy. Although both are significant, NTCP is only reduced from 1.0% to 0.2%, as both are clinically low. So, although the dose reductions are significant, the NTCP models show minor clinical benefit.

For the lungs, average V_{20Gy} doses are similar, being 13.1% for VMAT and 13.0% for IM-BECT; however, values are 14.1% and 9.2% for CW4, demonstrating patient variability. Average D_{mean} doses are reduced from 8.8 Gy to 7.1 Gy. Average NTCP is reduced from 2.8% to 0.2% and $SCCP_{lin}$ is reduced from 15.1% to 10.2%. These differences might further improve (increase) by optimizing the location of the abutting edge for IM-BECT Plan 5.

Table 4.2. Comparison of lungs dose and biologic metrics for IM-BECT and VMAT Plans. Plan 4 utilizes scanned, discrete energy beams for IM-BECT, and Plan 5 utilizes scanned, continuous energy beams for IM-BECT.

	Modality-Plan	V_{20Gy} (%)	D_{mean} (Gy)	NTCP (%)	$SCCP_{lin}$
Patient Set 1					
CW1	VMAT	13.4	8.7	2.7	14.9
	IM-BECT Plan 5	10.7	5.2	0.01	8.7
CW3	VMAT	13.1	8.8	2.8	15.1
	IM-BECT Plan 5	12.5	5.6	0.01	9.4
CW6	VMAT	14.3	9.9	3.4	16.8
	IM-BECT Plan 5	16.8	7.6	0.02	12.8
Mean (Std Dev)	VMAT	**13.6 (0.6)**	**9.1 (0.7)**	**3.0 (0.4)**	**15.6 (1.0)**
	IM-BECT Plan 5	**13.3 (3.1)**	**6.1 (1.3)**	**0.01 (0.01)**	**10.3 (2.2)**
Patient Set 2					
CW2	VMAT	13.5	8.5	2.7	14.7
	IM-BECT Plan 4	10.5	5.3	1.0	8.9
CW4	VMAT	14.1	9.2	3.0	15.7
	IM-BECT Plan 4	9.2	4.8	0.01	8.1
CW7	VMAT	11.0	8.6	2.7	14.6
	IM-BECT Plan 4	16.5	14.6	0.02	14.1
CW8	VMAT	12.4	8.0	2.4	13.8
	IM-BECT Plan 4	14.8	6.5	0.01	9.7
Mean (Std Dev)	VMAT	**12.8 (1.4)**	**8.6 (0.5)**	**2.7 (0.3)**	**14.7 (0.8)**
	IM-BECT Plan 4	**12.8 (3.5)**	**7.8 (4.6)**	**0.3 (0.5)**	**10.2 (2.7)**
Patient Sets 1 & 2					
Mean (Std Dev)	VMAT	**13.1 (1.1)**	**8.8 (0.6)**	**2.8 (0.3)**	**15.1 (0.9)**
	IM-BECT Plan 4/5	**13.0 (3.1)**	**7.1 (3.4)**	**0.2 (0.4)**	**10.2 (2.3)**

Chapter 5. Summary of Results, Conclusion, and Future Works

5.1. Summary of Results

5.1.1. IM-BECT Plans Using Different Electron Beam Machines

IM-BECT treatment plans were generated for seven left-sided postmastectomy radiotherapy patients previously treated at MBPCC using VMAT. The patients were divided into two sets: Patient Set 1, which was comprised of three patients (CW1,CW3,CW6) and required a single electron field to treat the chest wall PTV, and Patient Set 2, which was comprised of four patients (CW2,CW4, CW7, CW8) and required two electron fields of differing energies to treat the chest wall PTV. For this study, only the chest wall PTV was studied, and the supraclavicular field, which requires photon beams to treat, was excluded. For patients in Patient Set 2, the inferior edge of the upper field was feathered to match the penumbra of the lower field. Thus, three beams were used to cover the chest wall PTV for these patients.

Four IM-BECT treatment plans were made for each patient in Patient Set 1, and five IM-BECT plans were made for each patient in Patient Set 2. These plans spanned the spectrum from currently available electron radiotherapy technology, scattered, discrete energy beams, to hypothetical scanned, continuous energy beams. The treatment plans also included scattered, continuous energy beams and scanned, discrete energy beams. To determine the effects of using scattered vs. scanned beams, as well as the effects of using discrete vs. continuous energy spacing, the planar isodose plots, DVHs, and dose and biologic metrics were extracted from the dose distribution for each of 32 plans.

5.1.2. Impact of Machine Technology on Heart Dose

Compared to other PMRT techniques, IM-BECT treatment plans typically have low heart dose,[21] which is due to the use of conformal electron bolus and dose distributions of electron

beams. For the seven patients studied, the $V_{22.5Gy}$, V_{30Gy}, and D_{mean} maximum values were 12.7%, 6.4%, and 9.6 Gy for Plan 1, which uses currently deliverable scattered, discrete energy beams. These doses are low, having maximum NTCP of 0.9%.

When comparing scattered and scanned beam metrics, $\Delta V_{22.5Gy}$, ΔV_{30Gy}, and ΔD_{mean} (scattered beam value less scanned beam value) versus R_{90} showed these metrics increased as R_{90} increased, i.e. scanned beams showed the greatest effect (benefit) at the higher energies ($R_p \geq 5$ cm). For the seven patients studied, maximum $V_{22.5Gy}$, V_{30Gy}, and D_{mean} were reduced to 9.5%, 4.2%, and 7.0 Gy for Plan 4, which could be deliverable by scanned, discrete energy beams.

When comparing discrete and continuous energy beams, $\Delta V_{22.5Gy}$, ΔV_{30Gy}, and ΔD_{mean} (discrete energy beam value less continuous energy beam value) versus R_{90} suggested that these metrics increased as R_{90} increased. Although only data for three patients (Patient Set 1) was used, all showed improvement, that for the highest energy beam (R_{90} = 6 cm) being the greatest with $V_{22.5Gy}$, V_{30Gy}, and D_{mean} values being reduced by as much as 4.6 %, 2.2%, and 1.9 Gy, respectively. Of course, this effect could be negligible if the discrete energy selected was equal or near the optimal energy.

In some patient cases, the effects of using both scanned and continuous energy beams were observed. This is clearer for patients in Patient Set 1 because there were no abutment issues. If we compare Plan 5 and Plan 1 metrics for CW1, there were reductions in $V_{22.5Gy}$ from 10.4% to 2.2%, V_{30Gy} from 3.1% to 0.1%, D_{mean} from 8.3 Gy to 4.3 Gy, and NTCP from 0.4% to 0.1%.

For all patients, the beam energy required for the lower field (based on maximum PTV thickness) and the thickness of tissue between the distal edge of the PTV and the heart (Δt) affected heart dose. Looking at Plan 1 for all patients shows that heart dose (1) decreased as the thickness of tissue (Δt) between the distal PTV edge and the heart increased and (2) increased as the R_{90}

(hence energy) required for PTV coverage increased. Therefore, patient plans with the smaller Δt and greater R_{90} are those that possibly could benefit most from availability of scanned and/or continuous energy beams with regards to heart dose.

5.1.3. Impact of Machine Technology on Lung Dose

For all IM-BECT treatment plans, dose to the lung was low due to using electron beams with conformal bolus, as previously reported.[41] For the seven patients studied, V_{20Gy} values ranged from 11.8% to 20.6% for Plan 1, the only plan deliverable using current scattered, discrete energy beams. These doses are acceptably low, having NTCP values ranging from 0.01% to1.4%. However, reducing $SCCP_{lin}$ values, which ranged from 10.9% to 18.6%, could be of concern.

Effects of using scattered versus scanned beams were best assessed by comparing Plan 1 with Plan 4 and Plan 3 with Plan 5 for Patient Set 1, because they required only a single beam; however, comparisons for Patient Set 2 were also meaningful, even though Plans 3 and 5 did not have the optimal location of the abutment edge for the lower and upper fields. Plots of ΔV_{20Gy} and $\Delta SCCP_{lin}$ (scattered beam value less scanned beam value) versus R_{90} showed the general trend that lung sparing benefitted from scanned beams and that the benefit increased as R_{90} increased. For the seven patients studied, V_{20Gy} values ranged from 9.2% to 17.8% and $SCCP_{lin}$ values ranged from 8.1% to 13.7% for Plan 4 (scanned, discrete energy beams). Improving location of the abutting edge for the upper and lower electron fields should further increase the benefit for Patient Set 2.

Effects of using continuous versus discrete energy beams were assessed by comparing Plan 1 with Plan 3 and Plan 4 with Plan 5 for Patient Set 1. Plots of ΔV_{20Gy} and $\Delta SCCP_{lin}$ (discrete beam energy value less continuous beam energy value) versus R_{90} suggested the general trend that lung sparing benefitted from continuous beam energy and that the benefit increased as R_{90} increased. Although only data for three patients, all showed improvement. The greatest, Patient CW1 (R_{90} =

6 cm), showed V_{20Gy} and $SCCP_{lin}$ reduced by 3.1 % and 2.6%, respectively. As for the heart, this effect could be negligible if the discrete energy selected was the optimal energy.

In some cases, the effects of using both scanned and continuous energy beams are significant. This is clearest for patients in Patient Set 1 because there are no abutment issues. Comparing Plan 5 metrics with Plan 1 metrics for CW1 shows that lung metrics are significantly reduced, V_{20Gy} from 17.2% to 10.7% and $SCCP_{lin}$ from 14.4% to 8.7%.

5.1.4. Impact of Location of Abutting Edge

For patients in Patient Set 2, the location of the abutting edge had a significant impact on the dose distribution and the heart and lung metrics. Placing the edge too superior can result in having to increase the energy of the inferior field to the detriment of increasing heart dose. Placing the edge too inferior can result in greater dose than necessary to parts of the lung, as well as additional heart dose from the bulging of the high energy penumbra of the upper field into the heart. Such was the case in the present study by placing the edge 1 cm superior to the superior extent of the heart. This was illustrated by comparing the heart dose for Plan 2 and Plan 3 in Patient Set 2. For (CW2, CW4, CW7, and CW8), $V_{22.5Gy}$ heart dose generally increased or changed little, from (3.1, 0.4, 11.6, and 3.4 Gy) to (8.4, 0.6, 12.8, and 3.3 Gy), and D_{mean} heart dose generally increased or changed little, from (4.6, 3.8, 9.7, and 4.2 Gy) to (8.1, 3.6, 9.7, and 3.9 Gy); however, NTCP decreased or changed little, from (0.9, 0.01, 0.5, and 0.1%) to (0.3, 0.01, 0.6, and 0.1%). For CW2 the increased heart $V_{22.5Gy}$ was most indicative of the encroachment from the higher energy upper field.

5.2. Response to Hypothesis

Hypothesis: For seven post-mastectomy radiotherapy left-side chest wall patients previously treated with volumetric modulated arc therapy (VMAT), treatment plans using intensity modulated bolus electron conformal therapy (IM-BECT) with a scanned electron beam and/or the

capability of continuous energy spacing can be superior (increased sparing of heart and lung and reduced chance of secondary cancer) to plans made using IM-BECT with a passively scattered electron beam and discrete Elekta energy spacing.

True, although a small sample of patients (seven), this study showed that IM-BECT treatment plans using scanned and/or continuous energy beams provided plans superior to plans using current scattered, discrete energy beams for some, but not all, patient plans.

5.3. Potential Clinical Impact

5.3.1. Impact of Scanned, Continuous Energy Beams

Availability of scanned, continuous energy beams would provide treatment plans superior to those currently available, which use scattered, discrete energy beams. However, there are several caveats to consider and possibly further study.

Previous studies have shown that IM-BECT offers increased dose sparing to the heart as opposed to other PMRT techniques.[21] For some patients, that benefit can be further increased using scanned and/or continuous energy beams, as illustrated by this study. Better understanding of this benefit requires additional studies. Also, the NTCP for the scattered, discrete energy beam plan is quite low, perhaps minimizing the impact of improved plans.

Shown in this study, lung dose can be reduced using scanned, continuous energy beams; however, the impact on NTCP is small, but perhaps of value for some patients. $SCCP_{lin}$ is significantly less using scanned, continuous energy beams, and it could likely be further improved by optimizing the abutting edge.

The benefit of scanned, continuous energy beams depends on the patient geometry, specifically the depth of the PTV (hence R_{90}) and the distance between the PTV distal surface and the proximal

surface of the heart (Δt). The benefits of using these proposed modalities varied between the different patients in this study. Further studies could better identify patient indications for using scanned, continuous energy electron beams.

The current study was suboptimal due to its suboptimal methods of selecting the abutting edge of the upper and lower fields. Hence, benefit of scanned and/or continuous energy beams should improve with an optimized edge.

It appears that the benefit of scanned beam technology might be more significant than continuous beam technology. This is in part due to the discrete energy beam possibly being the optimal energy. However, the scanned beam always produces a sharper dose falloff, improving the dose distribution. Also, the improvement in dose falloff (R_{90-10}) is always more for scanned versus scattered beam than using a slightly lower beam energy available with continuous energy beams.

5.3.2. Comparison of IM-BECT and VMAT Treatment Plans

The best possible IM-BECT plans, Plan 5 for Patient Set 1 and Plan 4 for Patient Set 2, were compared with patient VMAT plans from our clinic.[20] Because the IM-BECT plans excluded the supraclavicular PTV, only lung and heart dose were compared.

For heart dose, the average $V_{22.5Gy}$ was reduced from 9.8% for VMAT to 3.0% for IM-BECT, and average D_{mean} was reduced from 9.3 Gy to 4.4 Gy. Although such reductions were significant, NTCP models showed only minor average reduction from 1.0% to 0.2%, both clinically low.

For lung dose, the average V_{20Gy} doses were similar, 13.1% for VMAT and 13.0% for IM-BECT; however, values were 14.1% and 9.2%, respectively for CW4, demonstrating patient variability for benefits of IM-BECT. Average D_a was reduced from 8.8 Gy to 7.1 Gy; however,

average NTCP was reduced from 2.8% to 0.2%, and average $SCCP_{lin}$ was reduced from 15.1% to 10.2%. $SCCP_{lin}$ was reduced from 15.7% to 8.1% for CW4, demonstrating the potential benefit for a single patient.

These results show that for some patients, IM-BECT can provide plans that are significantly superior to VMAT.

5.4. Recommendations for Future Investigation

5.4.1. Revised Simple Planning Method

In future studies, it is recommended that only four plans be generated for each patient in Patient Set 2, as was the done in Patient Set 1. The four plans should use (1) scattered, discrete energy beams, (2) scattered, continuous energy beams, (3) scanned, discrete energy beams, and (4) scanned, continuous energy beams. Each plan should use the following steps:

1. Location of Abutting Edge: Select the lowest continuous energy (R_{90}) possible for a field covering only the heart PTV. Then, move the superior edge of the lower field superiorly as much as possible, while treating the chest wall with the 90% dose surface. That field edge specifies the abutting edge of the lower and upper fields for Plans 1 – 4.
2. Lower and Upper Field Beam Energies: Select the lowest available energies available (discrete or continuous depending) for the lower and upper fields for which the 90% dose surface contains the PTV.
3. Edge Feathering: Use the same procedure for feathering of the upper field edge as specified in the present methods.

Alternatively, the lowest energy (continuous or discrete) possible for a field covering only the heart PTV can be used. Then, the superior edge of the lower field can be moved superiorly as

much as possible while treating the chest wall with the 90% dose surface. That field edge is used only for that plan.

5.4.2. Revised Complex Planning Method

This method optimizes the location of the abutting edge. It is recommended that a fast method be developed for finding the optimal location of the abutting edge between the upper, greater energy field and the lower, lesser energy field. This is needed for those patients in Patient Set 2, which required upper and lower fields of differing beam energy.

In the present study, in Plans 3 and 5, the edge was 1.0 cm superior to the superior aspect of the heart. This allowed selection of the lowest available energy for the field overlying the heart; however, it did not necessarily give the lowest heart dose, due to dose from the bulging edge of the higher energy upper field reaching the heart. Also, because the energy had to be sufficiently high to cover the superior aspect of the chest wall, where PTV depth can be deeper, it resulted in a higher dose than needed over portions of the lung. Although bolus electron conformal therapy places R_{90} at the distal PTV, a higher energy than necessary results in a greater $R_{90\text{-}10}$, giving greater than necessary dose to lung. As the field edge is moved superiorly, the lung receives less dose, as a greater portion of the lung is irradiated with the lower energy lower field. However, the heart dose can increase if a slightly greater energy is required. Therefore, any optimization criteria need to quantify the benefit of these competing effects of decreased lung dose at the expense of increased heart dose.

5.4.3. Increasing Number of Patients for the Study

It is recommended that the number of patients in the study be increased approximately an order of magnitude. Results showed that the amount of heart dose depended on the distance between the distal PTV surface and the heart R_{90} of the energy required for the lower field.

In addition, the benefit of continuous versus discrete energy beams, for both lung and heart dose, depends on how close the ideal continuous energy is to the next greatest discrete energy required. Also, the benefit of scanned versu[41]s scattered beams is greatest for higher energy beam (≥ 15 MeV). Therefore, for the right conditions, currently available scattered, discrete energy beams might be very close to optimal. Also, for the right conditions, scanned and/or continuous energy beams might significantly improve treatment than using currently available scattered, discrete energy beams. Hence, a larger number of patients is required to determine the fraction that might benefit and the amount they might benefit from either scattered, continuous energy; scanned, discrete energy; or scanned, continuous energy beams.

5.4.4. Including the Supraclavicular Field in the Study

New IM-BECT patient plans should also include comparison with VMAT treatment plans. To make that comparison complete, the supraclavicular PTV should be included with the electron plan, treated either with VMAT or opposed IMXT as demonstrated by Doiron (2018). This should demonstrate the benefit of IM-BECT over VMAT for currently available scattered, discrete energy beams, as well as potential future beams using scattered, continuous energy beams; scanned, discrete energy beams; or scanned, continuous energy beams.

Appendix A. Description of p.d Bolus Design Operators

Table A.1 Description of p.d Bolus Design Operators

Operators used to design the bolus for ECT using p.d are based on a subset of the operators of Low et al. (1992) with some small changes. For more detail, refer to the p.d user manual.

Construction and Extension Operators
Creation Operator, $C_p\,(R_t, \Delta_I)$ **R_t is a user specified therapeutic range (typically R_{90}).** Δ_I is a user specified target inner margin, which is a distance, in the plane of the isocenter, between the edge of the target volume and the solid angle within which the initial bolus is designed. This operator creates an initial bolus surface. With respect to the source, the proximal patient skin surface defines the distal bolus surface**.** C_p only defines proximal bolus surface for ray-lines intersecting the target volume less target inner margin **(TVLM)** by bolus thickness $b_{i,j}$ along each *(i,j)* ray-line, where $b_{i,j} = (R_t - d_{i,j})$ where: $d_{i,j}$ is the distance from the proximal patient surface to the distal target surface along the (i, j) ray-line**;** **Note**: If $b_{i,j} < 0.2\ cm, b_{i,j} = 0.2\ cm$. The bolus surface is extended laterally using the height extension operator below**.**
Height Extension Operator, $H_h\,(\Delta_I, \Delta_O)$ Δ_O is a user specified block outer border margin, which is the distance, in the isocenter plane, between the inner edge of the custom electron applicator (block) and the unmilled region of the wax bolus (i.e. the block outer border). This operator extends bolus height on *(i,j)* ray-lines within the TVLM to the block outer border. The extended bolus heights $H_{i',j'}$ are defined separately for three zones (Low et al. 1992). In this work bolus heights in zone 1 were defined as the shorter of $h_{i,j}$ or the harmonic mean of $(h_{i,j})_x$ and $(h_{i,j})_y$**.** Zones 2 and 3 are defined as per Low et al. **where:** **$h_{i,j}$ is the nearest neighbor of $H_{i',j'}$ within the TVLM.** **$(h_{i,j})_x$ is the nearest neighbor of $H_{i',j'}$, where $j = j'$.** **$(h_{i,j})_y$ is the nearest neighbor of $H_{i',j'}$, where $i = i'$.**

(table cont'd)

Table A.1 Description of p.d Bolus Design Operators, cont.

Modification Operators
Isodose Shift Operator, *I* $(\%D, \Delta_I)$ ***%D*** is a user definition of a distal percent dose surface $(\boldsymbol{d}_{i,j})_{\%D}$ specified as percent given dose. **(**Typically, **%D = 90%)** Isodose Shift tries to match $(\boldsymbol{d}_{i,j})_{\%D}$ to a distal target surface $(\boldsymbol{d}_{i,j})_{target}$ by modifying bolus thickness $(\boldsymbol{b}_{i,j})_{old}$ as $(\boldsymbol{b}_{i,j})_{new} = (\boldsymbol{b}_{i,j})_{old} + (\boldsymbol{d}_{i,j})_{\%D} - (\boldsymbol{d}_{i,j})_{target}$.
Smoothing Operator, $G_h(\mu, \eta, ps)$ $\boldsymbol{\mu}$ is a user specified exponential smoothing weight coefficient**.** $\boldsymbol{\eta}$ is a user specified smoothing region size factor. $\boldsymbol{a^2}$ is a predefined to be 15mm. $$(\boldsymbol{h}_{i,j})_{smooth}(\mu, \eta, ps) = \frac{\sum_{\eta a}[\boldsymbol{h}_{i',j'} e^{-\mu r^2/(2a^2)}]}{\sum_{\eta a}[e^{-\mu r^2/(2a^2)}]}$$ where: $(\boldsymbol{h}_{i,j})_{smooth}$ is the smoothed bolus height on each (i, j) ray-line. $\boldsymbol{a}$ is bolus point spacing $\boldsymbol{ps}$ projected on each (i, j) ray-line to the distal target surface. $\boldsymbol{h}_{i',j'}$ is unsmooth bolus height along (i', j') ray-lines within the region $\boldsymbol{\eta a}$**.** $\boldsymbol{r}$ is the distance from an (i, j) ray-line to an (i', j') ray-line, where $r \leq \eta a$**.**
Specified Shift Operator, *S* (δ, Δ_O) δ is a specified shift of the milled bolus surface. This operator shifts the entire proximal bolus surface inside the block outer border toward the beam source by δ, effectively changing the bolus thickness along each (*i,j)* ray-line to $\boldsymbol{b}_{i,j} = \boldsymbol{b}_{i,j} + \delta$**.** A negative value of δ shifts the entire proximal bolus surface inside the block outer border away from the beam source, shifting isodose lines (IDL) deeper into the patient.
Truncation Operator, *T* (Δ_O) This operator only modifies the proximal bolus surface outside the block outer border defined by Δ_O by truncating bolus height $\boldsymbol{h}_{i,j}$ on each (*i,j)* ray to $(\boldsymbol{h}_{i,j})_{max}$**.** where: $(\boldsymbol{h}_{i,j})_{max}$ is the maximum bolus surface height within the block outer border**.**
Modulate Intensity Operator, $M(\Delta_I, w_{max})$ This operator modifies weights $\boldsymbol{w}_{i,j}$ of each PBRA pencil beam intersecting the TVLM, i.e. within Δ_I, as $(\boldsymbol{w}_{i,j})_{new} = (\boldsymbol{w}_{i,j})_{old} \cdot \boldsymbol{min}[\boldsymbol{w}_{max}, \mathbf{100\%}/\boldsymbol{d}_{max(i,j)}]$**.** Presently, the 1st application of $\boldsymbol{M}$ in p.d uses $(\boldsymbol{w}_{i,j})_{old} = (\boldsymbol{w}_{i,j})_{initial} = \mathbf{1.0}$. where: $\boldsymbol{d}_{\mathbf{max}(i,j)}$ is the maximum dose along each *(i,j)* ray-line. $\boldsymbol{w}_{max}$ is the un-normalized maximum pencil beam weight (1.1 in this work). Outside the TVLM, IM weights are extended according to Low et al. The pencil beam weights are converted to a island block distribution for calculation as described by Hilliard[30]

Appendix B. Treatment Planning Results

B.1. Patient Set 1 (CW1, CW3, CW6)

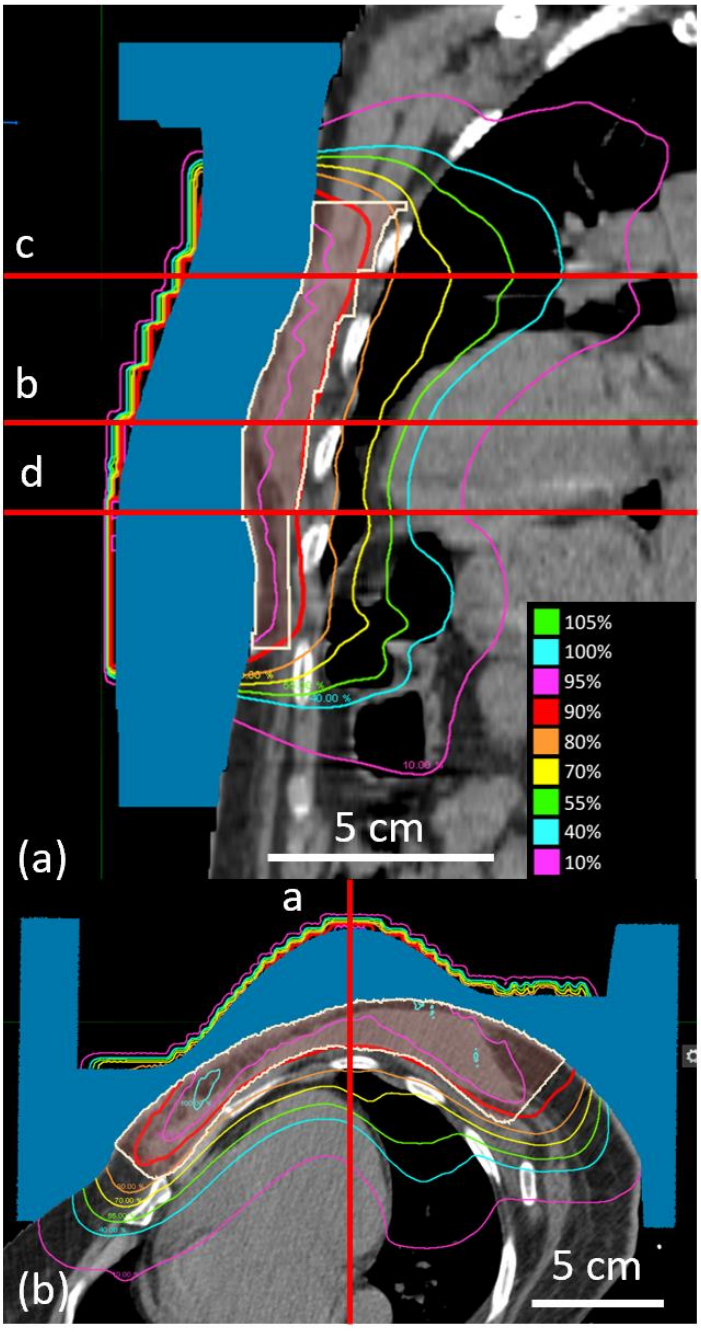

Figure B.1. **Sagittal and axial images of CW1, Plan 1**. CW1 (Patient Set 1) was planned using scattered electron beams and discrete energy spacing. (a) Dose plan in the sagittal-coronal, oblique plane demarcated by the red line in figure (b)'s transverse plane; (b) Dose plan in transverse plane passing through central heart region, demarcated by red line in figure (a)'s oblique plane. Bolus is shaded blue, and PTV is outlined in white. Key shows dose values.
(figure cont'd.)

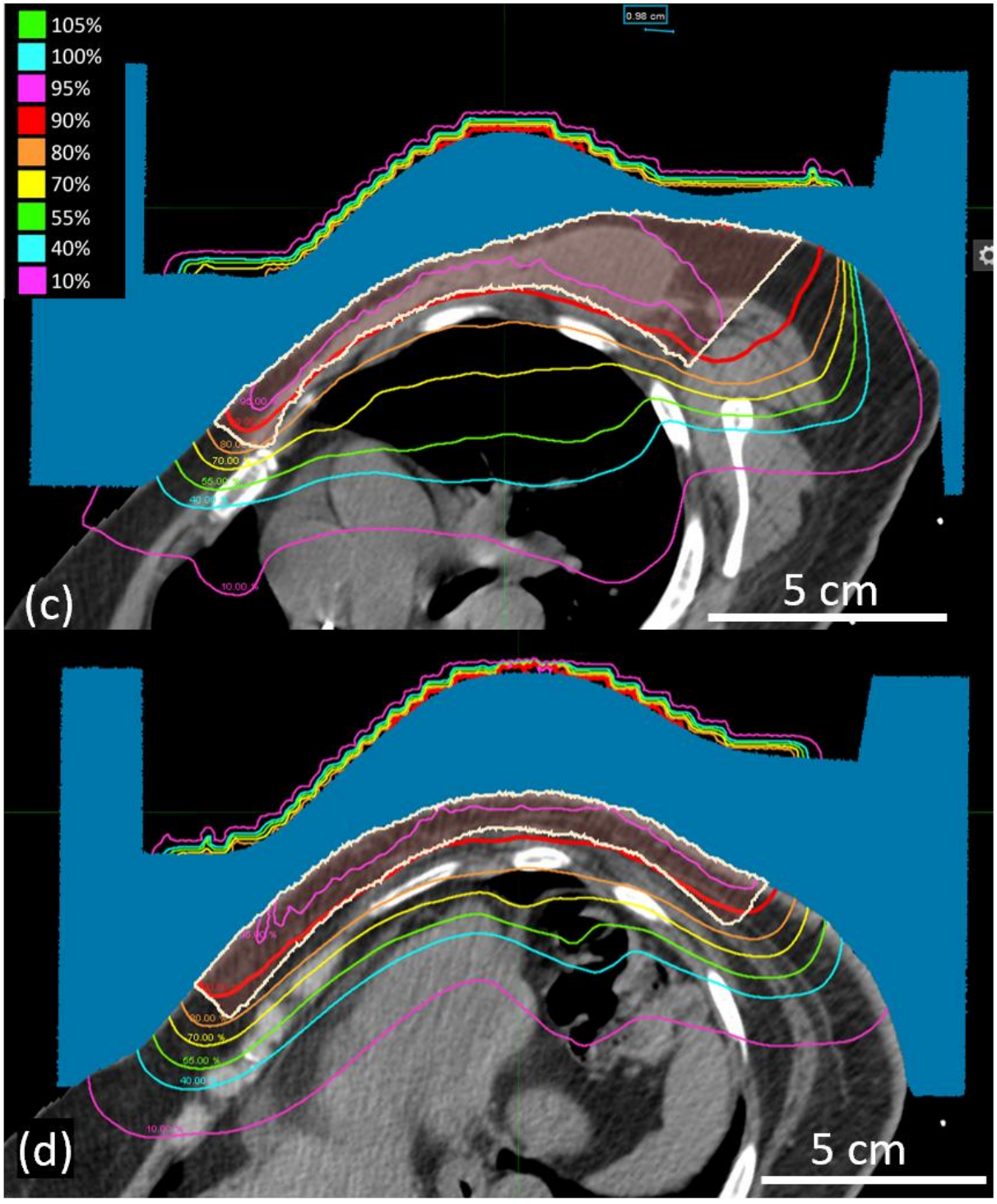
105%
100%
95%
90%
80%
70%
55%
40%
10%
0.98 cm
(c)
5 cm
(d)
5 cm

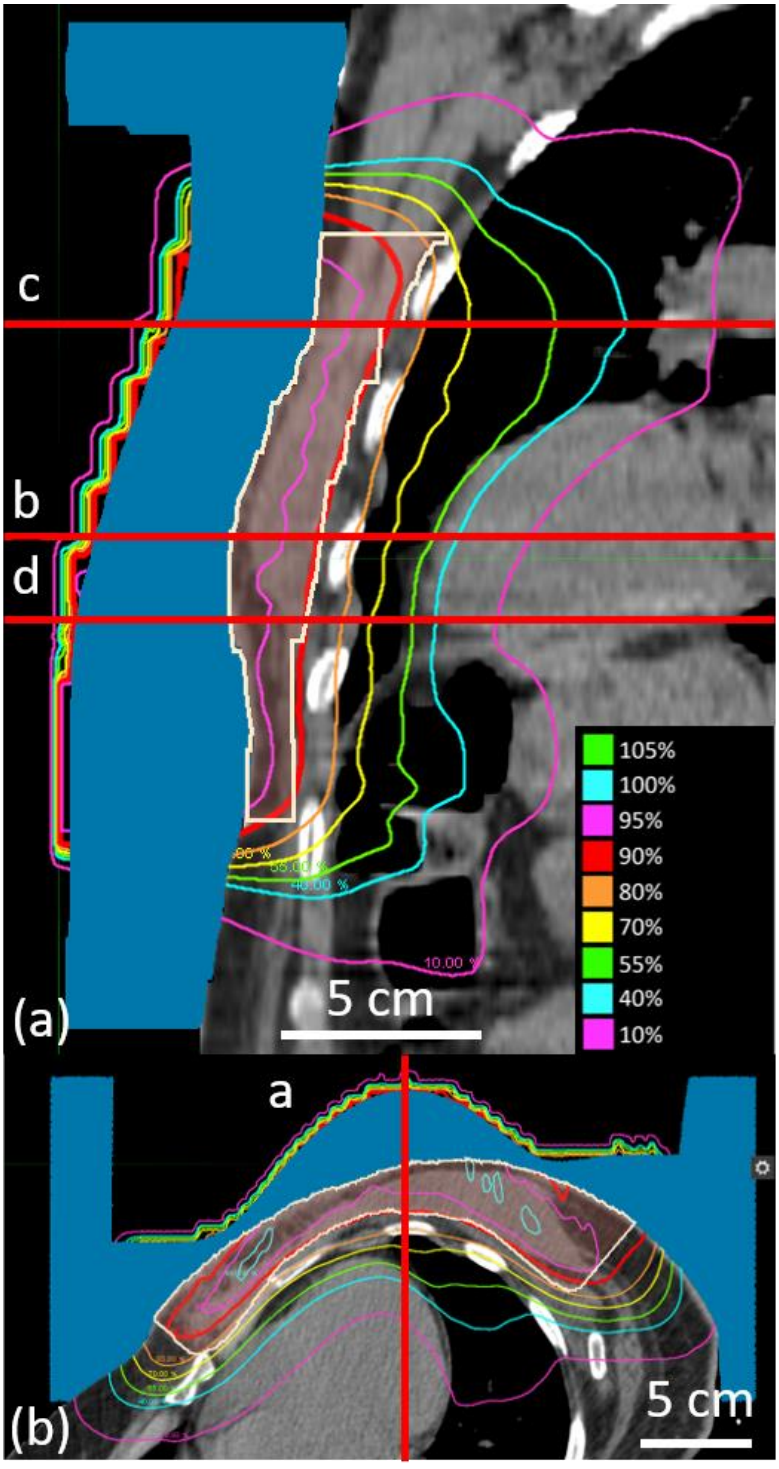

Figure B.2. **Sagittal and axial images of CW1, Plan 2**. CW1 (Patient Set 1) was planned using scattered electron beams and continuous energy spacing. (a) Dose plan in the sagittal-coronal, oblique plane demarcated by the red line in figure (b)'s transverse plane; (b) Dose plan in transverse plane passing through central heart region, demarcated by red line in figure (a)'s oblique plane. Bolus is shaded blue, and PTV is outlined in white. Key shows dose values.
(figure cont'd.)

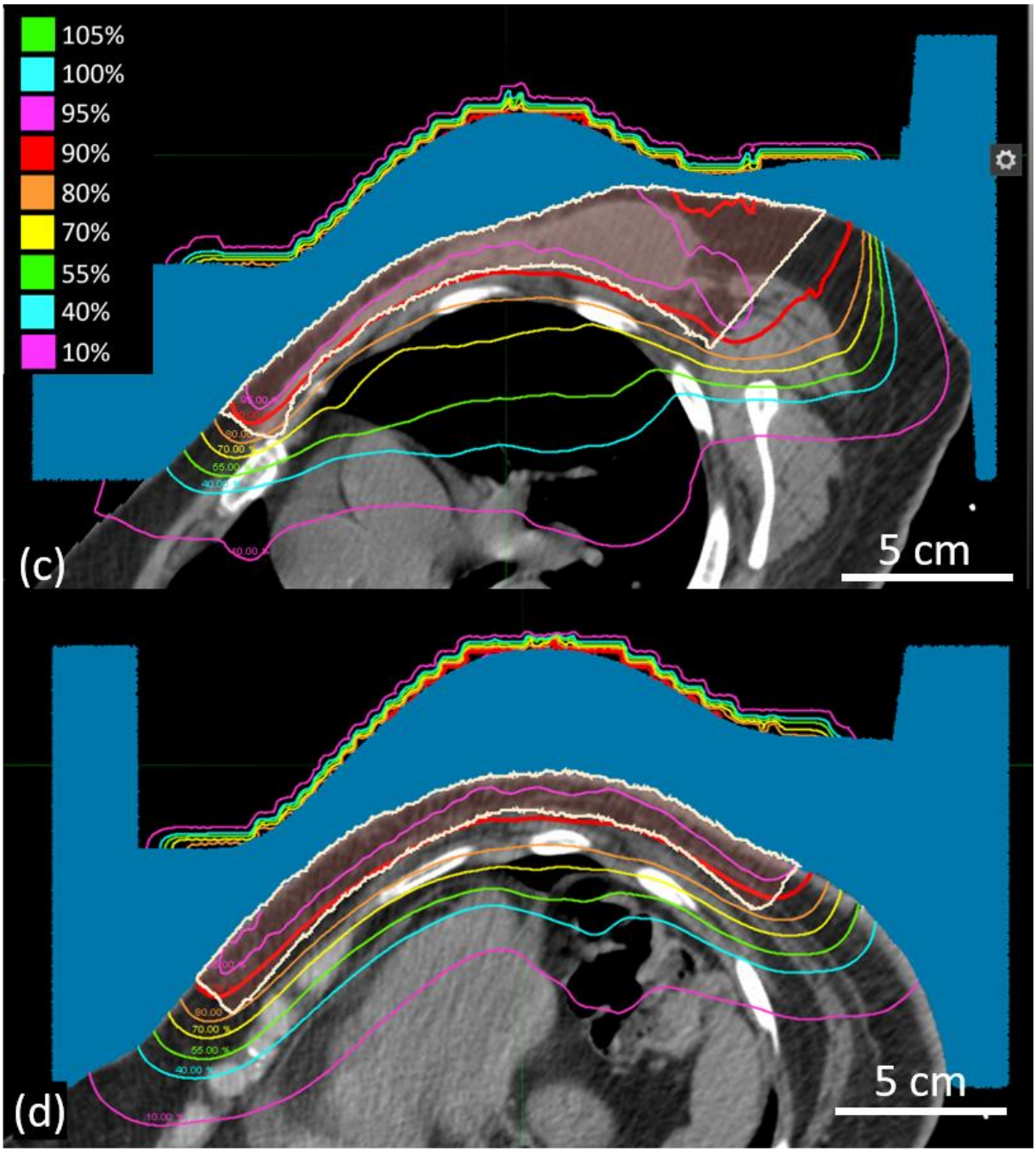
105%
100%
95%
90%
80%
70%
55%
40%
10%
(c)
5 cm
(d)
5 cm

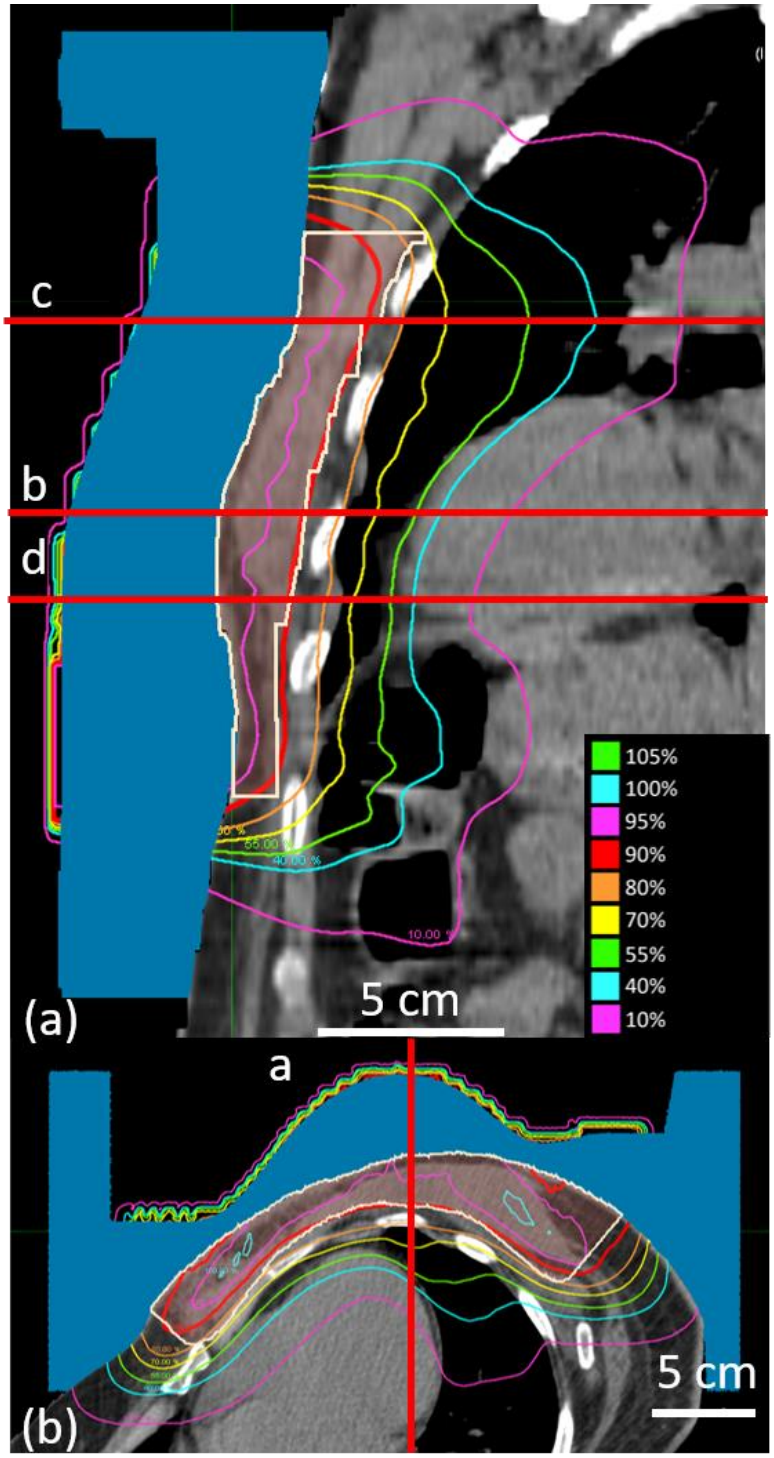

Figure B.3. **Sagittal and axial images of CW1, Plan 4**. CW1 (Patient Set 1) was planned using scanned electron beams and discrete energy spacing. (a) Dose plan in the sagittal-coronal, oblique plane demarcated by the red line in figure (b)'s transverse plane; (b) Dose plan in transverse plane passing through central heart region, demarcated by red line in figure (a)'s oblique plane. Bolus is shaded blue, and PTV is outlined in white. Key shows dose values.
(figure cont'd.)

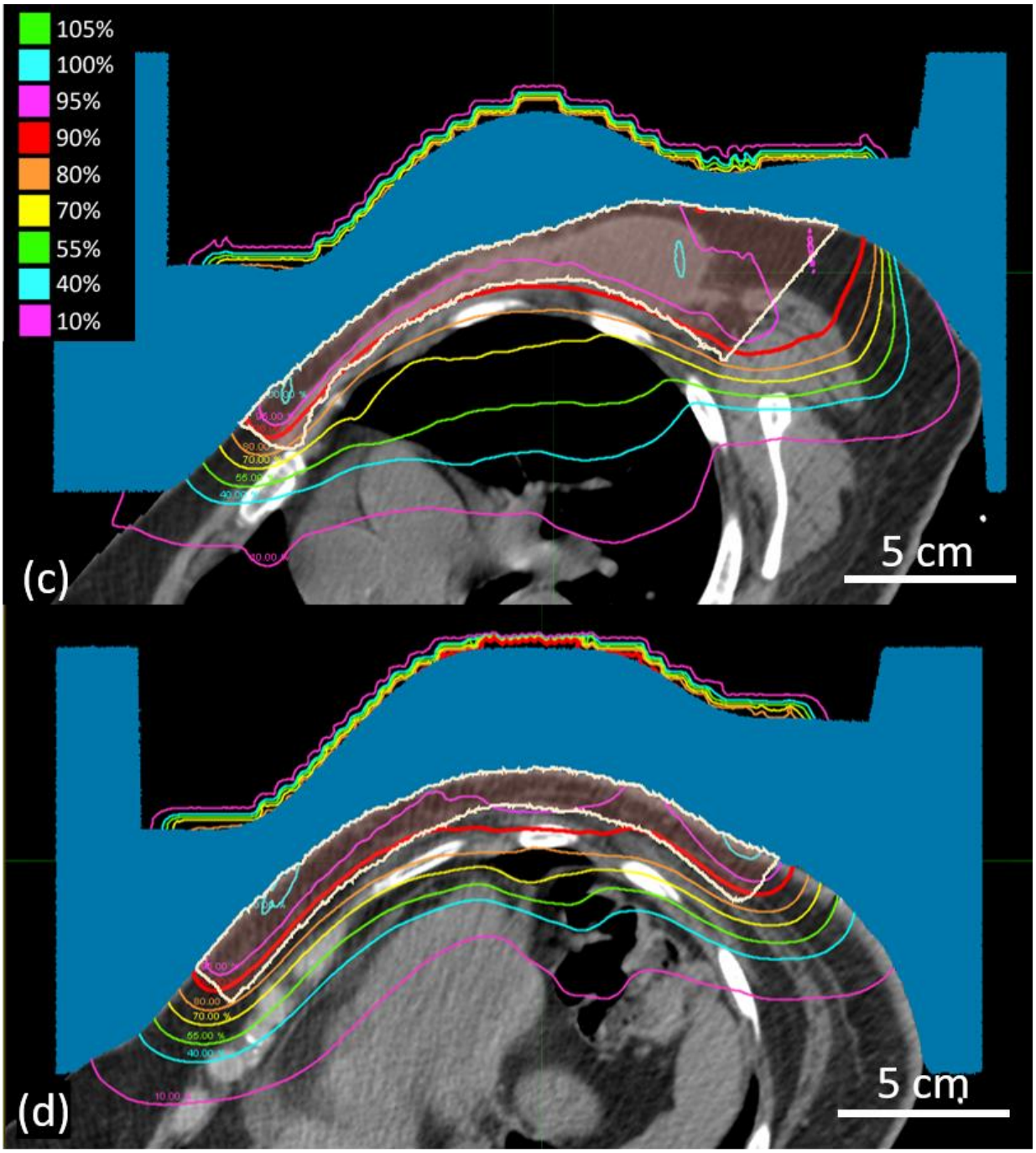
105%
100%
95%
90%
80%
70%
55%
40%
10%
(c)
5 cm
(d)
5 cm

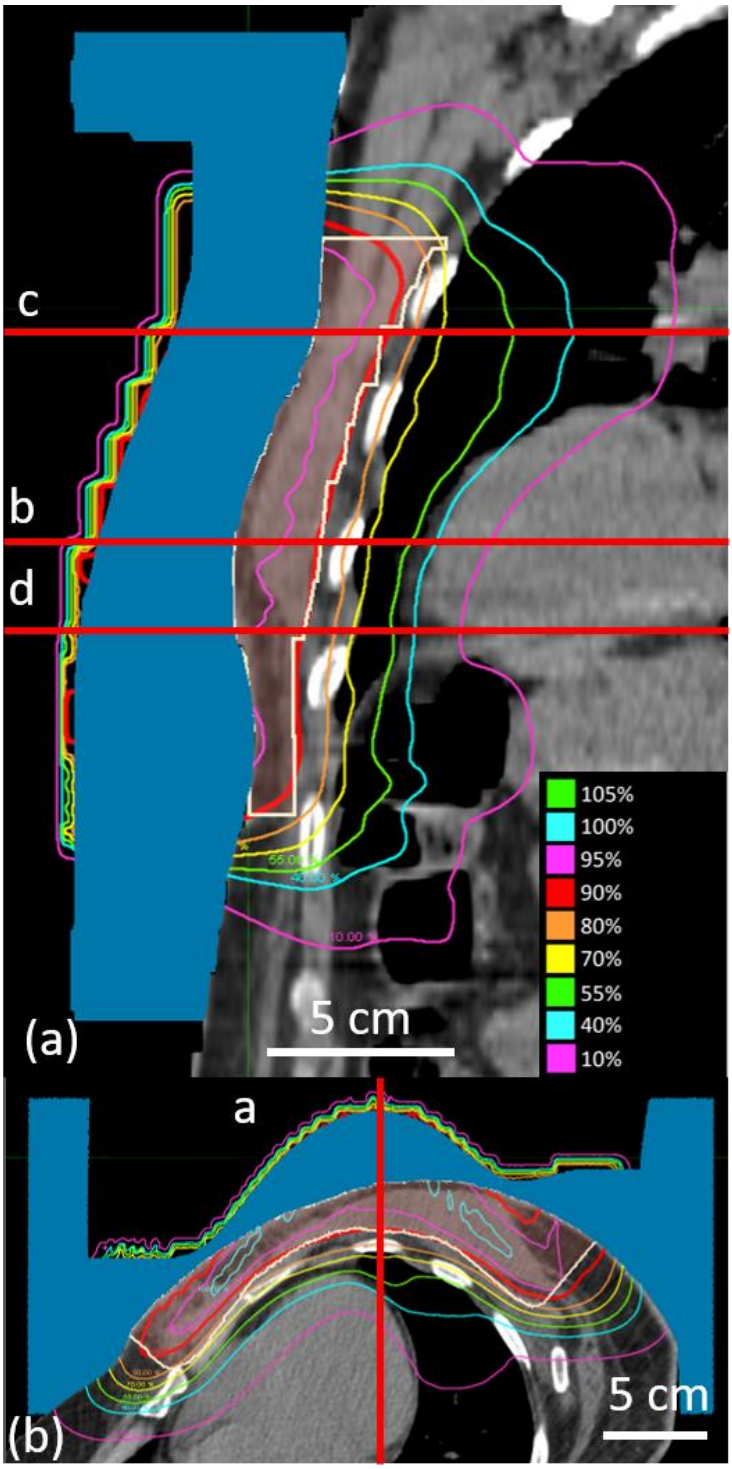

Figure B.4. **Sagittal and axial images of CW1, Plan 5**. CW1 (Patient Set 1) was planned using scanned electron beams and continuous energy spacing. (a) Dose plan in the sagittal-coronal, oblique plane demarcated by the red line in figure (b)'s transverse plane; (b) Dose plan in transverse plane passing through central heart region, demarcated by red line in figure (a)'s oblique plane. Bolus is shaded blue, and PTV is outlined in white. Key shows dose values.
(figure cont'd.)

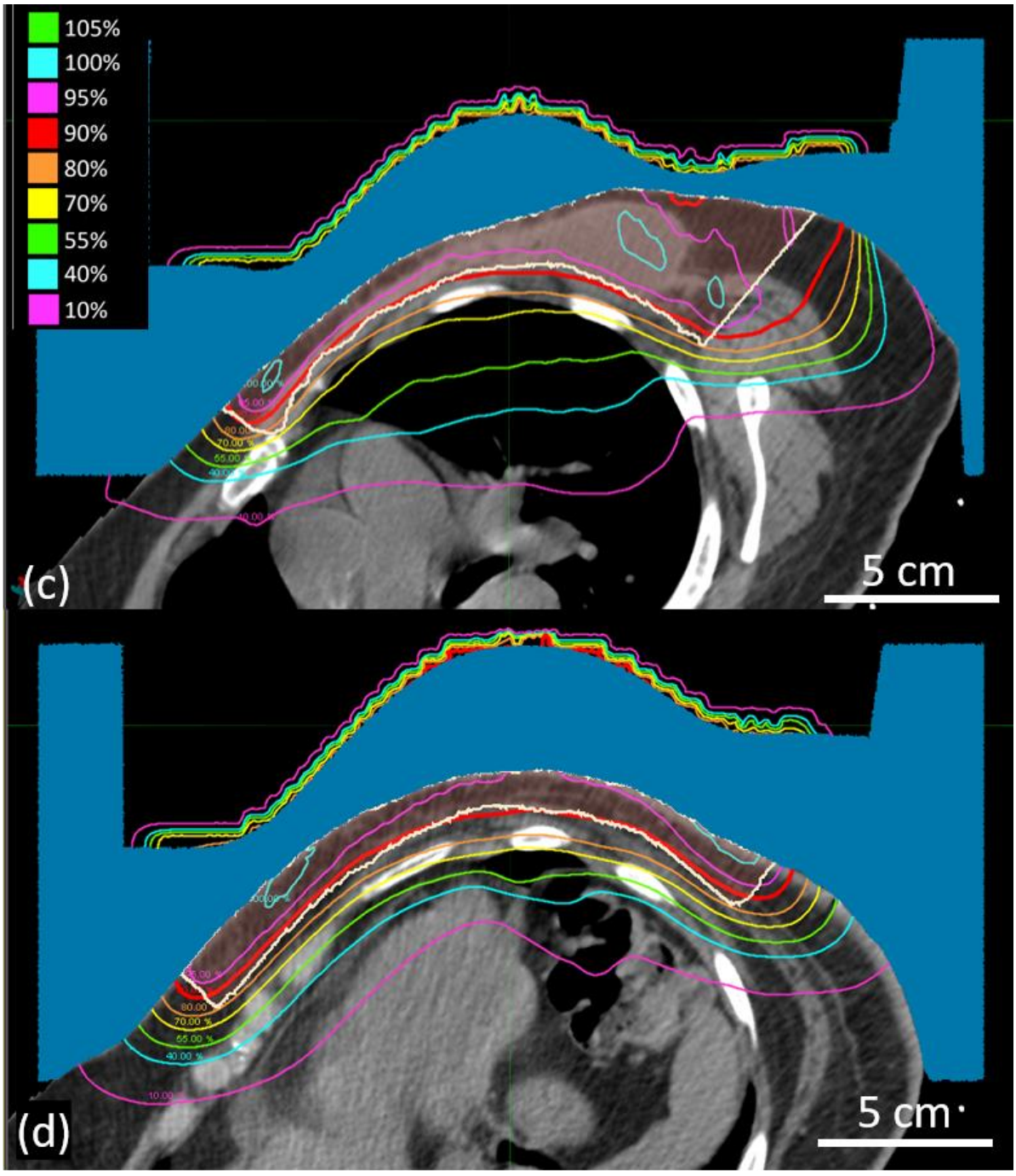
105%
100%
95%
90%
80%
70%
55%
40%
10%
(c)
5 cm
(d)
5 cm

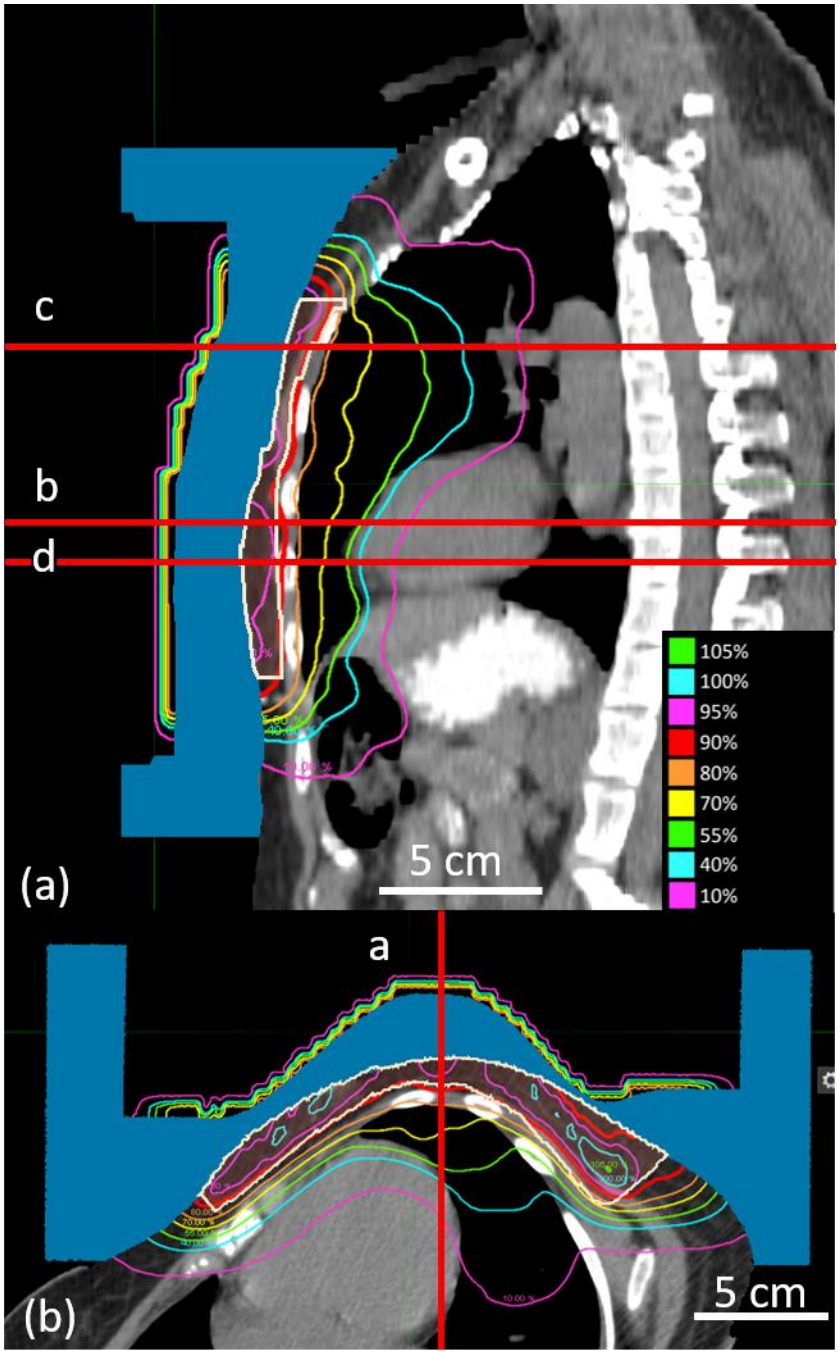

Figure B.5. **Sagittal and axial images of CW3, Plan 1**. CW3 (Patient Set 1) was planned using scattered electron beams and discrete energy spacing. (a) Dose plan in the sagittal-coronal, oblique plane demarcated by the red line in figure (b)'s transverse plane; (b) Dose plan in transverse plane passing through central heart region, demarcated by red line in figure (a)'s oblique plane. Bolus is shaded blue, and PTV is outlined in white. Key shows dose values.
(figure cont'd.)

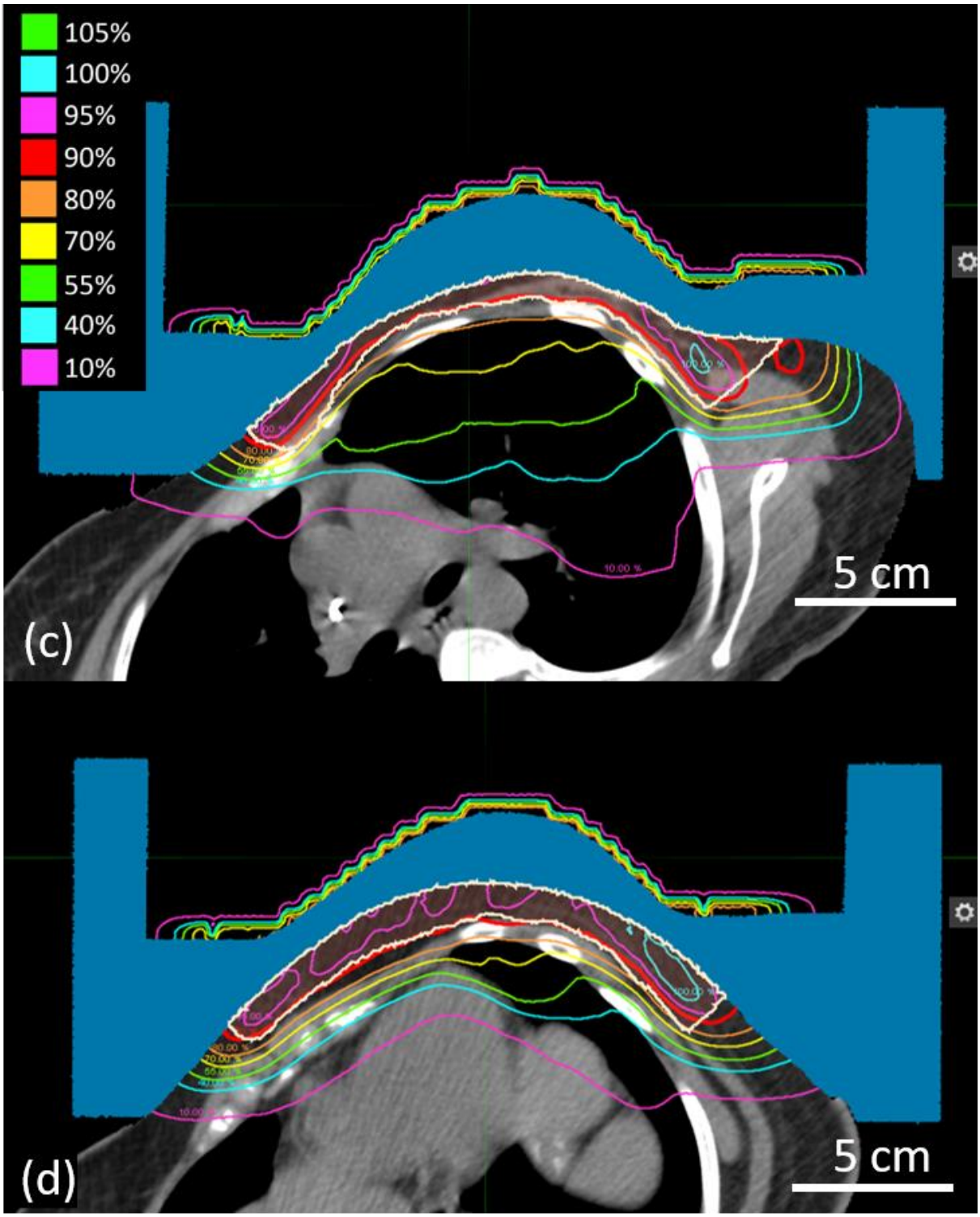
105%
100%
95%
90%
80%
70%
55%
40%
10%
5 cm
(c)
5 cm
(d)

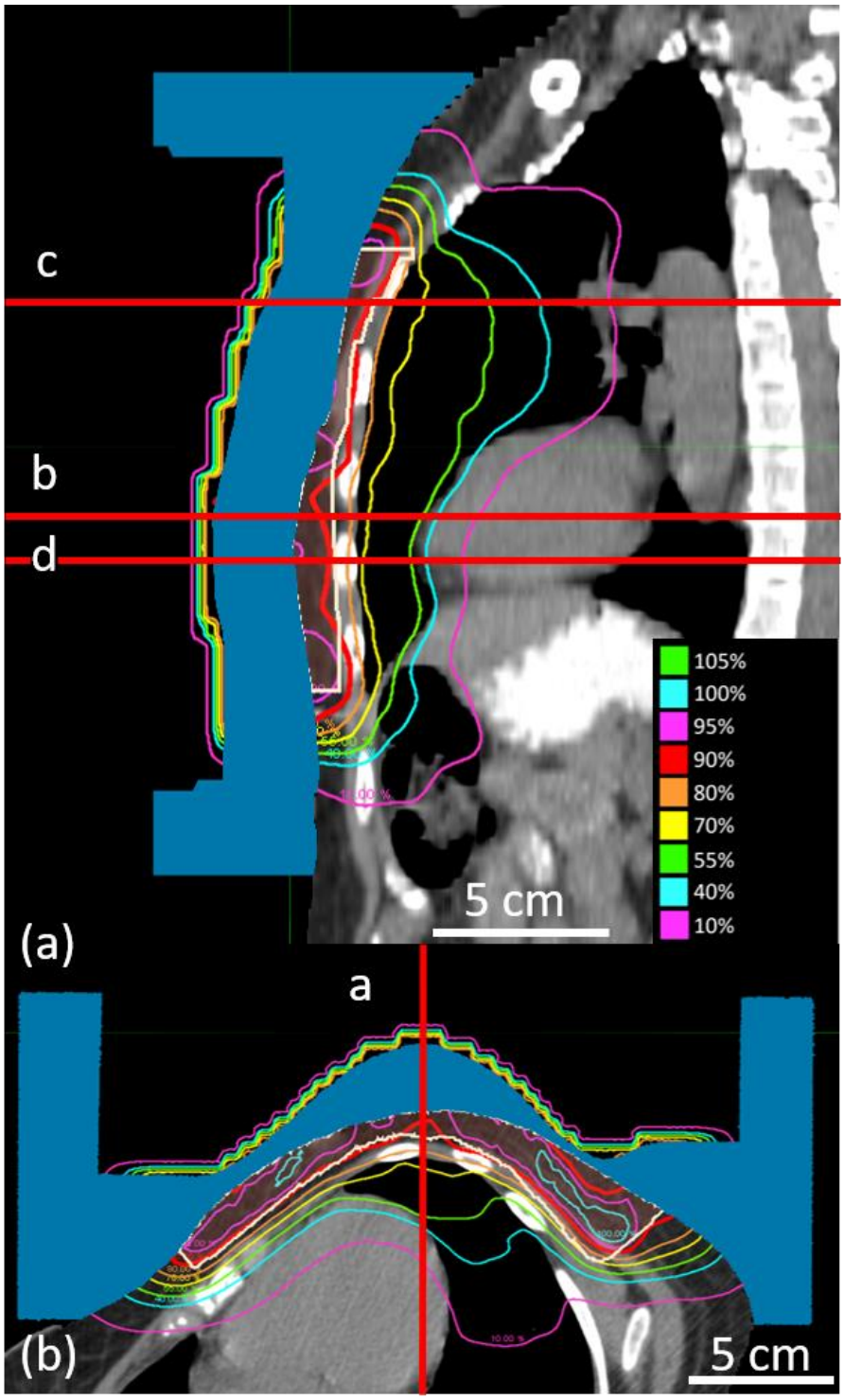

Figure B.6. **Sagittal and axial images of CW3, Plan 3**. CW3 (Patient Set 1) was planned using scattered electron beams and continuous energy spacing. (a) Dose plan in the sagittal-coronal, oblique plane demarcated by the red line in figure (b)'s transverse plane; (b) Dose plan in transverse plane passing through central heart region, demarcated by red line in figure (a)'s oblique plane. Bolus is shaded blue, and PTV is outlined in white. Key shows dose values.
(figure cont'd.)

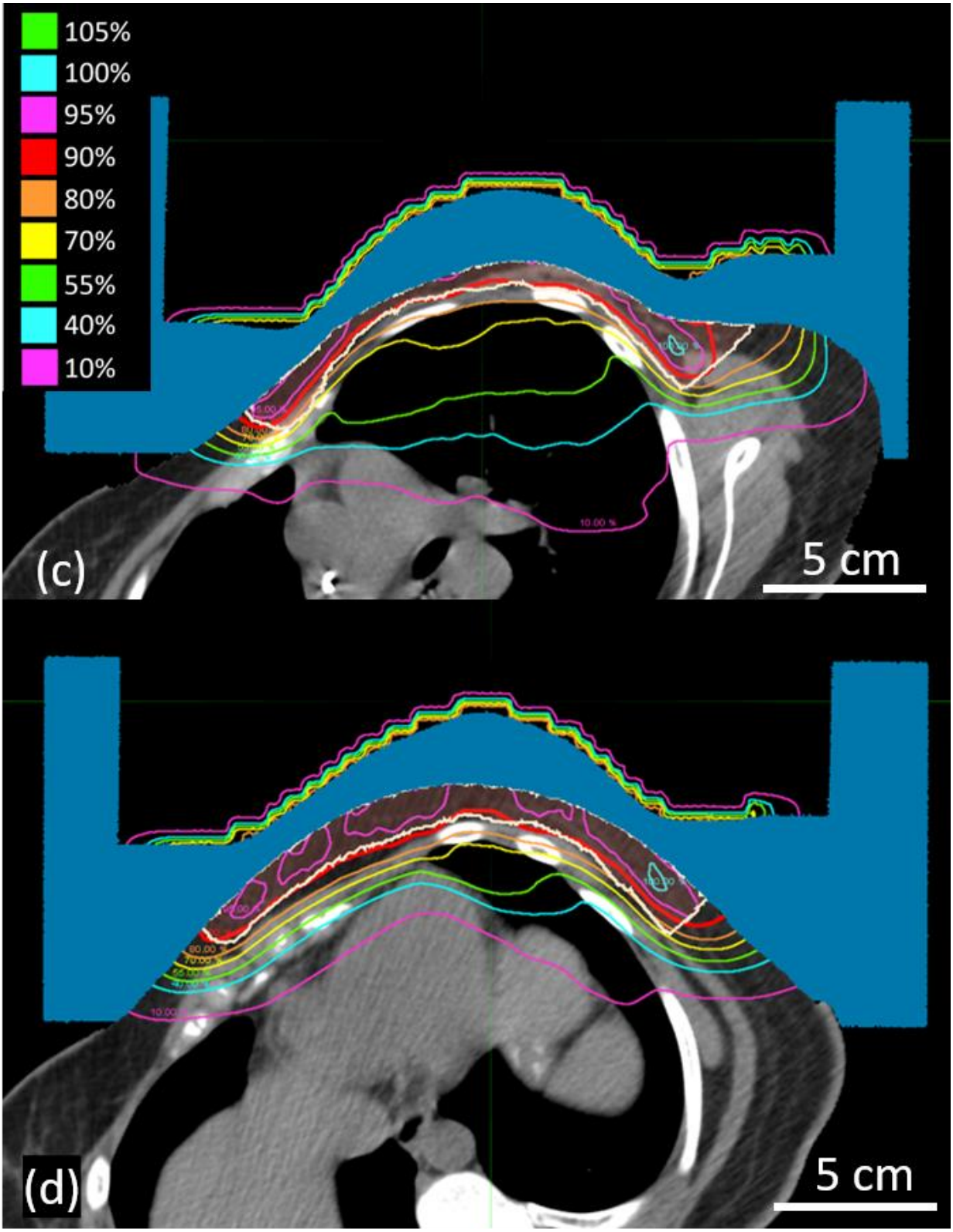
105%
100%
95%
90%
80%
70%
55%
40%
10%
(c)
5 cm
(d)
5 cm

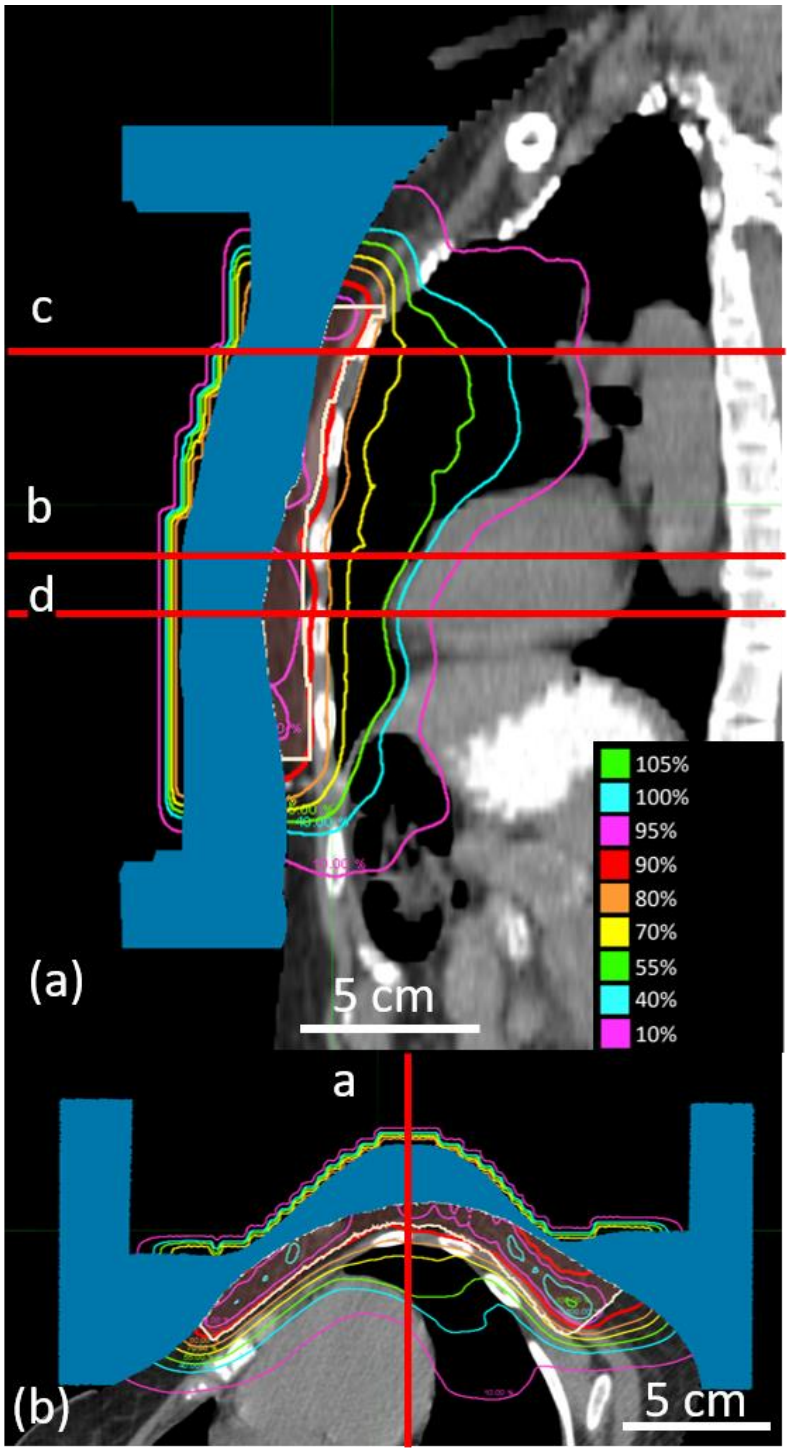

Figure B.7. **Sagittal and axial images of CW3, Plan 4**. CW3 (Patient Set 1) was planned using scanned electron beams and discrete energy spacing. (a) Dose plan in the sagittal-coronal, oblique plane demarcated by the red line in figure (b)'s transverse plane; (b) Dose plan in transverse plane passing through central heart region, demarcated by red line in figure (a)'s oblique plane. Bolus is shaded blue, and PTV is outlined in white. Key shows dose values.
(figure cont'd.)

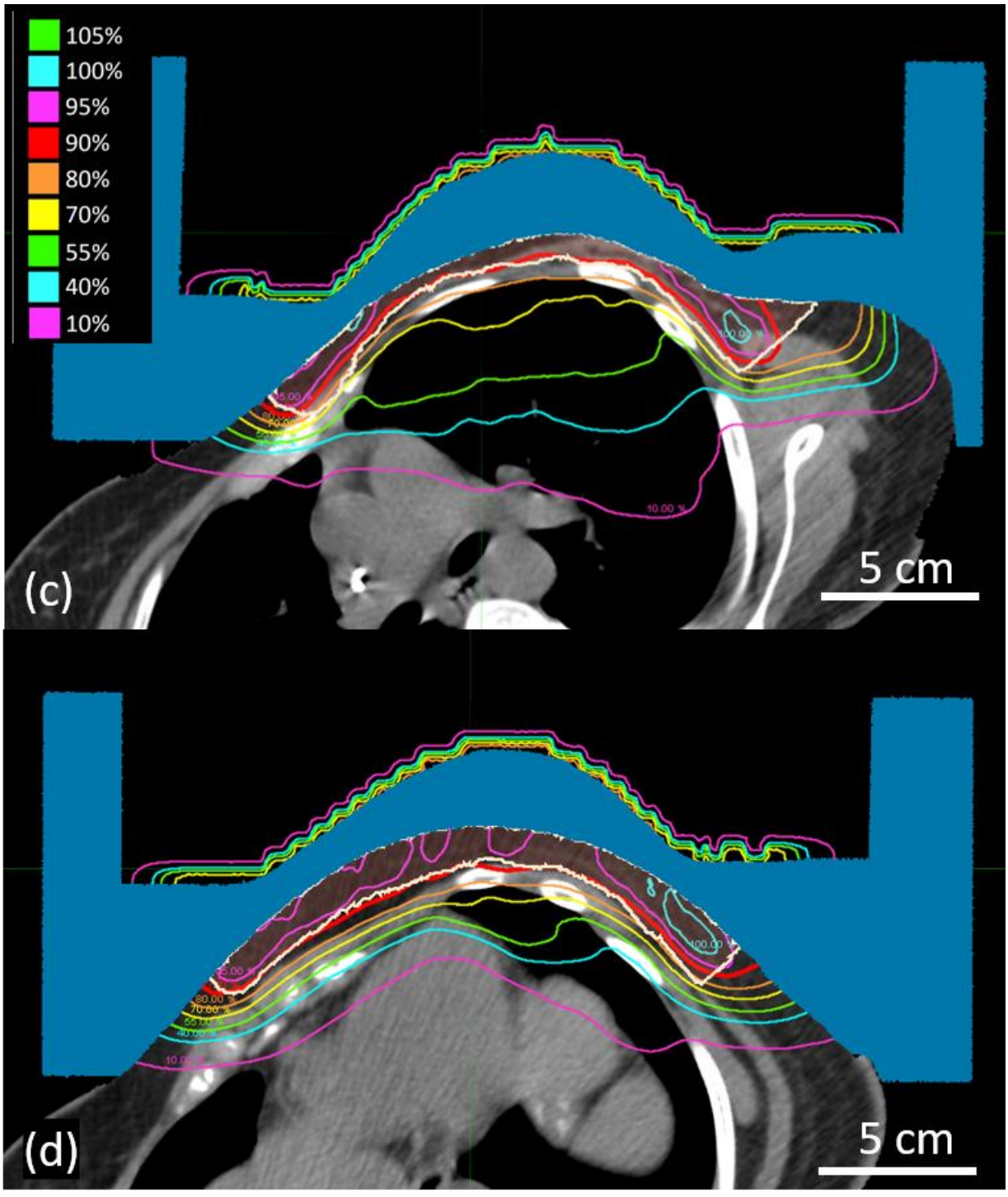
105%
100%
95%
90%
80%
70%
55%
40%
10%
(c)
5 cm
(d)
5 cm

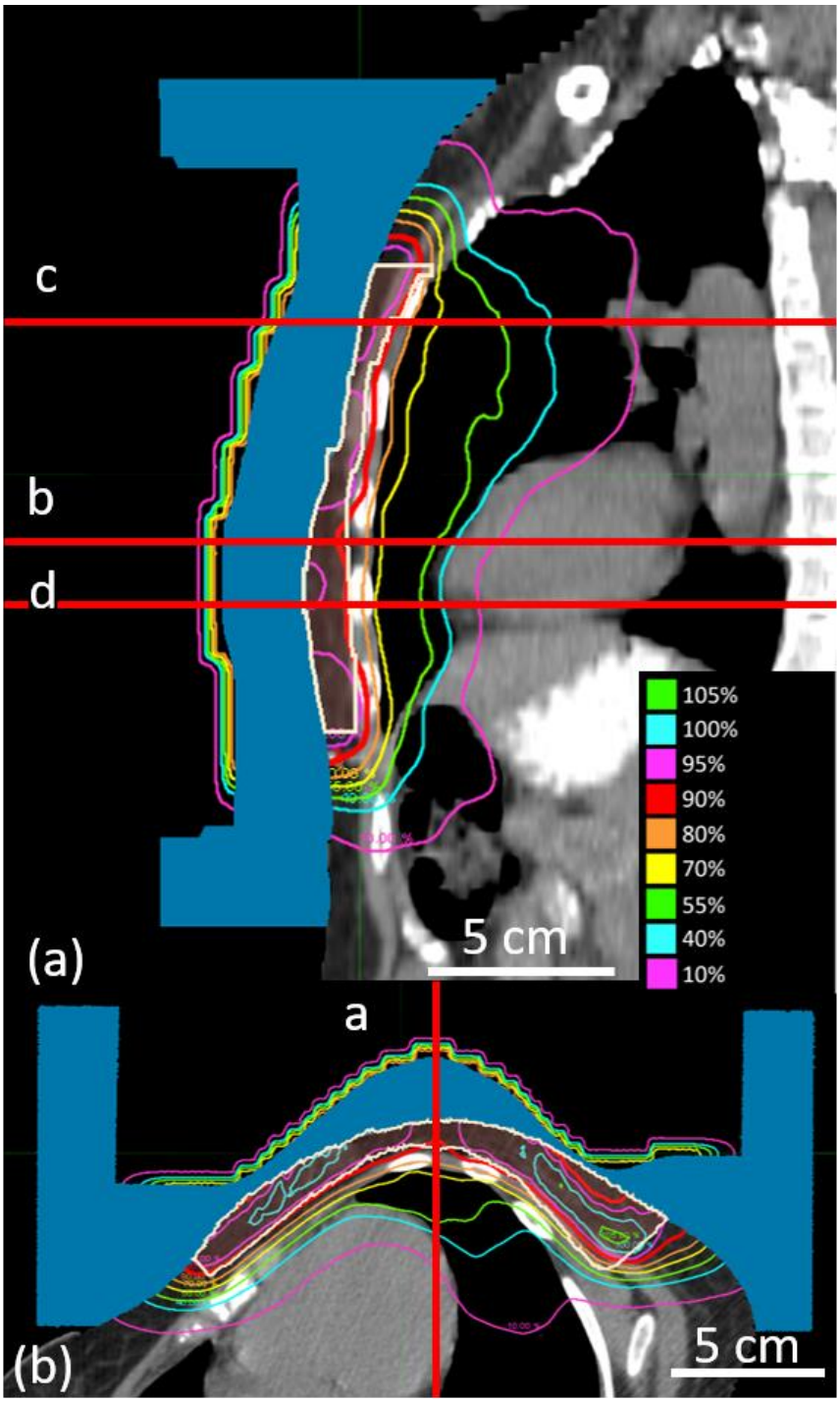

Figure B.8. **Sagittal and axial images of CW3, Plan 5**. CW3 (Patient Set 1) was planned using scanned electron beams and continuous energy spacing. (a) Dose plan in the sagittal-coronal, oblique plane demarcated by the red line in figure (b)'s transverse plane; (b) Dose plan in transverse plane passing through central heart region, demarcated by red line in figure (a)'s oblique plane. Bolus is shaded blue, and PTV is outlined in white. Key shows dose values.
(figure cont'd.)

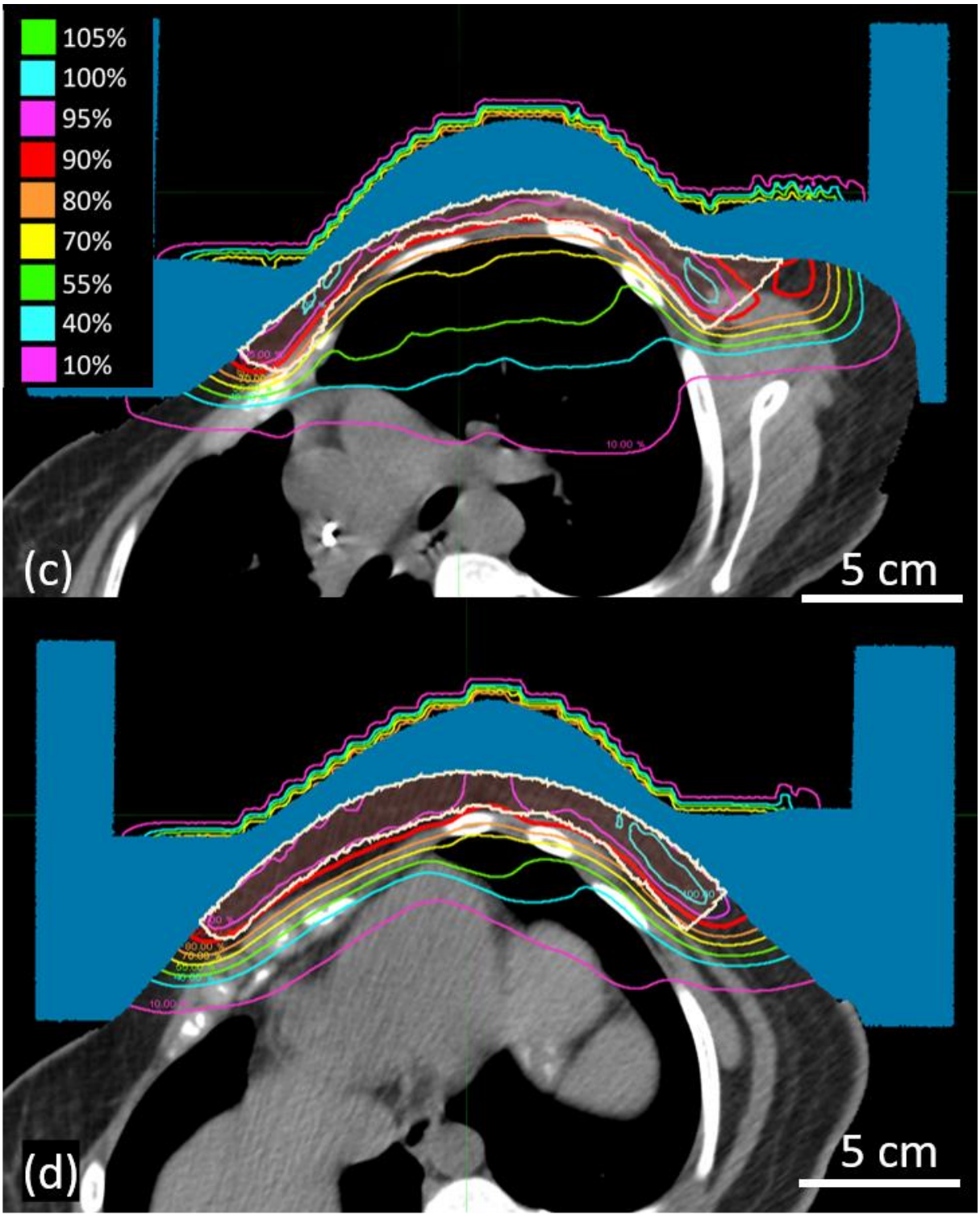
105%
100%
95%
90%
80%
70%
55%
40%
10%
(c)
5 cm
(d)
5 cm

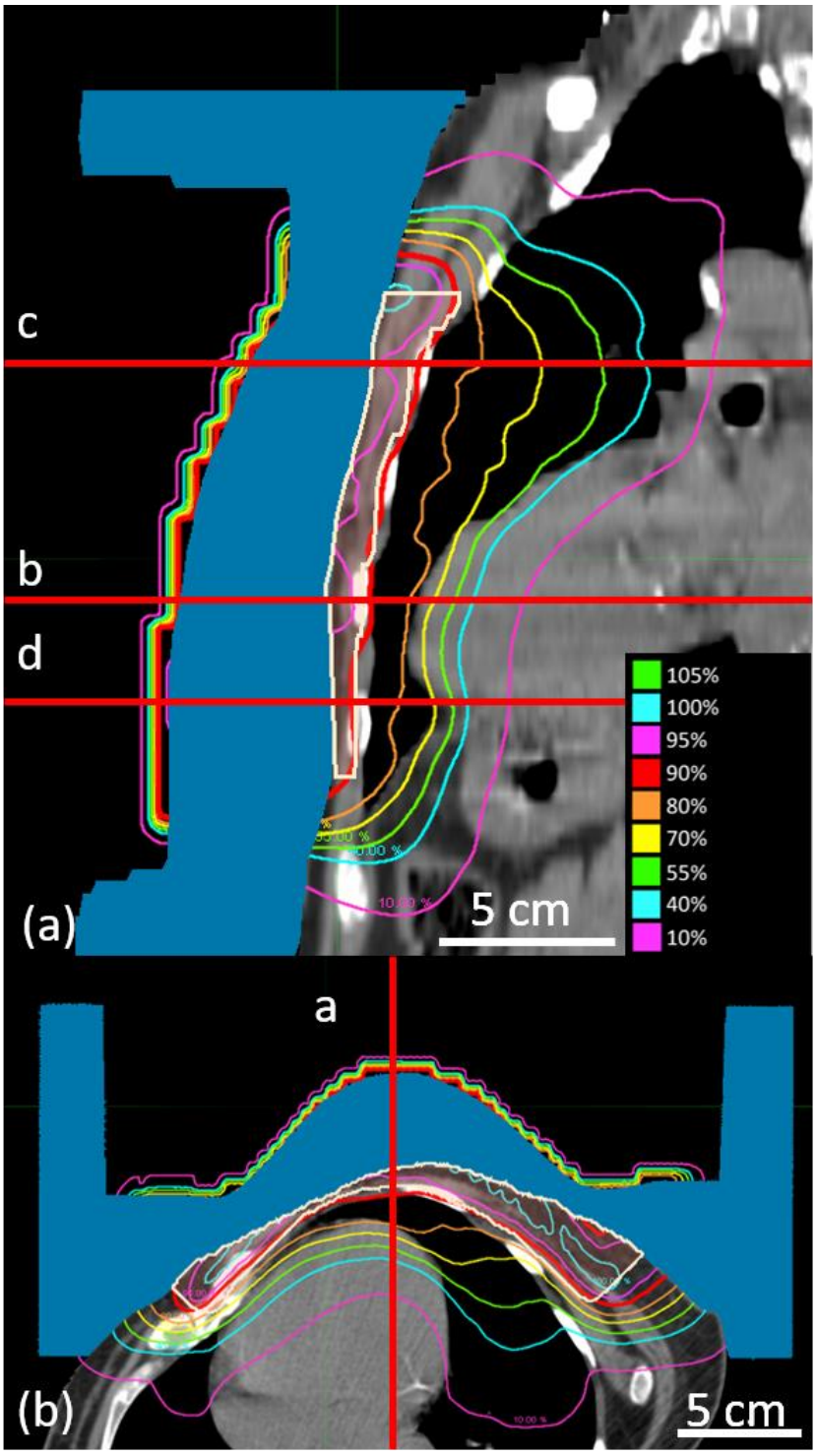

Figure B.9. **Sagittal and axial images of CW6, Plan 1**. CW6 (Patient Set 1) was planned using scattered electron beams and discrete energy spacing. (a) Dose plan in the sagittal-coronal, oblique plane demarcated by the red line in figure (b)'s transverse plane; (b) Dose plan in transverse plane passing through central heart region, demarcated by red line in figure (a)'s oblique plane. Bolus is shaded blue, and PTV is outlined in white. Key shows dose values.
(figure cont'd.)

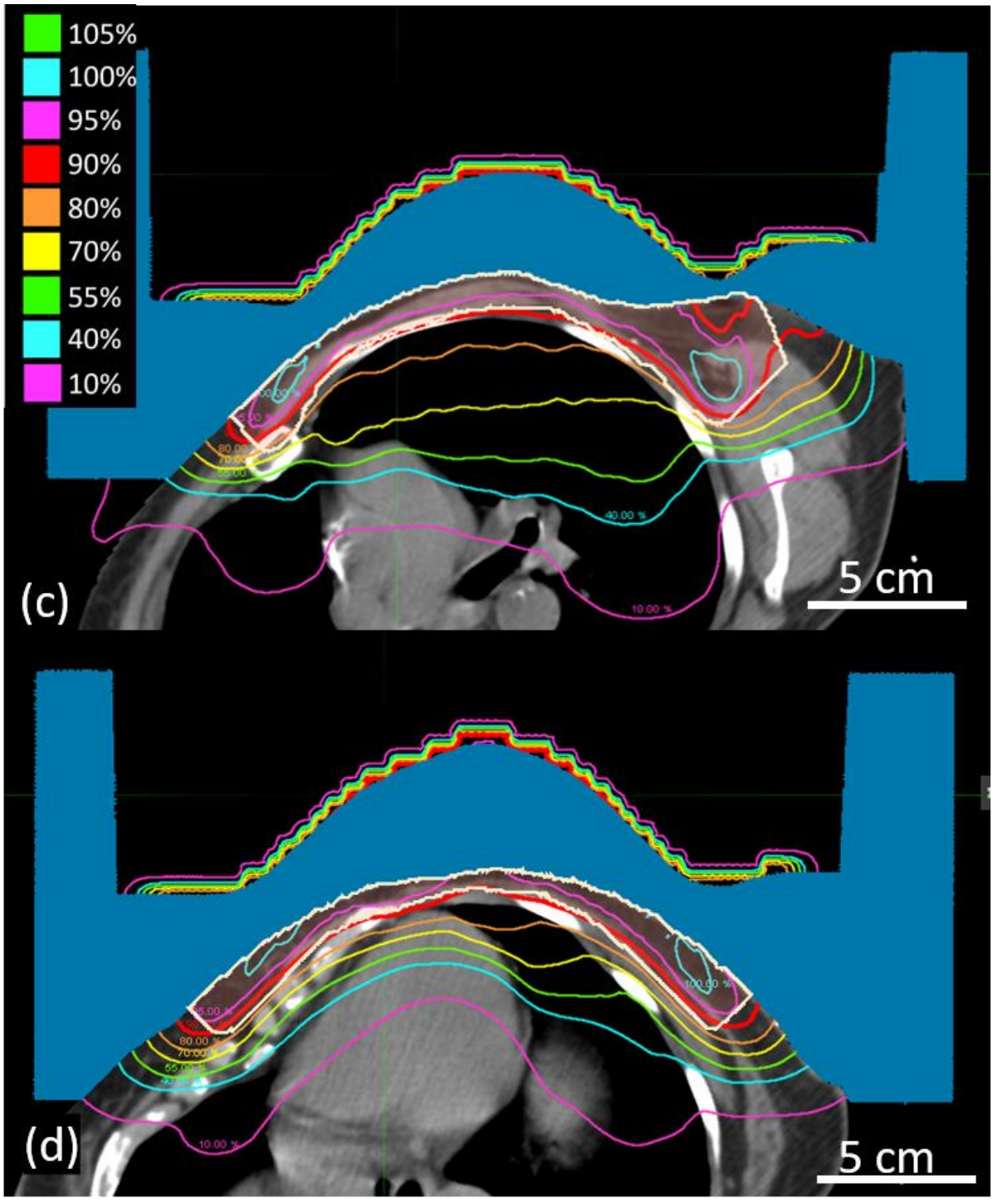
105%
100%
95%
90%
80%
70%
55%
40%
10%
(c)
5 cm
(d)
5 cm

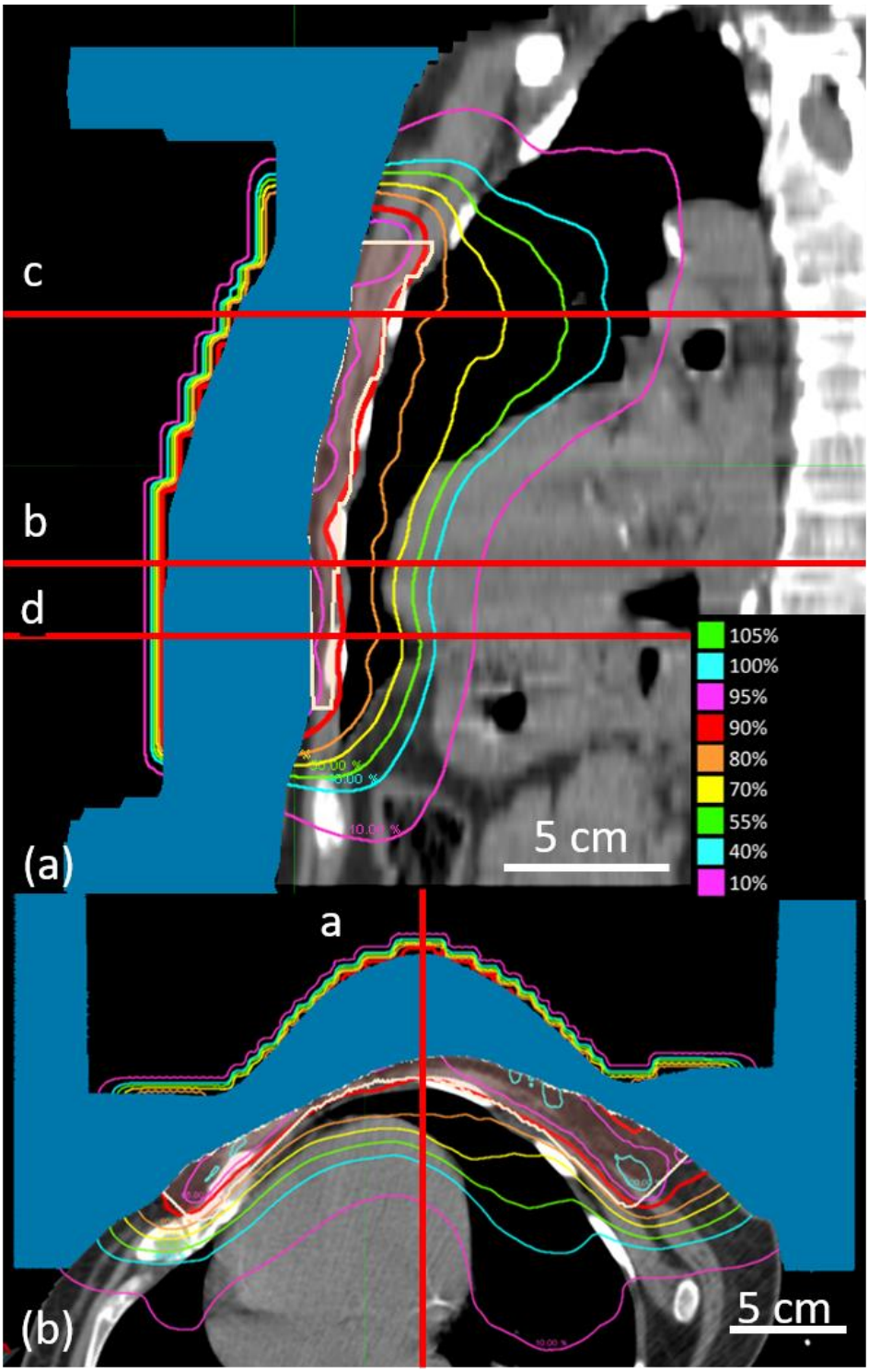

Figure B.10. **Sagittal and axial images of CW6, Plan 3**. CW6 (Patient Set 1) was planned using scattered electron beams and continuous energy spacing. (a) Dose plan in the sagittal-coronal, oblique plane demarcated by the red line in figure (b)'s transverse plane; (b) Dose plan in transverse plane passing through central heart region, demarcated by red line in figure (a)'s oblique plane. Bolus is shaded blue, and PTV is outlined in white. Key shows dose values.
(figure cont'd.)

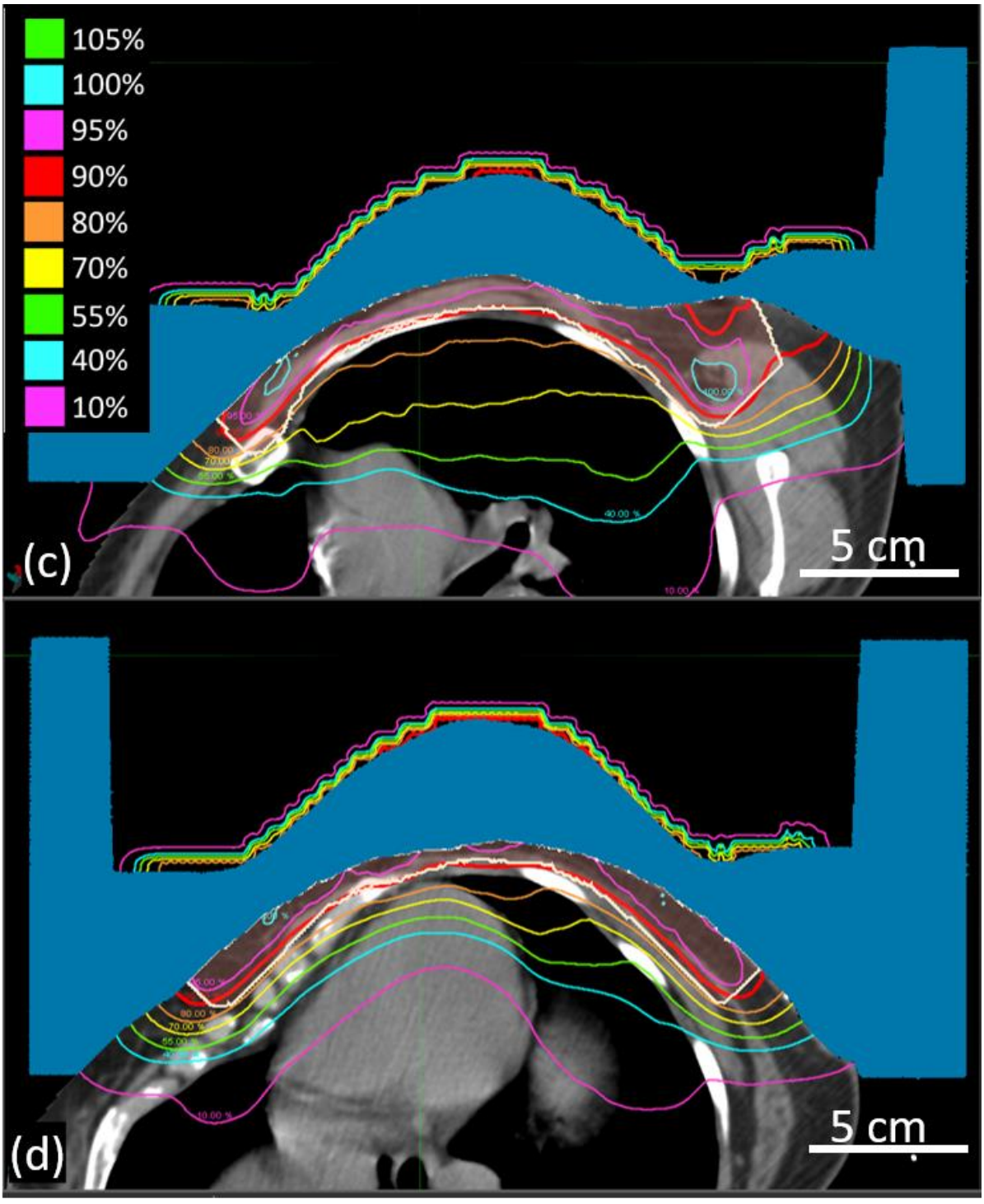
105%
100%
95%
90%
80%
70%
55%
40%
10%
(c)
5 cm
(d)
5 cm

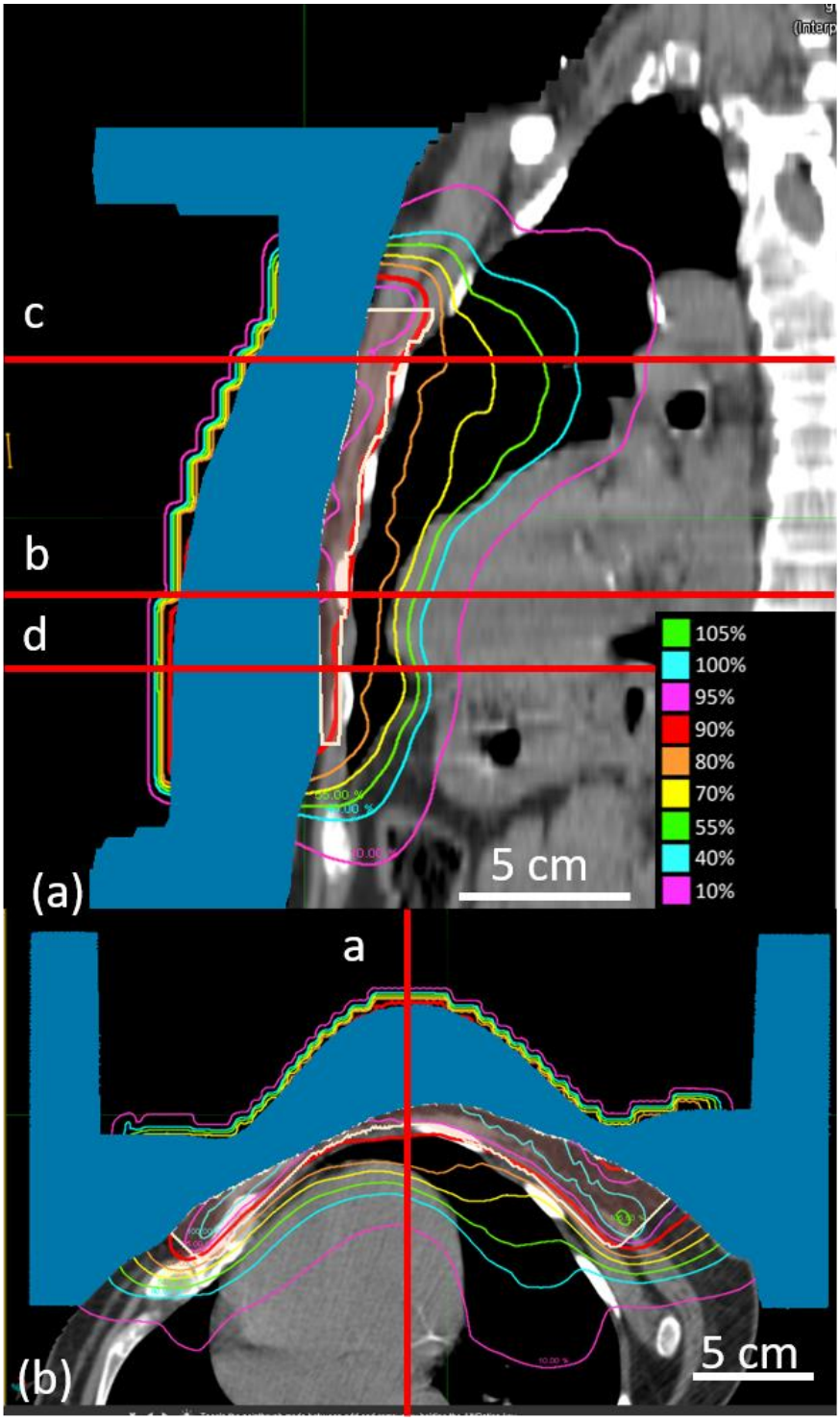

Figure B.11. **Sagittal and axial images of CW6, Plan 4**. CW6 (Patient Set 1) was planned using scanned electron beams and discrete energy spacing. (a) Dose plan in the sagittal-coronal, oblique plane demarcated by the red line in figure (b)'s transverse plane; (b) Dose plan in transverse plane passing through central heart region, demarcated by red line in figure (a)'s oblique plane. Bolus is shaded blue, and PTV is outlined in white. Key shows dose values.
(figure cont'd.)

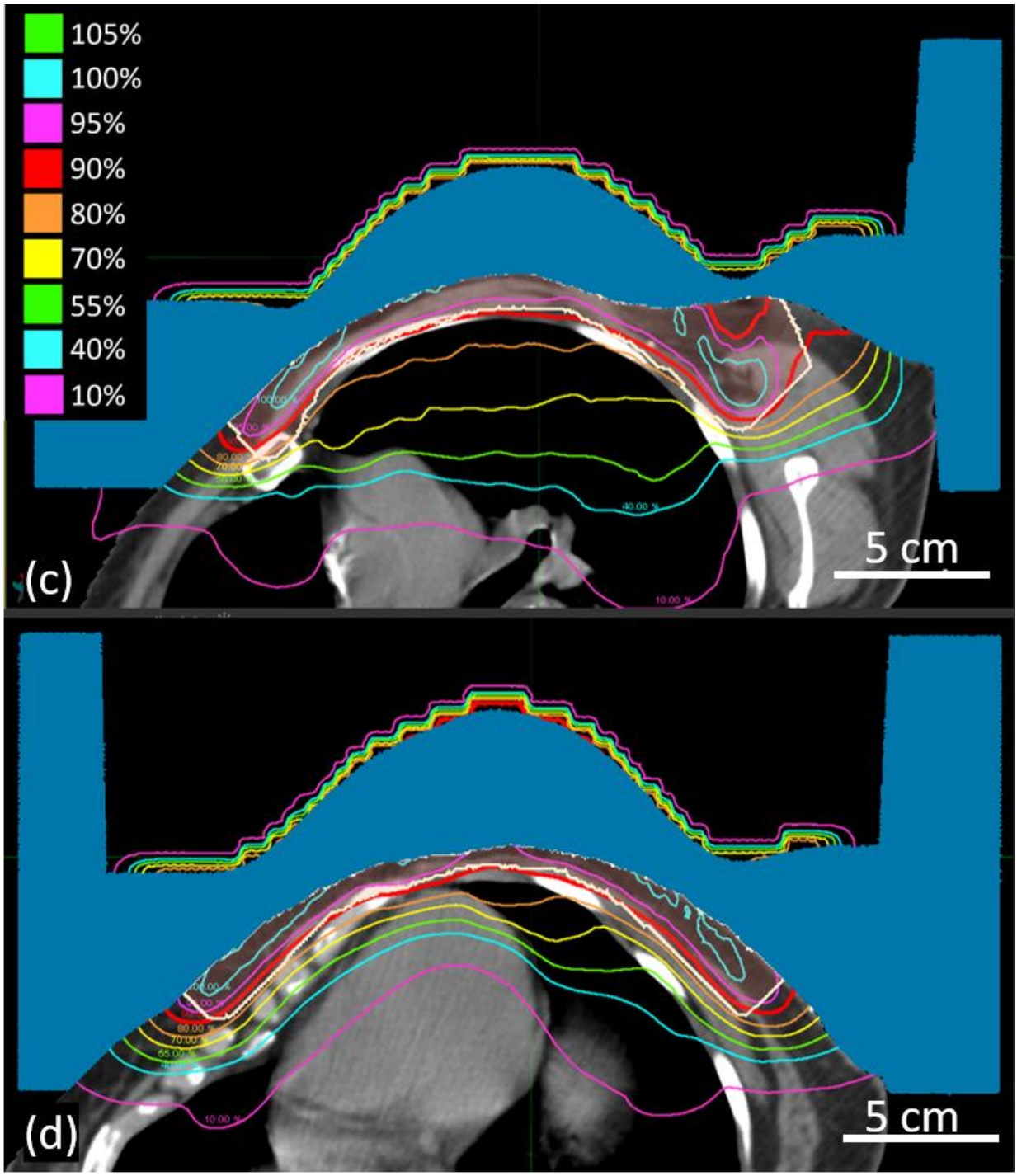
105%
100%
95%
90%
80%
70%
55%
40%
10%
(c)
5 cm
(d)
5 cm

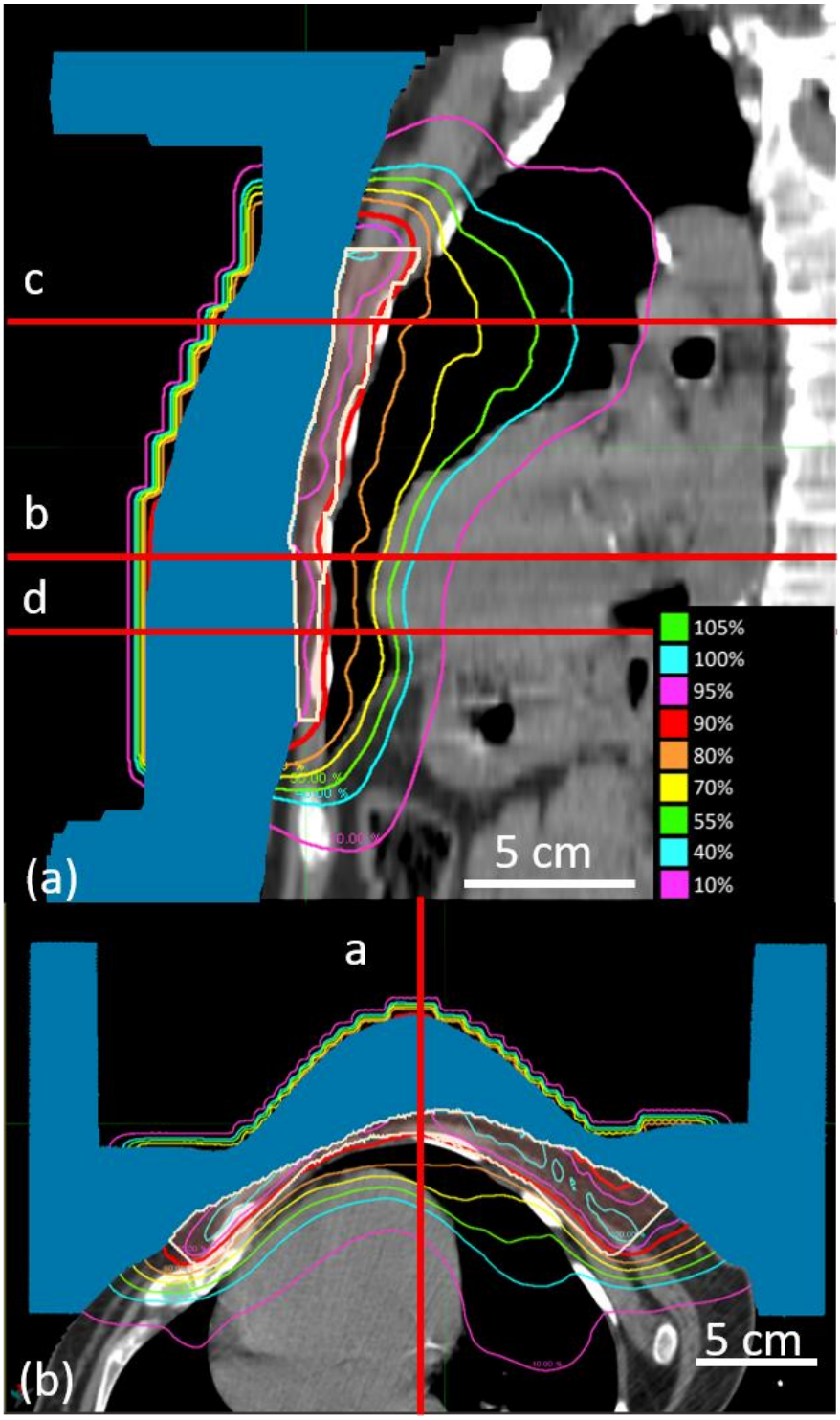

Figure B.12. **Sagittal and axial images of CW6, Plan 5**. CW6 (Patient Set 1) was planned using scanned electron beams and continuous energy spacing. (a) Dose plan in the sagittal-coronal, oblique plane demarcated by the red line in figure (b)'s transverse plane; (b) Dose plan in transverse plane passing through central heart region, demarcated by red line in figure (a)'s oblique plane. Bolus is shaded blue, and PTV is outlined in white. Key shows dose values.
(figure cont'd.)

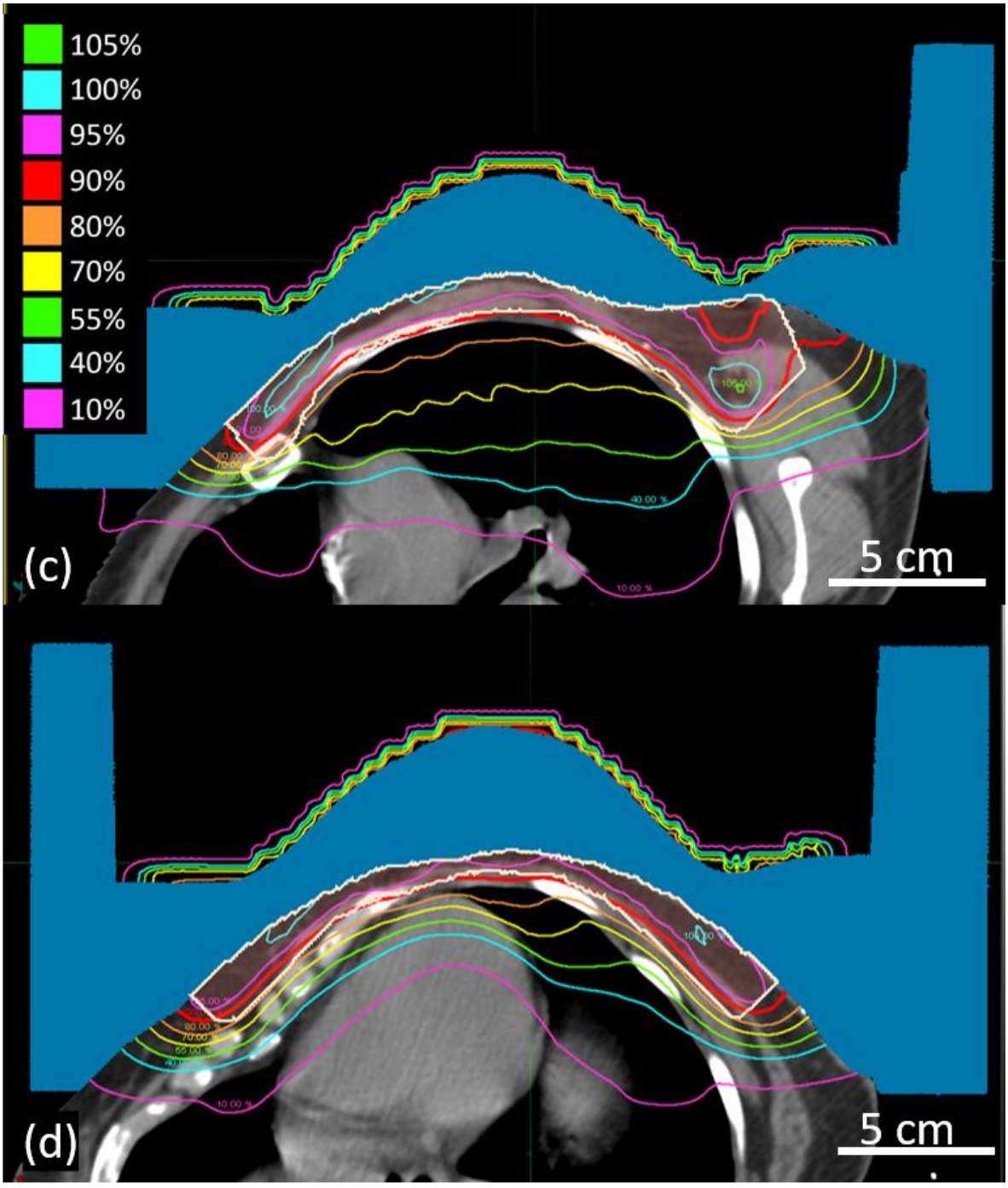
105%
100%
95%
90%
80%
70%
55%
40%
10%
(c)
5 cm
(d)
5 cm

B.2. Patient Set 2 (CW2, CW4, CW7, CW8)

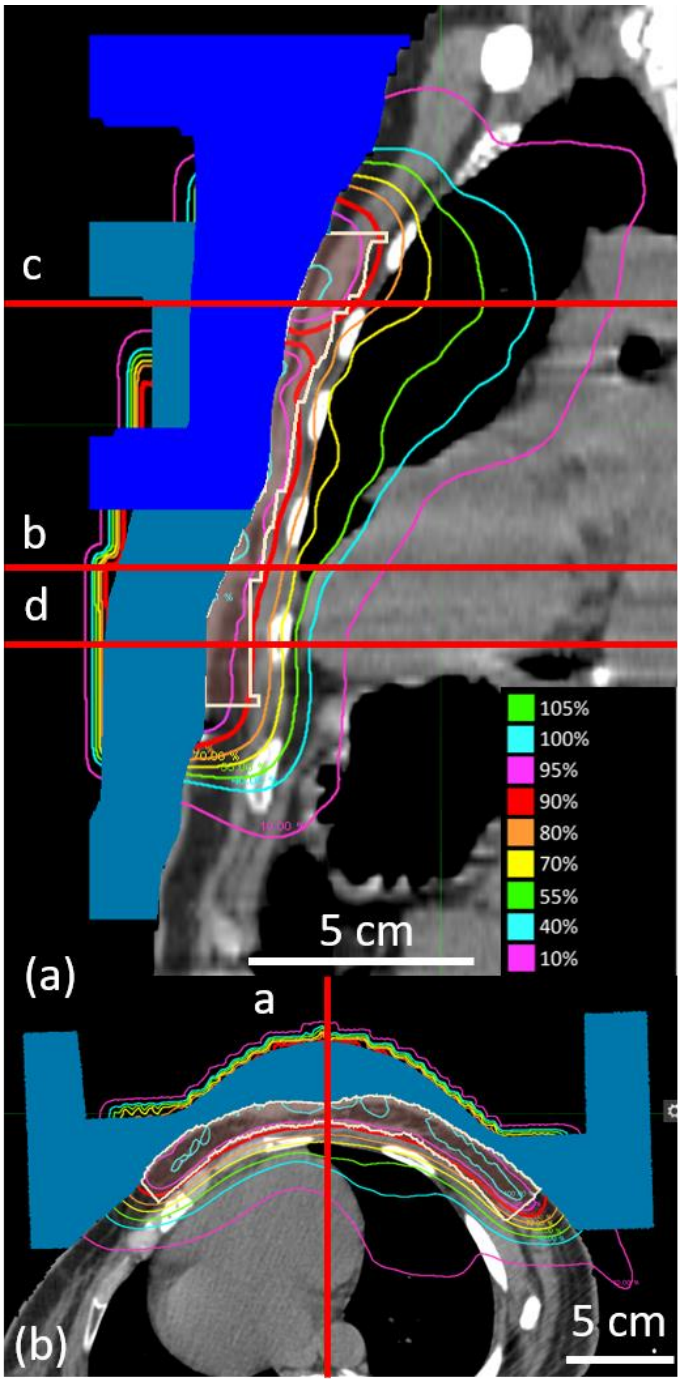

Figure B.13. **Sagittal and axial images of CW2, Plan 1**. CW2 (Patient Set 2) was planned using scattered electron beams and discrete energy spacing. (a) Dose plan in the sagittal-coronal, oblique plane demarcated by the red line in figure (b)'s transverse plane; (b) Dose plan in transverse plane passing through central heart region, demarcated by red line in figure (a)'s oblique plane. Upper bolus is shaded dark blue, lower bolus is shaded light blue, and PTV is outlined in white. Key shows dose values.
(figure cont'd.)

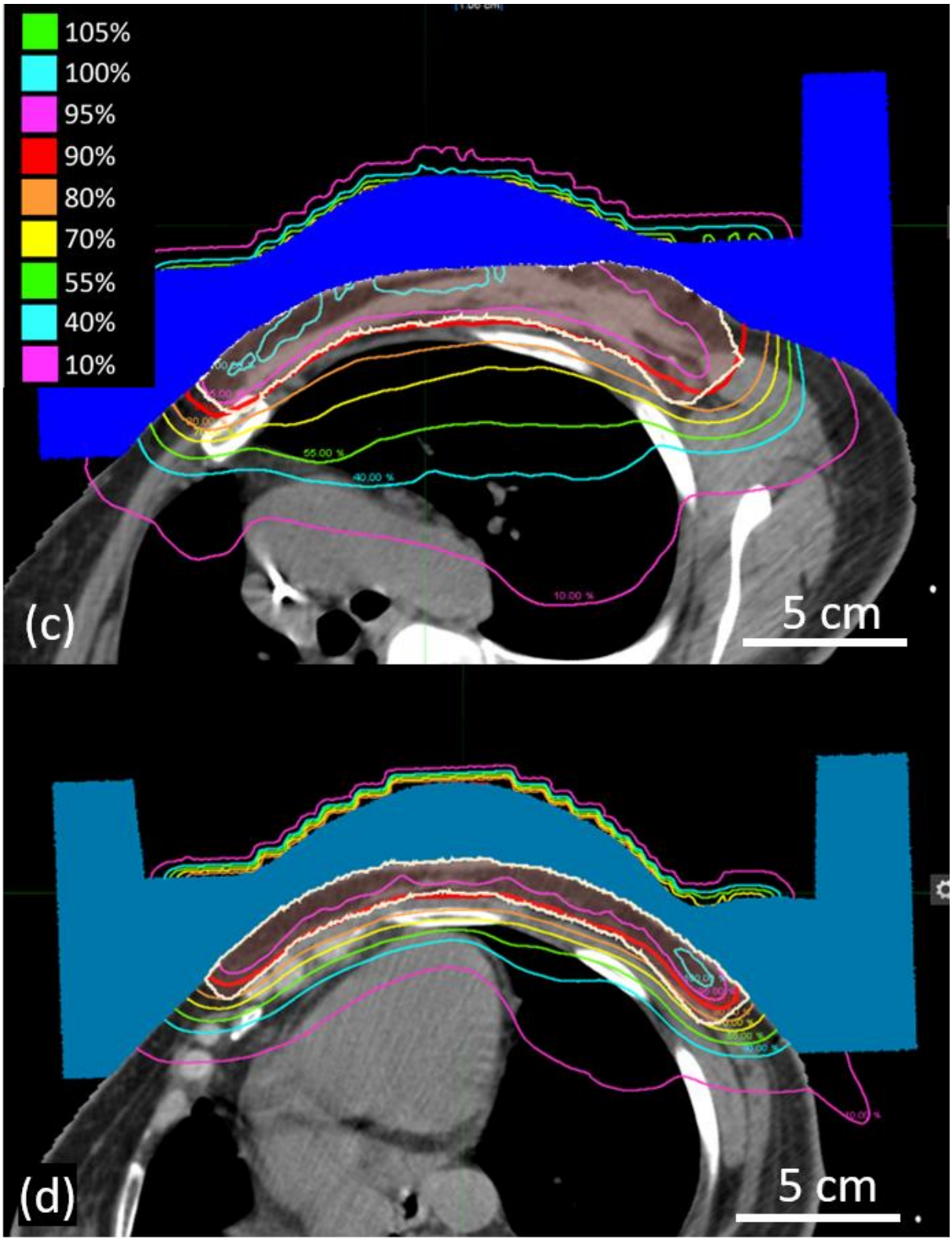
105%
100%
95%
90%
80%
70%
55%
40%
10%
55.00 %
40.00 %
10.00 %
(c)
5 cm
(d)
5 cm

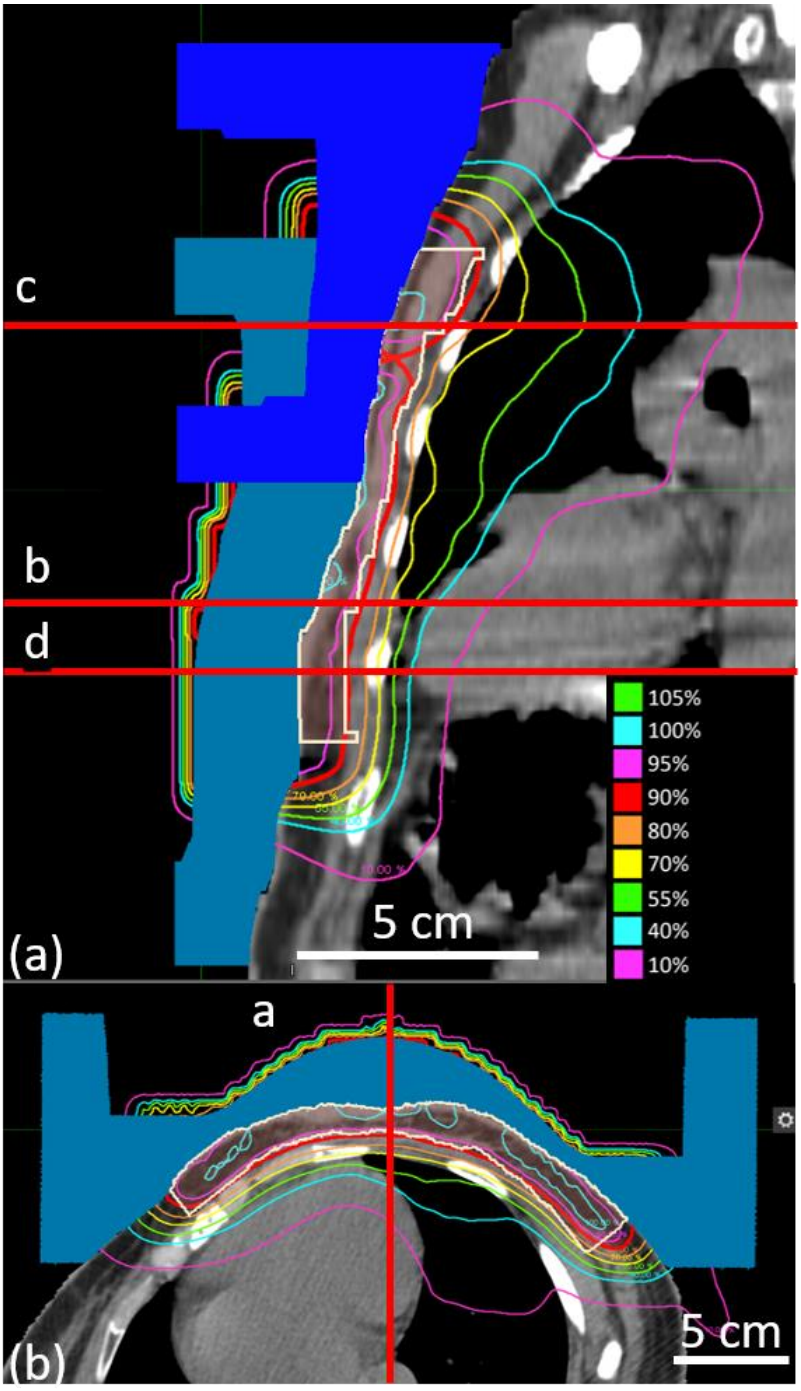

Figure B.14. **Sagittal and axial images of CW2, Plan 2**. CW2 (Patient Set 2) was planned using scattered electron beams and discrete (lower field)/continuous (upper field) energy spacing. (a) Dose plan in the sagittal-coronal, oblique plane demarcated by the red line in figure (b)'s transverse plane; (b) Dose plan in transverse plane passing through central heart region, demarcated by red line in figure (a)'s oblique plane. Upper bolus is shaded dark blue, lower bolus is shaded light blue, and PTV is outlined in white. Key shows dose values.
(figure cont'd.)

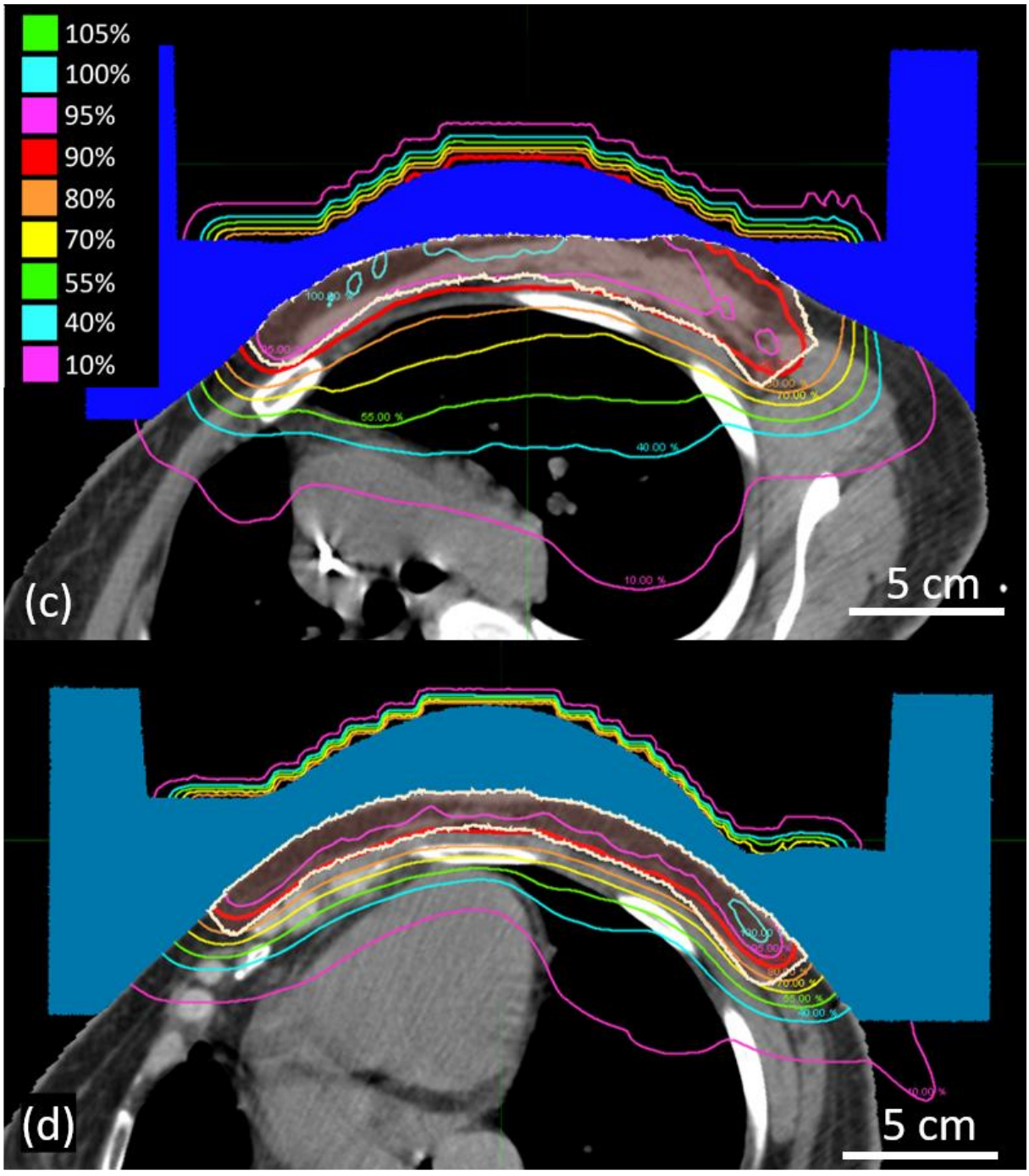
105%
100%
95%
90%
80%
70%
55%
40%
10%
(c)
5 cm
(d)
5 cm

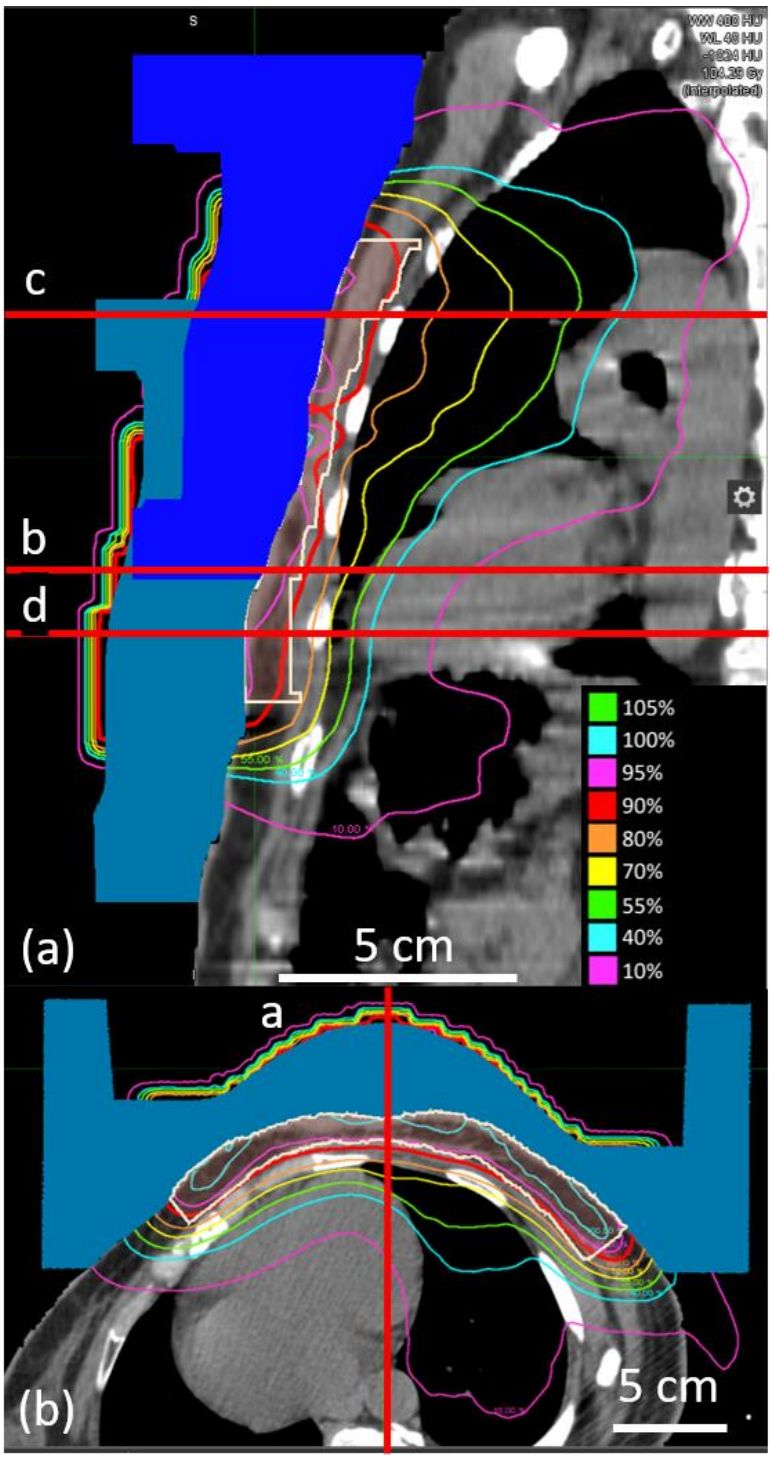

Figure B.15. **Sagittal and axial images of CW2, Plan 3**. CW2 (Patient Set 2) was planned using scattered electron beams and continuous energy spacing. (a) Dose plan in the sagittal-coronal, oblique plane demarcated by the red line in figure (b)'s transverse plane; (b) Dose plan in transverse plane passing through central heart region, demarcated by red line in figure (a)'s oblique plane. Upper bolus is shaded dark blue, lower bolus is shaded light blue, and PTV is outlined in white. Key shows dose values.
(figure cont'd.)

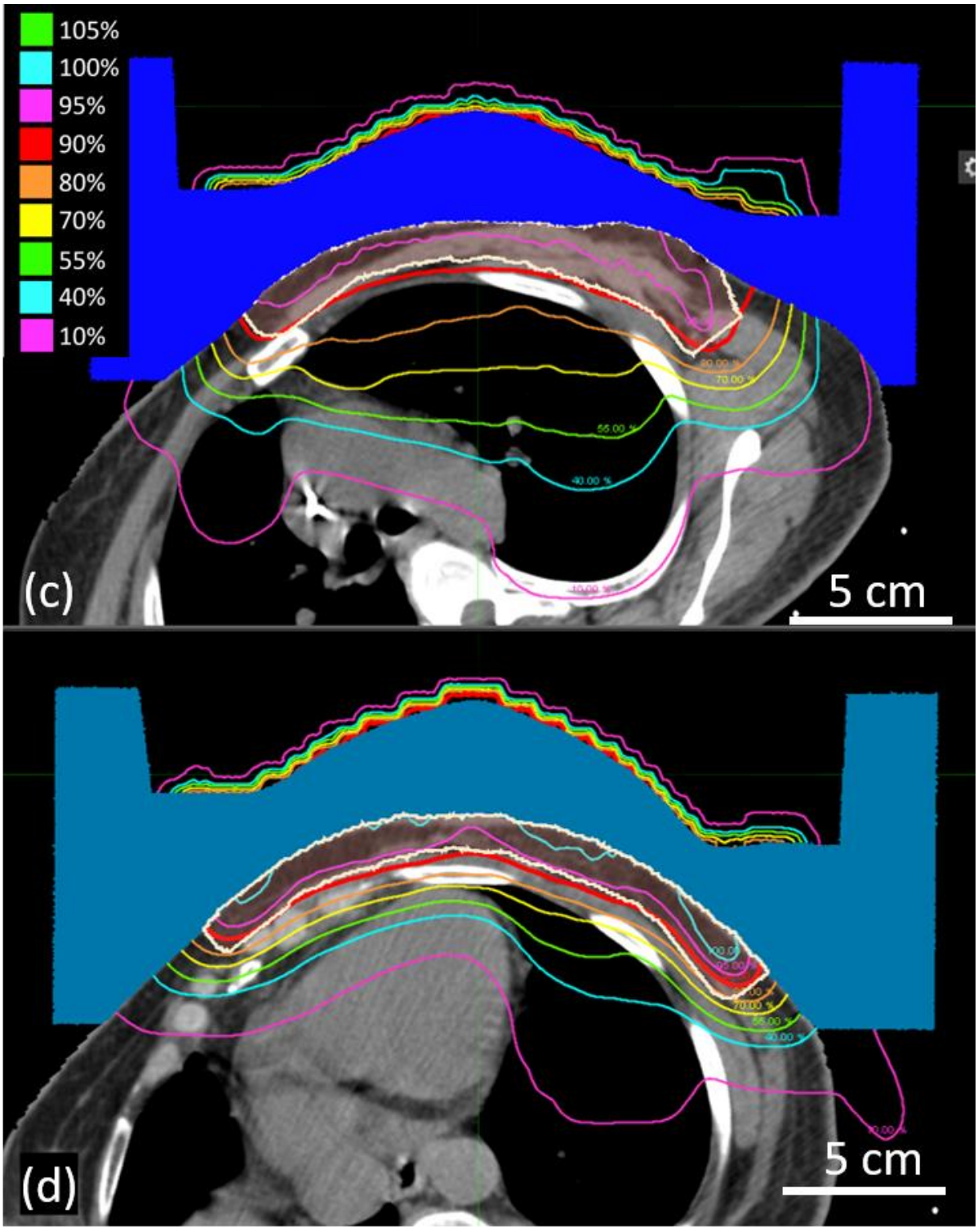
105%
100%
95%
90%
80%
70%
55%
40%
10%
(c)
5 cm
(d)
5 cm

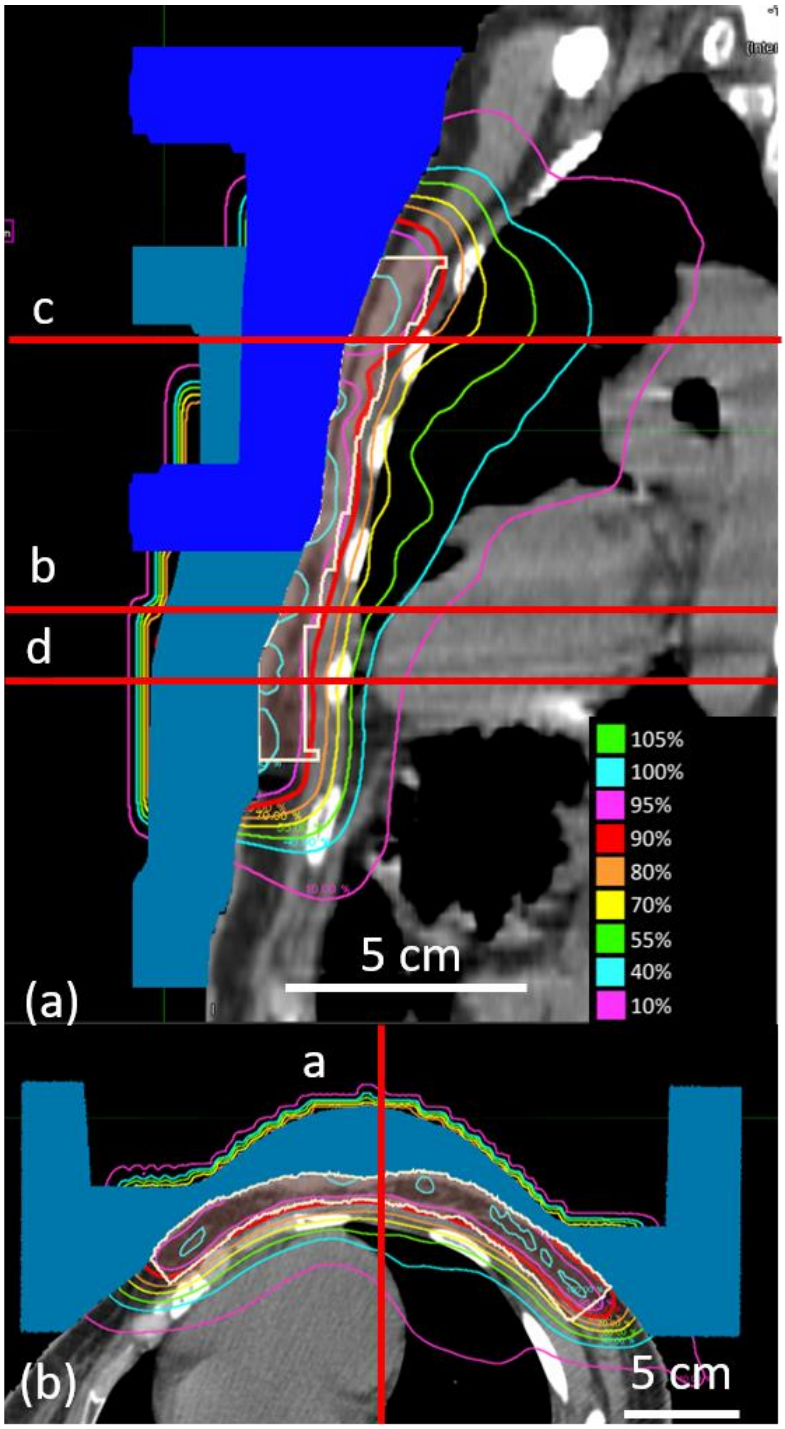

Figure B.16. **Sagittal and axial images of CW2, Plan 4**. CW2 (Patient Set 2) was planned using scanned electron beams and discrete energy spacing. (a) Dose plan in the sagittal-coronal, oblique plane demarcated by the red line in figure (b)'s transverse plane; (b) Dose plan in transverse plane passing through central heart region, demarcated by red line in figure (a)'s oblique plane. Upper bolus is shaded dark blue, lower bolus is shaded light blue, and PTV is outlined in white. Key shows dose values.
(figure cont'd.)

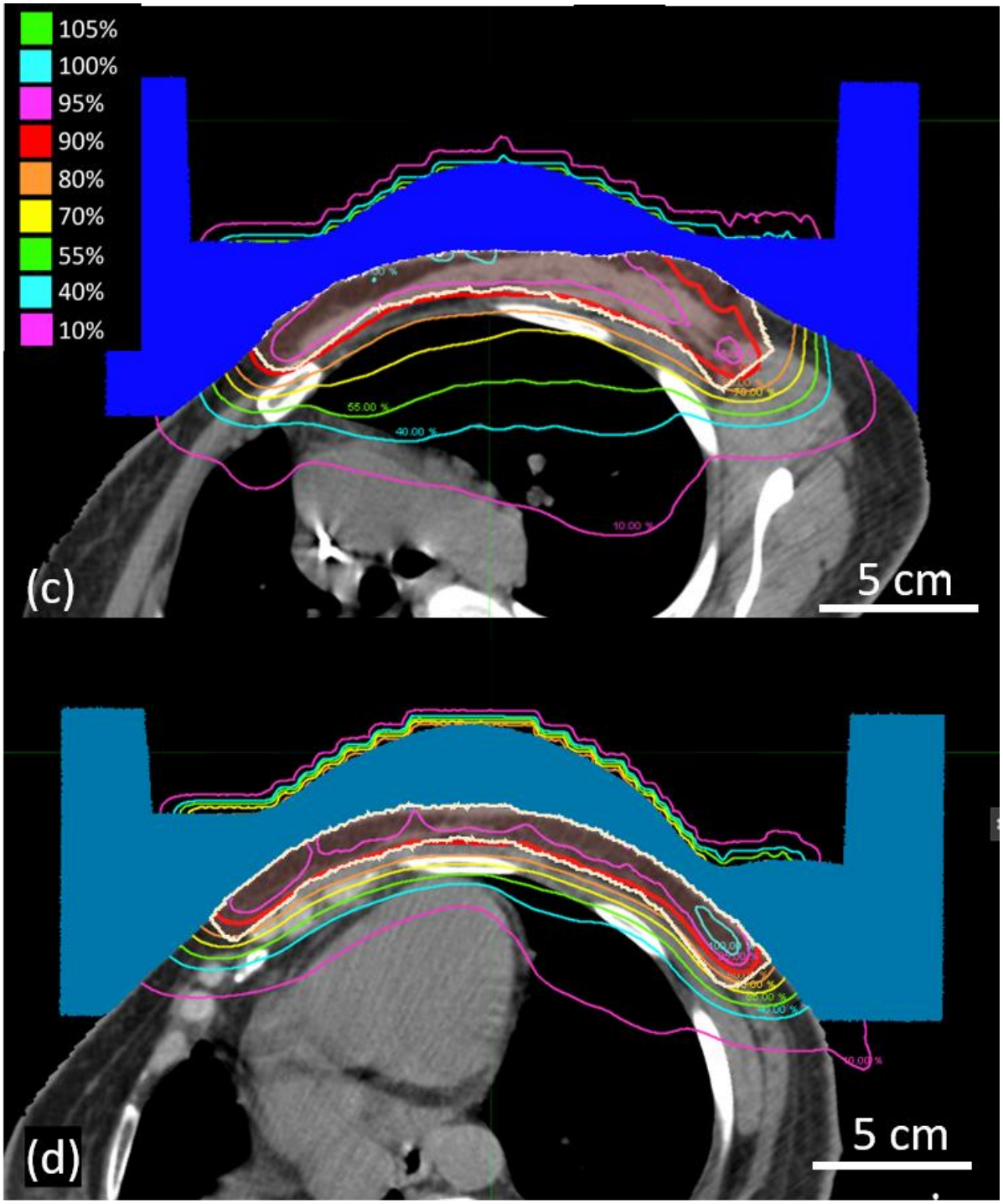

d

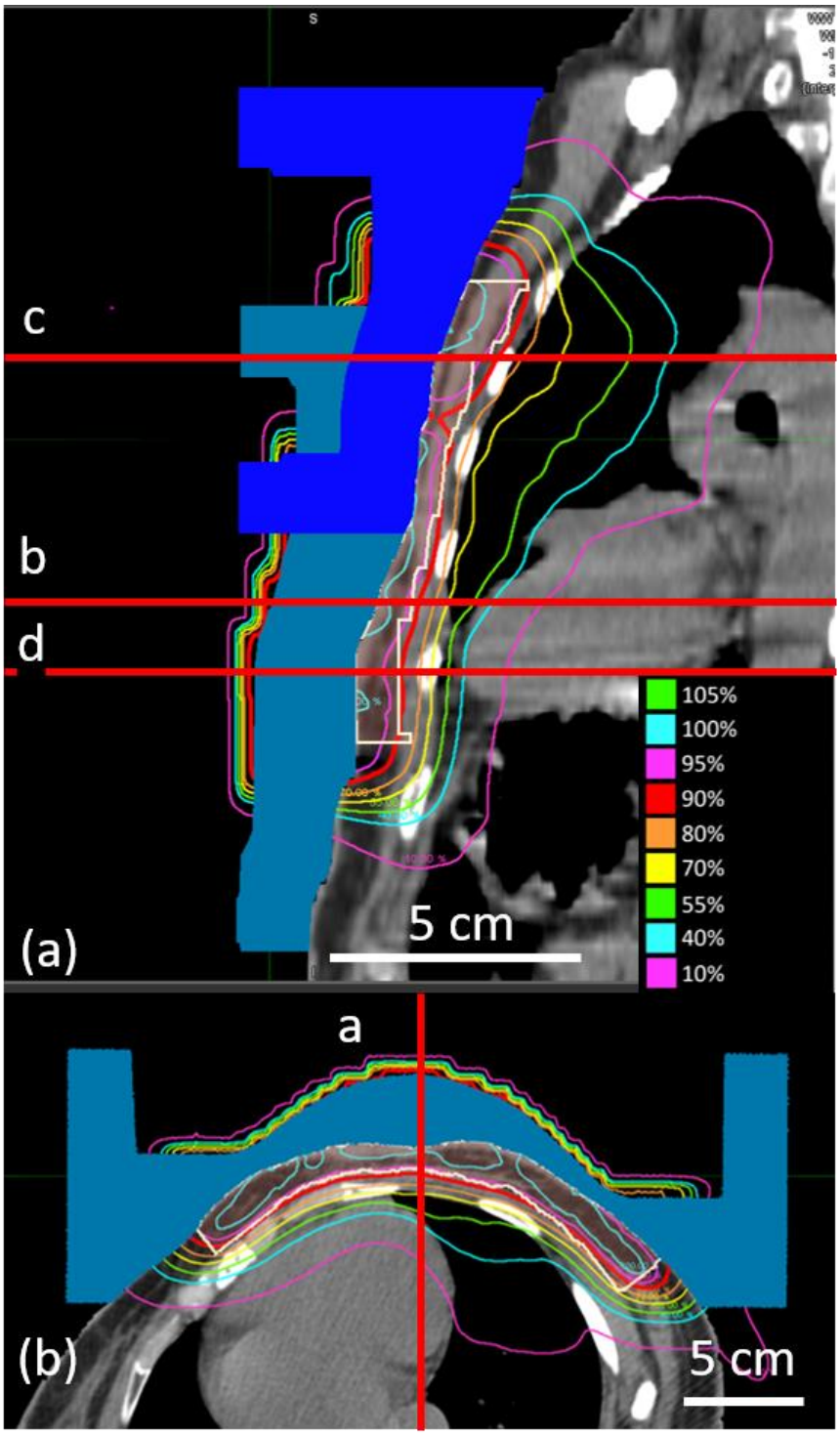

Figure B.17. **Sagittal and axial images of CW2, Plan 5**. CW2 (Patient Set 2) was planned using scanned electron beams and continuous energy spacing. (a) Dose plan in the sagittal-coronal, oblique plane demarcated by the red line in figure (b)'s transverse plane; (b) Dose plan in transverse plane passing through central heart region, demarcated by red line in figure (a)'s oblique plane. Upper bolus is shaded dark blue, lower bolus is shaded light blue, and PTV is outlined in white. Key shows dose values.
(figure cont'd.)

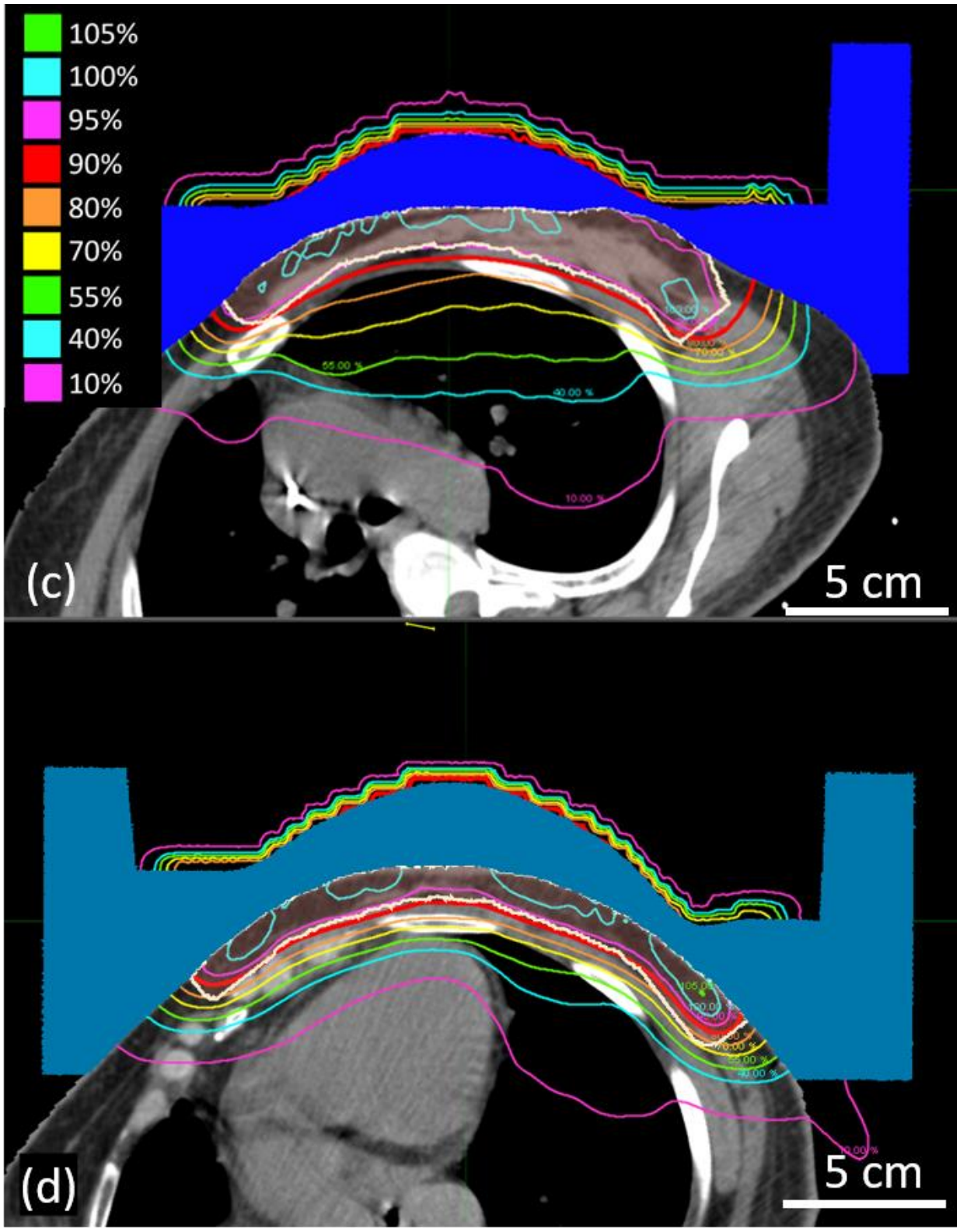
105%
100%
95%
90%
80%
70%
55%
40%
10%
(c)
5 cm
(d)
5 cm

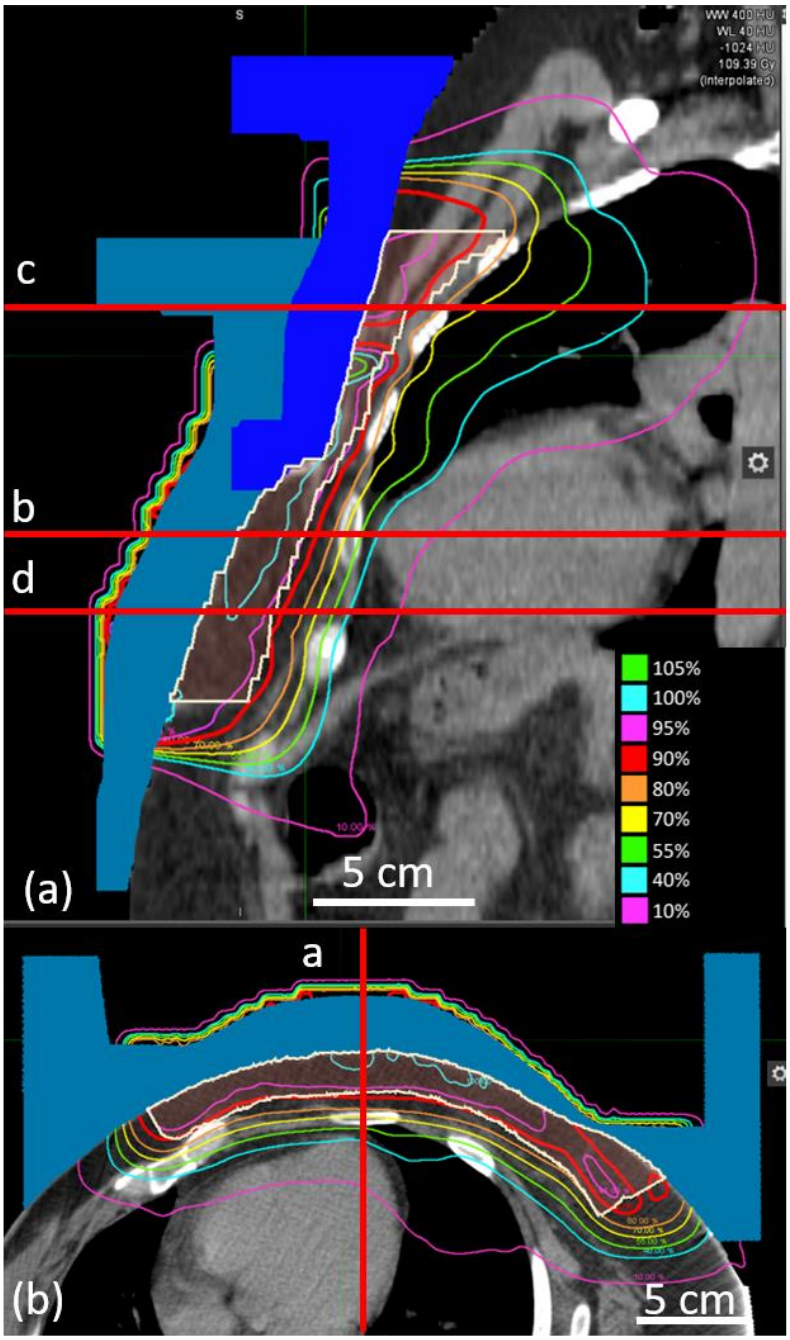

Figure B.18. **Sagittal and axial images of CW4, Plan 1 and Plan 2**. CW4 (Patient Set 2) was planned using scattered electron beams and discrete energy spacing for Plan 1 and discrete (lower field)/continuous (upper field) energy spacing for Plan 2. In this case, the optimal energy for the upper field was discrete so the Plans 1 and 2 are identical. (a) Dose plan in the sagittal-coronal, oblique plane demarcated by the red line in figure (b)'s transverse plane; (b) Dose plan in transverse plane passing through central heart region, demarcated by red line in figure (a)'s oblique plane. Upper bolus is shaded dark blue, lower bolus is shaded light blue, and PTV is outlined in white. Key shows dose values.
(figure cont'd.)

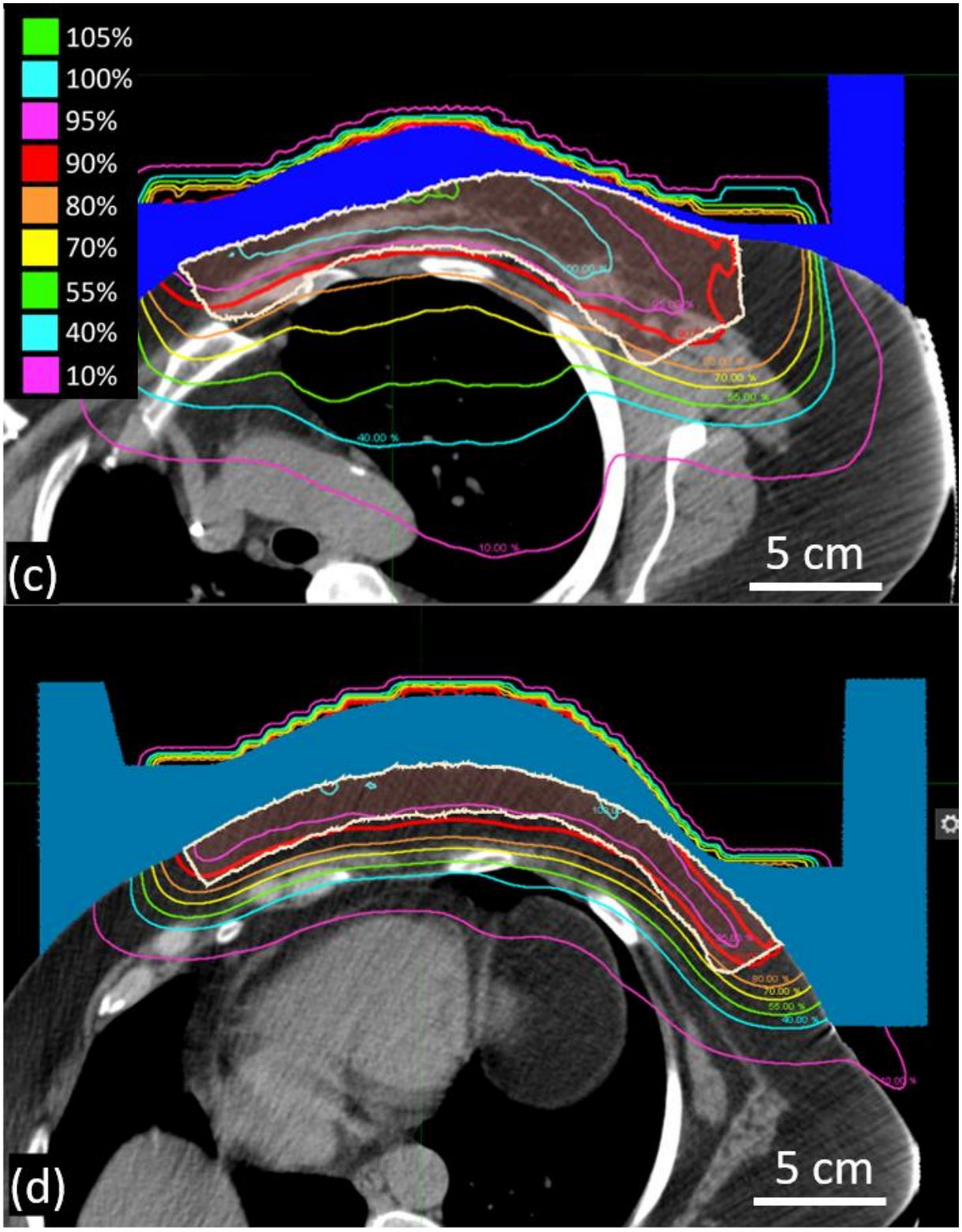
105%
100%
95%
90%
80%
70%
55%
40%
10%
(c)
5 cm
(d)
5 cm

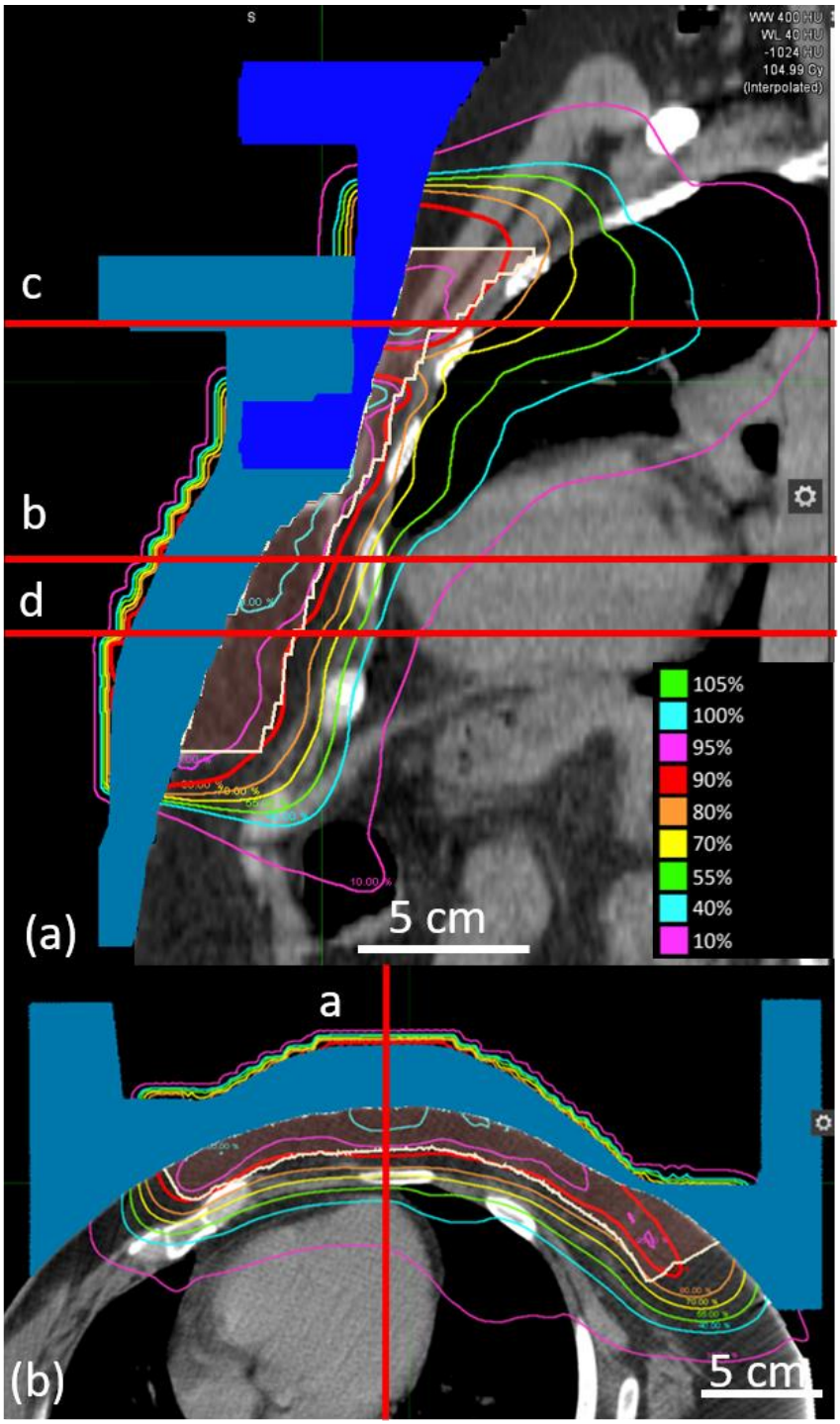

Figure B.19. **Sagittal and axial images of CW4, Plan 3**. CW4 (Patient Set 2) was planned using scattered electron beams and continuous energy spacing. (a) Dose plan in the sagittal-coronal, oblique plane demarcated by the red line in figure (b)'s transverse plane; (b) Dose plan in transverse plane passing through central heart region, demarcated by red line in figure (a)'s oblique plane. Upper bolus is shaded dark blue, lower bolus is shaded light blue, and PTV is outlined in white. Key shows dose values.
(figure cont'd.)

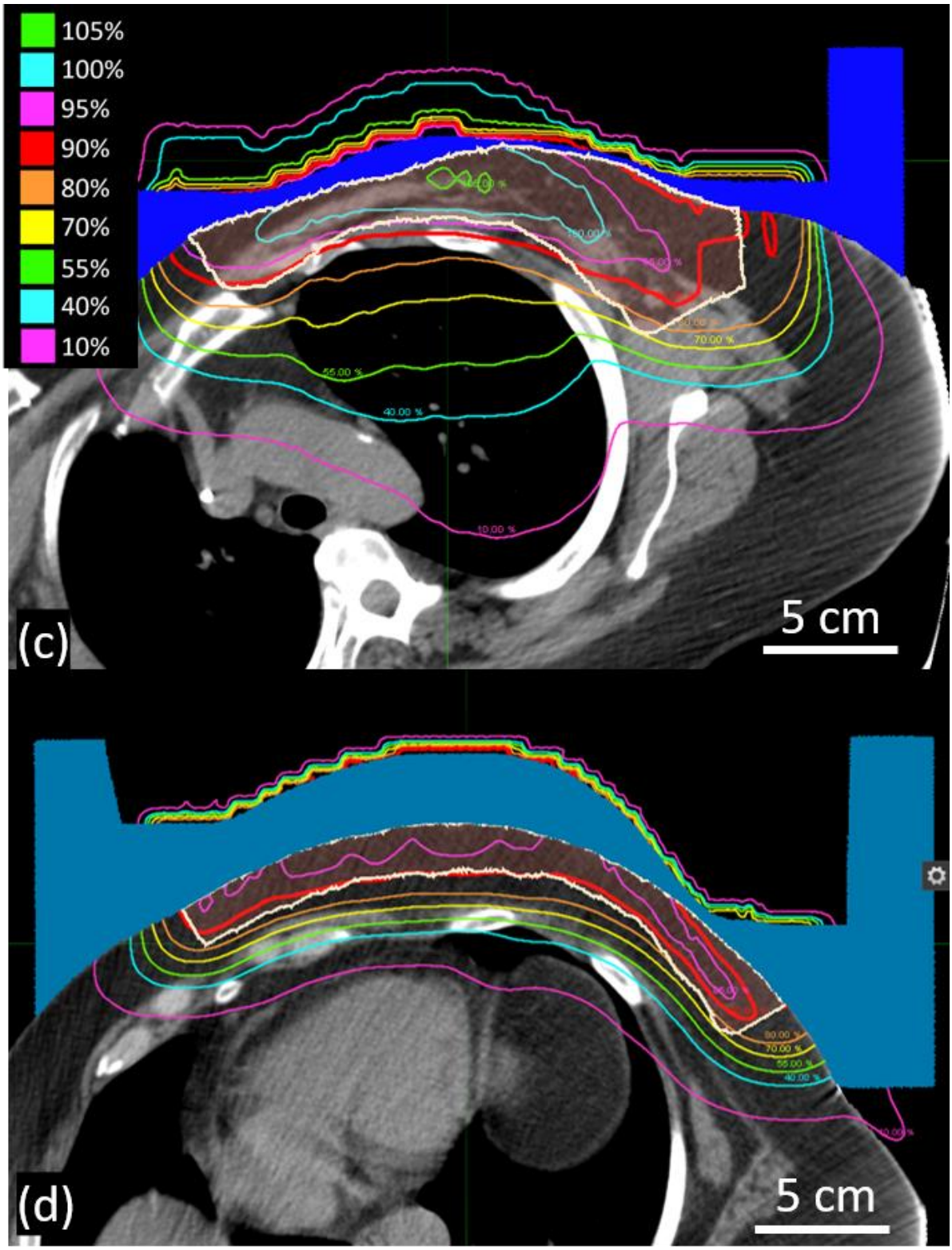
105%
100%
95%
90%
80%
70%
55%
40%
10%
(c)
5 cm
(d)
5 cm

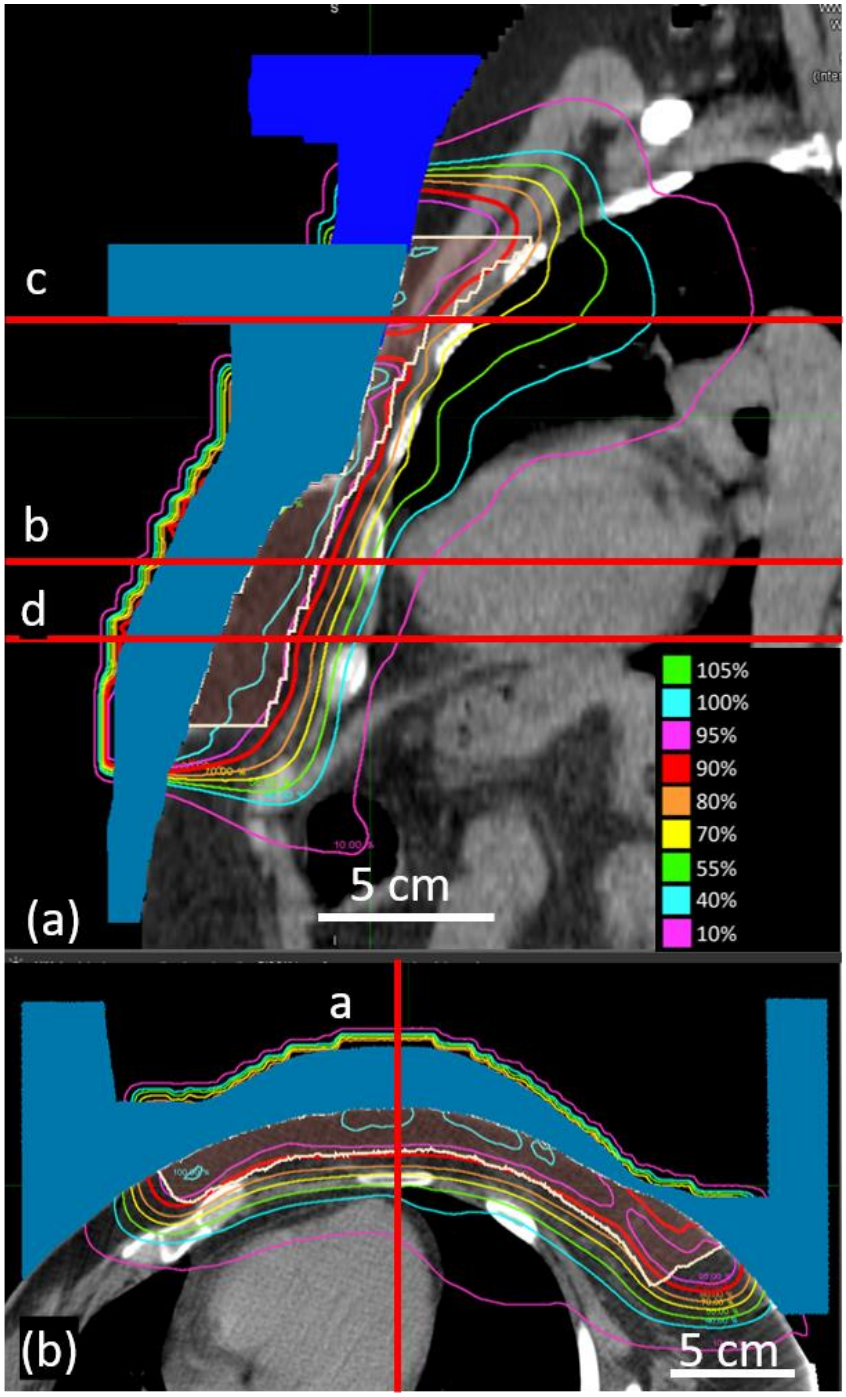

Figure B.20. **Sagittal and axial images of CW4, Plan 4**. CW4 (Patient Set 2) was planned using scanned electron beams and discrete energy spacing. (a) Dose plan in the sagittal-coronal, oblique plane demarcated by the red line in figure (b)'s transverse plane; (b) Dose plan in transverse plane passing through central heart region, demarcated by red line in figure (a)'s oblique plane Upper bolus is shaded dark blue, lower bolus is shaded light blue, and PTV is outlined in white. Key shows dose values.
(figure cont'd.)

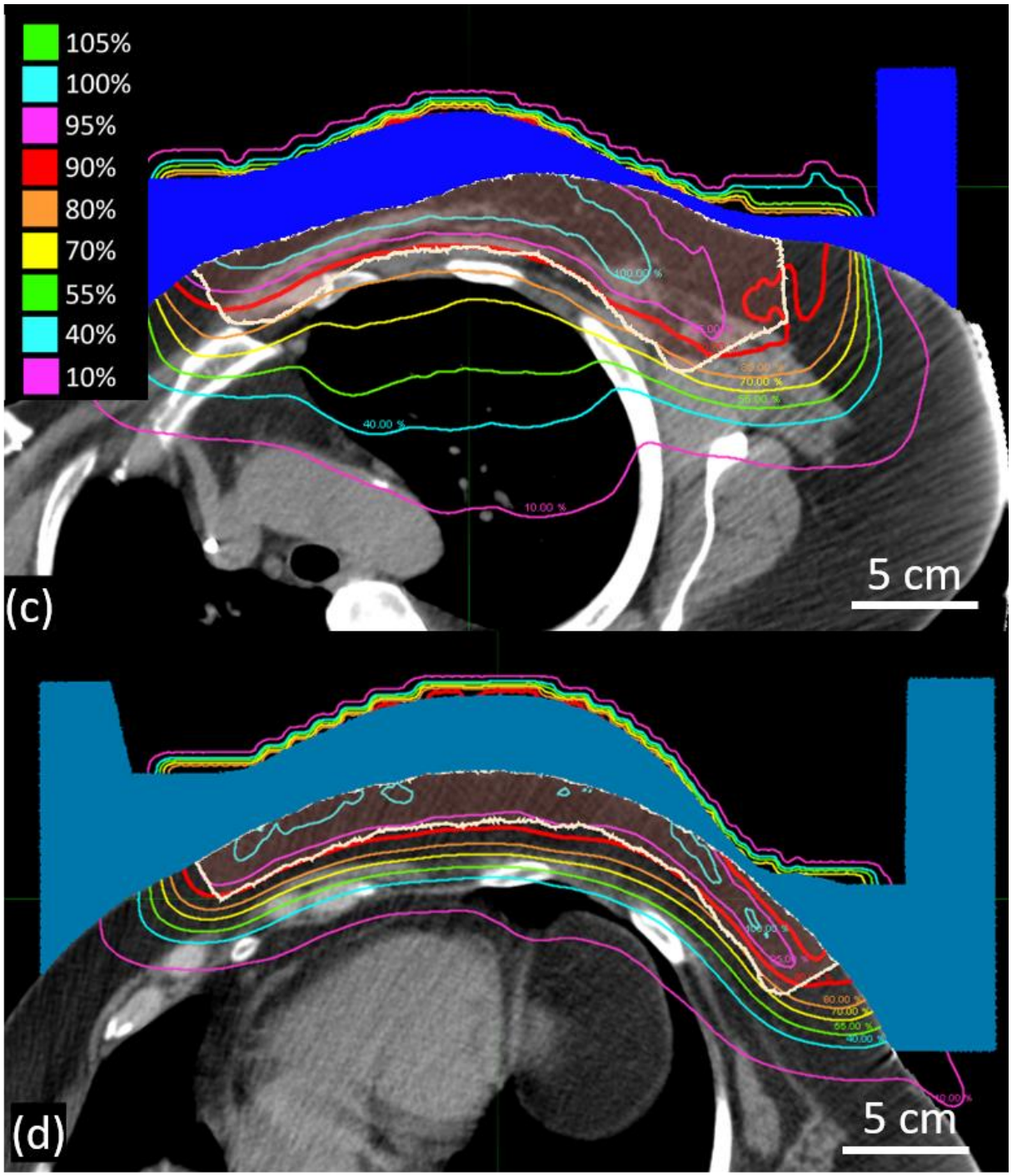
105%
100%
95%
90%
80%
70%
55%
40%
10%
40.00 %
10.00 %
5 cm
(c)
5 cm
(d)

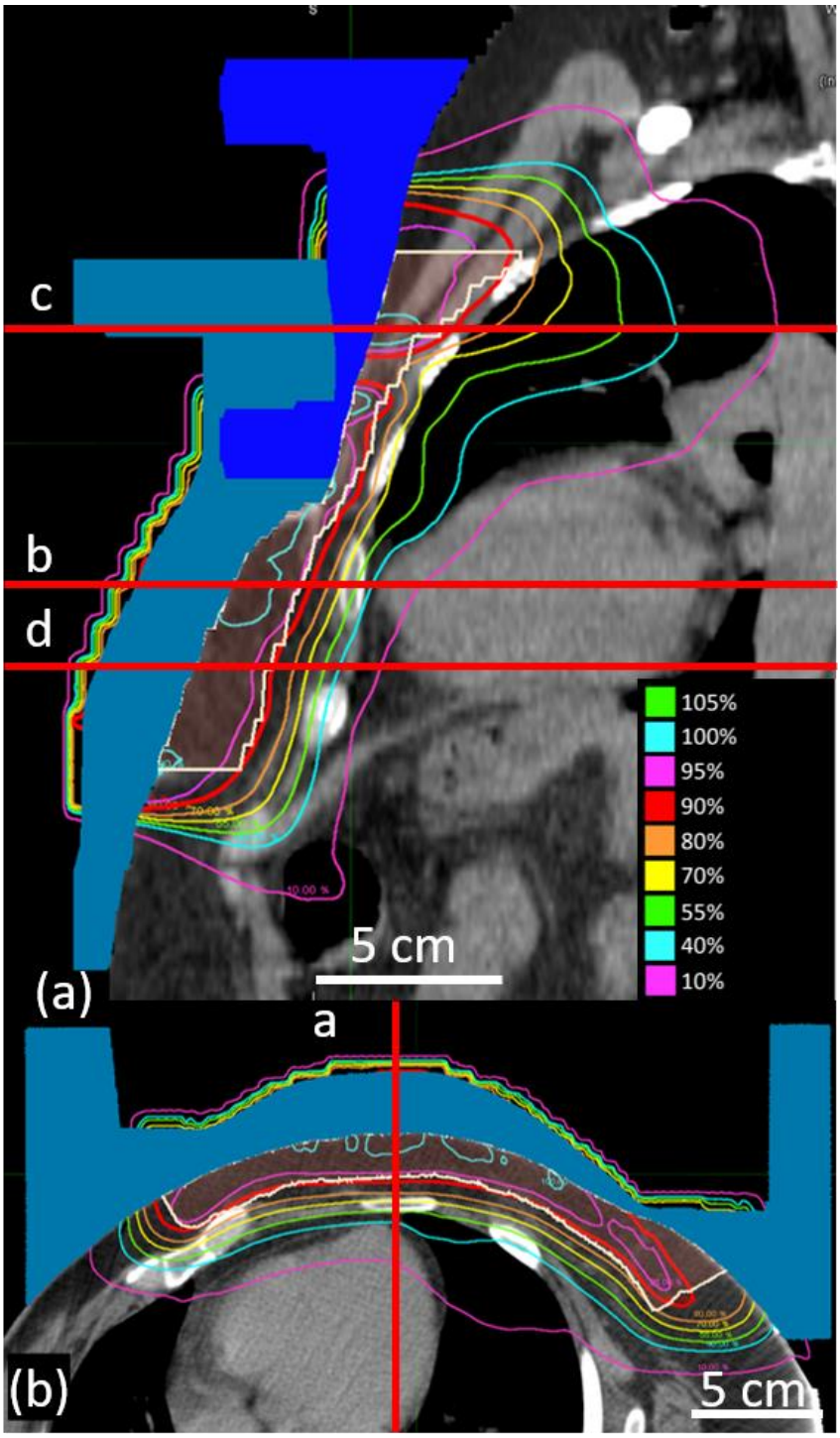

Figure B.21. **Sagittal and axial images of CW4, Plan 5**. CW4 (Patient Set 2) was planned using scanned electron beams and continuous energy spacing. (a) Dose plan in the sagittal-coronal, oblique plane demarcated by the red line in figure (b)'s transverse plane; (b) Dose plan in transverse plane passing through central heart region, demarcated by red line in figure (a)'s oblique plane. Upper bolus is shaded dark blue, lower bolus is shaded light blue, and PTV is outlined in white. Key shows dose values.
(figure cont'd.)

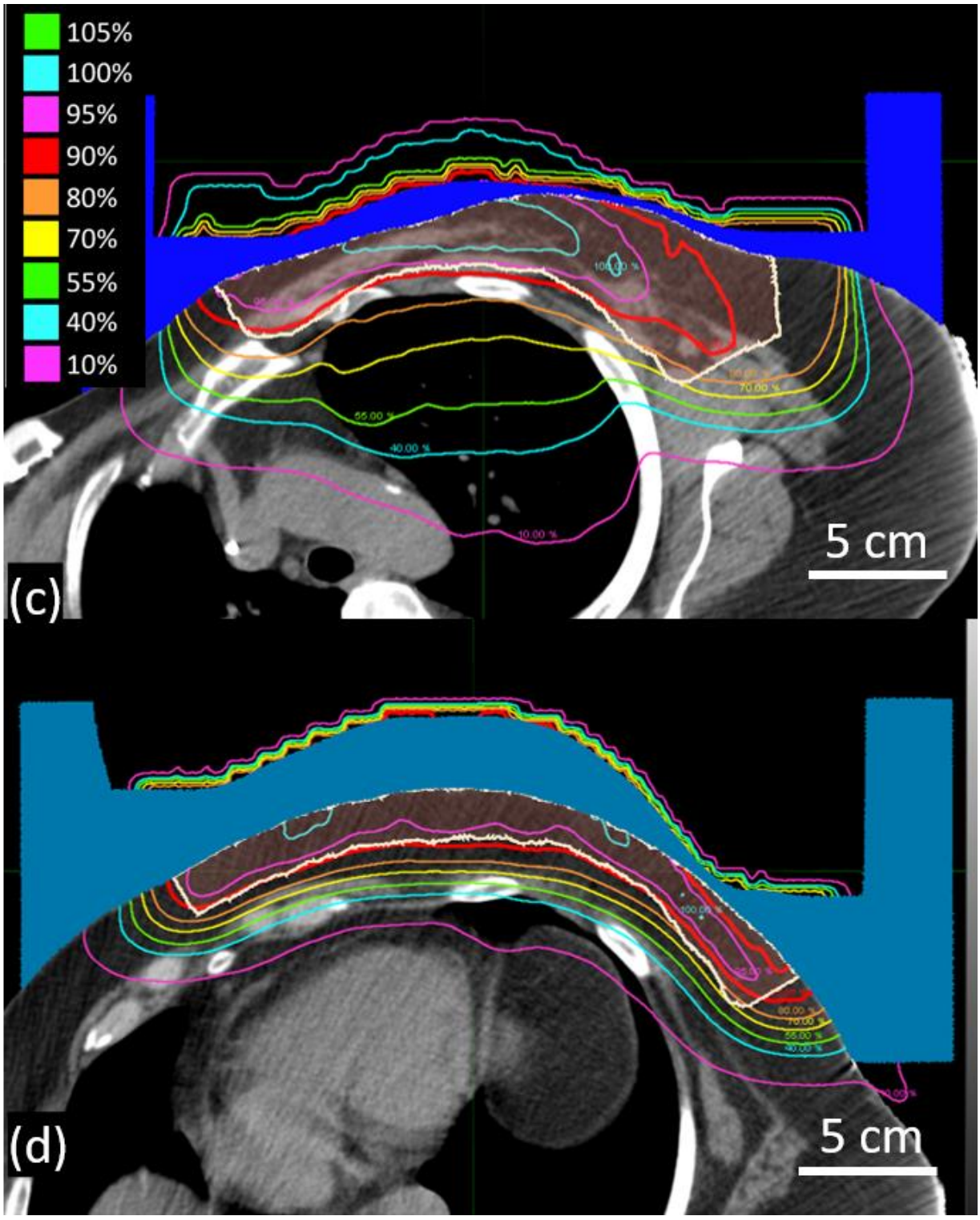
105%
100%
95%
90%
80%
70%
55%
40%
10%
5 cm
(c)
5 cm
(d)

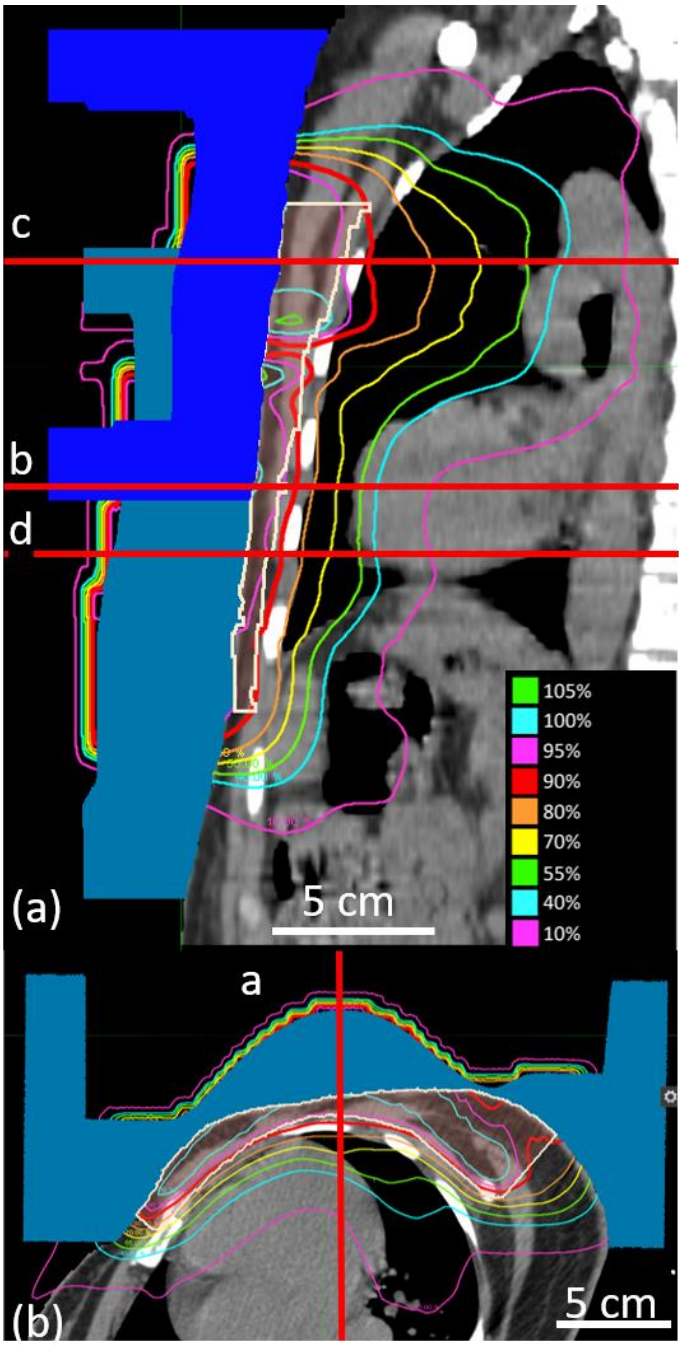

Figure B.22. **Sagittal and axial images of CW7, Plan 1 and Plan 2**. CW7 (Patient Set 2) was planned using scattered electron beams and discrete energy spacing for Plan 1 and discrete (lower field)/continuous (upper field) energy spacing for Plan 2. In this case, the optimal energy for the upper field was discrete so the Plans 1 and 2 are identical. (a) Dose plan in the sagittal-coronal, oblique plane demarcated by the red line in figure (b)'s transverse plane; (b) Dose plan in transverse plane passing through central heart region, demarcated by red line in figure (a)'s oblique plane. Upper bolus is shaded dark blue, lower bolus is shaded light blue, and PTV is outlined in white. Key shows dose values.
(figure cont'd.)

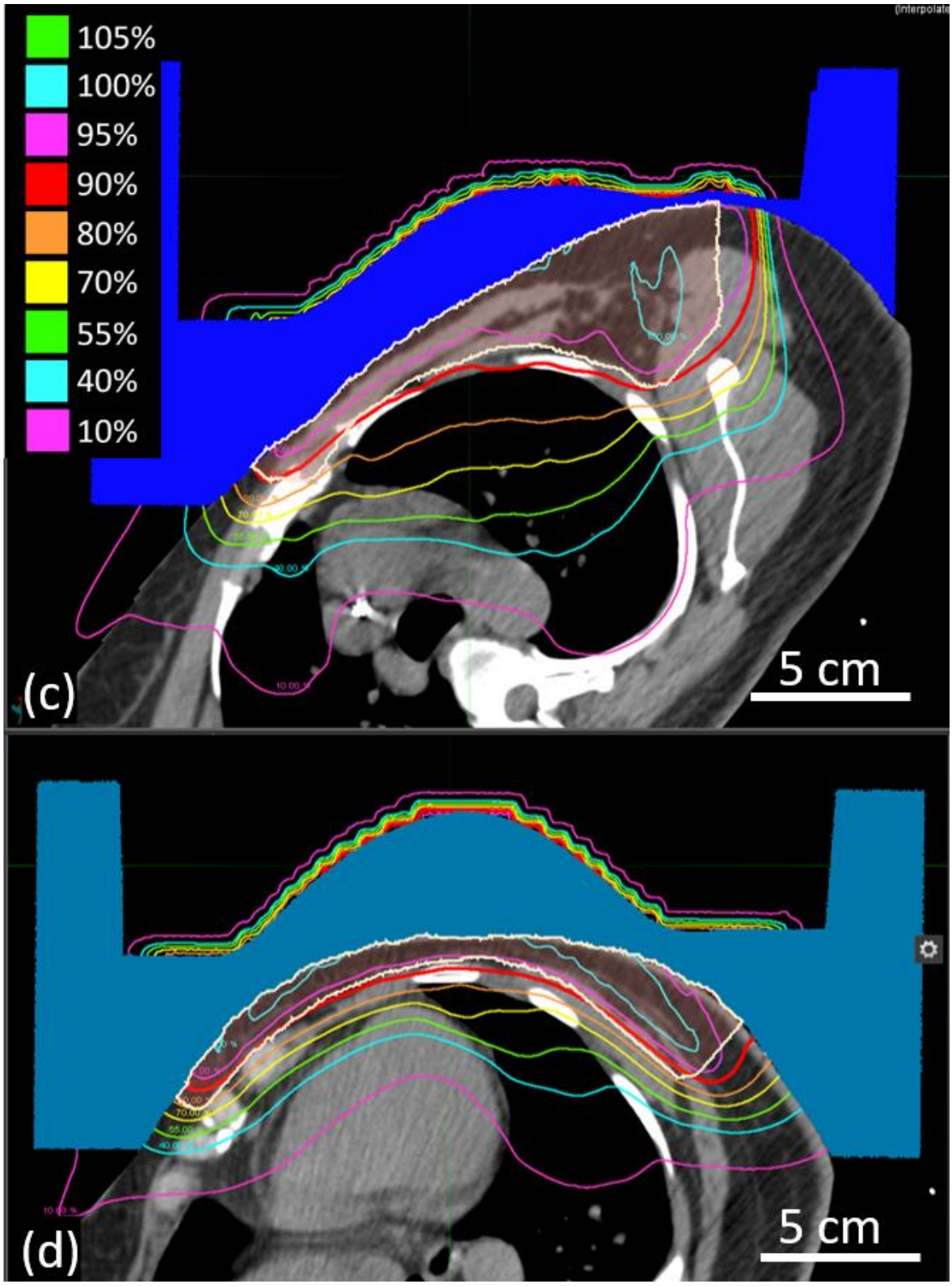
105%
100%
95%
90%
80%
70%
55%
40%
10%
(c)
5 cm
(d)
5 cm

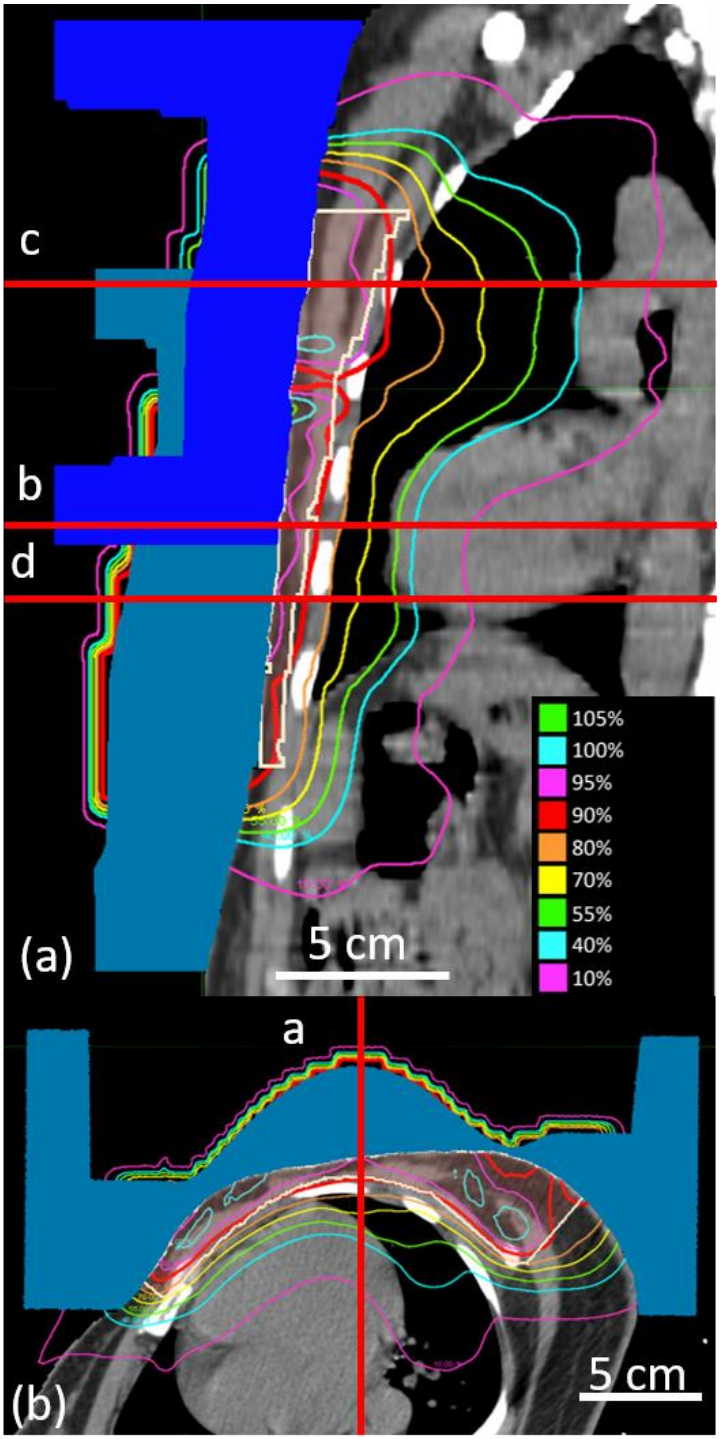

Figure B.23. **Sagittal and axial images of CW7, Plan 3**. CW7 (Patient Set 2) was planned using scattered electron beams and continuous energy spacing. (a) Dose plan in the sagittal-coronal, oblique plane demarcated by the red line in figure (b)'s transverse plane; (b) Dose plan in transverse plane passing through central heart region, demarcated by red line in figure (a)'s oblique plane. Upper bolus is shaded dark blue, lower bolus is shaded light blue, and PTV is outlined in white. Key shows dose values.
(figure cont'd.)

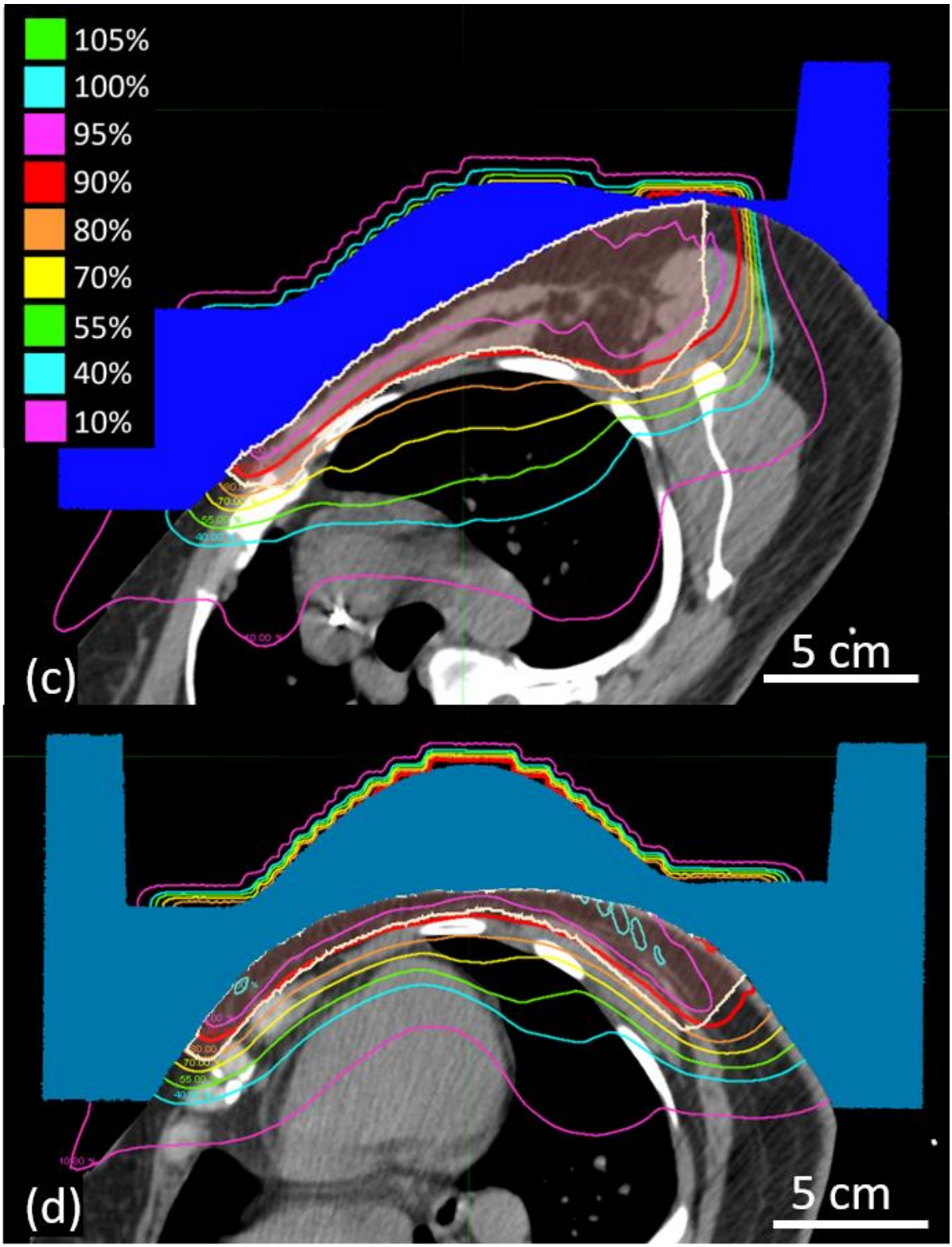
105%
100%
95%
90%
80%
70%
55%
40%
10%
(c)
5 cm
(d)
5 cm

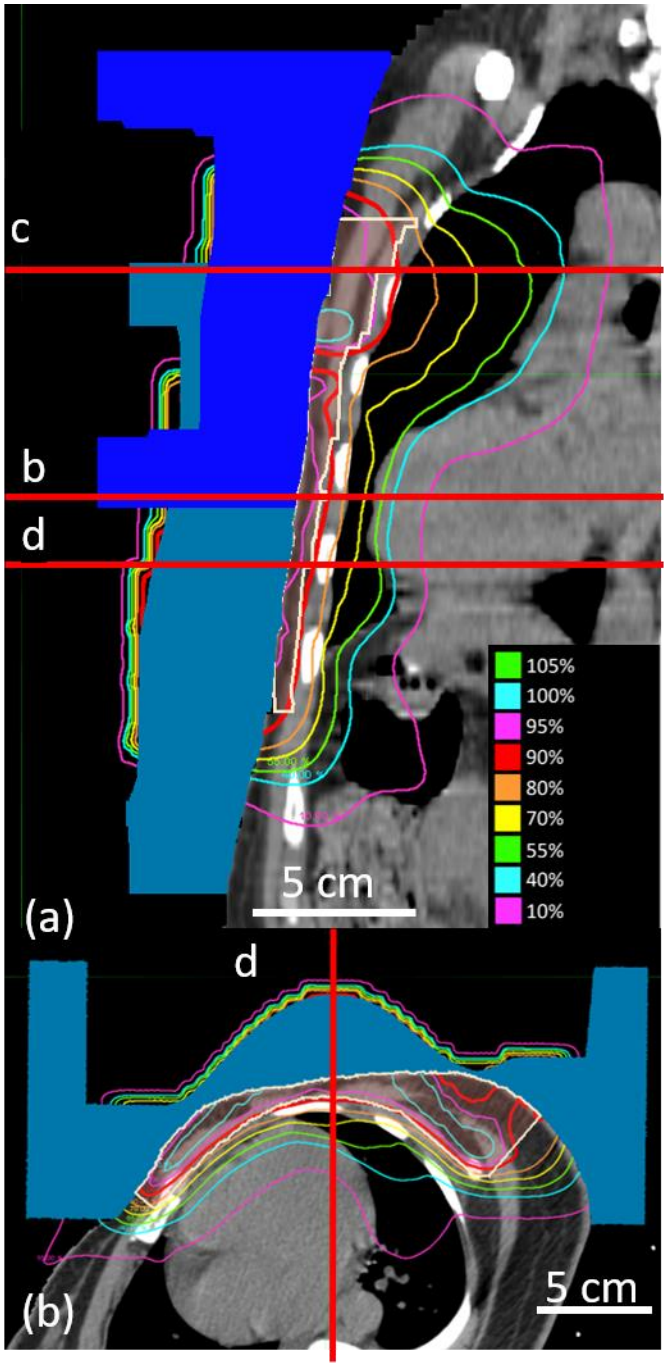

Figure B.24. **Sagittal and axial images of CW7, Plan 4**. CW7 (Patient Set 2) was planned using scanned electron beams and discrete energy spacing. (a) Dose plan in the sagittal-coronal, oblique plane demarcated by the red line in figure (b)'s transverse plane; (b) Dose plan in transverse plane passing through central heart region, demarcated by red line in figure (a)'s oblique plane. Upper bolus is shaded dark blue, lower bolus is shaded light blue, and PTV is outlined in white. Key shows dose values.
(figure cont'd.)

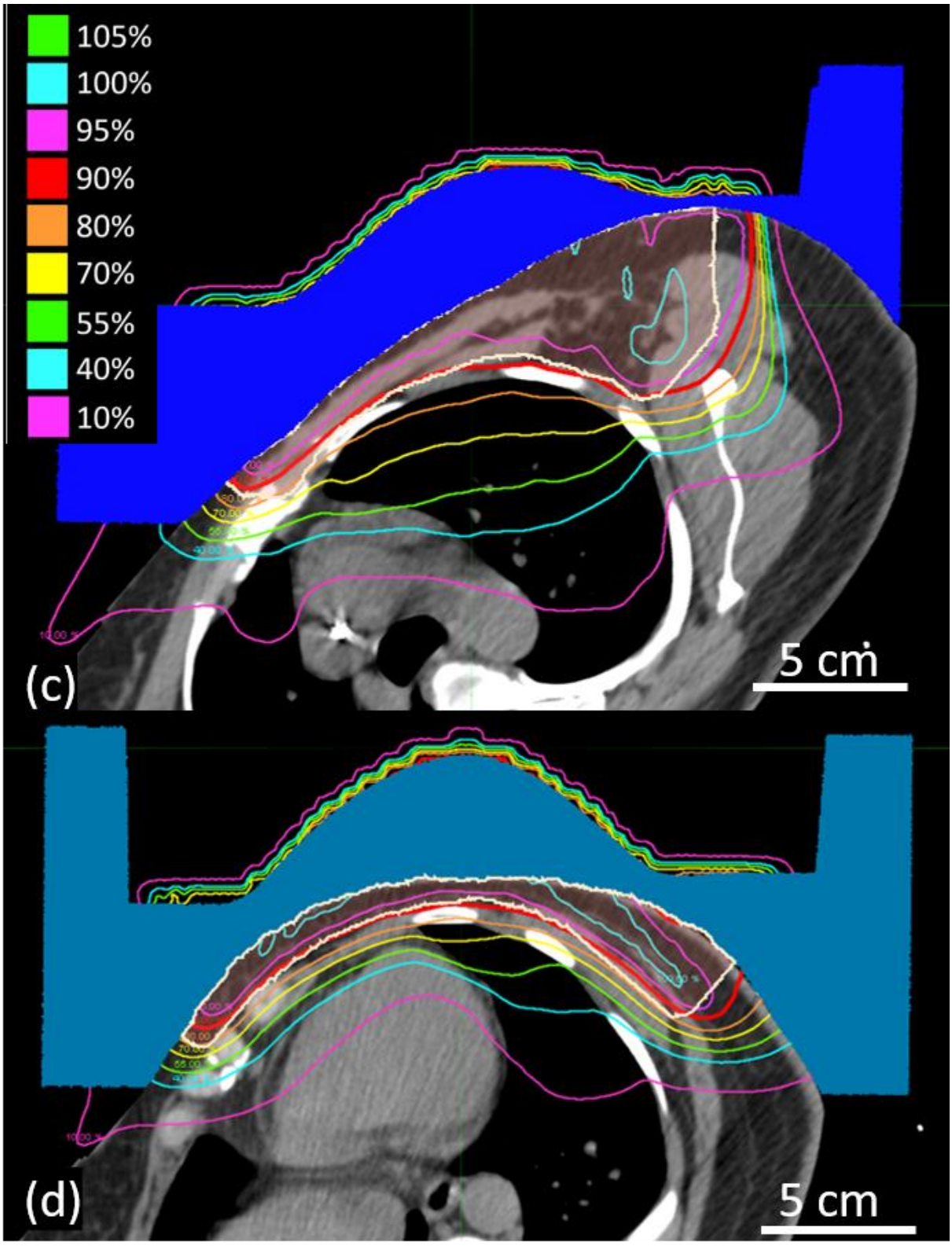
105%
100%
95%
90%
80%
70%
55%
40%
10%
(c)
5 cm
(d)
5 cm

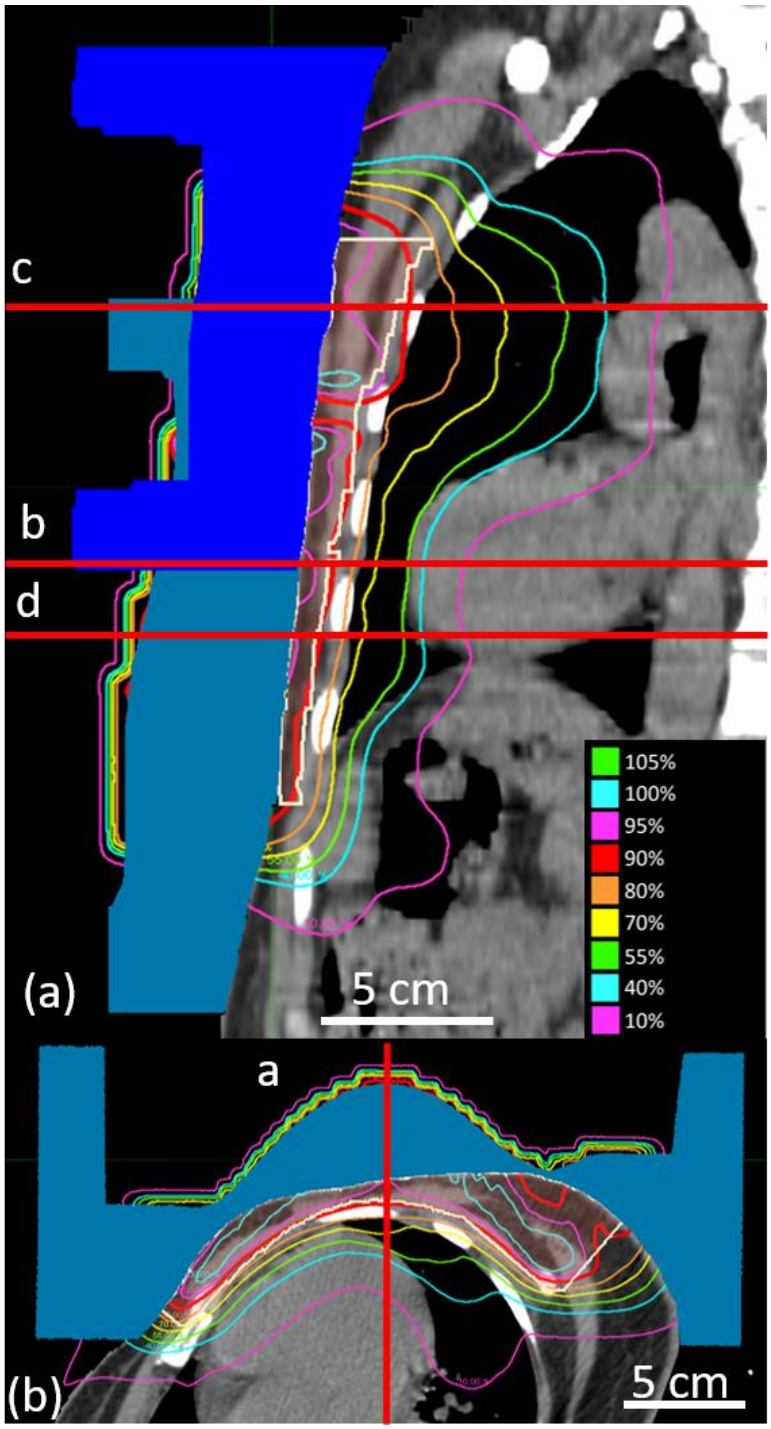

Figure B.25. **Sagittal and axial images of CW7, Plan 5**. CW7 (Patient Set 2) was planned using scanned electron beams and continuous energy spacing. (a) Dose plan in the sagittal-coronal, oblique plane demarcated by the red line in figure (b)'s transverse plane; (b) Dose plan in transverse plane passing through central heart region, demarcated by red line in figure (a)'s oblique plane. Upper bolus is shaded dark blue, lower bolus is shaded light blue, and PTV is outlined in white. Key shows dose values.
(figure cont'd.)

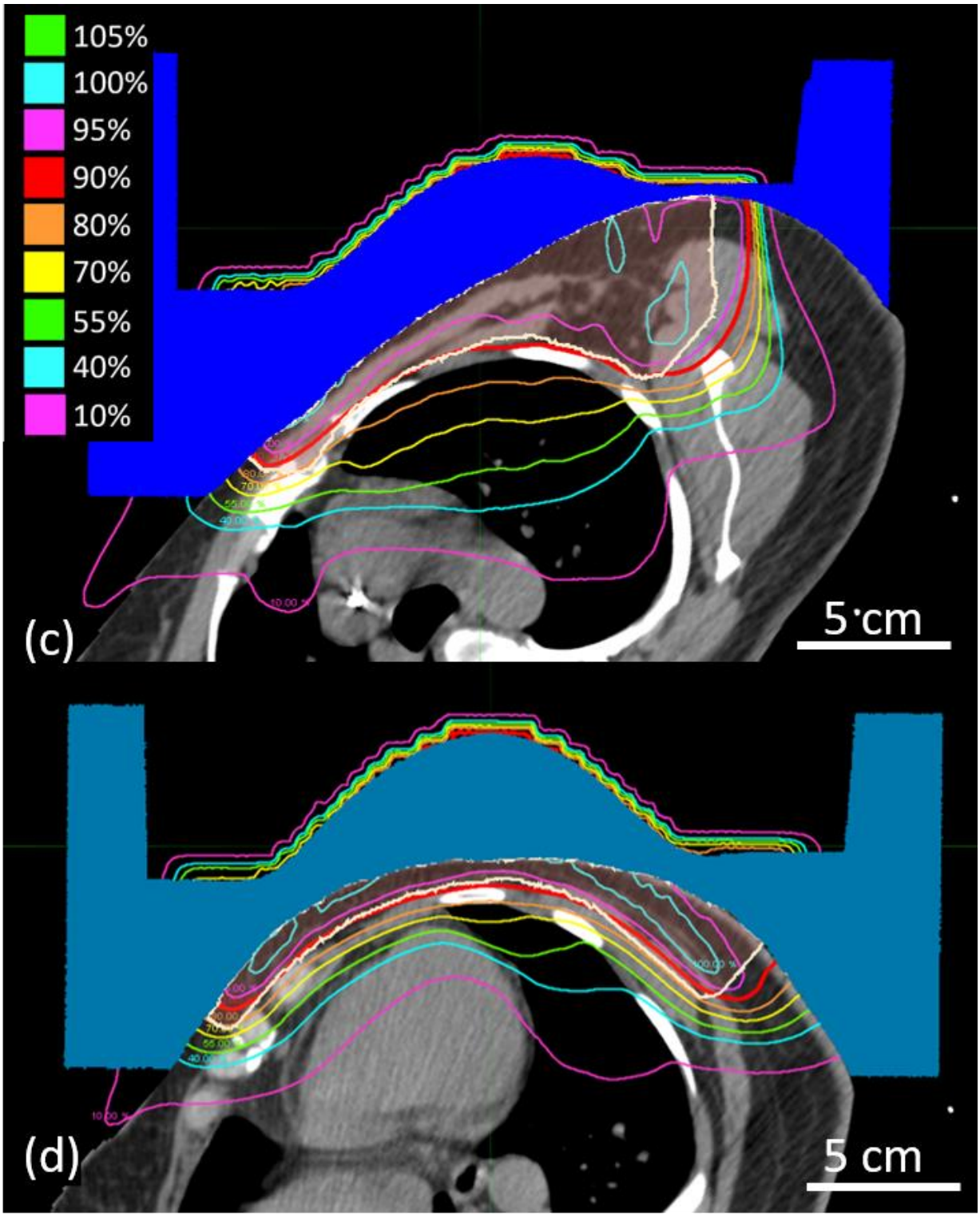
105%
100%
95%
90%
80%
70%
55%
40%
10%
(c)
5 cm
(d)
5 cm

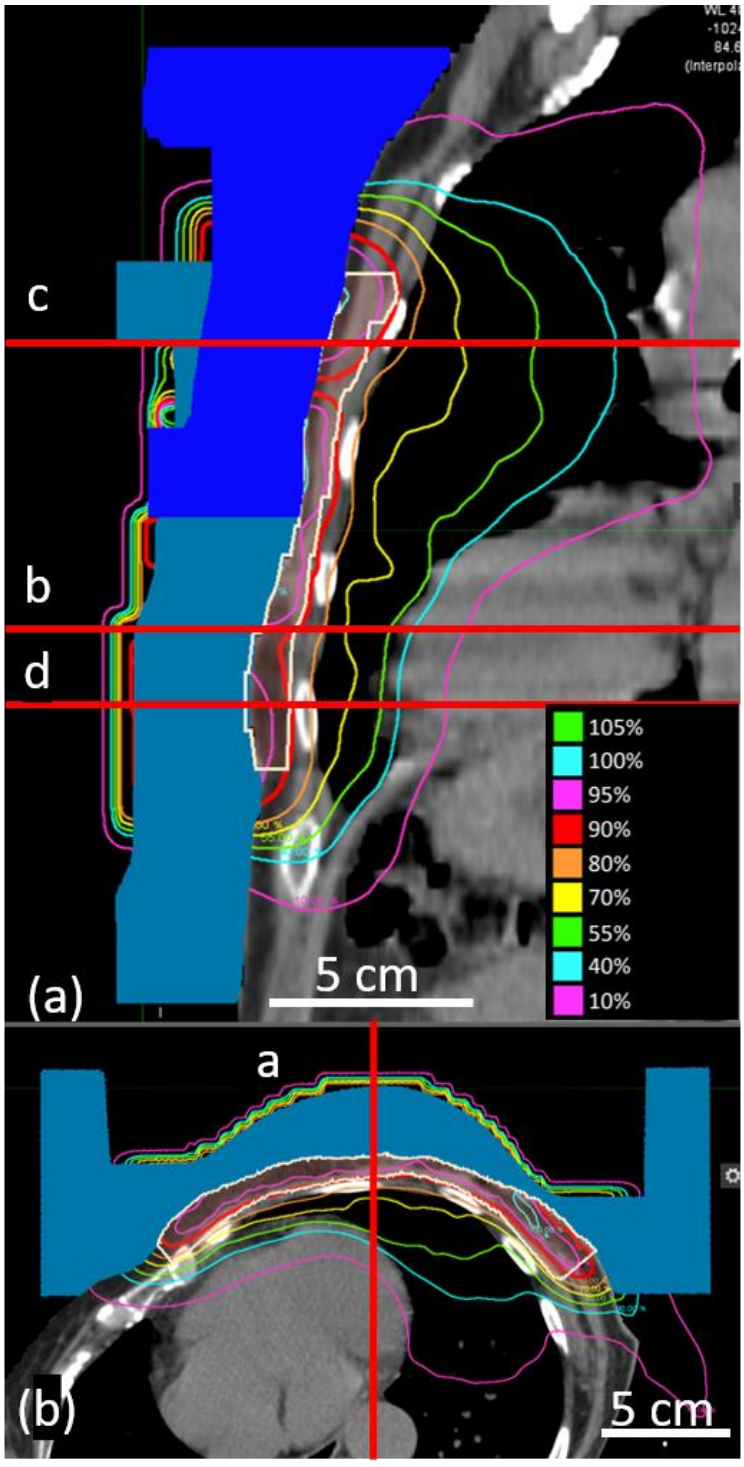

Figure B.26. **Sagittal and axial images of CW8, Plan 1**. CW8 (Patient Set 2) was planned using scattered electron beams and discrete energy spacing. (a) Dose plan in the sagittal-coronal, oblique plane demarcated by the red line in figure (b)'s transverse plane; (b) Dose plan in transverse plane passing through central heart region, demarcated by red line in figure (a)'s oblique plane. Upper bolus is shaded dark blue, lower bolus is shaded light blue, and PTV is outlined in white. Key shows dose values.
(figure cont'd.)

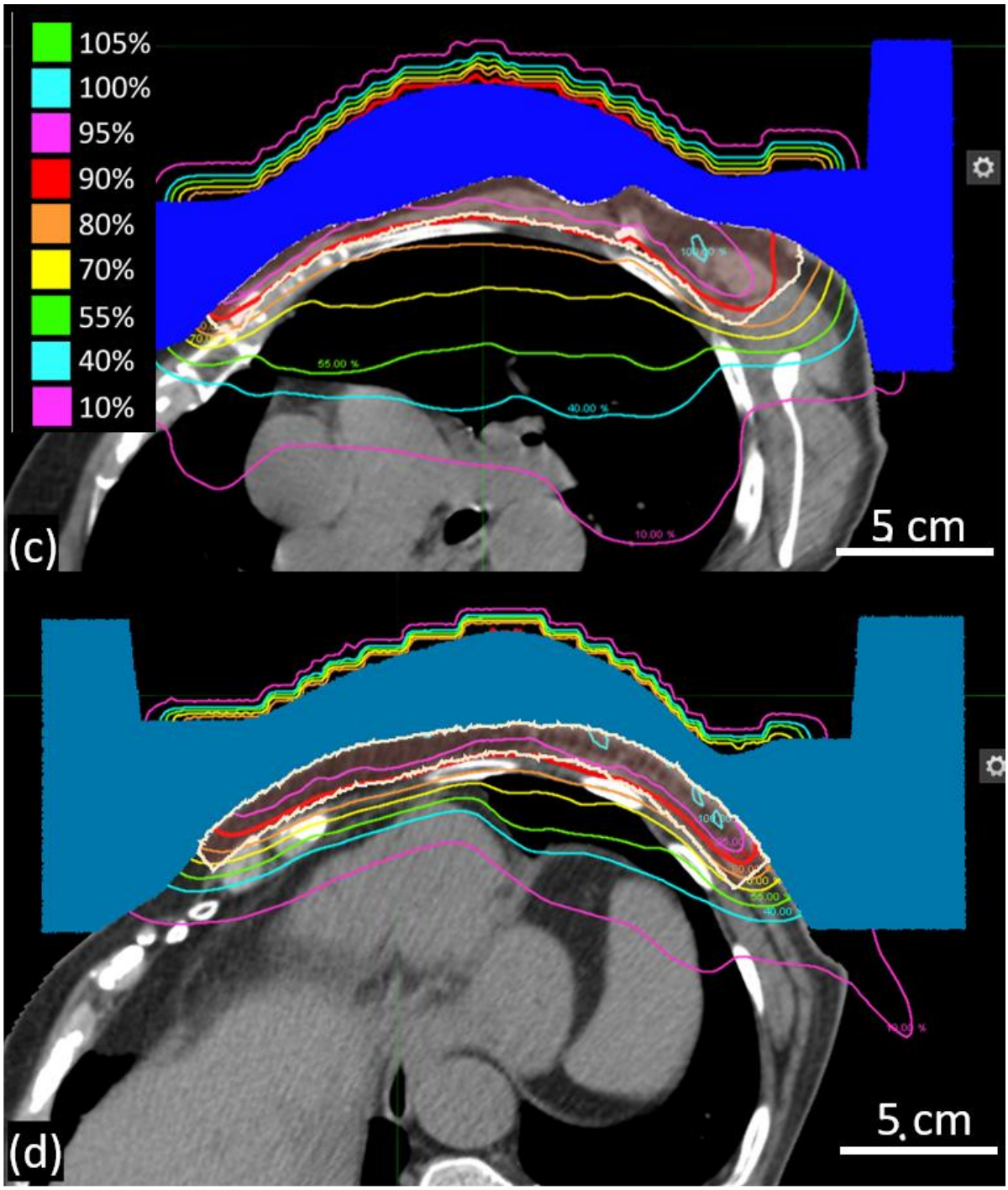
105%
100%
95%
90%
80%
70%
55%
40%
10%
55.00 %
40.00 %
10.00 %
(c)
5 cm
(d)
5 cm

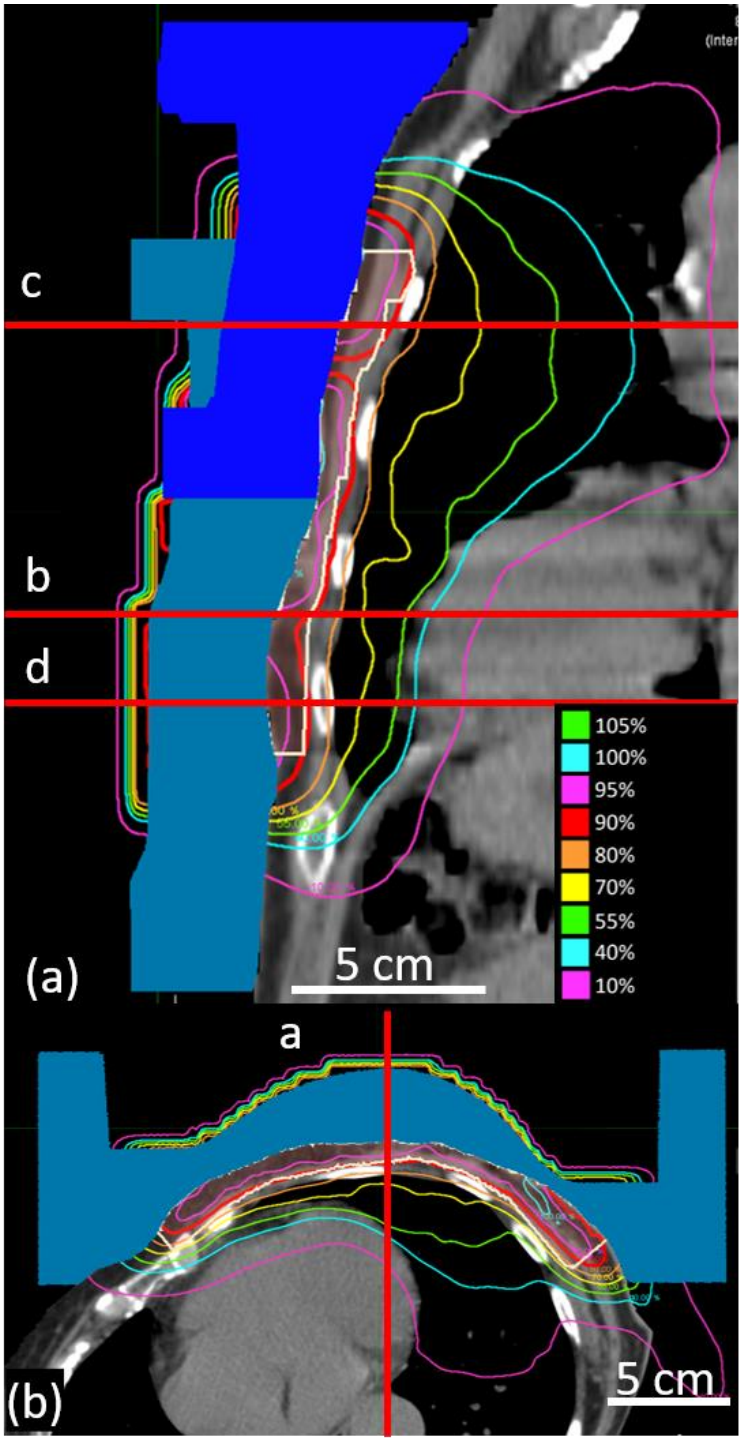

Figure B.27. **Sagittal and axial images of CW8, Plan 2**. CW8 (Patient Set 2) was planned using scattered electron beams and discrete (lower field)/continuous (upper field) energy spacing. (a) Dose plan in the sagittal-coronal, oblique plane demarcated by the red line in figure (b)'s transverse plane; (b) Dose plan in transverse plane passing through central heart region, demarcated by red line in figure (a)'s oblique plane. Upper bolus is shaded dark blue, lower bolus is shaded light blue, and PTV is outlined in white. Key shows dose values.
(figure cont'd.)

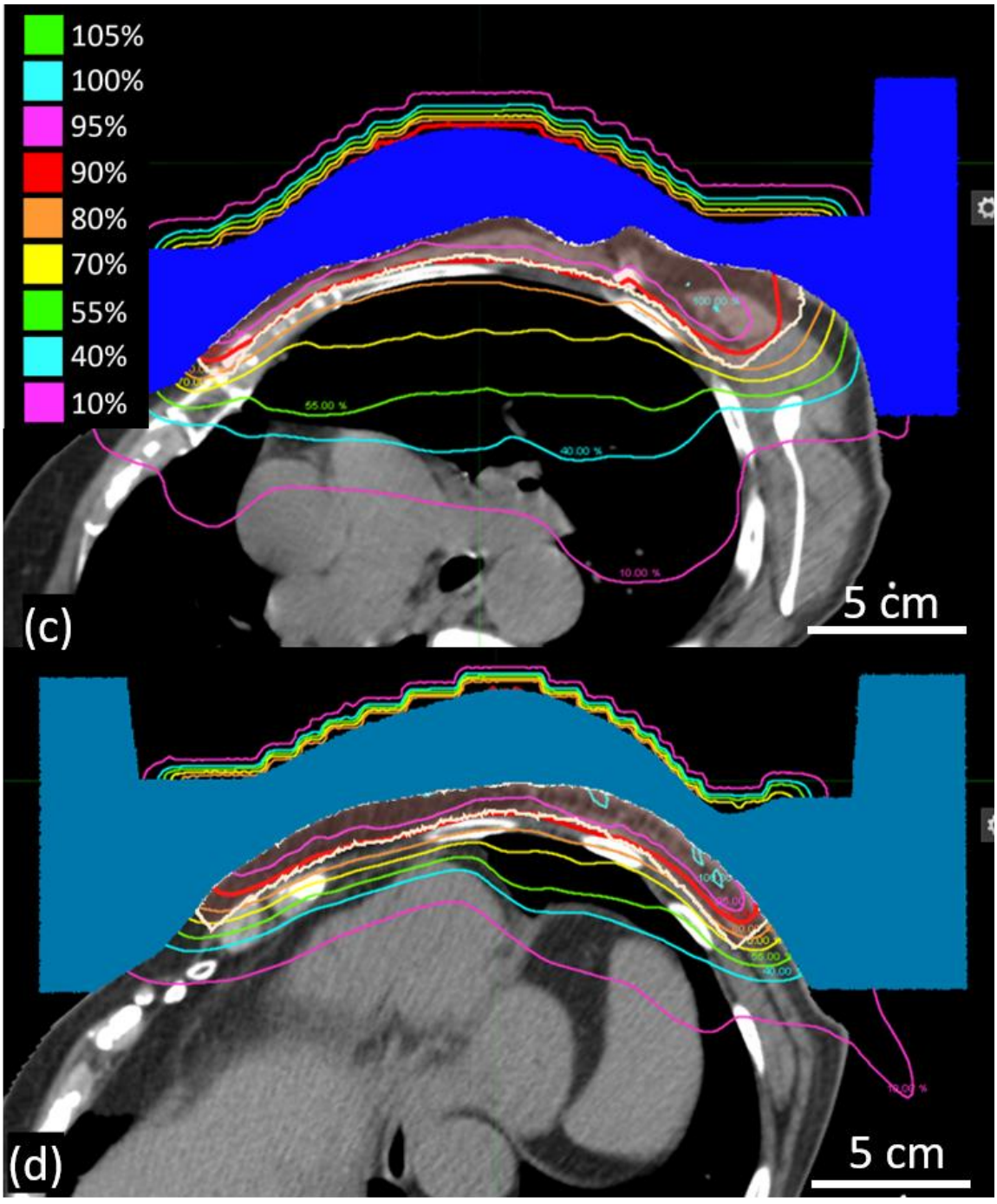
105%
100%
95%
90%
80%
70%
55%
40%
10%
(c)
5 cm
(d)
5 cm

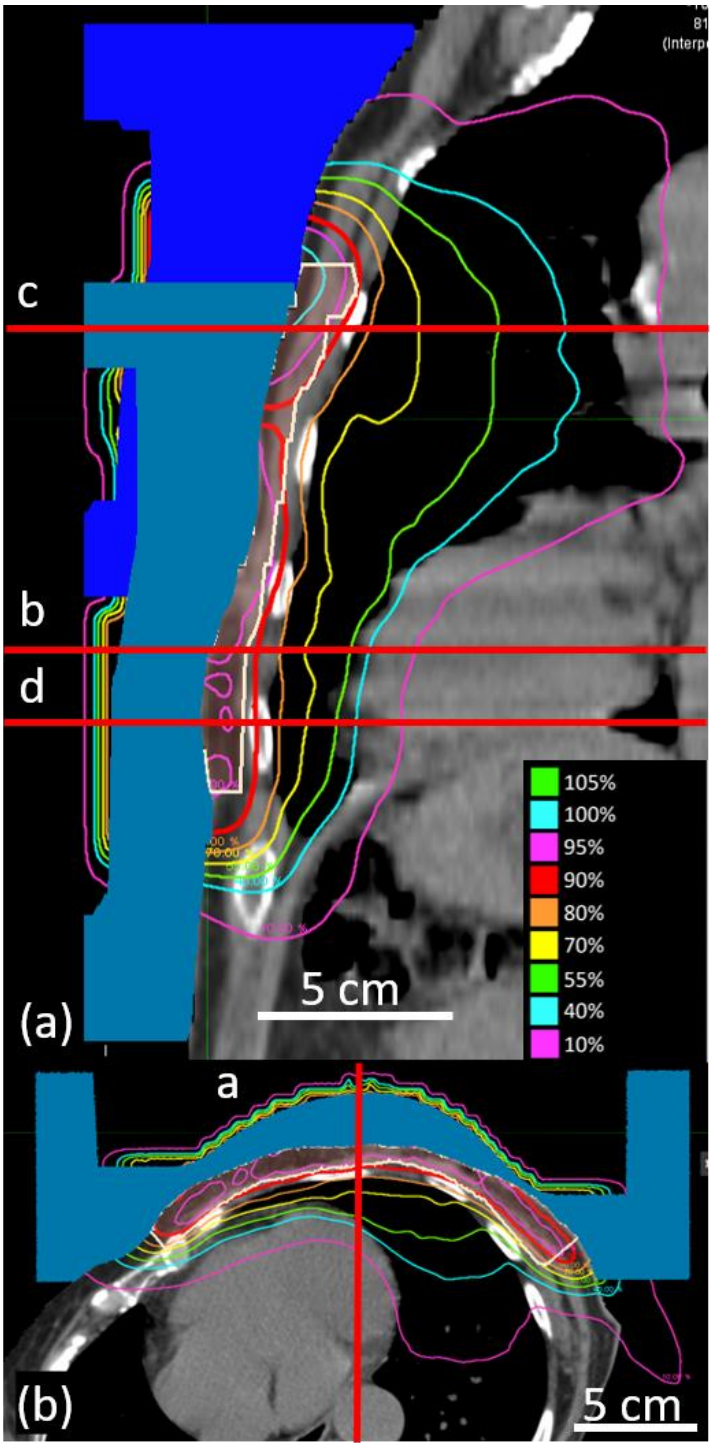

Figure B.28. **Sagittal and axial images of CW8, Plan 3**. CW8 (Patient Set 2) was planned using scattered electron beams and continuous energy spacing. (a) Dose plan in the sagittal-coronal, oblique plane demarcated by the red line in figure (b)'s transverse plane; (b) Dose plan in transverse plane passing through central heart region, demarcated by red line in figure (a)'s oblique plane. Upper bolus is shaded dark blue, lower bolus is shaded light blue, and PTV is outlined in white. Key shows dose values.
(figure cont'd.)

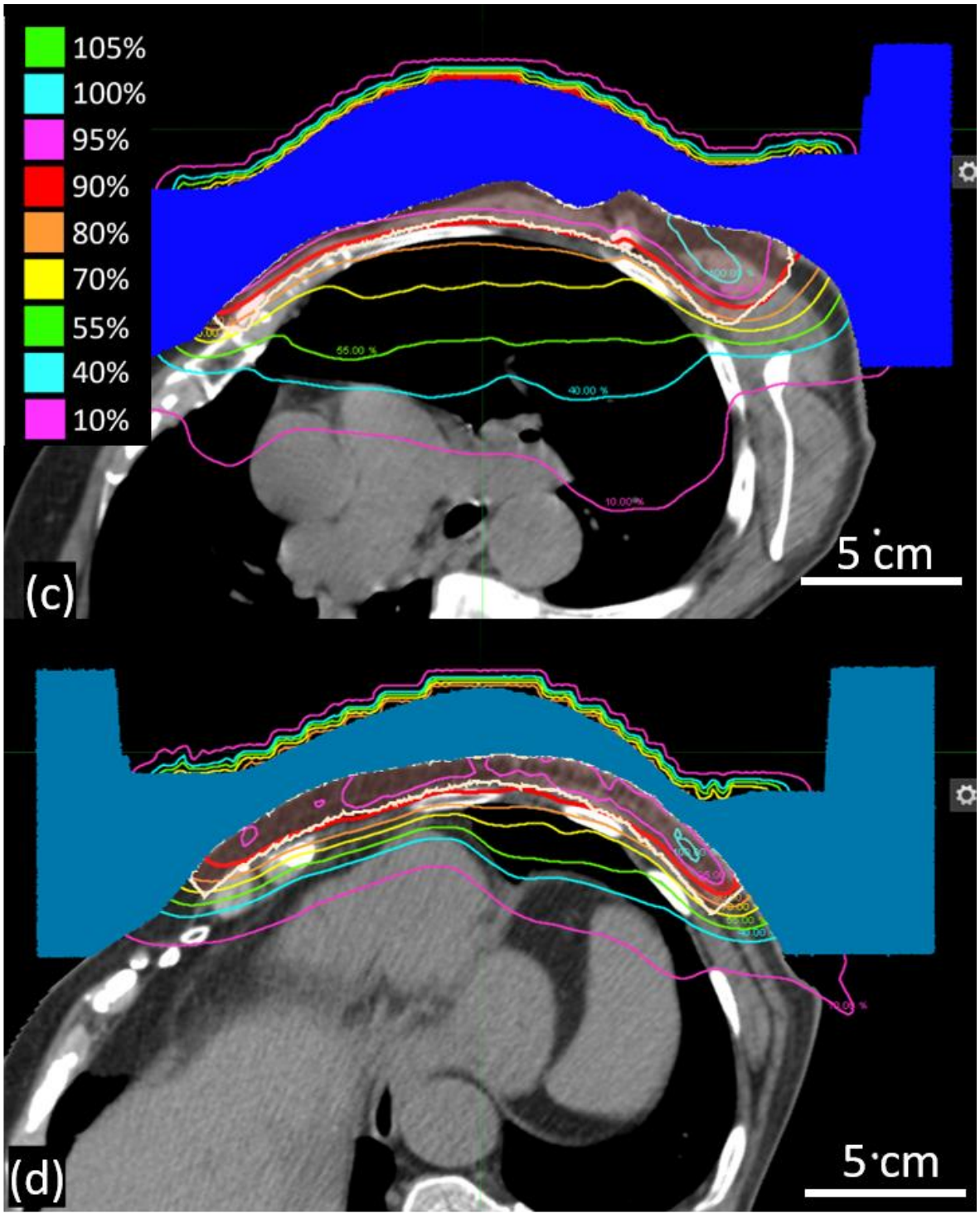
105%
100%
95%
90%
80%
70%
55%
40%
10%
55.00 %
40.00 %
10.00%
5 cm
(c)
5 cm
(d)

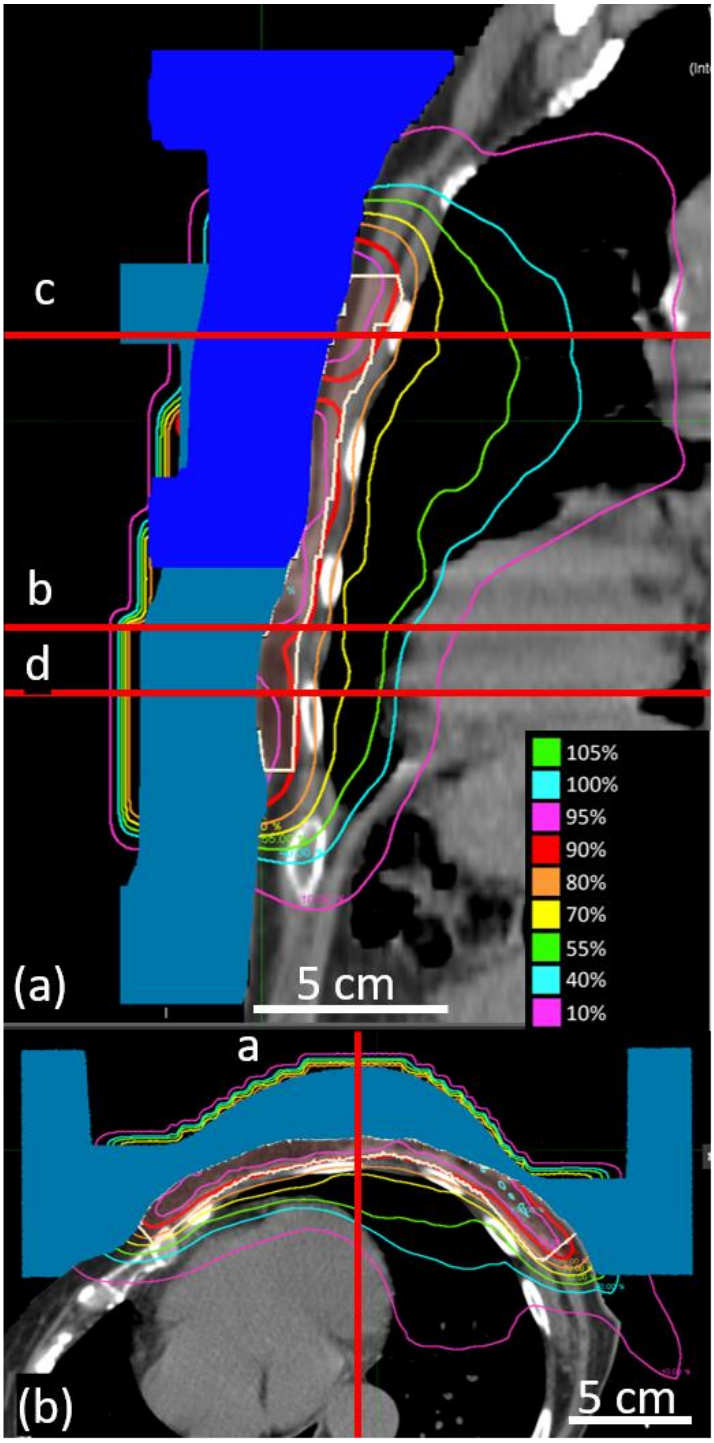

Figure B.29. **Sagittal and axial images of CW8, Plan 4**. CW8 (Patient Set 2) was planned using scanned electron beams and discrete energy spacing. (a) Dose plan in the sagittal-coronal, oblique plane demarcated by the red line in figure (b)'s transverse plane; (b) Dose plan in transverse plane passing through central heart region, demarcated by red line in figure (a)'s oblique plane. Upper bolus is shaded dark blue, lower bolus is shaded light blue, and PTV is outlined in white. Key shows dose values.
(figure cont'd.)

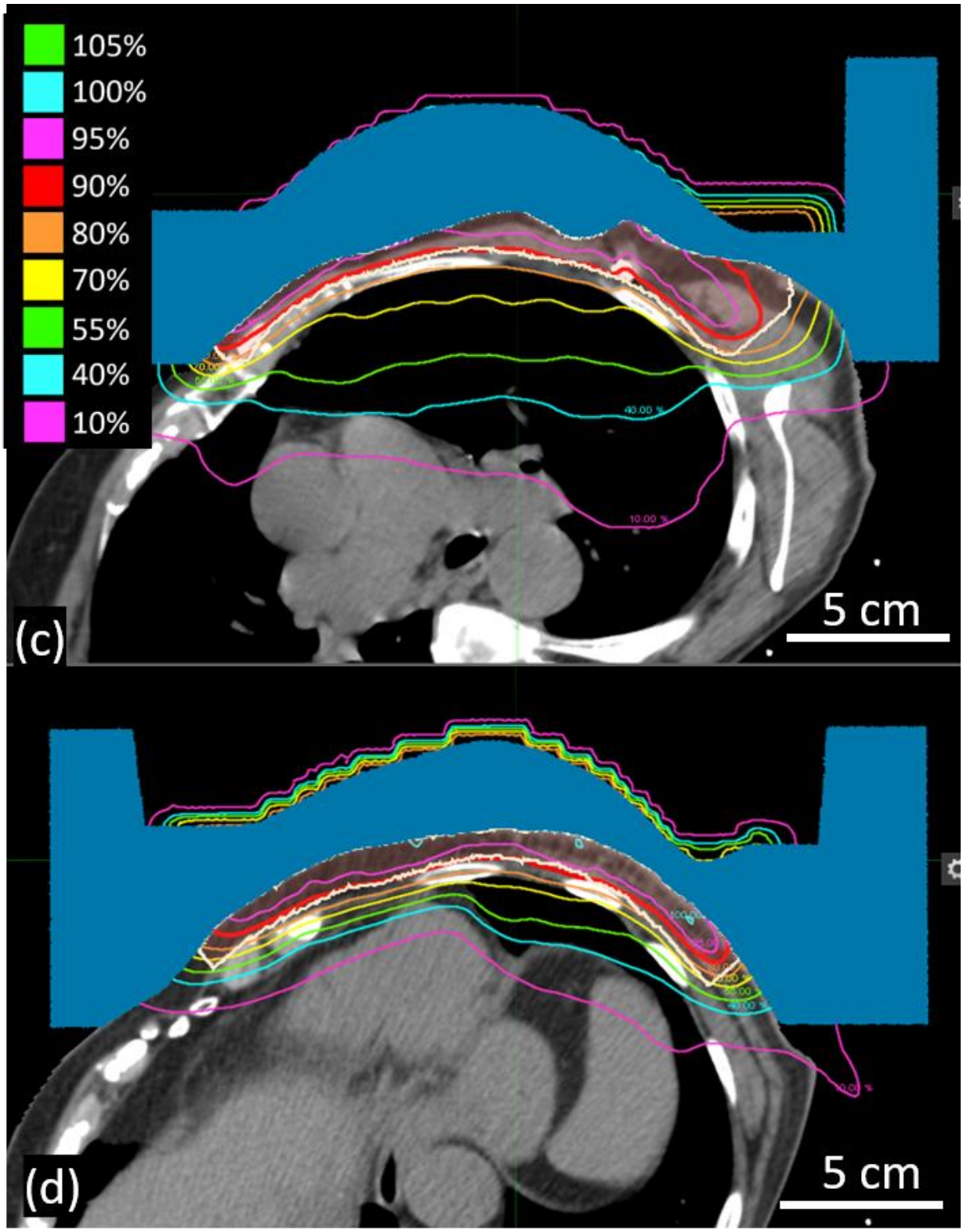
105%
100%
95%
90%
80%
70%
55%
40%
10%
40.00 %
10.00 %
5 cm
(c)
5 cm
(d)

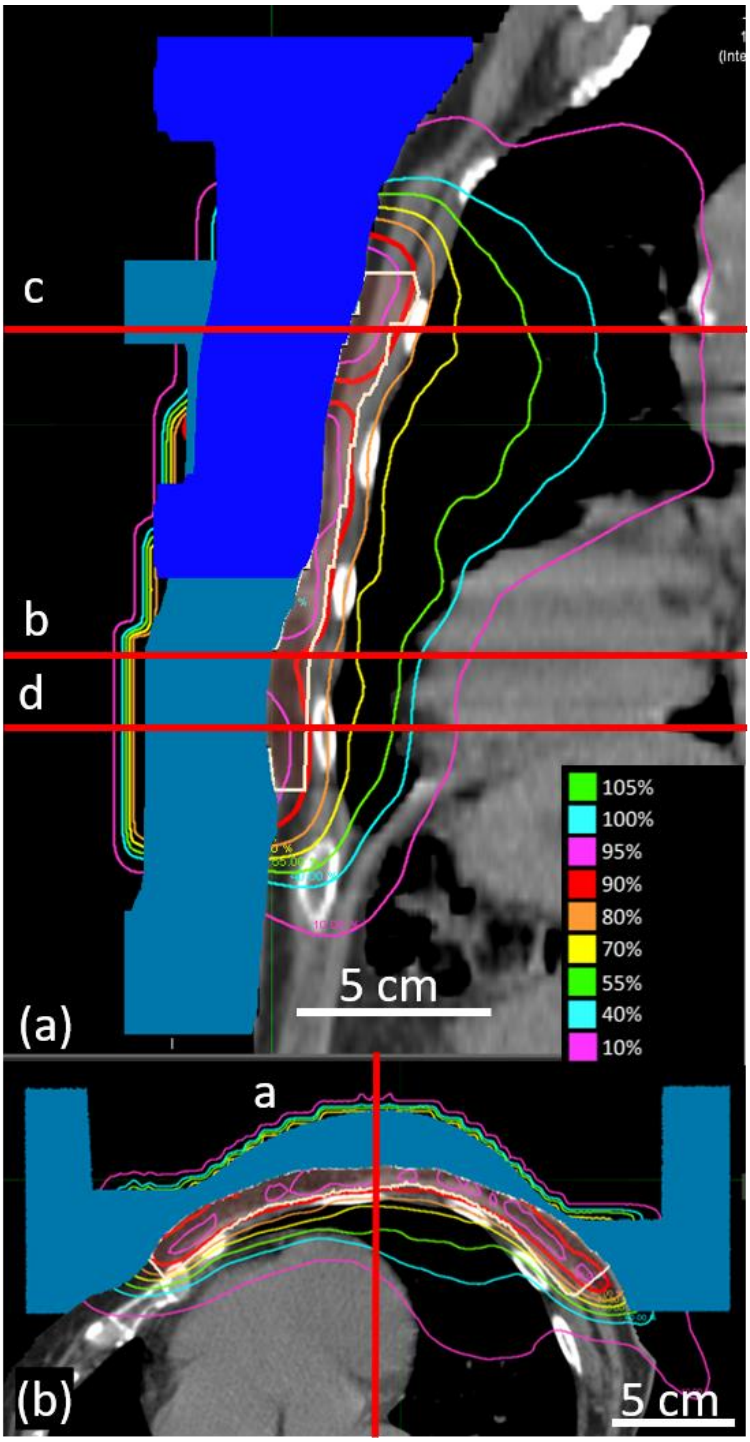

Figure B.30. **Sagittal and axial images of CW8, Plan 5**. CW8 (Patient Set 2) was planned using scanned electron beams and continuous energy spacing. (a) Dose plan in the sagittal-coronal, oblique plane demarcated by the red line in figure (b)'s transverse plane; (b) Dose plan in transverse plane passing through central heart region, demarcated by red line in figure (a)'s oblique plane. Upper bolus is shaded dark blue, lower bolus is shaded light blue, and PTV is outlined in white. Key shows dose values.
(figure cont'd.)

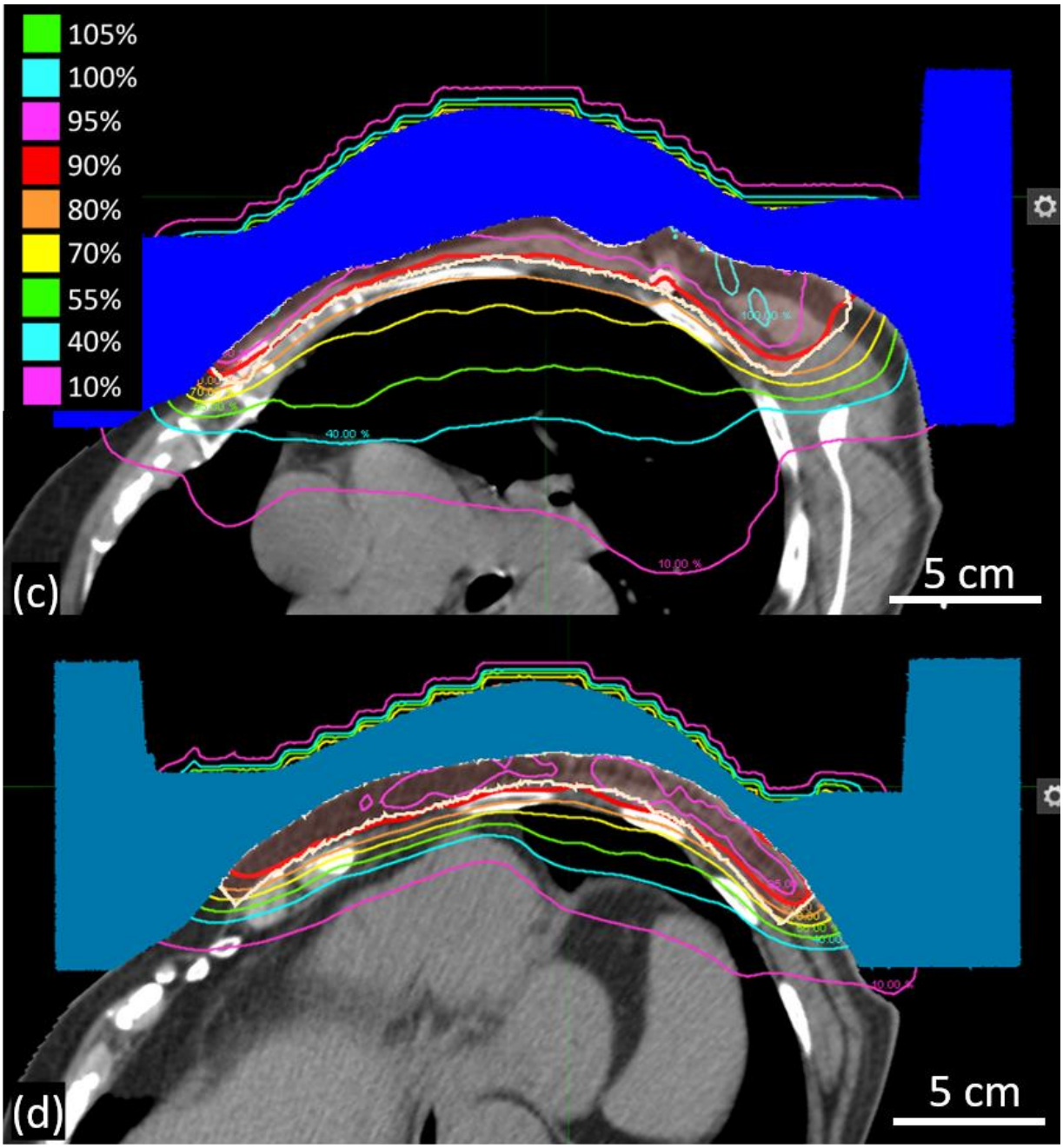
105%
100%
95%
90%
80%
70%
55%
40%
10%
40.00 %
10.00 %
(c)
5 cm
(d)
5 cm

References

[1] Siegel RL, Miller KD, Jemal A. Cancer statistics, 2019. *Cancer J Clin.* 2019; **69**(1): 7–34.

[2] Kummerow KL, Du L, Penson DF, Shyr Y, Hooks MA. Nationwide trends in mastectomy for early-stage breast cancer. *JAMA Surg.* 2015; **150**(1): 8–16.

[3] Kohler BA, Sherman RL, Howlader N, et al. Annual report to the nation on the status of cancer, 1975–2011, featuring incidence of breast cancer subtypes by race/ethnicity, poverty, and state. *J Natl Cancer Inst.* 2015; **107**(6): djv048, 1-25.

[4] Henley SJ, Ward EM, Scott S, et al. Annual report to the nation on the status of cancer, part I: national cancer statistics. *Cancer*. 2020; **126**(10): 2225-2249.

[5] Gee HE, Moses L, Stuart K, et al. Contouring consensus guidelines in breast cancer radiotherapy: Comparison and systematic review of patterns of failure. *J Med Imaging Radiat Oncol.* 2019; **63**(1): 102–115.

[6] Vargo JA, Beriwal S. RTOG chest wall contouring guidelines for post-mastectomy radiation therapy: is it evidence-based? *Int J Radiat Oncol.* 2015; **93**(2): 266–267.

[7] Gradishar WJ, Anderson BO, Balassanian R, et al. Invasive Breast Cancer. *J Natl Compr Cancer Netw*. 2016; **14**(3): 324–354.

[8] Heins DE. *Comparison of Advanced Radiotherapy Techniques for Post-Mastectomy Breast Cancer Patients, MS Thesis.* Baton Rouge, LA. Louisiana State University and Agricultural and Mechanical College; 2016.

[9] Lundkvist J, Ekman M, Ericsson SR, Isacsson U, Jönsson B, Glimelius B. Economic evaluation of proton radiation therapy in the treatment of breast cancer. *Radiother Oncol.* 2005; **75**: 179–185.

[10] Gagliardi G, Lax I, Ottolenghi A, Rutqvist LE. Long-term cardiac mortality after radiotherapy of breast cancer - application of the relative seriality model. *Br J Radiol.* 1996; **69**(825): 839–846.

[11] Marks LB, Bentzen SM, Deasy JO, et al. Radiation dose-volume effects in the lung. *Int J Radiat Oncol Biol Phys.* 2010; **76**(3): 70–76.

[12] Pierce LJ. Treatment guidelines and techniques in delivery of postmastectomy radiotherapy in management of operable breast cancer. *J Natl Cancer Inst Monogr*. 2001; **2001**(30): 117–124.

[13] Hernandez M, Zhang R, Sanders M, Newhauser W. A treatment planning comparison of volumetric modulated arc therapy and proton therapy for a sample of breast cancer patients treated with post-mastectomy radiotherapy. *J Proton Ther.* 2015; **1**(1): 119.

[14] Gauer T, Engel K, Kiesel A, Albers D, Rades D. Comparison of electron IMRT to helical photon IMRT and conventional photon irradiation for treatment of breast and chest wall tumours. *Radiother Oncol.* 2010; **94**(3): 313–318.

[15] Nichols GP, Fontenot JD, Gibbons JP, Sanders ME. Evaluation of volumetric modulated arc therapy for postmastectomy treatment. *Radiat Oncol.* 2014; **9**(1): 1–8.

[16] Tsai PF, Lin SM, Lee SH, et al. The feasibility study of using multiple partial volumetric-modulated arcs therapy in early stage left-sided breast cancer patients. *J Appl Clin Med Phys.* 2012; **13**(5): 62–73.

[17] Zhang R, Heins D, Sanders M, Guo B, Hogstrom K. Evaluation of a mixed beam therapy for postmastectomy breast cancer patients: bolus electron conformal therapy combined with intensity modulated photon radiotherapy and volumetric modulated photon arc therapy. *Med Phys.* 2018; **45**(7): 2912–2924.

[18] Hogstrom KR, Leavitt DD. Dosimetry of electron arc therapy. In: *Radiation Onocology Physics-1986: Proceedings of 1986 Summer School of the AAPM.* New York, NY: American Institute of Physics; 1987: 265–295.

[19] Ashenafi M, Boyd RA, Lee TK, et al. Feasibility of postmastectomy treatment with helical tomotherapy. *Int J Radiat Oncol Biol Phys.* 2010; **77**(3): 835–842.

[20] Xie Y, Bourgeois D, Guo B, Zhang R. Postmastectomy radiotherapy for left-sided breast cancer patients: comparison of advanced techniques. *Med Dosim.* 2020; **45**(1): 34–40.

[21] Opp D, Forster K, Li W, Zhang G, Harris EE. Evaluation of bolus electron conformal therapy compared with conventional techniques for the treatment of left chest wall postmastectomy in patients with breast cancer. *Med Dosim.* 2013; **38**(4): 448–453.

[22] Vaeth JM, Meyer JL. *The Role of High Energy Electrons in the Treatment of Cancer*. San Francisco, CA: Karger, 1991.

[23] Tapley N duV. *Clinical Applications of the Electron Beam.* New York, NY: Wiley, 1976.

[24] Gerbi BJ, Antolak JA, Deibel FC, et al. Recommendations for clinical electron beam dosimetry: Supplement to the recommendations of Task Group 25. *Med Phys.* 2009; **38**(1): 548–548.

[25] Kim MM, Kudchadker RJ, Kanke JE, Zhang S, Perkins GH. Bolus electron conformal therapy for the treatment of recurrent inflammatory breast cancer: a case report. *Med Dosim.* 2012; **37**(2): 208–213.

[26] Perkins GH, McNeese MD, Antolak JA, Buchholz TA, Strom EA, Hogstrom KR. A custom three-dimensional electron bolus technique for optimization of postmastectomy irradiation.

Int J Radiat Oncol Biol Phys. 2001; **51**(4): 1142–1151.

[27] Svensson H, Almond P, Brahme A, et al. *ICRU Report 35, Radiation Dosimetry: Electrons with Initial Energies Between 1 and 50 MeV*. Bethesda, MD: International Commission on Radiation Units and Measures; 1984.

[28] Khan FM, Doppke KP, Hogstrom KR, et al. Clinical electron-beam dosimetry: report of AAPM Radiation Therapy Trask Group No. 25. *Med Phys.* 1991; **18**(1):73-109.

[29] Bjärngard BE, Piontek RW, Svensson GK. Electron scattering and collimation system for a 12-MeV linear accelerator. *Med Phys.* 1976; **3**(3): 153–158.

[30] Carver RL, Hogstrom KR, Price MJ, LeBlanc JD, Pitcher GM. Real-time simulator for designing electron dual scattering foil systems. *J Appl Clin Med Phys.* 2014; **15**(6): 323–342.

[31] Taylor T, VanDyk G, Funk LW, Hutcheon RM, Schriber SO. Therac 25: A new medical accelerator concept. *IEEE Trans Nucl Sci.* 1983; **30**(2):1768-1771.

[32] Leveson NG, Turner CS. An investigation of the Therac-25 accidents. *Computer*. 1993; **26**(7): 18–41.

[33] Kudchadker RJ, Hogstrom KR, Garden AS, et al. Electron conformal radiotherapy using bolus and intensity modulation. *Int J Radiat Oncol Biol Phys.* 2002; **53**(4): 1023–1037.

[34] Hogstrom KR, Carver RL, Chambers EL, Erhart K. Introduction to passive electron intensity modulation. *Radiat Oncol Phys.* 2017; **18**(6): 10–19.

[35] Hogstrom KR, Antolak JA, Kudchadler RJ, Ma C-MC, Leavitt DD. Modulated Electron Therapy. In: *Intensity Modulated Radiation Therapy, The State of the Art: Proceedings of the 2003 AAPM Summer School.* Madison, WI: Medical Physics Publishing; 2003: 749–786.

[36] Su S, Moran K, Robar JL. Design and production of 3D printed bolus for electron radiation therapy. *J Appl Clin Med Phys.* 2014; **15**(4): 194–211.

[37] Kudchadker RJ, Antolak JA, Morrison WH, Wong PF, Hogstrom KR. Utilization of custom electron bolus in head and neck radiotherapy. *J Appl Clin Med Phys.* 2003; **4**(4): 321.

[38] Low DA, Starkschall G, Bujnowski SW, Wang LL, Hogstrom KR. Electron bolus design for radiotherapy treatment planning: bolus design algorithms. *Med Phys.* 1992; **19**(1): 115–124.

[39] Low DA, Hogstrom KR. Determination of the relative linear collison stopping power and linear scattering power of electron bolus material. *Phys Med Biol.* 1994; **39**(6): 1063–1068.

[40] Łukowiak M, Jezierska K, Boehlke M, et al. Utilization of a 3D printer to fabricate boluses used for electron therapy of skin lesions of the eye canthi. *J Appl Clin Med Phys.* 2017; **18**(1): 76–81.

[41] Doiron J. *Benefit of Intensity Modulated Bolus Electron Conformal Therapy for Post Mastectomy Chest Wall Irradiation, MS Thesis.* Baton Rouge, LA. Louisiana State University and Agricultural and Mechanical College; 2018.

[42] Hilliard EN. *Verification and Evaluation of a Passive Intensity Modulation Device for Bolus Conformal Therapy, MS Thesis.* Baton Rouge, LA. Louisiana State University and Agricultural and Mechanical College; 2018.

[43] Chambers EL. *Design of a Passive Intensity Modulation Device for Bolus Electron Conformal Therapy, MS Thesis.* Baton Rouge, LA. Louisiana State University and Agricultural and Mechanical College; 2016.

[44] Werner BL, Khan FM, Deibel FC. A model for calculating electron beam scattering in treatment planning. *Med Phys.* 1982; **9**(2): 180–187.

[45] Shiu S, Hogstrom KR. Pencil-beam redefinition algorithm for electron dose distributions. *Med Phys*. 1991; **18**(1): 7–18.

[46] Boyd RA, Hogstrom KR, Rosen II. Effect of using an initial polyenergetic spectrum with the pencil-beam redefinition algorithm for electron dose calculations in water. *Med Phys.* 1998; **25**(11): 2176–2185.

[47] Carver RL, Sprunger CP, Hogstrom KR, Popple RA, Antolak JA. Evaluation of the Eclipse eMC algorithm for bolus electron conformal therapy using a standard verification dataset. *J Appl Clin Med Phys*. 2016; **17**(3): 52–60.

[48] Seppenwoolde Y, Lebesque J V., De Jaeger K, et al. Comparing different NTCP models that predict the incidence of radiation pneumonitis. normal tissue complication probability. *Int J Radiat Oncol Biol Phys.* 2003; **55**(3): 724–735.

[49] Lyman JT. Complication probability as assessed from dose-volume histograms. *Radiat Res*. 1985; **8**: 13–19.

[50] Källman P, Ågren A, Brahme A. Tumour and normal tissue responses to fractionated non-uniform dose delivery. *Int J Radiat Biol.* 1992; **62**(2): 249–262.

[51] Schneider U, Kaser-Hotz B. A simple dose-response relationship for modeling secondary cancer incidence after radiotherapy. *Z Med Phys.* 2005; **15**(1): 31–37.

Vita

Stephanie Wang spent her formative years in both Phoenixville, PA and Montvale, NJ. She graduated from the College of William and Mary in Williamsburg, VA with a B.S. in Physics in 2017. In fall 2017, she matriculated into the M.S. in Medical Physics and Health Physics Program at Louisiana State University in Baton Rouge, LA. Stephanie plans to graduate with a M.S. degree in summer of 2020 and spend her next two years in a radiation oncology physics residency program.